2008

Heavy Stable Isotope Investigations in Environmental Science and Archeology

Sanghamitra Ghosh

FLORIDA STATE UNIVERSITY

COLLEGE OF ARTS AND SCIENCES

HEAVY STABLE ISOTOPE INVESTIGATIONS IN ENVIRONMENTAL SCIENCE AND ARCHEOLOGY

By

SANGHAMITRA GHOSH

A Dissertation submitted to the
Department of Geological Sciences
in partial fulfillment of the
requirements for the degree of
Doctor of Philosophy

Degree Awarded:
Summer Semester, 2008

The members of the Committee approve the Dissertation of Sanghamitra Ghosh defended on April 25, 2008.

Arthur Leroy Odom
Professor Directing Dissertation

William Landing
Outside Committee Member

Munir Humayun
Committee Member

Stephen Kish
Committee Member

Vincent Salters
Committee Member

Yang Wang
Committee Member

Approved:

Professor Arthur Leroy Odom, Department of Geological Sciences

The Office of Graduate Studies has verified and approved the above named committee members.

To my family

ACKNOWLEDGEMENTS

At the very outset I convey my gratitude to my supervisor Dr. Leroy Odom, for his valuable academic guidance and financial support. I specially thank Dr. Munir Humayun, who spent countless hours guiding me during my research. Words are inadequate to express his contribution to complete this dissertation.
I am grateful to Dr. Stephen Kish for giving me the opportunity to work on projects in archeology and lending academic support whenever required.
I would also like to thank my other committee members, Dr. Yang Wang and Dr. Vincent Salters, who have been a significant source of scientific support in my dissertation.

The National High Magnetic Field Laboratory, which houses the Isotope Geochemistry group, has been a wonderful place to work at. I take this opportunity to thank Ted Zateslo and Afi Sachi-Kocher for their continuous technical support. Special thanks go to Dr. Michael Bizimis who helped me learn the fundamental aspects of analytical geochemistry and provided insights into the technicalities of mass spectrometers.

I would also like to thank my friends Mabry Gaboardi, Soumen Mallick and his wife Indrani, and Sofia Khawaja for lending me their invaluable personal support during the most difficult times of my stay at Tallahassee and making my Tallahassee days memorable.

Finally, I would like to thank my parents and in-laws for their unending love and encouragement throughout my tenure as a PhD student. I am especially grateful to my father who motivated me to pursue a PhD degree and helped me reach my goals. Without his continuous inspiration and guidance, this would have been an impossible task for me to complete. I would also like to express my gratitude to my husband, Debasish, for his unconditional support and patience through our 6 years of long distance relationship.

TABLE OF CONTENTS

LIST OF TABLES

LIST OF FIGURES

ABSTRACT

A mercury isotope technique was developed using a *Neptune* Multi Collector Inductively Coupled Mass Spectrometer (MC-ICPMS) in low resolution mode. The amount of sample used was approximately 10 nanograms of Hg and the external precision obtained for $\delta^{198}Hg/^{202}Hg$ by sixty replicate analysis of Almaden cinnabar is 0.55‰. The mercury extraction chemistry developed in this study for various kinds of environmental samples (peat, vegetation, soil and shale) has a very high yield (96% -100%) and there is no observed isotope fractionation induced during the extraction chemistry. This study also demonstrates that drying and heating of samples can significantly fractionate mercury isotopes.

An ombrotrophic peat bog from Penido Vello, NW Spain has been analyzed for mercury isotopes and oxygen isotopes. The isotopic composition of mercury in the top of the core dominated by anthropogenic mercury is very similar to the isotopic composition of mercury from the bottom of the core dominated by pre-industrial mercury. This indicates that the Hg (0) emitted from the various sources probably homogenized quickly in the atmospheric pool and original isotopic source signatures were not preserved during deposition. A different explanation could be that since coal combustion, the main contributor of modern anthropogenic mercury releases all the mercury that has accumulated for thousands of years, essentially most of the modern anthropogenic mercury is representative of pre-industrial mercury, thereby showing no difference in isotopic composition. A third explanation could be that the analytical precision of the technique probably is insufficient to resolve meaningful isotopic variations that occur in mercury contributed from different sources. In the oxygen isotope record of the Penido Vello peat core, Medieval Warm Peiod (MWP), Little Ice Age (LIA) and Recent Warming (RW) are more pronounced whereas Roman Warming Period (RWP) and Dark Ages Cold Period (DACP) are less pronounced.

Mass Independent Fractionation (MIF) of mercury isotopes produced by both Nuclear Volume Effect (NVE) and Magnetic Isotope Effect (MIE) could be an important tool in constraining models of mercury sources and pathways in the environment. Deviations from mass-dependent fractionation were calculated as the difference between the measured $\delta^{199}Hg$ and $\delta^{201}Hg$ ($\delta^{A}Hg_{measured}$) of a sample and the $\delta^{199}Hg$ and $\delta^{201}Hg$ ($\delta^{A}Hg_{MD}$) obtained from the linear scaling defined by the even-mass isotopes. The NVE induces a MIF in the odd-A Hg isotopes in the ratio, $\Delta^{201}Hg/\Delta^{199}Hg \approx 0.5$, with the odd mass isotopes enriched in the reduced species such as Hg (0) and methylmercury and depleted in oxidized species such as Hg (II). The sediment samples and the Patagonia peat analyzed in this study are enriched in the odd-A Hg isotopes in approximately correct ratios for NVE. The Penido Vello peat core and Spanish moss samples are depleted in the odd-A Hg isotopes and exhibit $\Delta^{201}Hg/\Delta^{199}Hg \approx 1$ which is consistent with MIE.

Galena artifacts recovered at Late Archaic – Mississippian archaeological burial and habitation sites in southern and central United States have been provenanced by combining both lead and sulfur isotopes. The lead isotope database for the Mid Continental mineral deposits allows us to determine, with a high degree of certainty, the origin of galena artifacts found. Most of the seventeen archaeological burial/habitation sites contain galena artifacts which have lead isotopic characteristics that imply Central Missouri as a single source. Eight of the nine galena artifacts analyzed for sulfur show identical sulfur and lead isotope correlation with the Central Missouri lead district. From chemical and isotopic analysis, it seems that only certain areas especially the northern and

northeastern North America have galena artifacts sourced from Upper Mississippi Valley lead district. There is no evidence, except for one artifact from Poverty Point site in Louisiana that southern and eastern USA had any galena originating from Upper Mississippi Valley. Further the evidence doesn't show of any significant temporal change in galena sources over a time span of thousand years in the southern and eastern USA.

CHAPTER 1

DEVELOPMENT OF A METHOD FOR THE DETERMINATION OF LOW-ABUNDANCE, HIGH-PRECISION, MERCURY ISOTOPE RATIOS

1.1 Introduction

1.1.1 General

Mercury (Hg) is one of the most studied trace elements in the environment. Mercury is a global pollutant. Its toxic organic forms (such as methylmercury) can biomagnify through the aquatic food chain even in remote areas. As atmospheric component elemental mercury vapor can be transported long distances from its source of origin (possibly hundreds or thousands of kilometers away) and eventually be deposited back to the Earth's surface. Mercury has a complex biogeochemical cycle that involves exchanges between different reservoirs in the ecosystem. Mercury is emitted from both anthropogenic and natural sources. Moreover, mercury deposited from the atmosphere can be re-emitted over and over again; the re-emitted mercury can be either natural or anthropogenic in nature or both.

1.1.2 Global mercury cycle

The global biogeochemical cycling of mercury (**Figure 1.1**) has been often modeled using mass balance formulations (Fitzgerald, 1986; Fitzgerald, 1989; Fitzgerald and Clarkson, 1991; Hudson, *et al*., 1995; Lindqvist & Rodhe, 1985; Lindqvist, *et al*., 1991; Mason, *et al*., 1994; Mason and Sheu, 2002; Morel *et al*., 1998; Nriagu, 1989). These simulations in general show the atmosphere playing a prominent role in transporting and depositing mercury in different ecosystems. Direct anthropogenic releases of mercury are primarily from fossil fuel-fired power plants, chlor-alkali plants, pulp industries, metallic mining, and waste incineration (Pacyna *et al*., 2005; Streets *et al*., 2005) and represent approximately 50% -75% of current total atmospheric mercury emission (Fitzgerald, 1995; Mason, *et al*., 1994). The natural sources of mercury to the atmosphere are degassing from land especially from mercury rich ore deposits and soils (Gustin *et al*., 1996, 1997; Rasmussen, 1994), volcanic eruptions, biomass burning and degassing from the surfaces of ocean and other water bodies (Rasmussen, 1994).

The dominant (95% of total atmospheric mercury) atmospheric species of mercury is the gaseous, elemental Hg (0) which has an atmospheric residence time of about one to two year (Slemr & Langer, 1992). The Hg (0) is oxidized to Hg (II) by oxidants such as ozone, HClO, $HSO3^-$ and $OH^{\bullet}$(Munthe, *et al*., 1991; Munthe, 1992; Munthe & McElroy, 1992). Most of these oxidations occur at the liquid-solid interface of cloud and fog droplets (Morel, *et al*., 1998). Mercury gets deposited from the atmosphere to the Earth's surface by both dry deposition and wet precipitation of Hg (II). Especially over land, mercury gets adsorbed onto aerosols surfaces such as soot (Mason, *et al*., 1994). The long residence time of Hg (0) as compared to the mixing time of the atmosphere allows for global-scale mixing of this gas, before it is deposited to the Earth's surface by via precipitation and dry deposition.

30% of earth's surface is covered by land and also amount of precipitation is almost 3 times less on land compared to oceans. When atmospheric mercury gets deposited on Earth's surface, only 40% of it is deposited in oceans and 60% is deposited on land (Mason *et al*., 1994). The larger percentage of mercury gets deposited on land is probably because most of the modern mercury sources are on the land (Mason, *et al*., 1994). In the upper hundred meters of oceans, Hg (II) undergoes reductions to Hg (0) and is lost to the atmosphere by evasion (Mason & Fitzgerald, 1990) and only a very small fraction is permanently fixed in sediments (Mason, *et al*., 1994). These reductions can occur by photochemical processes (Amyot *et al*., 1994; Sellers *et al*., 1996), biotic processes (Barkay *et al*., 2005; Mason *et al*., 1995) and abiotic processes in presence of humic matter (Alberts *et al*., 1974; Allard and Arsenie, 1991). Oxidation/reduction reactions also occur on land but due to mercury's high affinity to form organic complexes, much of the mercury deposited on land becomes fixed in soils (Lindqvist, *et al*., 1991; Swain *et al*., 1992)

1.1.3 Mass fractionation of mercury isotopes

Mercury has seven stable isotopes (^{196}Hg, ^{198}Hg, ^{199}Hg, ^{200}Hg, ^{201}Hg, ^{202}Hg, ^{204}Hg), with a mass range of >3%, of which six are sufficiently abundant (7-30%) for precise measurement.. It undergoes complex redox reactions and is involved in chemical bonds with a high degree of covalent character. It has high vapor pressure at low temperature. All these factors suggest that mercury might undergo measurable isotopic fractionation in natural systems.

Although isotopes are characterized by similar chemical properties, due to their mass differences, their reaction rates slightly differ. The lighter isotopes react faster than the heavier ones thus causing products to be enriched with the lighter isotopes than reactants in irreversible reactions. In general, physical processes such as evaporation, condensation, and diffusion of ions/molecules due to concentration or temperature gradients cause isotopic fractionation in stable isotopes. It is most likely that along the complex pathways of the mercury cycle there are a number of natural processes, which will result in isotopic fractionation of mercury. These can be evaporation of mercury from soil or water surface and condensation of mercury vapor from the atmosphere. The lighter mercury isotopes would preferentially evaporate and the heavier mercury isotopes preferentially condense. Diffusion of mercury vapor in the soils, sediments, water and atmosphere could cause fractionation. The lighter isotopes would be more mobile than the heavier isotopes thus diffusing faster. Mercury is biologically very active and undergoes a variety of biological reactions like methylation and demethylation. Also, mercury binds in organic material more effectively than any other metal. Biological organisms preferentially use the lighter isotopic species because of the low energy associated with breaking the bonds in these molecules, resulting in maximum fractionations between the substrate (heavier) and the biologically mediated product (lighter).

Mercury is extracted from its principal ore cinnabar by metallurgical processes involving roasting and distillation. These vaporization processes most likely would fractionate mercury, with relative enrichment of lighter isotopes in the vapor phase and relative enrichment of heavier isotopes in the distillate. Anthropogenic mercury would therefore be expected to be isotopically distinct from some natural mercury.

1.1.4 Mercury isotopes as potential tool

The global mercury cycle is based on flux and concentration based models and many crucial uncertainties still exist. Most of the current models fail to accurately identify the importance of natural emissions and re-emissions of mercury due to lack of resources. This may be acceptable for local and regional models, but for global models over longer time periods, accuracy is needed. Also, the percentage of naturally emitted and re-emitted mercury is not very well known. First, it is quite impossible to differentiate between naturally emitted and re-emitted mercury. The only exceptions are in cases where there is a detectable natural mercury signal (e.g. natural mercury ore deposits, volcanic eruptions etc.). Secondly, there are only a handful of measurements available. The present estimates of re-emitted mercury are inferred from a few measurements and global mercury flux models. For example one of the biggest contributors of re-emitted mercury is the oceans; but data from oceanic re-emissions are limited to very specific sites. Moreover for anthropogenic sources the emission inventories need to be continuously updated and better informed on mercury speciation. The overall global contributions of the anthropogenic sources have been estimated quite well but large uncertainties exist for individual anthropogenic sources.

Stable isotope chemistry of many light elements such as H, N, S, C and O have been used as tracers for determining sources, sinks and dominant transformation pathways of nutrients and toxic substances in modern and paleoenvironments. Like the other stable isotopes, mercury isotopes can be used as a potential new tool to trace mercury transport pathways and degrees of recycling and to better understand the potential sinks for mercury in the environment. One of the biggest potential uses of mercury isotopes could be to distinguish between natural and anthropogenic sources of mercury. This could quantify the natural emissions which have a large influence in the global mercury background. Different anthropogenic sources could possibly emit mercury with different isotopic ratios. Coal-fired power plants emit mercury by direct burning and roasting of coal whereas chlor-alkali plants and landfills have diffused emissions of mercury. If these different physical processes change the isotopic composition of emitted mercury differently, then there will be a better knowledge of anthropogenic emission inventories not only on a regional/local scale but also on a global basis. Moreover, if coals from various coal-producing regions in the world vary in their mercury isotopic composition, then isotope studies might be used to distinguish and accurately quantify the actual amount of mercury being emitted from power plants. The oceanic contribution of mercury to the atmosphere although by natural biochemical transformations represents largely a recycled anthropogenic component. If re-cycled mercury is isotopically distinct, it would put a better constraint on global mercury mass balance budgets. Mercury isotopes can be useful tracers during biochemical transformation of mercury into toxic organic compounds like methylmercury in aquatic environments which are not yet completely understood. The processes of methylation and demethylation might also change the isotopic composition of mercury. This could be used to study and quantify the amount of mercury consumed by aquatic organisms and to understand its behavior in a lifetime of an organism.

Oxygen and hydrogen isotopes have been routinely used as paleoclimate tools. Mercury isotopes could potentially be used as a proxy for paleoclimate changes. Changes in different climatic factors such as temperature and/or humidity could fractionate oxygen and hydrogen isotopes and could also possibly fractionate mercury deposited from atmosphere and stored in soils and sediments. If such an effect is true, then isotopic composition of mercury deposited during colder

and dryer periods would be different than from warmer and wetter periods. Study of mercury isotopes archived in sediment and peat cores would probably provide climatological information for the past few thousand years.

1.1.5 Previous work

With increasing atomic mass, stable isotope fractionations generally tend to decrease strongly. Consequently, natural isotopic variations in heavier elements like mercury in different ecosystem reservoirs are expected to be quite small. Due to the low concentration of mercury in most environmental media, accurate and precise measurement of mercury isotope ratios becomes an additional analytical challenge. These analytical challenges had limited the number of previous investigations of the mercury stable isotope geochemistry and only a handful of mercury stable isotope studies had been conducted to date.

Nearly a century ago, Bronsted and von Hevesy reported in *Nature* that they had achieved a partial separation of mercury isotopes by evaporation at low pressure. In 1950, Nier suggested that the inability of researchers to obtain the same values for the isotopic composition of mercury might be due partly to real differences between the mercury reagents used. Neutron Activation Analysis has been used in the past to study mercury isotopes in meteorites (Reed and Jovanovic, 1967, 1990; Jovanovic and Reed, 1976a, b, 1987, 1990; Goel and Thakur, 1987; Thakur and Goel, 1989; Kumar and Goel, 1992a, b; Kumar *et al*., 2001). However, NAA can practically measure only two isotopes (^{196}Hg and ^{202}Hg) and had precision ranging from 0.5-30%. Zadnik *et al*. (1989) performed the study with noble gas mass spectrometer, in which he measured all the seven naturally occurring Hg isotopes: ^{196}Hg, ^{198}Hg, ^{199}Hg, ^{200}Hg, ^{201}Hg, ^{202}Hg and ^{204}Hg. The precisions that Zadnik achieved in his study are 0.9-1.2‰ (1RSD) for all the ratios of each isotope normalized to ^{202}Hg. Mercury has high vapor pressure due to which isotopic measurements cannot be performed by thermal ionization mass spectrometer (TIMS). Measurement of mercury isotopes by Quadrupole ICP-MS (Jackson, 2001) and Single Collector Magnetic Sector ICPMS (Krupp & Donard, 2005) has shown that these mass spectrometric techniques have an analytical precision which is not sufficient enough to establish meaningful natural variations of mercury isotopes in environmental samples.

1.1.6 Initial efforts of this research

Due to mercury's very high ionization potential and high volatility sputtering ionization was thought to be an efficient way to ionize mercury. Mitchell (1999) developed a technique to measure mercury isotope ratios in cinnabar grains (without dissolution or chemical processing) using the Isolab 54 in Secondary Ionization mode (England *et al*, 1992) in the National High Magnetic Field Laboratory. He showed for the first time natural variations in the isotopic composition of mecury.

Mitchell's study involved samples containing essentially unlimited amounts of mercury. It was recognized at the beginning of this project that in order to employ SIMS analyses to samples containing typical environmental levels of mercury, the mercury would have to be extracted from samples and concentrated in a single spot, not much larger than the size of the primary ion beam of the ISOLAB 54. Experiments began using small amounts of mercury from cinnabar solution. When, after many attempts of using a variety of different substrates, to precipitate HgS onto a small spot (to serve as the secondary ion source) failed to yield sufficiently large secondary ion currents, efforts turned to electroplating.

The mercury from a sample was purified by electroplating Hg on to a gold electrode. The electrode in reality was a tiny gold spot (100 microns in diameter) that had previously been electroplated on a stainless steel pin tip. After electroplating was done, the stainless steel pin was fitted on to the center of a stainless steel rod. The rod (1cm long) with the pin in center was fixed on a Cathodeon bead. The mercury amalgamated on the tiny gold spot was then targeted by 10 kV Ar^+ ion beam. The resulting secondary Hg^+ ions were analyzed in a double-focusing mass spectrometer and then detected on a series of adjustable Faraday cups. However, numerous problems were faced. Electroplating yield was very poor for mercury (less than 80%) which could be because of the tiny size of the gold spot serving as the electrode. The gold spot was of 100 microns diameter so that it would fit the aperture of the primary argon ion beam. The low yield can potentially induce mass fractionation in the sample which could overprint the natural fractionation. Also, due to mercury's affinity to amalgam with gold, the electroplated mercury diffused deep inside the gold. For ionization purposes it is essential for the mercury to stay on the surface of the gold. Moreover the ionization was achieved by sputtering without heat being applied. There were molecular interferences on mercury masses which were non- reproducible. The molecular interferences could be removed by applying heat but that would also cause the loss of mercury. Last but not the least, for high precision measurements of mercury isotopes, the amount of sample required for sputtering ionization was in the order of micrograms while environmental samples of mercury are in the levels of sub nanograms. A suitable method of making precise mesurements of mercury isotope ratios by SIMS at low concentrations was not achieved.

The recent advancement of multi collector inductively coupled plasma mass spectrometry (MC-ICPMS) technique has led to a successful high precision measurement of natural variations in the stable isotope composition of mercury. While this research was ongoing, there came reports of ranges of variations in $\delta\ ^{202}Hg/\ ^{198}Hg$ of up to 5.5 ‰ (relative to NIST SRM 3133) in cinnabar deposits (Smith *et al*., 2005). Hintelmann and Lu, 2003, investigated cinnabar samples from different places in the world of different ages and from a wide variety of geological settings. Values of $\delta^{198}Hg/\ ^{202}Hg$ varied from 0.0-1.33 ‰ relative to NIST SRM 1641d Hg standard and are in good agreement with those determined earlier by Mitchell (1999). The values of Smith *et al*. (2005) are considered to be too high. The extent of mercury fractionation in natural sediments and sediment cores has been investigated by several groups. The $\delta^{202}Hg/\ ^{198}Hg$ variation analyzed in sediment samples from different locations in the world having various sources of mercury are from +1‰ to -4 ‰ (Foucher and Hintelmann, 2006, relative to NIST SRM 1641d). In addition laboratory experiments conducted show a biologically induced -7‰ fractionation in $\delta\ ^{198}Hg/^{202}Hg$ (relative to NIST SRM 3133) measured by cold vapor generation and MC-ICPMS during reduction of Hg(II) to Hg(0) using a purely cultured bacterium *Escherichia coli* (Kritee *et al*., 2005, 2007).

This study focuses on the development of a mercury isotope analytical procedure by MC-ICPMS. The measurements are made by Thermo-Finnigan *Neptune* which is a Multicollector-ICPMS. The mercury isotope analytical technique employed a steady state continuous mercury reducing technique using stannous chloride as a reductant. A wide variety of environmental samples were studied for this purpose.

1.2 Materials and Methods

1.2.1 Samples and Reagents

The mercury solutions were prepared from the NIST SRM3133 10,000 μg/ml mercury standard stock solution (Hg^{+2} in HNO_3). A 1000ml intermediate standard solution with a concentration 10 μg/ml was made in 6M HCL and stored in the freezer. The standard solutions of 1ng/ml in 1M HCl was made on a daily basis from the intermediate standard solution. Other calibration solutions were made fresh (because of their very low concentration) by diluting the appropriate amount of 1ng/ml solution with 1M HCl. 2% tin chloride solution ($SnCl_2$, 98% purity, ACROS) was prepared in 1M HCl daily and purged prior to use with argon gas for approximately thirty minutes in order to release any trace mercury. Reagents used in this work included in-house doubly-distilled HNO_3 and HCl acids stored in PFA Teflon vessels, analytical grade H_2O_2 (30% Certified ACS, Fisher Chemical), and 18 MΩ QD H_2O.

Samples from two peat cores, Hg elemental abundances standards of sediment and shale, and vegetation, were analyzed for Hg isotope composition. A peat core was obtained from an ombrotrophic peat bog of Penido Vello, Spain, previously identified as having an anthropogenic Hg profile (Cortizas *et al*., 1999). The vegetation was also collected from the Spanish peat bog. A peat sample from Patagonia was obtained from Harold Beister from University of Heidelberg. The sediment and shale are NIST Standard Reference Materials Estuarine Sediment 1646 a and Green River Shale NIST SGR-1 respectively.

1.2.2 Mercury Extraction Chemistry

1.2.2.1 Sample Preparation

It is very important to recover mercury from the sample without introducing isotopic fractionation during sample chemistry. A cold acid (room temperature) leaching technique was applied on Standard Reference Materials NIST 2704 Buffalo River Sediment (1400 ppb) and NIST 1572 Citrus Leaves (80 ppb) to test the mercury recovery yield. Three samples of NIST 2704 (0.179, 0.158, 0.185 grams) and two samples of NIST 1572 (0.371, 0.317 grams) standards were weighed into screw top120 ml PFA vessel (Savillex) beakers. A mixture of ultrapure concentrated HCl and 30% H_2O_2 (30 ml, 2:1 v/v) was added to the sample and the vessels were closed. The samples were shaken for an hour on a C1 platform Shaker (New Brunswick Scientific Classic Series). The samples were then ultrasonicated for 48 hours in a bath of high purity water. The leachate was then filtered from the residual sample by passing through a 0.2 um Millipore Polycarbonate membrane filter in a vacuum filtration system. In between each sample, the filter system was cleaned with aqua regia.

1.2.2.2 Experimental setup

The recovery yield of mercury by cold acid leaching was tested by coupling of CETAC HGX-200 Hydride Generation and Cold Vapor System (Klaue and Blum, 1999) and Finnigan MAT "ELEMENT," high resolution sector ICP-MS. Elemental Hg vapor, formed by reacting sample solution with 2% $SnCl_2$, was introduced into the mass spectrometer by the Cold Vapor System. The HGX-200 system features a gas liquid separator (GLS), reagent vessels, clearly labeled tubing and connections, solution mixing blocks and coils, and a built-in gas flow meter. The special U-shaped GLS incorporates a "frosted" glass post that provides a high surface area for

liquid film evaporation and release of Hg (0). The GLS also features a porous PTFE membrane and droplet separator to achieve complete gas/liquid separation and reduced signal noise. The cold vapor generated from the $SnCl_2$ reduction is carried by Teflon tubes to the mass spectrometer. A Perimax Spectec peristaltic pump is used for controlling the intake rates of $SnCl_2$ and Hg sample solutions (Klaue and Blum, 1999).

The concentrated NIST 2704 and NIST 1572 solutions were diluted 5 fold with 0.5 M HCl to a final volume of approximately 25 ml. Hg Calibration standards of 0.1 ng/ml, 0.2 ng/ml, 0.4 ng/ml and 0.5 ng/ml were prepared by serial dilution of 1ng/ml NIST SRM 3133 standard solution. The 0.2ng/ml standard was run every two or three samples to check the sensitivity of the mass spectrometer. The whole system was cleaned by wash solution of 1M HCl for 2-3 minutes after each sample or standard to ensure that there was no carryover of mercury in the tubes. Random blank (called "system" blank) solutions made of 1M HCl were run with some of the samples to ensure that the hydride generator system had no carryover mercury and the mercury background was constant throughout the measurement period. Some of the NIST 2704 and NIST 1572 solutions were run in duplicates in the measurement sequence (**Table 1.1**). The Experimental conditions for the Element are listed in **Table 1.2**.The 0.2 ng/ml Hg standard solution used for tuning and monitoring plasma stability had a typical sensitivity varying between $1*10^6$-$2*10^6$ counts per second for ^{202}Hg. The typical mercury background varied between 16,000-20,000 counts per second for ^{202}Hg. The solution uptake rate was 1.1 ml/min

A multi elemental analytical method was setup (**Table 1.3**). ^{204}Pb isobaric interference on ^{204}Hg was monitored at mass 206 (^{206}Pb) and ^{198}Pt isobaric interference on ^{198}Hg was monitored at mass 195 (^{195}Pt). Linear regression analysis on the standard calibration curve yielded an R^2= 0.9992 (**Figure 1.2**). Since ICP-MS signal intensity drifts over the course of a measurement session, standard concentrations were calculated over the sample range by interpolating the 0.2 ng/ml standard signal intensities. This interpolation assumes linear changes in the sensitivity of the Element. The mercury recovery yield for both NIST 2704 and NIST 1572 was very high (varying from 96% to a 100%) (**Table 1.4**). The same technique was applied to all samples for the current study. The vegetation and peat sample from Penido Vello bog was kept in a freezer and were not dried for chemistry. The quantity of sample leached varied from 1-30 g depending on the concentration of mercury and was adjusted in such a way that final concentration was approximately 1ng/ml.

1.2.2.3 Blank Validation

The total procedure blank for the cold leaching technique was measured by preparing solutions following the same leaching and dilution steps as the NIST 2704 and NIST 1572 standards. Four total procedure blank solutions (named as A, B, C and D) (**Table 1.5**) were prepared by mixing ultrapure concentrated HCl and 30% H_2O_2 in approximately 2:1 v/v in screw top120 ml PFA vessel (Savillex) beakers. The solutions were shaken for an hour on the C1 platform Shaker and ultrasonicated for 48 hours in a bath of high purity water. The total procedure blank solutions were then filtered by passing through a 0.2 um Millipore Polycarbonate membrane filter in the vacuum filtration system. The total procedure blank solutions were further diluted to various concentrations with 0.5M HCl (**Table 1.5**) to an approximate final volume of 5ml in ICP vials. For calibration purposes four Hg standards were prepared by serial dilution of 0.2 ng/ml to a final concentration of ~ 0.0 ng/ml (no Hg standard added, only 0.5 M HCl), 0.001 ng/ml, 0.002

ng/ml and 0.005 ng/ml with 0.5M HCl and linear regression analysis on the calibration curve of the standards yielded a R^2=0.9962 (**Figure 1.3**). The total procedural blank including cold acid leaching of sample and vacuum filtration was approximately 211±115 pg (1 stdev, n=22) (**Figure 1.4, Table 1.5**).

1.2.3 Instrumentation

Mercury isotopic measurements were performed on a Thermo-Finnigan *Neptune* multicollector inductively coupled plasma mass spectrometer (MC- ICPMS) equipped with eight movable faraday cups and a fixed axial faraday collector. Elemental Hg vapor, formed by reacting sample solution with 2% $SnCl_2$, was introduced into the mass spectrometer by the CETAC HGX-200 Hydride Generation and Cold Vapor System (Klaue and Blum, 1999). The peristaltic pump speed was adjusted to 22 rpm which made the solution uptake rate 1.4 ml/min. The mercury solutions had a typical concentration of 1ppb (1ng/ml). In between samples the hydride generator system was washed with 1M HCl for 2-3 minutes until the mercury signal intensity returned to background level.

1.2.4 Measurement

For mercury isotope ratio measurements seven adjustable Faraday cups were used (**Table 1.6**). ^{204}Pb isobaric interference on ^{204}Hg was monitored at mass 206 (^{206}Pb). Operating conditions of the mass spectrometer are listed in **Table 1.7**. Data acquisition was done using 1 block of 50 cycles with an integration time of 8.418 seconds per cycle. A baseline measurement of 30 cycles (total time of 90 seconds) was performed by defocusing the ion beam at the beginning of each measurement. Peak centering was performed at the beginning of the block. For maximum efficiency gain calibration of the amplifiers associated with Faraday collectors were done on a daily basis. The method used for data acquisition took a total time of 510 seconds. Raw isotope ratios ^{198}Hg/^{202}Hg, ^{199}Hg/^{202}Hg, ^{200}Hg/^{202}Hg, ^{201}Hg/^{202}Hg and ^{204}Hg/^{202}Hg were calculated from baseline corrected signal intensities. Instrumental mass bias was determined to be about 3-4‰ based on replicate analyses of the NIST SRM 3133 solution. In order to minimize effects of instrumental fractionation, isotope ratios were determined by sample standard bracketing technique and reported in δ (‰) notation relative to NIST SRM 3133 Hg elemental standard.

$$\delta^{n}\mathrm{Hg}=\left[\frac{\left(\frac{^{n}\mathrm{Hg}}{^{202}\mathrm{Hg}}\right)_{\mathrm{sample}}}{\left(\frac{^{n}\mathrm{Hg}}{^{202}\mathrm{Hg}}\right)_{\mathrm{standard}}}-1\right]\times 1000\,‰ \qquad (1.1)$$

1.3 Results and Discussion

Instrument mass bias corrections can be achieved in several ways: a) internal correction using double isotope spiking where two isotopes of known ratio (gravimetric) are added to the sample b) external correction of sample standard bracketing and c) internal correction by measuring the isotopic composition of a different element added to the sample which has a similar mass. Several current reports have coupled the use of internal correction of thallium (mass very close

to mercury) addition to the sample with external sample standard bracketing for mass bias correction (Blum and Bergquist, 2007; Hintelmann and Lu, 2003; Foucher and Hintelmann, 2006; Ridley and Stetson, 2006; Smith et al., 2005). Mercury vapor is introduced and mixed with $TlNO_3$ of known $^{205}Tl/^{203}Tl$ isotopic composition to correct raw mercury isotope ratios. The usefulness of this particular approach to correct for mass discrimination is difficult to test because there is no mercury isotope standard available that has its isotopic ratio certified by any other technique than MC-ICP-MS. The current study has conducted all mass bias corrections externally by sample standard bracketing technique.

All absolute isotopic ratios are converted to per mil deviation (δ notation) with respect to the NIST SRM3133 Hg Standard. For mass dependent fractionation only one isotope ratio needs to be reported and the convention adopted in the present study was $^{198}Hg/^{202}Hg$. The intention was to put the highest atomic mass and major abundance isotope i.e. ^{202}Hg in the denominator and all other isotopes (^{198}Hg, ^{199}Hg, ^{200}Hg, ^{201}Hg and ^{204}Hg) in the numerator. Although ^{204}Hg (6.9%) has the highest mass among all the mercury isotope and would give the largest atomic mass difference (6 a.m.u instead of 4 a.m.u. now) but its abundance is low compared to ^{202}Hg (29.9%) and thus would magnify the error if put in the denominator. In addition, ^{204}Hg potentially suffers from isobaric interference with ^{204}Pb. A few publications have adopted the nomenclature of reporting mercury isotope ratios with ^{198}Hg as the denominator and all other isotopes as numerator (Blum and Bergquist, 2007; Foucher and Hintelmann, 2006; Kritee *et al*., 2007, Ridley and Stetson, 2006). The other researchers have focused on the fact that it is more important to be consistent with the δ nomenclature of commonly used isotopic systems. For instance, in the oxygen isotope system, $^{18}O/^{16}O$ variations are reported as $\delta^{18}O‰$ and sulfur isotope system, variations in $^{34}S/^{32}S$ are reported as $\delta^{34}S‰$ and so lighter isotope is always at the denominator. But in both cases of oxygen and sulfur, the lighter isotopes are the most abundant ones and have the highest precision which is certainly not the case in mercury. So, the current study will not follow the general convention of δ, firstly because the abundance of ^{198}Hg is 9.97%, again low compared to ^{202}Hg and second ^{198}Hg suffers from potential isobaric interference from ^{198}Pt (7%).To ensure that the instrumental fractionation followed the mass dependent fractionation law, some of the isotope ratios were plotted against Rayleigh mass dependent fractionation model (**Figure 1.5**).

Figure 1.6 shows the entire set of the $\delta\ ^{198}Hg/\ ^{202}Hg$ ‰ values of Almaden cinnabar after mass bias correction with sample standard bracketing technique. The total number of measurements is sixty (**Table 1.8**) and has been acquired during seven separate measurement sessions over a time period of four months (February 2007 to May 2007). The measurements show the long term consistency and analytical reproducibility of the δ measurements over time. There is absence of any systematic trend in the distribution of the corrected $\delta\ ^{198}Hg/\ ^{202}Hg$ ‰ values of the cinnabar over time (**Figure 1.6, Table 1.8**). Based on sixty measurements an average of 0.17 ‰ and a precision of 0.55 ‰ (external reproducibility, ± 2SD) is estimated for the $\delta\ ^{198}Hg/\ ^{202}Hg$ ‰ values of Almaden cinnabar solution (**Figure 1.6, Table 1.8**). Only a very few δ values (4-5) determined for the cinnabar are outside the ± 2SD confidence interval. The data set in **Figure 1.6** and **Table 1.8** implies that the current analytical technique is probably robust enough to measure meaningful and consistent δ values over longer periods of time.

In recent times several studies have explored the extent of mercury fractionation in natural materials like mercury ore minerals (primarily cinnabar), sediments and soil. Hintelmann and Lu, 2003, evaluated cinnabar samples of different ages and places from a wide variety of geological settings. Values of $\delta^{198}Hg/^{202}Hg$ varied from 0.0-1.33 ‰ relative to NIST SRM 1641d Hg standard. Their analysis of Almaden cinnabar showed a mean $\delta^{198}Hg/^{202}Hg$ ‰ of 1.13‰ (our mean $\delta^{198}Hg/^{202}Hg$ value of Almaden cinnabar is 0.17‰). The mercury isotopic variations relative to NIST 3133 Hg standard of two fossil hydrothermal systems from the National District and Ivanhoe district were studied by Smith *et al*. 2005. They grouped the mercury isotope variations of both the hydrothermal systems by dominant mineralogy and position; in the top of the systems dominated by cinnabar sinter $\delta^{202}Hg/^{198}Hg$ values varied from -3.5‰ to -0.4‰, -0.2‰ to +2.1‰ in metacinnabar dominated sinter, and the underlying veins had $\delta^{202}Hg/^{198}Hg$ values of -1.4‰ to +1.3‰ (Smith *et al*. 2005). The authors attributed the isotope differences to be a combined effect of redox and vaporization reactions (e.g. boiling of hydrothermal fluids). The extent of mercury fractionation in natural sediments and sediment cores has been investigated by several groups. The $\delta^{202}Hg/^{198}Hg$ variation analyzed in sediments from different locations in the world having various mercury sources are from +1‰ to -4 ‰ (Foucher and Hintelmann, 2006, relative to NIST SRM 1641d). Jackson *et al*. 2004 have examined the variations in isotopic composition of mercury in a historic Arctic lake sediment record from the Romulus Lake, Ellesmere Island, Canada. The age of the core varied from 1899 AD to 1997 AD. The core shows an overall $\delta^{198}Hg/^{202}Hg$ variation of approximately 2‰. The bottom of the core (around 1899 AD) shows higher value of approximately 3.00‰ whereas top of the core shows lower value of approximately 1.5‰ (Jackson *et al*. 2004).

The extent of mercury isotope fractionation has been investigated in this report and various samples containing mercury e.g. peat, vegetation, sediment standard and a shale standard have been analyzed (**Figure 1.7, Table 1.9**). The samples consisted of peat from Patagonia, peat and vegetation from Penido Vello peat bog in Spain as well as certified reference materials (NIST SRM 1646) and reference shale (NIST SGR-1). The measured solutions were diluted such that the final concentration was approximately 1 ng mL^{-1} and isotope ratios were determined as the average of 1 block with 50 ratios and an integration time of 8.418 seconds. The reported $\delta^{198}Hg/^{202}Hg$ ‰ is the mean of δ values from n runs, where n =50, or multiples of 50 for larger samples. The internal precision of each analysis was calculated as the 2 SE of the mean of n runs, where n = 50, or multiples of 50 for larger samples. The total amount of mercury needed in the method is approximately 10 nanograms which is very low compared to all previous reports (Jackson *et al*., 2004; Foucher and Hintelmann, 2006; Smith *et al*., 2005). Foucher and Hintelmann, 2006 used approximately a total of 50 nanogram of mercury to analyze sediment samples with a typical ±1SD external reproducibility varying from 0.035‰ to 0.275‰ and Jackson *et al*., 2004 had an Hg content adjusted between 3-5 ng/ml in analyzing their sediment core. Cinnabar samples analyzed by Smith *et al*., 2005 had a concentration approximately 40 ng/ml and the typical external precision for the δ values was 0.1‰ (2σ). Using a total amount of mercury varying between 15 ng- 60 ng in cinnabar samples, Hintelmann and Lu, 2003 obtained an external precision (±1SD) of 0.06‰ – 0.26‰. Although such a low mass of Hg is used in this study, the degree of external precision obtained is quite acceptable for a MC-ICPMS analysis. The observed δ values for the $^{198}Hg/^{202}Hg$ ratio extends from +0.08 to +4.06 ‰. The external uncertainty (±2SE) of the measurements is estimated between ±0.02 and ±0.15 ‰. The validity and reproducibility of the measurements for the environmental samples are confirmed by

analyses of samples for which the entire chemical procedure was repeated three times indicated by PVO 0-2: A, B and C, Patagonia Peat:1, 2 and 3 and NIST SRM 1646 Estuarine sediment: A, B and C. The $\delta\ ^{198}Hg/\ ^{202}Hg$ ‰ values of PVO 0-2 A, B and C agree within 0.1‰ of each other; Patagonia peat-1, 2 and 3 show a maximum scattering of 0.13‰ and NIST SRM 1646 Estuarine sediment: A, B and C match within 0.1‰ of each other. This confirms the fact that: i) leaching chemistry has not induced any mass discrimination effect in mercury isotopes and ii) the recovery yield of mercury from the peat samples with the leaching technique is probably close to a 100%. The degree of fractionation observed up to 4.06‰ in Sample Vegetation and 0.08‰ in NIST SGR-1, Green River Shale is larger in magnitude than the external uncertainties determined. The measurements demonstrate the fact that the current method is able to detect significant differences in mercury isotope ratios that occur within both similar and different types of samples.

Mercury is a very volatile element. Mass fractionation might be easily induced during sample preparation through processes like freeze drying, high temperature digestion and heating. In previous studies none of the researchers have taken into account of mass discrimination effects in their sample preparation techniques nor have they quantified their mercury recovery yield (Jackson *et al*., 2004; Foucher and Hintelmann, 2006). Sediments and soil usually were dried before digestion chemistry. During the process of digestion the samples were subjected to very high temperatures. Both of these processes could easily introduce matrix induced mass fractionation. To demonstrate this effect an experiment was conducted where a peat sample, PVO 6-8 cm was dried for a week at two different temperatures of 35 ºC and 90 ºC and subjected to the same type of extraction chemistry as the wet sample. When analyzed for mercury isotopes the dried samples showed a significant isotopic difference compared to the wet sample (**Figure 1.8, Table 1.10**). The error bars represent external reproducibility (±2SD) based on replicate analysis (6 times) of the sample aliquots. The $\delta\ ^{198}Hg/\ ^{202}Hg$ (5.66 ‰, ± 0.40‰) for PVO 6-8 cm in wet condition (denoted as 0 ºC, since sample was kept in freezer) show a depleted signature when dried at 35 ºC (2.09 ‰, ±0.44 ‰). This signature is expected to be a function of mass dependent isotope partitioning; the lighter isotopes would preferentially evaporate and heavier isotopes would be more refractory. The degree of isotope fractionation observed is larger than the external precision estimated in both the samples (**Figure 1.8, Table 1.10**). When heated at 90 ºC, the $\delta\ ^{198}Hg/\ ^{202}Hg$ shows an insignificant change compared to 35 ºC but lower than 0 ºC and has an external uncertainty (1.73 ‰, ± 0.26 ‰).

In recent times, the recognition that mercury displays both mass independent fractionation (MIF) and mass-dependent fractionation (MDF) in natural systems requires additional nomenclature. Schauble, 2007 has made estimations of equilibrium $^{198}Hg/^{202}Hg$ separation factors for a number of mercury species relative to Hg^0 vapor. He showed that the nuclear field shift (due to changes in nuclear volume) is far more significant than zero-point energy differences (vibrational frequency) in effecting isotopic separation. Although, nuclear radii are to first approximation a simple function of mass, in detail the nuclei of odd isotopes exhibit a smaller $\Delta r/A$ than the nuclei of the even isotopes so that the nuclear field shift deviates from mass-dependent isotope fractionation (Schauble, 2007). For mercury isotopes, Buchachenko et al., 2004, 2007 demonstrated a mass independent magnetic isotope effect in the thermal reaction between creatine kinase with methylmercury chloride (CH_3HgCl) and photochemical decomposition of an organomercury compound. Such effects are expressed in the odd-A Hg isotopes (^{199}Hg: -1/2,

^{201}Hg: -3/2), due to their non-zero nuclear spin, relative to the even-A Hg isotopes (^{198}Hg, ^{200}Hg, ^{202}Hg, ^{204}Hg). Deviations from mass-dependent fractionation were calculated as:

$$\Delta^{A}Hg = \delta^{A}Hg_{measured} - \delta^{A}Hg_{MD} \quad (1.2)$$

The value Δ^{199}Hg and Δ^{201}Hg is defined as the difference between the measured δ^{199}Hg and δ^{201}Hg ($\delta^{A}Hg_{measured}$) of a sample and the δ^{199}Hg and δ^{201}Hg ($\delta^{A}Hg_{MD}$) obtained from the linear scaling defined by the even-mass isotopes. Linear and exponential mass bias correction laws yield Δ^{199}Hg and Δ^{201}Hg values within the uncertainty of our analyses (~±0.1‰). In this paper, the linear scaling factors are derived by least squares fitting of the δ values of the even A isotopes. From the Δ^{199}Hg and Δ^{201}Hg values calculated for the NIST SRM 3133 Hg standard and Almaden cinnabar we infer that the external precision of our Hg measurements is better than 0.1‰ (2σ) for both Δ^{199}Hg and Δ^{201}Hg (**Figure 1.9a and 1.9b**). No routine trend is observed in the distribution of the Δ^{199}Hg and Δ^{201}Hg ‰ values of the NIST and cinnabar (**Fig. 1.9a and 1b**). Since mercury is introduced to the plasma in the elemental vapor form (Hg^0), no matrix effects are expected.

1.4 Conclusions

The mercury extraction chemistry developed in this study for various kinds of environmental samples (peat, vegetation, soil and shale) has a very high recovery yield (96% -100%) and also there is no noticeable isotope fractionation effect induced during the leaching chemistry. Previous reports had not considered induced mass fractionation effects through processes like heating and drying during sample preparation chemistry. This report demonstrates that drying and heating of samples can significantly fractionate mercury isotopes. The method detailed here represents a robust and reliable way to determine accurate and precise mercury isotope ratios of natural samples using MC-ICPMS. The measurements demonstrate the method is capable in distinguishing significant variations in mercury isotope ratios that exists within similar kind of samples for e.g., between different peats. Although the absolute mass of sample (10 ng of mercury) used in this study is very low compared to previous reports, the external precision obtained is acceptable for a typical MC-ICPMS analysis. The study also reports mass independent fractionation and both δ and Δ values of Almaden cinnabar with respect to NIST SRM 3133 Hg standard. With this new approach stable isotope studies of mercury can now be applied to very low mercury level in aquatic, snow, biological and atmospheric samples.

Table 1.1 Sequence for the testing of Hg recovery yield in cold acid leaching process by ICPMS

System_Blank_001
Hg_Standard_100ppt_002
Hg_Standard_200ppt_003
Hg_Standard_400ppt_004
Hg_Standard_500ppt_005
System_Blank_006
Hg_Standard_200ppt_007
NIST 1572_0.3713gms_008
NIST 1572_0.3713gms_009
Hg_Standard_200ppt_010
NIST 1572_0.317gms_011
System_Blank_012
Hg_Standard_200ppt_013
NIST 2704_0.1790gms_014
NIST 2704_0.1790gms_015
NIST 2704_0.158gms_016
Hg_Standard_200ppt_017
System_Blank_018
NIST 2704_0.185gms_019
NIST 2704_0.185gms_020
Hg_Standard_200ppt_021
NIST 2704_0.185gms_022
System_Blank_023
Hg_Standard_200ppt_024
System_Blank_025

System blanks are solutions made of 1M HCl
NIST 2704 is the Buffalo River Sediment standard and NIST 1572 is the Citrus leaf standard

Table 1.2 ICPMS and Hydride generator run parameters

ICP-MS (*Element*)	
Plasma tune parameters	Values
Cool Gas (Ar)	13.00 L/min
Auxiliary Gas (Ar)	0.99 L/min
Sample Gas (Ar)	0.955 L/min
Additional Gas (Ar)	0.35 L/min
RF Power	1300 Watt
Peripum Speed	5.51 rpm
Cetac HGX-200 Hydride Generation and Cold Vapor System	
Solution uptake rate	1.1 ml/min
Sensitivity of ^{202}Hg vapor	$1*10^6$-$2*10^6$ cps for 0.2 ng/ml Hg

Table 1.3 Analytical Method to measure mercury concentration by ICPMS

Isotope	Mass Window	Settling Time (s)	Sample Time (s)	Samples per peak	Search Window	Integration Window	Runs/Passes
^{198}Hg	5	0.001	0.01	160	10	10	40/40
^{195}Pt	5	0.3	0.01	160	10	10	40/40
^{200}Hg	5	0.001	0.01	160	10	10	40/40
^{202}Hg	5	0.001	0.01	160	10	10	40/40
^{204}Hg	5	0.001	0.01	160	10	10	40/40
^{208}Pb	5	0.3	0.01	160	10	10	40/40

Table 1.4 Conditions and results for mercury cold acid leaching experiment

Hg Std.	Weight (grams)	Sample in Sequence	True mass of Hg (ngs)	Acid used for leaching (ml)		Total Solution Volume (ml)	Measured Conc. of Hg (ng/ml)	Measured Mass of Hg (ng)	Yield
				HCl	H_2O_2				
NIST 2704	0.179	NIST 2704_0.1790gms_015	250.60	20.01	10.06	30.07	8.13	244.54	98%
		NIST 2704_0.1790gms_016					8.08	242.86	97%
	0.158	NIST 2704_0.158gms_017	221.06	20.46	10.34	30.80	6.90	212.49	96%
	0.185	NIST 2704_0.185gms_020	259.00	20.74	10.02	30.76	8.19	251.91	97%
		NIST 2704_0.185gms_021					8.11	249.45	96%
		NIST 2704_0.185gms_022					8.22	252.83	98%
NIST 1572	0.371	NIST 1572_0.3713gms_008	29.70	20.09	10.15	30.24	0.95	28.62	96%
		NIST 1572_0.3713gms_009					0.98	29.64	100%
	0.317	NIST 1572_0.317gms_011	25.36	20.51	10.01	30.51	0.81	24.72	97%

Table 1.5 Total blank validations

Zero Blank Stock Solution	Acid used for leaching (ml)		Total Solution Volume (ml)	Zero Blank Diluted Solutions	Volume of Zero Blank solution used for dilution (ml)	Volume of 0.5 M HCl used for dilution (ml)
	HCl (ml)	H_2O_2 (ml)				
				A1	0.11	4.48
				A2	0.22	4.55
A	26.247	10.461	36.708	A3	0.44	4.38
				A4	0.66	4.25
				A5	0.88	4.13
				B1	0.11	4.10
				B2	0.23	4.57
B	22.366	16.275	38.641	B3	0.45	4.17
				B4	0.67	4.44
				B5	0.89	4.23
				C1	0.11	4.43
				C2	0.23	4.34
C	21.348	14.393	35.741	C3	0.45	4.37
				C4	0.66	4.44
				C5	0.86	4.53
				D1	0.10	4.18
				D2	0.22	4.23
D	24.092	10.664	34.756	D3	0.44	4.05
				D4	0.66	4.58
				D5	0.88	4.21
A	26.247	10.461	36.708	A-500	0.53	3.97
B	22.366	16.275	38.641	B-500	0.52	4.03
C	21.348	14.393	35.741	C-500	0.53	4.04
D	24.092	10.664	34.756	D-500	0.55	3.74

Table 1.5 continued

Zero Blank Diluted Solutions	Dilution factor	Measured Concentration (ppt)	Calculated Final Concentration (ppt)	Zero Blank Stock Solution	Calculated Total Hg (ρg) in Zero blank stock solutions
A1	41.5	0.20	8.25		303
A2	20.7	0.28	5.85		215
A3	10.0	0.42	4.17	A	153
A4	6.4	0.41	2.63		97
A5	4.7	0.60	2.81		103
B1	39.0	0.30	11.65		450
B2	20.1				
B3	9.3	0.51	4.72	B	182
B4	6.6	0.84	5.55		214
B5	4.7	0.70	3.30		127
C1	42.2	0.15	6.35		227
C2	19.3	0.35	6.81		243
C3	9.6	0.39	3.76	C	134
C4	6.7	0.61	4.08		146
C5	5.3	0.90	4.75		170
D1	41.8	0.42	17.59	D	611

Table 1.5 continued

Zero Blank Diluted Solutions	Dilution factor	Measured Concentration (ppt)	Calculated Final Concentration (ppt)	Zero Blank Stock Solution	Calculated Total Hg (ρg) in Zero blank stock solutions
D2	19.7	0.40	7.87	D	273
D3	9.3	0.51	4.72		164
D4	7.0	0.81	5.62		195
D5	4.8	0.88	4.23		147
A-500	7.5	0.57	4.24	A	156
B-500	7.7	0.72	5.52	B	213
C-500	7.6	0.63	4.77	C	170
D-500	6.8	0.65	4.44	D	154

Table 1.6 Configuration of the Faraday Collectors for mercury isotope ratio measurements

Measurement	L4	L3	L2	L1	C	H1	H2	H3	H4
Hg & Pb	____	____	198	199	200	201	202	204	206

Table 1.7 Operating conditions of *Neptune* mass spectrometer and Hydride Generator

MC-ICPMS (*Neptune*)	
Plasma tune parameters	Values
Cool Gas (Ar)	15.00 L/min
Auxiliary Gas (Ar)	0.75-0.85 L/min
Sample Gas (Ar)	0.7-0.9 L/min
Additional Gas (Ar)	0.23 L/min
RF Power	1200 Watt
Peripum Speed	22 rpm
Cetac HGX-200 Hydride Generation and Cold Vapor System	
Solution uptake rate	1.418 ml/min
Sensitivity of ^{202}Hg vapor	600-700 (mV)/(ng/mL)
Background	8-10 mV

Table 1.8 $\delta\ ^{n}Hg / ^{202}Hg$ ‰ values of sixty replicate analyses of Almaden cinnabar solution relative to NIST SRM 3133 Hg Standard

Replicate No.	$\delta^{198}Hg/^{202}Hg$	$\delta^{199}Hg/^{202}Hg$	$\delta^{200}Hg/^{202}Hg$	$\delta^{201}Hg/^{202}Hg$	$\delta^{204}Hg/^{202}Hg$
1	0.70	0.46	0.34	0.10	-0.44
2	0.26	0.10	0.11	-0.02	-0.19
3	0.45	0.27	0.21	0.01	-0.28
4	0.56	0.30	0.24	0.09	-0.24
5	0.17	0.04	0.05	0.06	-0.01
6	0.43	0.25	0.21	0.06	-0.23
7	0.15	-0.05	0.03	-0.09	-0.09
8	0.18	0.05	0.09	-0.10	-0.05
9	-0.68	-0.59	-0.34	-0.28	0.41
10	0.08	-0.04	0.02	-0.08	-0.14
11	-0.04	-0.21	-0.09	-0.23	-0.08
12	-0.12	-0.19	-0.07	-0.14	0.03
13	0.28	0.28	0.15	-0.05	-0.10
14	0.14	-0.01	0.03	-0.10	-0.01
15	0.18	-0.01	-0.01	-0.13	-0.14
16	0.71	0.49	0.37	0.07	-0.26
17	0.07	-0.04	-0.02	-0.06	-0.03
18	0.15	0.06	0.02	0.00	0.08
19	0.28	0.18	0.15	0.09	0.05
20	0.41	0.16	0.16	0.06	-0.13
21	0.36	0.21	0.13	0.06	-0.02
22	0.53	0.26	0.24	0.06	-0.22
23	0.16	0.07	0.10	0.03	-0.11
24	-0.02	-0.06	-0.02	-0.12	-0.14
25	0.28	0.11	0.13	0.05	-0.26
26	0.48	0.26	0.22	0.04	-0.21
27	0.05	-0.01	0.04	-0.13	0.07
28	0.92	0.57	0.40	0.17	-0.28
29	-0.25	-0.28	-0.12	-0.16	0.17
30	0.23	0.07	0.11	-0.09	-0.13
31	0.01	-0.22	-0.02	-0.15	-0.06
32	0.21	-0.02	0.07	-0.07	0.00
33	-0.08	-0.18	-0.08	-0.17	0.02
34	0.00	0.00	0.01	-0.06	0.10
35	-0.45	-0.34	-0.24	-0.15	0.09
36	-0.27	-0.24	-0.14	-0.12	0.06
37	-0.03	-0.04	-0.03	-0.03	0.04
38	0.22	-0.01	0.03	-0.05	-0.08
39	0.07	-0.07	-0.02	-0.17	-0.09

Table 1.8 continued

Replicate No.	$\delta^{198}Hg/^{202}Hg$	$\delta^{199}Hg/^{202}Hg$	$\delta^{200}Hg/^{202}Hg$	$\delta^{201}Hg/^{202}Hg$	$\delta^{204}Hg/^{202}Hg$
40	0.07	-0.03	0.02	-0.11	0.00
41	0.30	0.16	0.21	0.08	-0.13
42	0.16	0.06	0.06	0.03	-0.03
43	0.15	0.08	0.08	-0.02	-0.06
44	0.01	-0.05	0.01	-0.01	0.03
45	0.13	0.07	0.07	-0.05	-0.15
46	0.25	0.03	0.07	0.01	-0.05
47	0.27	0.07	0.10	-0.03	-0.10
48	0.09	-0.03	0.02	-0.04	-0.16
49	0.01	-0.11	-0.02	-0.04	0.04
50	0.06	0.02	0.04	-0.11	-0.12
51	0.24	0.17	0.16	0.01	-0.21
52	0.39	0.21	0.14	-0.01	-0.25
53	0.22	0.11	0.10	0.00	-0.10
54	0.31	0.20	0.17	0.03	-0.18
55	0.42	0.20	0.15	0.01	-0.11
56	0.27	0.15	0.15	-0.01	-0.16
57	-0.41	-0.29	-0.19	-0.08	0.26
58	-0.04	0.00	-0.01	0.40	0.02
59	0.18	0.14	0.10	0.07	-0.03
60	0.24	0.14	0.11	0.00	-0.13

	$\delta^{198}Hg/^{202}Hg$	$\delta^{199}Hg/^{202}Hg$	$\delta^{200}Hg/^{202}Hg$	$\delta^{201}Hg/^{202}Hg$	$\delta^{204}Hg/^{202}Hg$
Average	0.17	0.05	0.07	-0.03	-0.08
2 SD	0.54	0.40	0.27	0.21	0.28

Table 1.9 δ ^{n}Hg / ^{202}Hg ‰ values for different peat, vegetation, shale and sediment samples relative to NIST SRM 3133 Hg Standard

Sample	ID	δ ^{198}Hg/^{202}Hg	
		Average	2SE
Vegetation	1	4.06	0.04
PVO 0-2A	2	4.02	0.04
PVO 0-2B	3	3.97	0.02
PVO 0-2C	4	3.92	0.04
Patagonia Peat1	5	1.13	0.02
Patagonia Peat2	6	1.15	0.08
Patagonia Peat3	7	1.26	0.08
NIST SRM 1646, Estuarine SedimentA	8	2.36	0.07
NIST SRM 1646, Estuarine SedimentB	9	2.26	0.15
NIST SRM 1646, Estuarine SedimentC	10	2.26	0.14
NIST SGR-1, Green River Shale	11	0.08	0.04

Data acquisition was done in 1 block, 50 cycles with an integration time of 8.418 seconds per cycle. The internal precision of each measurement was calculated as the 2SE of the mean of n runs, where n=50, or multiples of 50 for larger samples

Table 1.10 δ ^{n}Hg/^{202}Hg ‰ values for a peat sample PVO 6-8 cm analyzed wet and dried relative to NIST SRM 3133 Hg standard

T (ºC)	δ^{198}Hg / ^{202}Hg		δ^{199}Hg / ^{202}Hg		δ^{200}Hg / ^{202}Hg		δ^{201}Hg / ^{202}Hg		δ^{204}Hg / ^{202}Hg	
	Average	2SD	Average	2SD	Average	2SD	Average	2SD	Average	2SD
0	5.66	0.40	4.07	0.32	2.81	0.24	1.17	0.24	-2.74	0.38
35	2.09	0.44	1.21	0.34	1.04	0.21	0.15	0.15	-1.05	0.16
90	1.73	0.26	0.92	0.19	0.87	0.10	0.08	0.07	-0.84	0.21

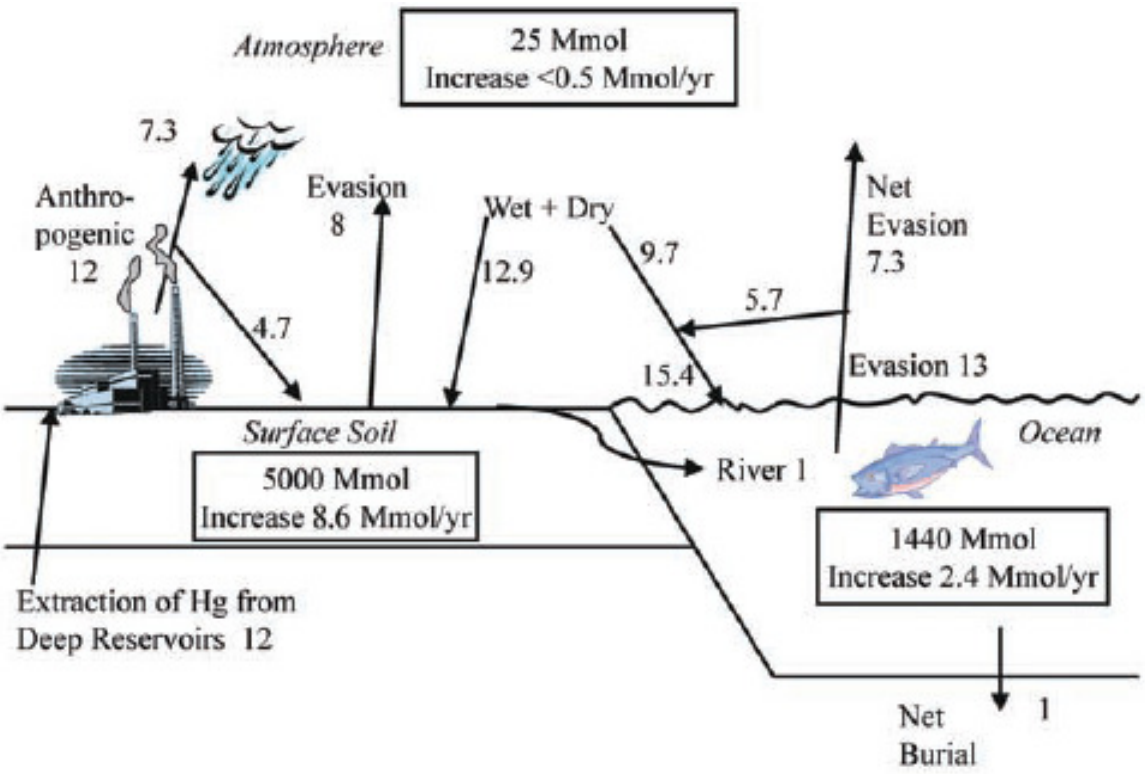

Figure 1.1 The current global mercury cycle adapted from Mason and Sheu, 2002. All fluxes are in Mmol yr^{-1}.

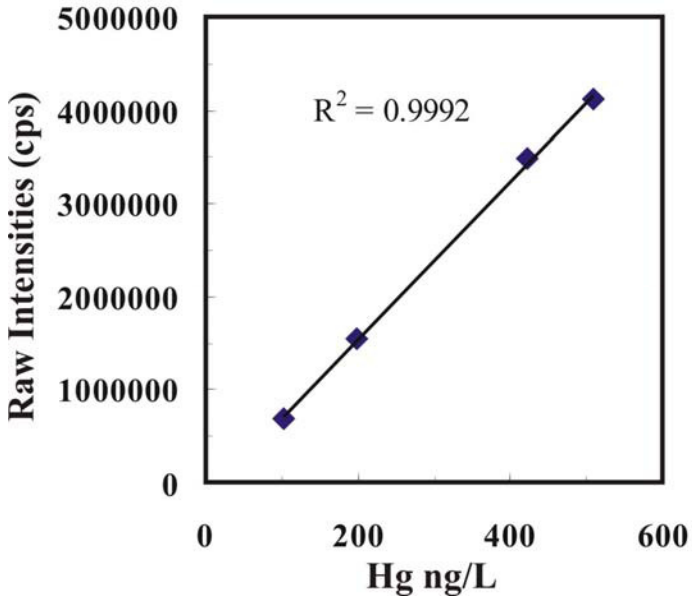

Figure 1.2 Standard calibration curve and linear regression analysis on mercury standards used for measuring the total mercury recovery yield by the cold acid leaching technique.

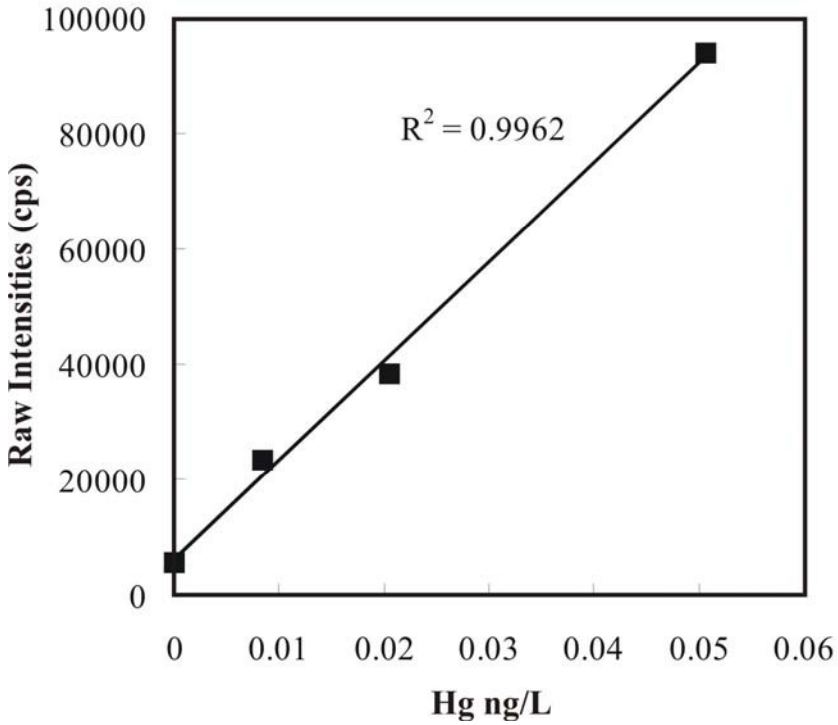

Figure 1.3 Standard calibration curve and linear regression on mercury standards prepared for blank validation.

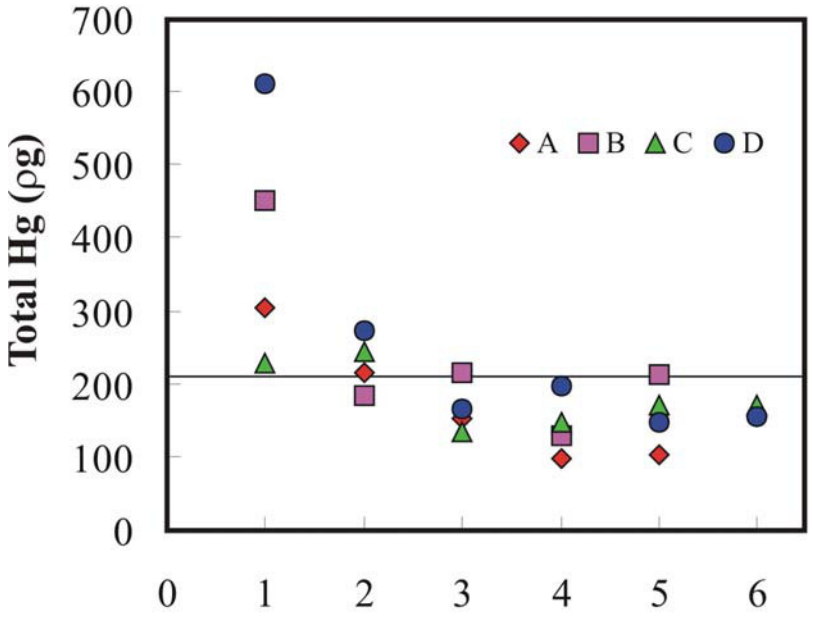

Figure 1.4 Total mercury blank concentrations in total procedure blank solutions. See **Table** 1.5 and text for the description of solutions A, B, C and D.

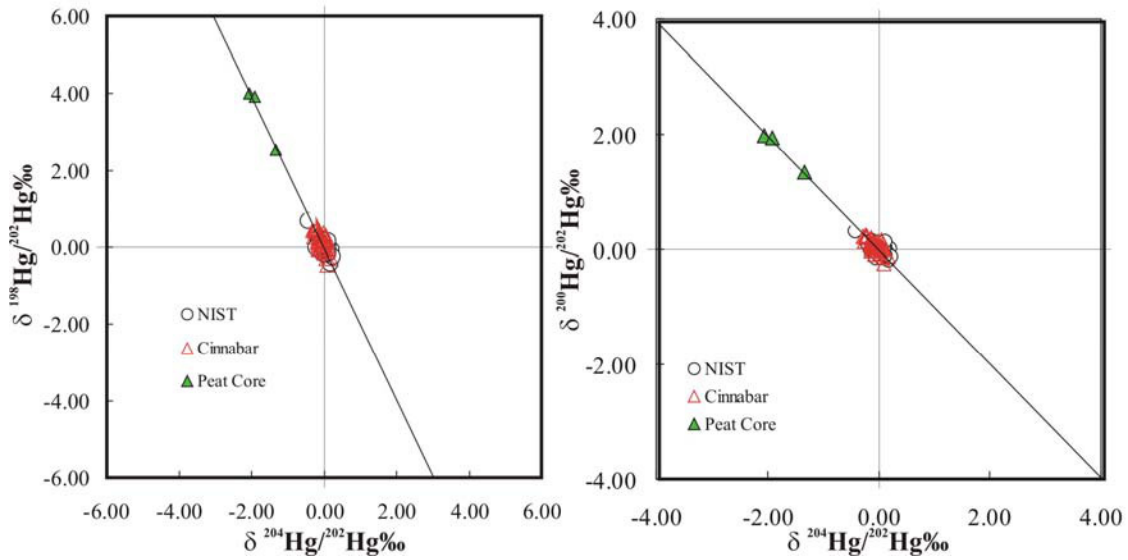

Figure 1.5 Mass dependence of fractionation. **a)** $\delta^{198}Hg / {}^{202}Hg$ vs. $\delta^{204}Hg / {}^{202}Hg$ **b)** g **c)** $\delta^{200}Hg / {}^{202}Hg$ vs. $\delta^{204}Hg / {}^{202}Hg$ for the NIST SRM3133 standard, Almaden cinnabar and some peat samples analyzed in the present study. The line is the calculated mass dependent fractionation line based on Rayleigh distillation model.

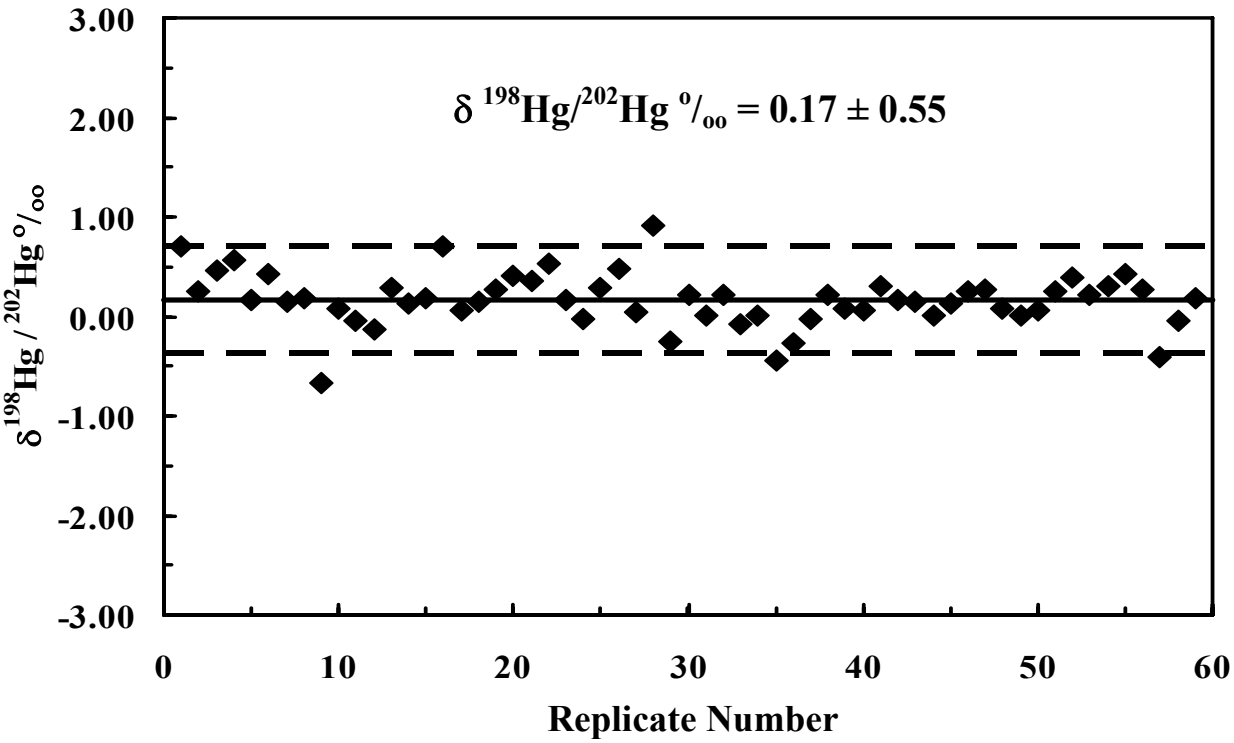

Figure 1.6 $\delta^{198}Hg/ {}^{202}Hg$ (‰) values relative to NIST SRM 3133 Hg Standard of Almaden cinnabar as a function of replicate measurements. The bold line and the dashed lines above and below represent the average and the ± 2SD interval determined from all 60 replicate measurements respectively

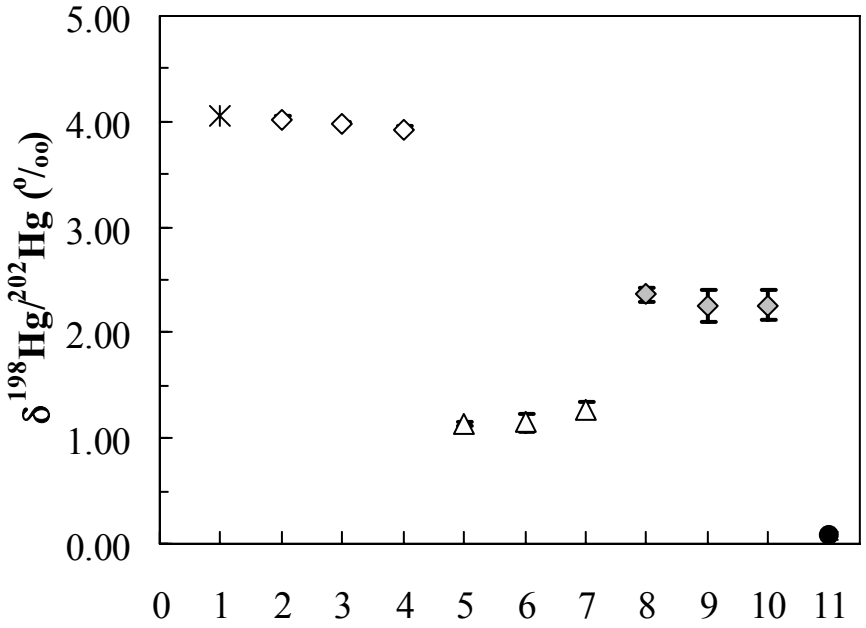

Figure 1.7 δ ^{198}Hg/ ^{202}Hg (‰) values relative to NIST SRM 3133 Hg standard of different peat, vegetation, shale and sediment samples**.** *Error bars* represent ±2SE on mean. See Table 1.9 for Sample IDs and descriptions.

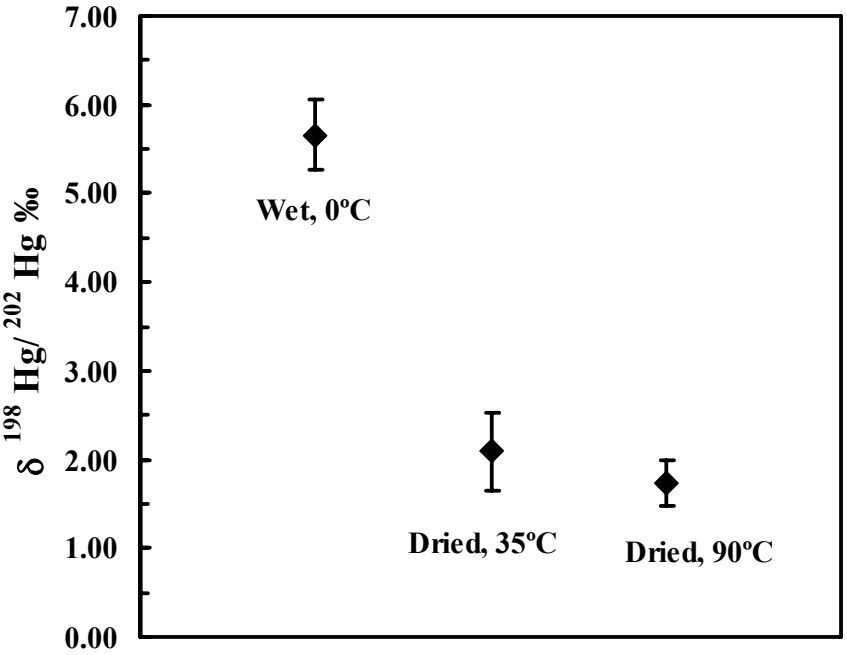

Figure 1.8 δ ^{198}Hg/ ^{202}Hg (‰) values relative to NIST SRM 3133 Hg standard of peat sample PVO 6-8 cm**.** *Error bars* represent ±2SD observed among replicate analysis of sample aliquots. The mercury extraction chemistry was applied on wet (0 ºC) and two dried specimens (35 ºC and 90 ºC) of sample PVO 6-8 cm.

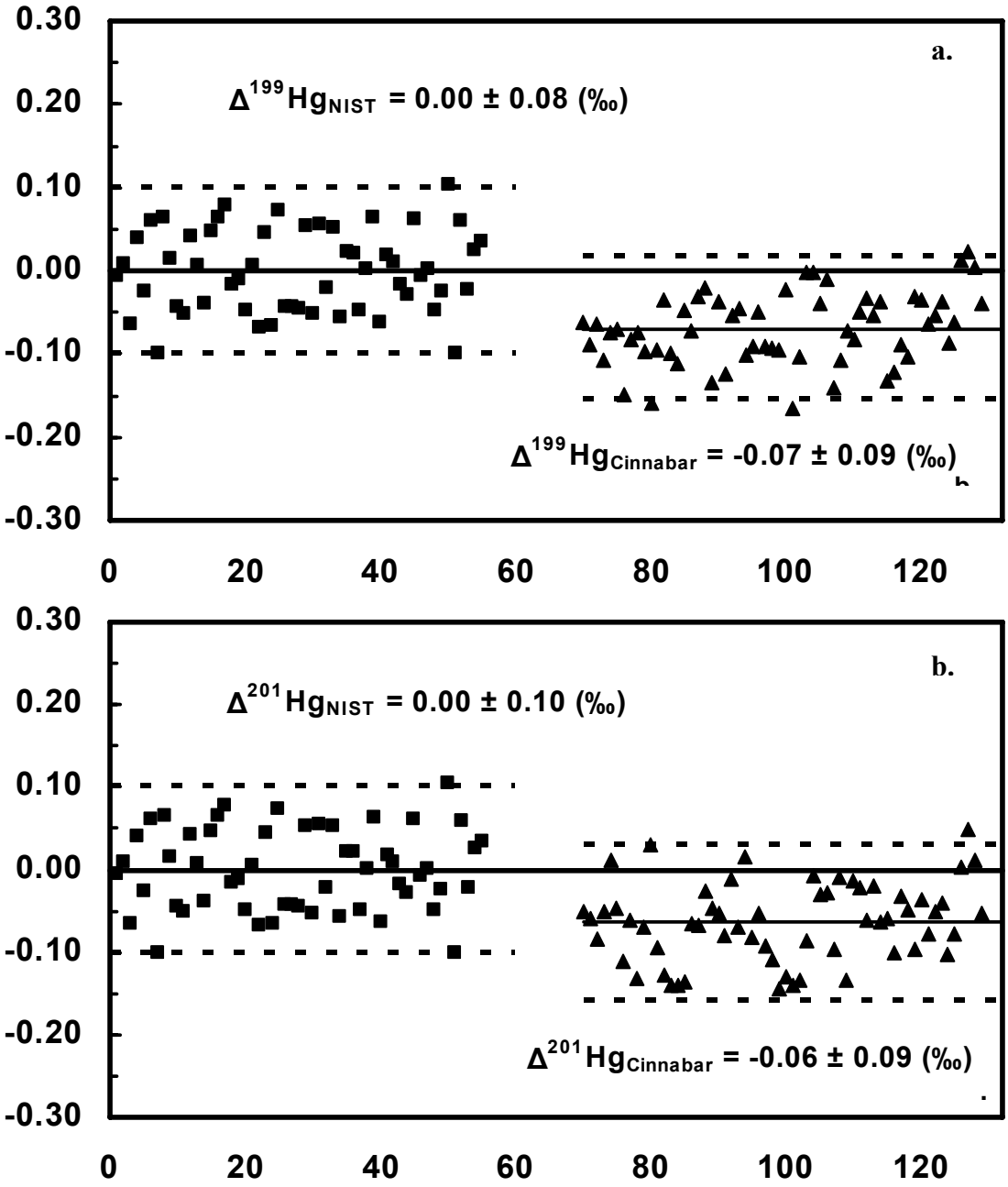

Figure 1.9 Long term reproducibility for Hg isotope ratios determined at NHMFL by MC-ICP-MS: a) Δ^{199}Hg (‰) for 55 replicate measurements of Hg from NIST SRM 3133 (1 ng mL^{-1}), and 60 replicate measurements of Hg from Almaden cinnabar (1 ng mL^{-1}), representing four months of data collection, and b) the same as in (a) for Δ^{201}Hg (‰). The bold lines represent the estimated average and the dashed lines represent the ± 2σ uncertainty.

CHAPTER 2

APPLICATION OF MERCURY AND OXYGEN ISOTOPES ON AN OMBROTROPHIC PEAT BOG OF PENIDO VELLO IN NORTHWESTERN SPAIN

2.1 Introduction

2.1.1 General

Ombrotrophic bogs are peatlands in which the only form of water supply is meteoric precipitation is. The advantage of ombrotrophic peat records over any sediment or soil cores is that they receive their nutrients and trace elements exclusively from the atmosphere via wet and dry precipitation and show no groundwater effects (Weiss *et al*., 1999). Also, as opposed to glaciers and ice cores, if precipitation is sufficient enough peat bogs usually form nearly at all latitudes. Pre and/or post industrial atmospheric deposition of metals has often been investigated in ombrotrophic peat bogs (Biester *et al*., 2003; Cortizas *et al*., 1997, 1999; Oldfield *et al*., 1981; Shotyk *et al*., 1990; Shotyk *et al*., 1998). Interpretations of temporal trace element records are usually based on changes in accumulation rates and concentrations.

Mercury Hg (II) has an extremely strong affinity for humic matter. Mercury forms stable organic complexes with humic acid fractions by being preferentially attached to reduced sulfur groups (Xia *et al*., 1999; Yudovich and Ketris 2005). Mercury, when deposited from the atmosphere (in both wet and dry forms) is absorbed onto the surface layer of organic matter and retained in the peat layers as the bog continues to grow vertically, producing a record of changes in atmospheric deposition over time. Ombrotrophic peat core records have often been used to evaluate historical records of atmospheric mercury (Hg) deposition (Benoit *et al*., 1998; Biester *et al*., 2002; Bindler 2002; Madsen 1981; Cortizas *et al*., 1999; Roos-Barraclough *et al*., 2002; Shotyk *et al*., 2003; Steinnes and Andersson 1991). The major aims of these investigations had been to estimate the increase in atmospheric mercury flux during the modern period compared to preindustrial natural times; to study the global cycle of mercury and to quantify the effect of natural mercury background and anthropogenic emissions on mercury deposition.

2.1.2 Mercury

Cortizas, *et al,* (1999), investigated a peat core from the ombrotrophic bog of Penido Vello, Spain for net accumulation of atmospheric mercury since 4000 BP. Total mercury was measured in a 2.5 m peat core sampled at 2 cm intervals in the upper 1 m and 5 cm intervals below that depth. Based on mercury desorption studies by pyrolysis (Biester and Scholz, 1997) they concluded that the mercury with low thermal stability was probably represented exclusively by elemental mercury, and mercury with high thermal stability was represented by mercury chlorides and organic mercury complexes (Cortizas *et al*., 1999). The record separated out into anthropogenic and natural components of mercury with the substantial anthropogenic mercury component beginning 2500 BP by the onset of Celtic mercury mining of Almaden mines, Spain. Anthropogenic mercury had been predominant in the deposition record through all the major mining periods (Roman, Germanic, Islamic, Christian and Modern). Moreover, Cortizas, *et al*.

(1999) observed that during cold climates there was an enhanced preservation and accumulation of mercury species which have low thermal stability and during warm climates there was lower accumulation and predominance of mercury species which have moderate to high thermal stability. Based on this thermal stability of the accumulated mercury they built a paleotemperature index (Cortizas *et al*., 1999). Positive values of the index represented periods which have higher temperature and negative values represented periods which have lower temperature. Their record showed that Neoglacial Period and Little Ice Age were the prominent cold periods; and Roman Warm Period and Medieval Warm Period were the most prominent warm periods of northwestern Spain.

Mercury shows a cold condensation effect quite comparable to that of some organic chemicals like hexachlorocyclohexane (HCHs) and hexachlorobenzene (HCB). Based on simple thermodynamic principles, Mackay, *et al*. (1995) developed a mercury flux model for an atmosphere – lake water ecosystem. The model showed a temperature dependence of mercury depositional fluxes. The net annual depositional flux of mercury from atmosphere to lake was three times greater at 0 ºC than at 25 ºC, although the total concentration of mercury in the atmosphere remained the same. As a result there is enhanced concentration of mercury in condensed media like water, soil and biota at colder temperatures. Isotopic fractionation factors are also temperature dependent. In general, the isotope fractionation factor for a particular reaction increases with decreasing temperature. So, it can be expected that the isotopic composition of mercury deposited from the atmosphere in the peat bog would be different in cold and warm periods. Also according to Mackay's model the depositional flux depends on the atmospheric concentration of mercury but the isotopic composition of deposited mercury is independent of the atmospheric concentration.

2.1.3 Oxygen isotopes

Cellulose is one of the predominant organic compounds present in plant tissues. The oxygen isotope composition of plant cellulose depends on three factors: a) cellulose-water biochemical fractionation factor (DeNiro and Epstein, 1981; Sternberg, *et al*., 1986a); b) the isotopic composition of meteoric water or source water that is used in the synthesis of cellulose (DeNiro and Cooper, 1989; Sternberg, *et al*., 1986a) and c) depletion of lighter isotopes in leaf water due to processes like evapotranspiration (Bricout, 1978; Dongman, *et al*., 1974; Gonfiantini, *et al*., 1965). The cellulose-water biochemical fractionation factor varies for different plant species and does not seem to depend on temperature at mid & high latitudes (DeNiro and Epstein, 1981; Sternberg *et al*., 1986a). Under steady state conditions, the leaf water enrichment is related to the oxygen isotope ratios of meteoric water, the oxygen isotope ratio of atmospheric water vapor and relative humidity (Allison *et al*., 1985; Bariac, *et al*., 1990; Dongman, *et al*., 1974). Since the oxygen isotopic composition of meteoric water is well correlated with temperature (Dansgard, 1964), significant correlation between temperature and oxygen isotope ratio of plant cellulose are observed (Burk and Stuiver, 1981; Edwards and Fritz, 1986; Switsur and Waterhouse, 1998). Previous studies have also reported the correlation between oxygen isotopes in plant cellulose and relative humidity (Burk and Stuiver, 1981; Edwards and Fritz, 1986; Lipp *et al*., 1996; Ramesh, *et al*., 1986). Accordingly models were developed based on the aforementioned empirical relationships to calculate the cellulose oxygen isotopic composition in terrestrial plants from the $\delta^{18}O$ values of meteoric or source water and leaf water (Aucour, *et al*., 1996; Burk and Stuiver, 1981; Edwards, *et al*., 1985).

$$\delta_c = (1-f)[\varepsilon^* + \varepsilon_k (1-h) + h\delta_a + (1-h)\delta_{sw}] + f\delta_{sw} + \varepsilon_b \quad (2.1)$$

where, δ_c, δ_{sw} and δ_a are the $\delta^{18}O$ values of cellulose, source water and atmospheric water vapor respectively. *f* is fraction of leaf water that undergoes evaporation (Allison, *et al*., 1985); *h* is the relative humidity of air; ε^* is the equilibrium fractionation factor between water vapor and liquid (Baertschi, et al., 1969), ε_k is the kinetic fractionation factor between water vapor and liquid and ε_b is the biological fractionation factor (De Niro and Epstein, 1979; De Niro and Epstein, 1981; Sternberg, 1989). The term (1-f) in the equation attempts to address the issue that not all the water in the leaf is subjected to evaporation and also the evaporation will vary depending on the plant type (Buhay, et al., 1996). The values of ε^*, ε_k and δ_a are dependent on temperature and humidity. Therefore, by studying the oxygen isotope composition of fossil cellulose, this model can probably be applied to interpret past changes in hydrological cycle (Aucour, et al., 1996; Brenninkmeijer, et al., 1982; Edwards, et al., 1985). The δ_a is the mean annual δ value of the water vapor and is calculated by following the assumption that in Europe, the water vapor is in the atmosphere is in isotopic equilibrium with the annual precipitation, i.e., $\delta_a = \delta_{sw} - \varepsilon^*$, (Förstel and Hutzen, 1983; Ménot-Combes et al., 2002). Equation 1 can be then rewritten as:

$$\delta_c = \delta_{sw} + (1-h)(1-f)[\varepsilon^* + \varepsilon_k] + \varepsilon_b \quad (2.2)$$

The present study therefore, included $\delta^{18}O$ measurements of the peat core to correlate with δ Hg values.

2.1.4 Purpose of the study

The subject of the present study is a peat core collected from the Penido Vello ombrotrophic bog of Spain. The core is 1 m long, and radiocarbon dating on bulk peat cellulose indicates the age of the bottom of the core to be 2183 BP. The first objective is to determine if modern atmospheric mercury, dominated by anthropogenic input, can be distinguished isotopically from natural atmospheric mercury deposited throughout a long pre-industrial period. The various factors controlling mercury output from sources such as marine emissions, biomass burning, degassing from mineralized areas and the variability of volcanic emissions, had made it difficult to quantify the amount of mercury released naturally. Previous attempts based on mercury fluxes to separate the natural mercury background and anthropogenic fractions of the oceanic and atmospheric pools involve considerable uncertainties. However, isotopes as a fingerprinting tool on long-term records of metal deposited from atmosphere such as the peat bog core in the current study might enable us to distinguish different sources of mercury to the atmosphere. Also it might allow us to compare preindustrial with modern industrial atmospheric mercury deposition rates and therefore quantify the effect of natural vs. anthropogenic emissions on mercury deposition. The bottom ~20 cm of the peat core mostly represents mercury from pre-industrial times with natural sources dominating whereas the top ~20 cm of the core represents predominantly industrial mercury. The second objective is based on the historic mercury deposition record by *Cortizas et al*. (1999) and cold condensation effect of mercury modeled by Mackay *et al*. (1995). If any temperature and/or humidity effect on isotopic composition of the atmospheric mercury is recorded in the peat core then mercury isotopes could potentially be used as a tool for quantitative palaeoclimate reconstruction.

In addition, stable oxygen isotope studies on bulk cellulose have also been conducted. The $\delta^{18}O$ values of bulk peat cellulose from the core should provide proxy data on climatic parameters such as palaeohumidity in Northwestern Spain during the last 2200 years. The $\delta^{18}O$ values of

modern cellulose data should document the present relationship between the $\delta^{18}O$ values of plant cellulose, probably the $\delta^{18}O$ values of the meteoric precipitation used by the plants and the relative humidity of the air. Data for oxygen isotope of present day precipitation is available for Northwestern Spain from IAEA/GNIP stations. Investigation of modern plants would thus test the applicability of the above mentioned mechanistic model by Burk and Stuiver, (1981), Edwards, *et al*.(1985), and Aucour, *et al*. (1996) in the case of Penido Vello peat bog. The $\delta^{18}O$ values of fossil cellulose from the core should provide proxy data on climatic parameters such as palaeohumidity. The palaeoclimate information obtained by studying oxygen isotopes and mercury isotopes (if such an effect is recorded for Hg isotopes) would be a good test to see if it confirms with the paleotemperature index of Cortizas, *et al*. (1999).

2.2 Study Area

The northwestern Iberian Peninsula is a mid-latitude area of transitional climates varying from continental to oceanic (coastal mountains, coastal regions and western and northern sides of the interior Cantabrian- Atlantic mountains) and also influenced by Submediterranean environments. The climate with the aid of acidic (pH<5) lithological substrata produced a suitable environment for the development of peatlands (Ramil-Rego *et al.*, 1996a). The peatland is part of an extensive area where blanket bogs developed during the Holocene. The Penido Vello bog, ombrotrophic in nature, is located in the Sierras Septentrionales of Galicia, northwestern Spain. The Penido Vello bog is at 700 m above sea level on a summit. The bog overlies on weathered granite rock or periglacial stoney deposits (Cortizas, *et al*., 1997). One of the peat cores at Penido Vello was sampled to a depth of 100 cm for the present study (adjacent to core sampled by Cortizas *et al*., 1997). **(Figure 2.1).**

The mean annual temperature in the area ranges from 10°C-7.5°C and annual precipitation from 1350-1700 mm. There is an intense north-south gradient of decreasing temperature and increasing precipitation with altitude (Cortizas, *et al*., 1997). The present day vegetation in the bog area is mainly *Spaghnum papilosum*, *Eriophorum angustifolium*, *Morina caerulea* and *Carex duriei* as well as some sporadic heathers *Erica mackaiana* and *Calluna vulgaris* (Ramil, *et al*., 1996).

The total depth of the peat in the bog is approximately 3.5 m. Previous radiocarbon date indicate total 4000 years of peat accumulation (Cortizas, *et al*., 1997). The bog was sampled to a depth of 1 m for the purpose of the present study. A total of five radiocarbon dates were obtained for the peat core. Bulk cellulose extracted from different sections of the peat core was sent to National Ocean Science AMS facility at WHOI for radiocarbon analysis **(Table 2.1).** The peat is composed mainly of *Sphagnum* and *Eriophorum* residues (*Cortizas et al*., 1997). The organic carbon content is high varying from 45% to 58% (*Cortizas et al*., 1997).

2.3 Materials and Methods

The peat was sampled by cutting cores of 25 × 25 × 25 cm with a serrated stainless steel knife, to a depth of 100 cm. The fresh core were then sliced into 2 cm slices and wrapped in plastic bags and shipped to the NHMFL laboratory from Spain. The samples were then kept in a freezer.

For the purpose of oxygen isotope study, subsampling was done for every 2 cm interval. The peat samples are dried at a temperature of approximately 60°C. The cellulose extraction procedure is based on Green (1963) but adapted from Epstein *et al*. (1977). The dried samples undergo Soxhlet extraction to remove the resin and lipid fractions by using three different organic solvents: first a mixture of benzene and methanol (1:1), second a pure acetone solution and finally de-ionized water. With a solution of $NaClO_2$ mixed with acetic acid at 70°C, the lignin fraction is removed next. This 'bleaching' step is repeated multiple times until the sample color turns white completely. Samples are then washed with de-ionized water until the pH of the rinsing solution turns neutral. At this point, samples consist of only hemicellulose. With a 17% NaOH solution the hemicellulose fraction is extracted. After washing the samples in de-ionized water, the residual tissue is incubated in 10% acetic acid. As a final step, α-cellulose is rinsed for several days with de-ionized water and then dried at 60°C.

$\delta^{18}O$ values in hemicellulose were determined by an on-line continuous flow method. Approximately 500 µg of sample was used for analysis. Sample was pyrolyzed in the Thermo Finnigan High Temperature Elemental Analyzer TC/EA. The gases after pyrolization were separated by passing them through a GC column in the carrier gas helium. The oxygen isotopic composition of CO was measured with a Thermo Finnigan Delta Plus XP stable isotope ratio mass spectrometer. All measurements were calibrated using three different laboratory standards analyzed with each batch of samples: two benzoic acid standards obtained from IAEA (IAEA-601: $\delta^{18}O$ value 23.3‰, IAEA-602: $\delta^{18}O$ value 71.4‰) and a potassium phosphate standard (Karen-Low, $\delta^{18}O$ value 8.92 ± 0.32 ‰). The results are reported in standard δ notation as:

$$\delta^{18}O_{sample} = \left[\frac{\left(\frac{^{18}O}{^{16}O} \right)_{sample}}{\left(\frac{^{18}O}{^{16}O} \right)_{VSMOW}} - 1 \right] \times 1000 \text{‰} \qquad (2.3)$$

For mercury isotope sample preparation a cold acid leaching technique was applied to the peat in the current study. The peat samples were not dried and leaching chemistry was applied at room temperature. A mixture of ultrapure concentrated HCl and 30% H_2O_2 (45 ml, 2:1 v/v) was added to wet sample in a tightly capped 120 ml PFA vessel (Savillex). The samples were shaken for an hour on a C1 platform Shaker (New Brunswick Scientific Classic Series). The samples were then ultrasonicated for 48 hours in an ultrasonic bath of high purity water. The leachate was then filtered from the residual sample by passing through a 0.2 um Millipore Polycarbonate membrane filter in a vacuum filtration system. The quantity of sample leached varied from 1-30 g (wet weight) depending on the concentration of mercury and was made to a final concentration of approximately 1ng/ml of mercury. The total procedural blank including cold acid leaching of sample and vacuum filtration were below 30 ρg.

The measurements were made using a Thermo-Finnigan *Neptune* in National High Magnetic Field Laboratory, which is a Multicollector-ICPMS with high mass resolution capabilities.

Measurements were conducted in low resolution mode. Elemental Hg vapor, formed by reacting sample solution with 2-5% $SnCl_2$, is introduced into the mass spectrometer by a Cetac HGX-200 Hydride Generation and Cold Vapor System (Klaue and Blum, 1999). A Perimax Spectec peristaltic pump controlled the uptake rates of $SnCl_2$ and Hg sample solutions. The Hydride Generation and Cold Vapor System have been described in full detail by Klaue and Blum, 1999. The mercury vapor generated from the reduction is transferred by Teflon PFA tubes to the mass spectrometer. In order to minimize effects of instrumental fractionation, isotope ratios were determined by sample standard bracketing technique and reported in δ (‰) notation relative to NIST SRM 3133 Hg elemental standard.

$$\delta^{n}\mathrm{Hg}=\left[\frac{\left(\frac{^{n}\mathrm{Hg}}{^{202}\mathrm{Hg}}\right)_{\mathrm{sample}}}{\left(\frac{^{n}\mathrm{Hg}}{^{202}\mathrm{Hg}}\right)_{\mathrm{standard}}}-1\right]\times 1000‰ \qquad (2.4)$$

2.4 Results

Variations of $\delta^{198}Hg$ / ^{202}Hg observed in the peat core section are presented in **Table 2.2** and **Figure 2.2a**. For each analysis, the internal precision was calculated as the 2 SE of the mean of n runs, where n = 50, or multiples of 50 for larger samples (**Table 2.2, Appendix A.1**) and varies from 0.02 ‰-0.09 ‰.The range of observed $\delta^{198}Hg$ / ^{202}Hg values for the peat core is from 2.96 ‰ to 5.66 ‰ **(Table 2.3).** Overall the entire peat core profile shows an average enrichment of 4.03‰ with respect to NIST SRM3133 Hg standard (**Figure 2.2a**). The reproducibility and validity of the measurements for the core sections are confirmed by the analyses of peat samples where mercury separation chemistry was replicated (**Table 2.2).** The δ-values for the repeat analysis of the Sample 0-2 (0-2A, 0-2B and 0-2C) and Sample 6-8 (6-8A and 6-8B) agree remarkably well with the original δ-values (**Table 2.2)** for all isotope ratios. This also confirms the fact that: i) leaching chemistry has not induced any mass discrimination in mercury isotopes or ii) the recovery yield of mercury from the peat samples with the leaching technique is probably close to 100%.

The interpolated time depth curve for the Penido Vello peat core is based on the five available radiocarbon ages **(Table 2.1).** The accumulation rates from the surface to 33 cm depth are 0.4 mm $year^{-1}$. The accumulation rate between ca. 1012 AD and ca. 587 AD (33 cm – 47 cm) is 0.3 mm $year^{-1}$. Between ca. 587 AD and ca. 457 AD (47 cm – 63 cm) the accumulation of peat increased to 1.2 mm $year^{-1}$ and from 63 cm to bottom of the core (ca. 457 AD until ca. 233 BC) the accumulation rate decreased to 0.5 mm $year^{-1}$.

The analytical precision (external reproducibility) is defined by the replicate analysis of Almaden cinnabar (**Figure 2.2a**) with a 2σ of 0.55‰ represented by dashed lines in **Figure 2.2a**. The topmost 6 cm of the peat core (1788 AD to present) have $\delta^{198}Hg$ / ^{202}Hg values varying between 3.9 to 4.3 ‰. The high $\delta^{198}Hg$ / ^{202}Hg peaks occur at 7 cm (ca. 1751 AD or ca. 199 BP), 11 cm

(ca. 1637 AD or ca. 313 BP) of 5.66‰ and 5.00‰ respectively which is almost a 6σ variation wrt average and 47 cm which represents ca. 587 AD (ca. 1363 BP) of 5.26‰ which is almost a 4σ variation wrt average. The minimum $\delta^{198}Hg$ / ^{202}Hg peaks are observed at 59 cm; ca 489 AD (ca. 1461 BP) and 63 cm (ca. 457 AD or ca. 1493 BP) of 2.97‰ and are siginificant as they represent almost a 4σ variation from average. All other peaks are within the 2σ error bar of Almaden cinnabar (**Figure 2.2a**) and are probably not significant. From 86 cm, ca. 16 AD (ca. 1934 BP) to the bottom of the core (99cm, ca. 233 BC or ca. 2183 BP) $\delta^{198}Hg$ / ^{202}Hg values vary from 4.07‰ to 3.25‰. The most important point to note is that the upper 5 cm of the peat core spanning from ~ 1800 AD – present day represents mercury deposited in modern and industrial times. Estimates are that 50-75% of mercury emission in the modern period is anthropogenically related (Fitzgerald 1995). The bottom 10 cm of the core represents mercury deposited during pre-Roman mining times and is predominantly natural. The mercury isotope ratios at the top and bottom of the core are remarkably similar (97 cm depths has a 3.25‰ $\delta^{198}Hg$ / ^{202}Hg value; 1 cm depth has a $\delta^{198}Hg$ / ^{202}Hg value of 3.92‰).

The $\delta^{18}O$ values of the peat core show a large scatter (**Figure 2.2b, Table 2.3**). In the top 23 cm of the core (present – ca. 1296 AD, 0 BP- ca. 654 BP) the highest $\delta^{18}O$ value observed is 23.7‰ (1cm, ca. 1922 AD, ca. 28 BP) and the lowest ratio observed is 14.4‰ (19 cm; ca. 1410 AD, ca.540 BP). The $\delta^{18}O$ sharply increases to 23.8‰ (25 cm; ca.1239 AD, ca. 711 BP) and until ca. 571 AD (49 cm, ca. 1379 BP) the $\delta^{18}O$ values vary lowest from 20.4‰ (35 cm; ca 951 AD, ca. 999 BP) to highest of 24.9‰ (49 cm; ca. 571 AD, ca. 1379 BP). There is a low peak of 17.0‰ at ca. 522 AD (55 cm, ca. 1428 BP) which increases to 20‰ (63 cm; ca. 457 AD, ca. 1493 BP). From ca. 227 AD/ca. 1723 BP (75 cm, 19.5‰) until bottom of the core (ca. 233 BC, 2183 BP) the $\delta^{18}O$ show a large scattering with low peaks of 17.4‰ (83 cm, ca. 74 AD, ca. 1876 BP), 16.6‰ (91 cm; ca. 80 BC, ca. 2030 BP) and 17.0‰ (97 cm; ca. 195 BC, ca. 2145 BP); and high peak from 77 cm to 81 cm (24.5‰ to 23.7‰, ca. 189 AD-ca. 112 AD, ca. 1761 BP-ca. 1838 BP) and 26.4‰ (93 cm; ca 118 BC, ca. 2068 BP). The overall average of the measured $\delta^{18}O$ for the entire peat core profile is 20.9 ‰.

2.5 Discussion

2.5.1 Evidences for past climate changes in NW Iberia

Broad scale models on climatic reconstructions of the past 2500 years describe a warming, the Roman Warm Period (RWP) from ca. 250 BC-ca. 450 AD (Codrón, 1996; Hass 1996; McDermott *et al*., 2001; Tullot, 1988; Zapata, 1999), followed by generally cold conditions (Dark Ages Cold Period, DACP) between ca. 450 AD and ca. 1000 AD (Lamb, 1985, McDermott *et al*., 2001); later a Medieval Warming Period (MWP) beginning around ca.1000 AD– ca. 1400 AD (Bradley, 2000; Broecker, 2001; Hass 1996; McDermott *et al*., 2001). Around ca. 1450 AD, the Little Ice Age (LIA) began (Bradley, 2000; Broecker, 2001; Fischer *et al*., 1999; Grove, 1988; Haas, 1996; Thompson *et al*., 1986). The Little Ice Age can be subdivided into several climate phases (Mann *et al*., 1998), with lower temperatures around ca.1450 AD and in the 18th and 19th centuries. The Little Ice Age has been said to be a winter phenomenon in Europe, with normal summer temperatures (Pfister 1985).

From the 4000 year old record of atmospheric mercury deposition in the Penido Vello peat bog (**Figure 2.3**), a proxy record of climate change was reconstructed which showed that during

periods of cold climate there is an enhanced accumulation of mercury with low thermal stability and during periods of warmer climate there is lower accumulation of mercury with a higher thermal stability (Cortizas *et al*., 1999). Based on the observed thermal stability of mercury, a temperature and a humidity index was developed (Cortizas *et al*., 1999). For the last 4000 years, the temperature index identified two major periods of warm climate (Roman Warm Period and Medieval Warm Period) and two major cooling phases (Neoglacial period and the Little Ice Age). The shift of mercury from higher stability to lower stability was used to establish the humidity index. The conclusions of this study were that during warm and wet climates mercury with higher thermal stability are more abundant and the variations fit with other humidity records for that part of Spain.

In addition palynological studies have also revealed past climate in the Iberian region (Desprat *et al*., 2003; Mighall *et al*., 2006). High-resolution pollen influx sequence study of Vir-18 core from Ría de Vigo (North West Iberia) covering past 3000 years demonstrated the first cold phase of the Subatlantic period (ca. 975 BC – ca. 250 BC) followed by the Roman Warm Period (ca. 250 BC – ca. 450 AD); another successive cold period, the Dark Age Cold Period (ca. 450 AD – ca. 950 AD) terminated by the start of the Medieval Warm Period (ca. 950 AD – ca. 1400 AD). The Little Ice Age (ca. 1400 AD – ca. 1850 AD) which included the Maunder Minimum (at around ca. 1700 AD) preceded the period of Recent Warming (ca. 1850 AD - present) (Desprat *et al*., 2003). Mighall *et al*. (2006) tried to infer changes in past climate by using pollen and non-pollen palynomorphs (NPP) data from two ombrotrophic peat cores: the Pena da Cadela (PDC) and Borralleiras da Cal Grande (BLL) situated in the Montes do Cabaleiros and Xistral Mountains in Northwestern Spain. Six major wet and humid periods were shown: at ca. 850 BC, ca. 560–250 BC, ca. 240 AD–770 AD (with two probably severe droughts at ca. 280 AD–300 AD and ca. 560 AD–580 AD), ca. 1100 AD–1130 AD, ca. 1330–1460 AD and ca.1810– 1860 AD.

Valero-Garcés *et al*. (1999) when investigating the Salada Mediana and Salada Chiprana records (Ebro valley, NE Iberia) found that during the 14^{th}-15^{th} centuries there was a rise in lake levels which coincided with the end of the Medieval Warm Period. High-resolution sequential analysis of the upper 3.80 cm of a sediment core from Lake Sanabria, an oligotrophic freshwater lake in the granitic zone of the NW Iberian Peninsula revealed that there was a sedimentary episode between14^{th} and 16^{th} centuries during which there was low lake productivity and this was correlated to an episode of low temperature during the Little Ice Age (Luque and Juliá, 2001).

2.5.2 Paleoclimate relevance from Oxygen and Mercury isotopes

2.5.2.1 Species dependence of oxygen isotopes

Recently a few studies had reconstructed Holocene climate variations at various time scales using $\delta^{18}O$ as the paleoclimate tool in ombrotrophic peat cores (Aucour *et al*., 1996; Brenninkmeijer *et al*., 1982; Hong *et al*., 2000). In all these studies oxygen isotope analysis was conducted on bulk peat cellulose and the isotopic variations were directly interpreted in terms of paleohydrological/paleohumidity/paleotemperature changes. In contrast few other studies conducted their isotope studies on cellulose separated from each species and indicated that the amplitude of any $\delta^{18}O$ response signal is species dependent (Aravena and Warner 1992; Ménot-Combes *et al*., 2002; Zanazzi and Mora, 2005).

Study conducted on five species of *Spaghnum* moss from three different peat lands indicated that microenviromental water relations regulated evapotranspiration in Sphagnum species (Aravena and Warner, 1992). *Spaghnum* moss species collected from hummock tops (*S. fuscum, S. capillifolium)* showed a consistent enrichment in $\delta^{18}O$ when compared to species representing depressions or hollows (*S. magellanicum, S. papillosum, S.fallax)* in peat lands. The maximum enrichment in the hummock species was found to be 3.8 ‰ higher than the hollow species (Aravena and Warner, 1982). The enriched oxygen isotope values in the hummock species indicated that the source water used in photosynthesizing the cellulose in hummock species was probably much more affected by evaporation and transpiration than in species which grow in adjacent hollows (Aravena and Warner, 1992). One of the most important factors controlling photosynthetic activity in *Spaghnum* mosses is the differences in moisture conditions between different micro sites in peat lands. When the moisture conditions are low the hollow species show lower rates of growth compared to hummock species (Luken 1985) and the reverse is true in case of high moisture conditions (Luken 1985). Because of their more efficiently developed capillary network, hummock species are more capable in acquiring and retaining water compared to hollow species (Rydin 1985; Titus & Wagner 1984; Wagner & Titus 1984).

The study conducted by Ménot-Combes *et al*. (2002) on temperate peat bogs in Switzerland reported that the $\delta^{18}O$ of the mosses *S. capillifolium* and of the cotton sedge *Eriophorum vaginatum* appeared to be more responsive to climatic variations. The other *Spaghnum* species (*S. magellanicum, S. cuspidatu*m) do not appear to be linked with any changes in hydrological conditions or are heavily influenced by the microenvironmental conditions at the surface of the bog (Ménot-Combes *et al*., 2002).The result is that some species are more sensitive to the actual variation in source water (precipitation in case of Penio Vello peat core) than others. The unresponsive species would therefore be difficult to be linked with climatic variations and in such cases the use of bulk peat cellulose i.e. without separating out each individual species would certainly lead to erroneous interpretations of climate. In addition to the species dependent $\delta^{18}O$ response signal, Ménot-Combes *et al*. (2002) also reported $\delta^{18}O$ variation of surface water correlating with the microtopography of the surface of the bog. Surface water from raised hummocks had enriched $\delta^{18}O$ values due to higher rate of evaporation whereas water from depressions had depleted $\delta^{18}O$ values. The total variation was reported to be as high as 4‰ in one bog (Ménot-Combes *et al*., 2002). The large $\delta^{18}O$ variation observed in the bog surface waters was however found to be quite averaged in the plant cellulose by almost 5-10 times for some plant species. This indicated that the source water used to synthesize cellulose reflects the annual precipitation isotopic composition (Ménot-Combes *et al*., 2002).

Due to the relatively large uncertainties associated with the biochemical fractionation factor ε_b for mosses (27±3 ‰) (Aucour *et al*., 1996; Aravena and Warner, 1992; Deniro and Epstein, 1981; Epstein *et al*., 1977), the use of peat moss cellulose oxygen isotope composition as a proxy for paleohydrological and paleoclimatic reconstructions has been limited (Zanazzi and Mora, 2005). *Sphagnum* moss species from the hummock tops are the ones which show the larger variability 27±3 ‰, whereas species from hollows show smaller variability 27±1 ‰ (Zanazzi and Mora, 2005). Thus, $\delta^{18}O$ isotopic shifts which are larger than 3–4‰ in peat cellulose should be the ones linked to climate shift (Zanazzi and Mora, 2005). Species specific isotopic analysis

would probably reduce this uncertainty thus improving paleoclimate reconstructions (Zanazzi and Mora, 2005).

2.5.2.3 Isotopic links between source water and modern cellulose

The IAEA/GNIP stations located closest and in the same latitude to the Penido Vello bog area are in La Coruna and Santander in NW Iberian Peninsula. The mean monthly and annual $\delta^{18}O$ values of precipitation are available from 2000 to 2004 for both of these stations (**Table 2.4, 2.5**). During this period the maximum and minimum monthly mean temperatures that were recorded was approximately 18.9ºC (September) and 11.1ºC (January) in La Coruna and 20.6ºC (August) and 10.8ºC (January-February) in Santander respectively (**Figure 2.4, Table 2.4)**. Both the stations show a higher amount of precipitation during the winter months of October-January (**Figure 2.4, Table 2.4)** and low precipitation in summer months of May-September. This is typical for NW Iberia as precipitation over the peninsula has a strong seasonal character. During winter, precipitation is mainly related to air masses moving eastward from the Atlantic Ocean and in contrast, the sparse summer precipitation depends on local thunderstorms associated with ground heating and high moisture content (Serrano et al., 1998). The relative humidity has been calculated from the water vapor pressure and temperature data provided by IAEA/GNIP and saturated water vapor pressure data from Donald 1994. In Santander the relative humidity is higher in summer than in winter but in La Coruna the relative humidity is almost constant throughout the year (**Figure 2.4, Table 2.4**).

Linear regression analysis of $\delta^{18}O$ precipitation was carried out with respect to the major climatic factors: observed average monthly temperature, observed average monthly precipitation, calculated average monthly relative humidity (**Figure 2.5**) and yearly means of amount of precipitation, temperature and relative humidity (**Figure 2.6**) for the meteorological stations La Coruna and Santander between 2000 and 2004. La Coruna and Santander show strong seasonal variations of $\delta^{18}O$ content of monthly precipitation, with precipitation isotopically depleted in winter and enriched in summer (R^2 = 68% and 53% respectively). During the months of summer (May-September), low amount of precipitation resulted in relatively higher $\delta^{18}O$ values whereas for winters (October-January) higher amount of precipitation resulted in lower values of $\delta^{18}O$ (**Figure 2.5**). The monthly temperature effect on $\delta^{18}O$ precipitation in La Coruna and Santander is lower than the seasonality (R^2 = 40% and 36%) respectively. The strongest correlation (positive) is for the summer months June-August where higher temperatures resulted in higher $\delta^{18}O$ values of precipitation. This effect is more prominent for La Coruna site than Santander (**Figure 2.5**). On other hand, correlation of $\delta^{18}O$ precipitation with the estimated relative humidity values demonstrates two very different effects in La Coruna and Santander with R^2 = 0% and 67% respectively (**Figure 2.5**). The relative humidity control on $\delta^{18}O$ precipitation is most prominent for the months April-October in Santander. For the months November-March, the humidity effect does not seem to be important (**Figure 2.5**). Regression analysis of $\delta^{18}O$ precipitation with annual means of precipitation, annual mean temperature and annual relative humidity (**Table 2.5**) demonstrate that for both La Coruna and Santander, there is no significant correlation in $\delta^{18}O$ precipitation with change in total annual precipitation (**Figure 2.6**). In La Coruna, the highest precipitation amount recorded for the year 2000 is 1274 mm and lowest is 672 mm in 2004 and the corresponding isotopic shift is 0.98‰ (**Table 2.5**) whereas a shift from 1182 mm (2003) to 672 mm (2004) causes a larger isotopic shift of 2.84‰. There is no significant variation in $\delta^{18}O$ precipitation (total shift of ~0.4‰) corresponding to the highest

precipitation amount in 2000 (1168 mm) and lowest in 2001 (808 mm) in Santander. Annual mean temperature for both the sites seem to be fairly constant for the years 2000-2004 and so no correlations are observed between temperature and $\delta^{18}O$ precipitation (**Figure 2.6**). The significant $\delta^{18}O$ precipitation-temperature correlation on the monthly scale is certainly diminished at the annual scale for both the stations. In Santander humidity (R^2 =64%) show a high positive correlation with $\delta^{18}O$ precipitation (**Figure 2.6**) although a relative humidity change from 93 (2004) to 88 (2001) causes only a change of 0.86‰ in $\delta^{18}O$ precipitation. From such limited modern data available (only for 5 years) it is difficult to use this as a modern analog to interpret past climate variations. Also it is difficult to say with certainty which climatic effect (precipitation amount, temperature or humidity) is the major controlling factor in causing significant oxygen isotopic shifts in precipitation.

To test the validity of the mechanistic model described in equation 2, vegetation (Sample Vegetation, **Table 2.6**) collected from the surface of the peat core is used as a proxy to estimate the oxygen isotope value of modern precipitation. The bog surface has highly stratified air (Brennikmeijer, 1983) and boundary conditions are stagnant which fixes the value of ε_k = 28‰ (Buhay *et al*., 1996). The value of the water vapor-liquid equilibrium fractionation factor ε^* has been calculated to be 9.8 ‰ (Baertschi and Thürkauf, 1969). For all C_3 plants, the biological fractionation factor ε_b is thought to be nearly constant with an average value of 27±3 ‰ (Baertschi and Thürkauf, 1969). Previous studies conducted on mosses growing in various climatic zones such as equatorial and temperate found that ε_b varied from 25 to 27 ‰ (Aucour *et al*., 1996; Aravena and Warner, 1992; Deniro and Epstein, 1981; Epstein *et al*., 1977). For *Spaghnum* moss *f* can vary from 0.3 (70% evaporation) to 0 (100% evaporation) (Ménot-Combes *et al*., 2002). The humidity index is assumed to vary between 1 (100% relative humidity) to 0.80 (80% relative humidity) which is probably reasonable for a bog area near the coast (**Table 2.6**). In the equation that derives $\delta^{18}O_c$ from $\delta^{18}O_{sw}$ (oxygen isotope value of source water, in this case probably precipitation) relative humidity plays a predominant role. Decreasing humidity index leads to depleted $\delta^{18}O_{sw}$ values and vice versa. For a fixed humidity index h (exception is 100% humidity) and biological fractionation factor ε_b, an increasing *f* results in enriched $\delta^{18}O_{sw}$ values (**Table 2.6**). This necessarily does not reflect an isotopic change in source water over time but probably accounts more for the heterogeneous leaf water reservoir. Lastly, as expected, varying biological fractionation factor value from 25 to 27 ‰ has a significant effect in altering the isotope value of the source water (**Table 2.6**). In any case, the evident dependence of the estimated isotopic values of source water (precipitation) on *f* and ε_b calls for the fact that peat-based palaeoclimate reconstruction probably should not be carried out on bulk peat but at the species level. There are a few combinations (indicated by bold font in **Table 2.6**) by varying the mechanistic model parameters (*f*, h and ε_b) the estimated value of $\delta^{18}O_{sw}$ closely matches with the IAEA $\delta^{18}O$ precipitation data. In all these case, the assumed humidity varies between 85%-100%. It had been suggested that the Penido Vello bog area has a strong oceanic influence (being 20-25 kms away from ocean) and is subjected to a continuous advance of cyclonic fronts (Ramil-Rego *et al*., 1998). This would probably make humidity a more important climatic parameter than temperature (Mighall *et al*., 2006). On the other hand, the mechanistic model requires the humidity parameter to be assumed. Measurements have shown that in the first top few centimeters of air at the surface of the bog, relative humidity is close to a 100% (Brennikmeijer, 1983). Assuming a fixed humidity index in the model for the last 2200 years of the peat core would certainly yield a meaningless and erroneous paleoprecipitation reconstruction. It seems for

the case of Penido Vello peat bog the mechanistic model linking oxygen isotope ratio of cellulose and source water (precipitation) is certainly not applicable.

2.5.2.2 Climatic inference from $\delta^{18}O$ cellulose

Three important factors control variations observed in $\delta^{18}O$ of cellulose. One factor is the species composition, second is the isotope enrichment in leaf water, which relates to relative humidity and the third is the isotope ratio of meteoric water. The isotope ratio of meteoric water (precipitation) is generally influenced by certain meteorological conditions such as temperature effect and amount effect. $\delta^{18}O$ values in modern precipitation have long been known to correlate with temperature, as a result of temperature-dependent distillation processes in the atmosphere (Craig 1961; Dansgaard, 1964). During winter or cooler weather there is depletion $\delta^{18}O$ and during summer or warmer weather there is enrichment of $\delta^{18}O$ in meteoric water. In general, a sinusoidal distribution pattern for the $\delta^{18}O$ precipitation with low values during winter and high values during summer is observed. For mid to high latitudes, the empirical relationship between the annual average $\delta^{18}O$ precipitation and local surface air temperature is typically 0.58‰/^{o}C (Fricke and O'Neil, 1999). The amount effect is also an important effect (Dansgaard, 1964) in the tropical areas and mid-latitudes in summer. When temperatures are warmer and there is significantly higher humidity and/or precipitation, the $\delta^{18}O$ values in meteoric water (precipitation) are lower (Dansgaard 1964). Strong convective systems (tropical thunderstorms, cold fronts etc.) are usually controlled by the amount effect.

The results from previous studies indicate that paleoclimate and paleohydrological inferences based on the oxygen isotope values of moss peat cellulose must consider both changes in hydrological conditions and moss species distribution. Reconstructions based just on bulk peat cellulose would probably lead to erroneous results. Nevertheless, the present study was conducted by measuring $\delta^{18}O$ on cellulose extracted from bulk peat material. Conducting species specific analysis was beyond the scope of the present study. The total range of variation in $\delta^{18}O$ cellulose in the Penido Vello peat core is from 16.6 ‰ to 26.4 ‰ which yields a $\Delta^{18}O$ of 9.8‰ (**Table 2.3**). Change in species composition from hummock to hollow and vice versa would probably account for a 4‰ shift in $\delta^{18}O$ cellulose. Thus, $\delta^{18}O$ isotopic shifts which are larger than 4‰ in peat cellulose should be the ones linked to local climate shift. If all other factors remain constant, then a $\Delta^{18}O$ of 9.8‰ will correspond to a $\Delta T \sim 17\ ^{o}C$ and a $\Delta^{18}O$ of 5.8‰ (remaining 4‰ accounted by species change or uncertainty in biological fractionation factor) will correspond to a $\Delta T \sim 10\ ^{o}C$ over a period of 2200 years. Both seem to be an unreasonable change over a period of 2200 years and there is no other supporting evidence available. Moreover, analysis of modern yearly precipitation data (**Figure 2.6**) from both the La Coruna and Santander stations show temperature to be an insignificant factor controlling oxygen isotope fractionation of precipitation. Although, with limited 5 data points the above statement is rather inconclusive. The seasonality based on amount of precipitation is more significant when compared on a monthly scale compared to the annual scale (**Figure 2.5**). Also there are very few annual data available. The time resolution in the Penido Vello peat core (each data point approximately varies from 20-60 years) is too low for any seasonal effect to be recorded. Thus the source water that was used by the plants to synthesize cellulose would reflect the isotopic composition of the average annual precipitation rather than any monthly or seasonal effect. A change in relative humidity from 100% to 80% with all other factors remaining constant (**Table 2.6**) causes an oxygen isotope shift in precipitation of approximately 5‰. This is a significant

change and could probably explain some of the shift in oxygen isotope values observed in the Penido Vello peat cellulose but according to the modern data there is a pronounced humidity correlation in Santander and completely absent in La Coruna. Both the sites are sub coastal and have the same latitude. For the past 2200 years temperature and humidity both could have contributed significantly in changing $\delta^{18}O$ values in peat cellulose but humidity could have been a more dominant factor. Again, with the current limitations and discrepancy of the annual modern data the observations are only suggestive and not conclusive.

The raw $\delta^{18}O$ bulk peat cellulose record of the peat core is compared for correlation with the main climatic variations identified for the past 2200 years (**Figure 2.7**). However, the application of these large-scale climate changes (RWP, DACP, MWP and LIA) to the study area may not be appropriate based on analysis of only one peat core. The overall average of the measured $\delta^{18}O_c$ for the entire peat core profile is 20.9 ‰. In the bottom part of the core, the period between ca. 252 BC-ca. 450 AD (ca. 2205 BP- ca. 1500 BP) there is large scattering in the $\delta^{18}O_c$ trend. There are two peaks in the oxygen record (**Figure 2.7**) from ca. 137 BC-ca. 99 BC (ca. 2087 BP-ca. 2049 BP) and ca. 93 AD-ca. 208 AD (ca.1857 BP- ca. 1742 BP) with enriched $\delta^{18}O$ values with respect to the mean $\delta^{18}O_c$. The longer term trend shows enrichment in $\delta^{18}O$ between ca. 2106 BP-ca. 2011 BP and ca. 1819 BP-ca. 1723 BP and depleted values between the periods of ca. 2011 BP-ca.1915 BP. The enriched values could represent a natural warming period coinciding with the RWP (Codrón, 1996; Haas, 1996; McDermott *et al*., (2001); Tullot, 1988; Zapata, 1999). The depleted event could either reflect a change form warmer conditions to cooler period or a change to more humid conditions or a combined effect of both. Since, there is no alternative supporting record and appropriate modern analog to compare with, the suggestions are all speculative. There is a period of severe drought spanning from ca. 280 AD-ca. 300 AD (ca. 1670 BP-ca. 1650 BP) (Mighall *et al*., 2006) which is not prominent in the $\delta^{18}O_c$ record. During drought which is essentially an arid period, it is expected that due to higher rates of evapotranspiration, $\delta^{18}O$ in cellulose would be enriched. The peak with low $\delta^{18}O_c$ values in the period ca. 481 AD-ca. 530 AD (ca.1469 BP-ca. 1420 BP) could well indicate the onset of another cooling period, the DACP (Lamb, 1985, McDermott *et al*., (2001)). Another period of drought reported by Mighall *et. al* (2006) seems to be coinciding with the increase in $\delta^{18}O_c$ value in the oxygen record in the period between ca. 563 AD-ca.587 AD (ca. 1387 BP-ca.1363 BP). There is another period between ca. 800 AD-ca. 860 AD (ca. 1150 BP-ca. 1090 BP) with an enriched oxygen peak probably indicating a warming or drought event but there is no previous record to compare with. Between the period ca. 940 AD-ca. 1390 AD marked as MWP (ca. 1010 BP-ca. 560 BP, **Figure 2.7**) there is a humid event identified in the bog record of Mighall *et al*., 2006, at ca. 1110 AD-1130 AD which is not indicated in the oxygen isotope record here. The MWP in general is quite prominent in the oxygen isotope record as the long term $\delta^{18}O_c$ trend shows an overall enriched signature which is consistent with a warming period. The minima between the period ca. 1268 AD-ca. 1325 AD (ca. 682 BP-ca. 625 BP) coinciding with the end of the MWP phase and start of a humid period (Mighall *et al*., 1996) could be indicative of the onset of another cooling event, namely the LIA (Bradley, 2000; Broecker, 2001; Fischer *et al*., 1999; Grove, 1988; Haas, 1996; Thompson *et al*., 1986). In the period from about ca. 1382 AD-ca.1438 AD (ca. 568 BP-ca. 512 BP) a large minima in the oxygen isotope record definitely corresponds with the LIA cold period. The LIA is thought to include two cooling periods ca. 1600 AD-ca. 1750 AD & ca. 1800 AD-ca. 1850 AD separated by a warm episode ca. 1750 AD-ca. 1800 AD (Fischer *et al*., 1999). The warming episode and the last cooling period in the LIA

record coincides well with the peat cellulose oxygen isotope record by showing substantial increase and subsequent decrease in isotopic ratios (**Figure 2.7**). There is also another wet period (ca. 1810 AD-ca. 1860 AD) reported by Mighall *et al*., 1996 which is prominent in the oxygen isotope record. This wet period also coincides with the last cooling event between ca. 1800 AD-ca. 1850 AD (Fischer *et al*., 1999) in Little Ice Age. Overall the long term $\delta^{18}O_c$ trend shows a depleted oxygen isotope signature in the range of LIA which is consistent with the cooling event. During the Recent warming period the oxygen isotope ratios show a sharp increase agreeing well with the chronology of the event (**Figure 2.7**).

2.5.2.4 Climatic inference from mercury isotopes

The mercury isotope record of the Penido Vello peat core when compared with past climate records (**Figure 2.8**) does not seem to show any direct or consistent relationship. None of the chronology attributed to the warm and cold periods coincide with any change in isotopic pattern within the analytical uncertainties. It could be that in spite of the predictions from the cold condensation model of Mackay *et al*., 1995 and findings of Cortizas *et al*. 1999, mercury does not show any isotopic fractionation effect. Oxygen and hydrogen isotopes have been routinely used as a paleoclimate tool for a very long time. Generally, both oxygen and hydrogen show enrichment in heavier isotopes during warmer climate and depletion during colder climate. But unlike oxygen and hydrogen isotopes, probably the isotopic composition of mercury deposited during colder and dryer periods are not different than from warmer and wetter periods. Another reason could be the limitations of the technique employed to measure mercury isotopes. The analytical precision of the technique probably is insufficient to resolve meaningful isotopic variations that occur in mercury due to changes in temperature and humidity. Even if small isotopic variations occur in the mercury deposited from the atmosphere due to climate fluctuations it might be overwhelmed by differences in regional sources of mercury. The model of MacKay *et al*. (1995) has both temporal and spatial boundaries, a condition that can not be assumed for atmospheric mercury.

2.5.3 Various sources of mercury to the PV peat bog

The possible sources of mercury to the Penido Vello peat core, both natural and anthropogenic, over a period of 2200 years are discussed in details below. Marine emissions, volcanic eruptions, natural and human influenced output of mercury from the Almaden deposits and the release of mercury during forest fires are amongst the important ones. The quantity of mercury emitted from these sources probably depends on a number of physical, chemical, biological and climatic factors which are not fully understood.

2.5.3.1 Volcanoes

One of the major natural sources of mercury to the atmosphere is volcanic eruptions (Nriagu, 1989; Varekamp and Buseck, 1986). These volcanic emissions may constitute important point sources of various mercury species such as particulate Hg (P), reactive Hg (II) and gaseous mercury Hg (0) (Pyle and Mather, 2003). After a volcano erupts, mercury concentration could be increased by direct degassing form the volcanic emissions and also by formation of mercury compounds in acidic water droplets in the atmosphere. When gaseous mercury is emitted from volcanoes, to it is injected high into the stratosphere and is more likely to be deposited far from the volcano. It has proved difficult to quantify the amount of mercury released to the atmosphere since quantity and species of mercury differs from volcano to volcano and also there could be

different emission points on one volcano. Current time-averaged volcanic mercury flux is estimated to be ~700 t/yr or 20-40 % of natural emissions (Nriagu and Becker, 2003; Pyle and Mather, 2003). If there are several large individual eruptions in a century it can very well overwhelm the entire global mercury budget, and will transport almost 10^3–10^4 t Hg into the atmosphere (Pyle and Mather, 2003). The record of such past large volcanoes emitting mercury is preserved in ice cores and ombrotrophic peat deposits (Barraclough *et al*., 2002; Schuster *et al*., 2002).

In the 14500 year old ombrotrophic peat core from Swiss Jura Mountains, short term peaks in mercury concentration (Barraclough *et al*., 2002) matched the time period of some known volcanic eruptions (Simkin and Siebert, 1994) in Europe**.** During the late Boreal (ca. 7191 to ca. 7099 BC) and older Atlantic periods (ca. 6800 BC to ca. 5090 BC) elevated mercury signals corresponded to several known clusters of European volcanic eruptions in Iceland, Turkey, Germany, Italy and France (Barraclough *et al*., 2002). Other than peat cores, ice core records from the Upper Fremont Glacier, Wyoming, also have a high-resolution record of total atmospheric mercury deposition (ca. 1720 AD-ca.1993 AD) in which volcanic events contributed 6% to the total mercury in the ice-core samples. Krakatau (1883 AD) and Tambora (1815 AD), although in the southern hemisphere and 20,000 km from the glacier in Wyoming, reached high into the stratosphere and were point sources of mercury origin followed by global scale deposition (Schuster *et al*., 2002). The Mt. St. Helens eruption in 1980 (600 km distant from the glacier), although orders of magnitude smaller in scale than Krakatau and Tambora showed up as a corresponding mercury peak in the glacier record as a regional source.

There are major volcanic eruptions that could have acted as sources for significant amount of mercury to the Penido Vello peat core (**Figure 2.9a**, **Table 2.7**). There are two well known eruptions of Vesuvius in Italy within a brief interval of 512 AD and 472 AD (Simkin and Siebert, 1994). The minimum $\delta^{198}Hg$ / ^{202}Hg values at 58 -60 cm (ca. 498 AD–ca. 481 AD, ca.1452 BP-ca. 1469 BP) and 62 - 64 cm (ca. 465 AD – ca. 449 AD, ca.1485 BP-ca. 1512 BP) of 2.97 ‰ could have been caused by these eruptions. The peak of 5.66 ‰ at ca 1779 AD-1723 AD (6-8 cm depth) and the peak of 5.00 ‰ at ca. 1666 AD-ca. 1609 AD (10-12 cm depth) correspond in time to a cluster of European eruptions; Vesuvius (1631 AD in Italy), Hekla (1597 AD; 1693 AD;1766 AD in S Iceland), Katla (1626 AD; 1660 AD;1729 AD;1755AD in S Iceland), Oraefajokull (1727 AD in SE Iceland), Grimsvotn (1783 AD in NE Iceland) and Etna (1787 AD in Italy). There are also smaller and numerous volcanic eruptions during the past 2200 years (Simkin and Siebert, 1994). Some of these eruptions could have affected the global mercury pool but the volcanic signal is likely to be subdued by the natural mercury background or strong anthropogenic signals (for recent years). Also, because of the uncertainties involved in the dating of both the volcanic eruption dates and peat samples, it is not possible to say with absolute certainty which volcano in the past record could have caused a peak in the mercury isotope profile.

A volcanic eruption is a short episode and would not last longer than several months or a couple of years. Even if an eruption event releases a vast amount of mercury to the atmosphere, the signal would not cover more than 3-5 years because mercury has a residence time of approximately one year in the atmosphere. The distance of the nearest volcanoes to the Penido Vello peatland site are all located in Italy and Iceland and are at least 1500 kilometers away. It is

unlikely that mercury signals from distant erupions would be apparent in this bog core. Even if the eruptions are large, most of the particulate mercury Hg (P) and reactive mercury Hg (II) would deposit quickly locally via wet and dry precipitation. The gaseous mercury Hg (0) would join the atmospheric mercury pool and is the likely candidate to appear as a volcanic signal in the bog. It is more likely that gaseous mercury extruded from the volcanoes would get homogenized isotopically with the atmospheric gaseous mercury pool and get widely dispersed. What fraction of that would actually be trapped in the PV peat bog is very unclear. There are also large uncertainties regarding isotopic signature of mercury emitted from volcanic eruptions. It is not known if mercury from different volcanoes is isotopically distinct; it is also not known if mercury from various other geological sources can be distinguished isotopically. What comes out of volcanoes is all juvenile mercury vapor (Hg (0)) which has never gone through the mercury global cycle. If it is assumed by definition that juvenile mercury would have an isotopic composition of ~0.0‰, when it joins the atmospheric pool it would be fractionated by photochemical reactions etc. and be of a different isotopic makeup deposited via wet or dry precipitation in the bog. Analysis of volcanic ash in the peat core given that it has preserved the juvenile mercury isotope signal would probably answer a lot of these uncertainties but this is beyond the scope of this study. Moreover, the time resolution in the Penido Vello peat core (each data point approximately varies from 20-60 years) (**Figure 2.9a**) is too low for a clear mercury signal of a volcanic source located at least 1500 kilometers away to be produced. Current estimates based on Hg/SO_2 ratio (Edner *et al*., 1994; Varekamp and Buseck, 1981; Ferrara and Maserti, 1990) demonstrate that volcanic emissions in the Mediterranean region (Etna, Vulcano, Stromboli) do not represent an important source of atmospheric mercury (Ferrara *et al*., 2000) compared to Hawaiian volcanoes (Siegel and Siegel, 1984). There is no available data on the quantity of mercury released from these past eruptions. With such crucial uncertainties existing, it is questionable to link the mercury isotopic peaks in Penido Vello bog record with known volcanic eruptions.

2.5.3.2 Biomass burning

Forest fires are believed to mobilize mercury and redistribute it into the atmosphere as elemental Hg (0), divalent Hg (II) and particulate Hg (P) forms of mercury (Porcella *et al*., 1996). A recent study by Sigler *et al*., 2003 determined an annual release of 3.5 tonnes mercury from Canadian boreal forest fires which is roughly equal to 30% of Canada's annual anthropogenic mercury emission (Environment Canada, 2000)**.** In a forest fire in the Amazon, concentrations of mercury as high as 1,000 mg/kg were measured in smoke particles smaller than 2.5 μm in diameter (Kaufmann *et al*., 1992). Mercury measured in the plume of a wild land fire in South Africa had an estimated global contribution to the atmospheric budget of 1000 t/year (Brunke *et al*. 2001). Laboratory experiments suggest that release of mercury from fires may be 104-526 t y^{-1} or 3.5-17.5% of natural Hg emissions (Friedli *et al*., 2001).

Santos *et al*., 2001 estimated mercury accumulation rates in a sediment core from Lagoa da Pata, a remote lake in São Gabriel da Cachoeira, northern Amazon. They observed a three-fold increase in mercury deposition rate approximately 20,000 years ago, after the Last Glacial Maximum and linked it to drier periods and a higher frequency of forest fires during Holocene, which released larger amounts of mercury from the biomass and the soils.

Evidence for an increased frequency of pre-historic forest fires/biomass burning usually comes from charcoal deposits in soils (Pessenda *et al*. 1998a, 1998b) and sediments (Cordeiro 1995;

Cordeiro *et al*. 1997; Lacerda *et al*. 1999; Turcq *et al*. 1998). Charcoal may be deposited as a result of atmospheric transport of the finer particles after biomass burning or it could be generated *in situ*. Palynological studies conducted on two pollen sequences from two Galician Sierras, the Courel and Queixa Sierras in NW Iberian Peninsula (Santos *et al*., 2000) and ombrotrophic peat bogs Pena da Cadela (PDC) from the Xistral Mountains in the NW Iberian Peninsula (Cortizas *et al*., 2005; Mighall *et al*., 2006) show the presence of substantial microcharcoal particles (**Figure 2.9b**) since ca. 2000 BP (Roman times). The abundance of microcharcoal particles probably suggests the occurrence of regional fires related to anthropogenic activity in the NW Iberian Peninsula. From the peat core PDC some high microcharcoal concentration peaks (Cortizas *et al*., 2005; Mighall *et al*., 2006) which could be indicating biomass burning (thus releasing mercury to the atmosphere) were compared to the mercury isotope plot (**Figure 2.9b**).

The large peak at ca. 617 AD-ca. 579 AD (46-48cm, ca.1333BP- ca. 1371 BP, $\delta^{198}Hg$ / ^{202}Hg of 5.26 ‰) could signify change in mercury source thus causing change in isotopic fractionation pattern (**Figure 2.9b**). Historical and other records support the interpretation that human activities are mostly responsible for significant clearance in forests and change in vegetation pattern at least for the past 2500 years in NW Iberian Peninsula (Cortizas *et al*., 2005; Mighall *et al*., 2006; Santos 2004; Sobrino *et al*., 1997). There are known periods of intense forest clearance coinciding with the Roman period (100 BC-400 AD) and Germanic Period (Visigoth Kingdom) starting with the seventh century AD (Cortizas *et al*., 2005). Historical records show that burning practices were very common in both the periods mainly to clear forest for agriculture. After the Roman Empire fell in the 4th AD, the forests recovered and remained stable until the onset of the Visigoth Kingdom in seventh century AD, when it underwent the most dramatic retreat in the vegetation history of northwestern Spain (Cortizas *et al*., 2005; Mighall *et al*., 2006). The mercury isotopic peaks coincide with the high microcharcoal peaks from the Roman period and Germanic period (**Figure 2.9b**).

Experiments suggest that during biomass burning elemental mercury can be emitted from 50% (Pacyna and Münch, 1991) to as high as 95% (Friedli *et al*., 2003). If 50% -95% of the mercury released due to burning was in the form of Hg (0) it is unclear how much fraction of the mercury recorded by the Penido Vello bog reflects the total emission flux, i.e. the percentage of mercury emitted from biomass burning and deposited in the bog and percentage of mercury dispersed globally. Moreover, the isotopic discrimination pattern of mercury emitted during biomass burning is not known. Also, uncertainties exist in the dating of both the peat samples and the microcharcoal records.

2.5.3.3 Marine emissions

Marine mercury emissions are believed to be one of the largest contributors of elemental mercury to the atmosphere. Marine emissions contribute towards 54% of surface atmospheric mercury in the southern hemisphere where anthropogenic sources are relatively less abundant, while in the northern hemisphere the marine contribution is on an average 36% (Strode, *et al* 2007). Aqueous mercury in the ocean is present in the form of various mercury species: elemental, monomethyl and dimethyl, divalent, particulate and colloidal (Morel *et al*., 1998). The reduction of Hg species to Hg (0) vapor can occur by photochemical (Amyot *et al*., 1994; Sellers *et al*., 1996) biological (Barkay *et al*., 2005; Mason *et al*., 1995), or abiotic organically mediated

(Allard and Arsenie, 1991) mechanisms. Modeling experiments show that on an average 56% of the total mercury depositing in the ocean by atmospheric deposition reduces to Hg (0) and joins the global atmospheric mercury pool (Strode *et al*., 2007).

In general ocean-atmosphere mercury emission- deposition fluxes are thought to be in equilibrium with each other but can change due to change in oceanic productivity (Kim and Fitzgerald, 1986; Mason and Fitzgerald, 1990). In upwelling regions, aqueous Hg (0) concentrations get elevated and also show seasonal variations. Usually high concentrations occur during times of higher biological productivity (Strode *et al*., 2007). The oceanic productivity depends on upwelling, turbulence and soil dust input (Kim and Fitzgerald, 1986; Pongratz and Heumann, 1999). In the Vostok ice core record, the peak in mercury concentrations during the Last Glacial Maximum (approximately 20,000 years ago) was thought to be because of increase in oceanic productivity (Vandal *et al*., 1993).

From the variation in benthic foraminifera distribution and sediment grain size records collected in the Galicia Mud Deposit, from the NW Iberian peninsula outer continental shelf two main episodes leading to more eutrophic conditions were interpreted (Martins *et al*., 2006). These two periods spanning from ~ ca. 2200-1200 BP and ~ ca. 500-100 BP were characterized by an increased supply of finer sediment highly rich in organic matter and possibly coupled with increased oceanic upwelling. This could have possibly caused higher elemental mercury evasion from the ocean to the surface atmosphere. The two main intervals (~ ca. 2200-1200 BP and ~ ca. 500-100 BP) have been related to occur during two colder periods: the Dark Age Cold Period and the Little Ice Age (Martins *et al*., 2006). In the Nordic sea regions, there are in general good correlations between colder phases and strong northerly winds generated in the Nordic Seas (Bond *et al*., 1992). In the NW Iberian Peninsula the intensity of oceanic upwelling is in general related to the strengthening of northerly winds (Martins *et al*., 2006). The higher productivity and upwelling period around 500 BP could probably be correlated with the high peaks in the mercury isotope record (**Figure 2.9b**) observed at ca. 1779 AD-1723 AD (ca.171 BP-ca. 227 BP, 6-8 cm depth, 5.66 ‰) and ca. 1666 AD-ca. 1609 AD (ca. 284 BP-ca. 341 BP, 10-12 cm depth, 5.00 ‰). Although the increase in gaseous mercury emission during the upwelling period of ca. 500-100 BP is not known in a quantitative sense, if the ocean had acted as the predominant source of mercury to the PV peat bog during that time, it could very well be responsible for the isotopic change observed in the PV record (**Figure 2.9b**).

2.5.3.4 Output from Almaden Mines

Mercury from ore deposits can be released to the atmosphere in various ways. During the periods of mining and related metallurgical activity, roasting and smelting of ores release various mercury species to the atmosphere. Once mines are abandoned the mercury mine wastes, heaps of the low grade ore and enclosing rocks enriched in mercury can release mercury to the atmosphere by continuous degassing (Loredo *et al*., 2007; Rytuba, 2003). The mercury degassing rates from wastes and polluted soils are affected by various factors like soil composition, temperature, sunlight radiation, wind speed etc (Loredo *et al*., 2007). Ore refining by roasting results in short-term, high concentration source of mercury and mine wastes and naturally enriched deposits result in long-term sources of mercury to the atmosphere (Gustin *et al*., 2003). If Hg(II) is the species of mercury that is emitted from roasting of ore, mine waste and pits, and naturally enriched areas then it would impact local ecosystems. If emitted mercury species is Hg

(0), then this will join the atmospheric mercury pool and get broadly transported and dispersed, although there are reports which have shown that it can also get deposited locally and regionally (Gray *et al*., 2004; Gustin *et al*., 2003; Veiga and Hinton, 2002) .

Cinnabar is the dominant ore of mercury in the Almaden but some Hg (0) is also present and in some places inside the deposit it is abundant locally. During ore refining processes, some mercury compounds get reduced to elemental Hg (0) and escape to the atmosphere. Estimates have shown almost 25% of the recovered total mercury from mines can be lost to environment (Hines *et al*., 2000). Mercury degassing rates were observed to be the highest of up to 110μg/m^2h in Almaden mines over the roasted cinnabar banks from past and present mining activity (Ferrara *et al*., 1997). The total mercury flux from the Almaden district represents around 0.1% of the modern global anthropogenic emission rate (Hudson *et al*., 1995). Mining, roasting, and waste disposal processes at mercury mine site have all contributed to local and regional mercury contamination. The contamination could be significant up to a hundred kilometers from the source (Gray *et al*., 2000; Gray *et al*., 2002; Hines *et al*., 2000; Nevado *et al*., 2003).

Mining in the Almaden area had been active since Roman times (approximately 2000 years ago) with almost no interruptions except by mining disasters (floods, fires) or by other factors such as wars and fall of civilizations. During the Roman period (ca. 1932 BP–ca. 1650 BP) of extensive gold extraction between ~18 AD to 300 AD, alchemy was practiced in which cinnabar reacted with oxygen to produce Sulphur dioxide and mercury vapor, both of which were released to the environment (*Cortizas et al*., 1999; *Cortizas et al*., 2002; Sun *et al*., 2006). Evidence of Roman exploitation of mercury is found to be recorded in peat deposits (*Cortizas et al*., 1999, Roos-Barraclough *et al*., 2002) and a recent study on seal hairs (Sun *et al*., 2006). The mercury concentration has been found to decrease between ca.1650-1200 BP (*Cortizas et al*., 1999; Sun *et al*., 2006;) with the fall of the Roman civilization between 300 AD and 750 AD (Brading and Cross, 1972). The Almaden mines were exploited again and for the first time metallurgy got introduced to the Islamic Kingdom (*Cortizas et al*., 1999; Sun *et al*., 2006) spanning a period ~ from ca. 1200-1050 BP (750 – 900 AD). During the Christian Kingdom period of 12th to 15th century (~ca 700-450 BP), new silver mines were discovered in Europe and there was a rise in mercury mining activity due to the silver rush (Sun *et al*., 2006; *Cortizas et al*., 1999). A new way of amalgamation process was first developed in 1554 AD (~400 BP) known as “patio” process in Spanish Mexico (Lacerda, 1997). In the "Patio" process, powdered ore of silver and gold were spread over large, paved flat surfaces and mixed with salt brine, copper and iron pyrites and mercury metal. The amalgamation reaction was set for days to weeks depending on the conditions of the weather. Gold and silver were then recovered from the amalgam through roasting (Brading and Cross, 1972; Fisher, 1977; Mellor, 1952; Nriagu, 1994; Rose, 1915). Especially between ca. 250-150 BP (1700-1800 AD) due to the “patio” amalgamation process, an annual use of mercury of 800-1200 ton/year has been estimated (Sundelin and Eriksson, 2001) and this mercury were mainly came from the Almaden mines. After that period, the mercury mining in Spain declined due to the break out of the early 19th century Independence war of South America (Brading and Cross, 1972; Cortizas *et al*., 1999; Cuadra and Dunkerley, 1991). The third metallurgical revolutions happened in 1940’s and the more efficient cyanidization process replaced mercury amalgamation process. This resulted in lower mercury pollution (Benoit *et al*., 1998) but still there was steep rise in mercury concentrations (Sun *et al*., 2006; Cortizas *et al*., 1999). This is so because since the 1840’s industrial revolution, modern

industries such as chlor-alkali plants, oil refining industries and coal combustion plants became the most important contributors of mercury (Biester *et al*., 2002; Lockhart *et al*., 2000; Pirrone *et al*., 1998; Slemr and Langer, 1992).

The high peaks in the mercury isotope record observed at ca. 1779 AD-1723 AD (ca.171 BP-ca. 227 BP, 6-8 cm depth, 5.66 ‰) and ca. 1666 AD-ca. 1609 AD (ca. 284 BP-ca. 341 BP, 10-12 cm depth, 5.00 ‰) could probably be linked to the period between 1650 AD-1800 AD of the New World where mercury amalgamation "patio" process reached its apogee (**Figure 2.9c**). Fischer (1977) calculated emission factors for the Spanish "patio" process as ~ 1.0 kg of Hg/kg of metal produced. As a consequence of gold and silver mining, the cumulative losses of mercury to the environment totaled ~257400 tonnes (Nriagu, 1994) between 1580 AD-1900 AD Approximately 60-65% of the mercury lost is believed to have been released to the atmosphere (Nriagu, 1994).

2.5.3.5 Correlation of mercury concentration and mercury isotopes

The potential sources of mercury discussed in this study: oceanic upwelling, volcanic eruptions, biomass burning and mining in Almaden since historic times all cause increase in concentration of mercury in the atmosphere. If the isotopic excursions observed have indeed been caused by the different sources and the source related isotopic effects are preserved in the core, then the isotopic record could probably be related to variations in the total mercury concentration of the core. The adjacent peat core investigated by Cortizas, *et al,* 1999 for net accumulation of atmospheric mercury is compared with the isotopic record (**Figure 2.10**). Total mercury was measured by pyrolysis in a 2500 cm peat core sampled at 2 cm intervals in the upper 100 cm and 5 cm intervals below that depth (Cortizas, *et al*., 1999). The isotopic maxima observed between ca.1857 BP- ca.1896 BP (ca. 93 AD- ca. 54 AD), ca.1333BP- ca. 1371 BP (ca. 617AD-ca. 579 AD) and isotopic minima observed between ca.1452 BP-ca. 1469 BP (ca. 498 AD–ca. 481 AD), ca.1485 BP-ca.1512 BP (ca. 465 AD – ca. 449 AD) are unrelated to variations in the total mercury record (**Figure 2.10**). There are no prominent changes in total mercury concentration which can be correlated with the isotopic peaks. The biggest maxima observed from (ca.171 BP-ca. 227 BP) (ca. 1779 AD-1723 AD) and ca. 284 BP-ca. 341 BP (ca. 1666 AD-ca. 1609 AD) corresponds with the "second metallurgical revolution" where "patio" amalgamation process became prevalent for mining gold and silver throughout the world and correlates very well with the two fold increase in mercury concentration in the peat core analyzed by Cortizas, *et al*., 1999. No significant isotope fractionation is observed between ca. 171 BP-present although due to modern industrial output the total concentration of mercury in the bog core is increased by four-five fold (**Figure 2.10**).

2.5.3.6 Correlation of mercury isotopes and various sources

This study was initiated to determine if the recent anthropogenic contribution to environmental mercury could be isotopically distinguished from the dominating natural sources of pre-industrial times. If it could be, the temporal increase in anthropogenic mercury as inferred from the total mercury profile by Cortizas *et al*., 1999 in their Penido Vello peat core section will be corresponded with a change in mercury isotope composition. The mercury isotope record (**Figure 2.2a**) doesn't seem to show such an effect. The top 5 cm of the core dominated by anthropogenic mercury released from coal fire plants, waste incineration, chlor-alkali plants and modern industries seem to share a similar isotopic composition with the lower 10 cm of the core which represents mercury from pre-industrial times (mostly natural). A plausible explanation could be that mercury isotopes do get fractionated differently from natural and anthropogenic

sources, but when the emitted mercury join the atmospheric pool get homogenized quickly (before the average life time of 1 year) and thus in the process are unable to preserve isotopic signatures of individual sources. During coal combustion all of the mercury stored in the coal is released in the form of Hg (0), Hg (II) and Hg (p) (Galbreath and Zygarlicke, 2000. The mercury released into the atmosphere due to coal burning for the last 200 years is essentially the same mercury that has been stored in the peat/coal in pre industrial times. As a result the isotope composition of mercury deposited at the top of the core (represented by mercury stored in coal for thousands of years) is similar to mercury deposited at the bottom of the core. This holds true only if it is assumed that coal combustion does not induce any additional fractionation of the isotopes and source of modern mercury is essentially dominated by coal fired power plants. An alternate third explanation could be the limitations of the technique employed to measure mercury isotopes. The analytical precision of the technique perhaps is insufficient to resolve meaningful isotopic variations that occur in mercury contributed from different sources.

A recent report by Biester *et al*., 2003 demonstrated that biochemical alteration of the peat during humification can strongly influence concentrations and accumulation rates of mercury in peat cores. Due to mercury's strong binding with humic matter, the concentrations of mercury in peat increase as a result of mass losses during peat humification and the temporal changes in mercury concentrations in peat cores do not necessarily reflect the temporal changes in atmospheric mercury fluxes to the bog (Biester *et al*., 2003). Especially in the case of ombrotrophic peatlands, cores which are less humified and degraded tend to overestimate atmospheric mercury accumulation rates compared to peat cores which are more degraded and have lost a large mass due to humification (Biester *et al*., 2003). If mercury is diagenetically mobile during peat humification processes, which is not known, then isotopic consequences need to be taken into consideration. In such a case diagenesis could obliterate any significant isotopic differences between natural and anthropogenic mercury components.

Although the isotopic record does not provide substantial proof for preservation of mercury isotope signatures from individual natural or anthropogenic sources, this in itself does not exclude the possibility of source dependent effects as some small and larger peaks are seen in the profile (**Figure 2.11**). These could have resulted from temporal changes in the percent contributions from various mercury sources due to changes in rates of mercury degassing, or wind factors such as wind direction, speed etc or both. Since any other natural or anthropogenic source of mercury is not known that could have produced the two minima between ca. 498 AD– ca. 481 AD (ca.1452 BP-ca. 1469 BP) and (ca. 465 AD – ca. 449 AD (ca.1485 BP-ca. 1512 BP) it is suggested they are related to emissions from Mt. Vesuvius (**Figure 2.11**). The next prominent peak coinciding with the start of the Germanic Period (approximately 7th century AD) spans from at ca. 617AD-ca. 579 AD (ca.1333BP- ca. 1371 BP). It could be related to the intense vegetation and forest burning with the onset of the Germanic Period. Although the biomass burning continues until the fall of the Visigoths (**Figure 2.9b**) there is no other isotopic variation recorded during that period (**Figure 2.11**). Since there is no other source known to this study, the biomass burning associated with the Visigoth Kingdom provides the best match with the peak in the isotope profile, although the temporal overlap is not exact and so not very convincing. The largest peak observed in the mercury isotope record (**Figure 2.11**) spanning from ca. 1779 AD-1723 AD (ca.171 BP-ca. 227 BP) and ca. 1666 AD-ca. 1609 AD (ca. 284 BP-ca. 341 BP) could have been caused by a number of sources namely : Cluster of volcanic eruptions in Iceland and

Italy; oceanic upwelling in Northwest Iberia and thus higher emission of mercury and lastly the "second metallurgical revolution" where "patio" amalgamation process became prevalent for mining gold and silver throughout the world. It is most likely that the anthropogenic event (related to gold and silver mining worldwide) acted as the predominant source of mercury and thus the large peak in the isotopic profile. Alternatively, the large peaks in the peat record could have been produced by the combined contributions of all the different sources of mercury that are known to us (**Figure 2.11**) during this period. In any case, the correlations of all these sources to the isotopic profile are suggestive and do not necessarily guarantee the fact that source-related isotope signatures are preserved in the Penido Vello peat core. Homogenization and fractionation of mercury isotopes in the atmosphere or other environmental compartments has probably erased whatever isotopic signatures were impressed on mercury at point of its emission. If the correlation with the sources as mentioned above is indeed present, then the possible explanation for it would be that there has been partial preservation of relict isotopic signatures inherited from these individual sources.

2.6 Conclusions

An ombrotrophic peat bog from Penido Vello, NW Spain has been analyzed for mercury and oxygen isotopes. The mercury results conducted on bulk peat provide the first detailed record of changes in isotopic composition of mercury preserved in a peat bog during the past 2200 years. The oxygen isotope study examines the relationship between changes in oxygen isotopes recorded in bulk cellulose and climate change in NW Iberian peninsula.

The mechanistic models linking isotope composition of modern cellulose to isotope compositions of source water (precipitation in case of Penido Vello) do not seem to be applicable in the present study. Furthermore peat-based paleoclimate reconstruction on oxygen isotope data needs to be carried out at the species level, and interpretations of previous studies using bulk cellulose should be considered with caution. Roman warming period (RWP) and Dark Ages Cold Period (DACP) do not seem to be well preserved in the bulk cellulose oxygen isotope record of Penido Vello peat core (**Figure 2.7**). On the other hand Medieval Warm period (MWP), Little Ice Age (LIA) and Recent Warming seems to be more prominent in the oxygen isotope record. A period of drought between ca. 563 AD-ca.587 AD (ca. 1387 BP-ca.1363 BP), two humid events between ca. 1268 AD-ca. 1325 AD (ca. 682 BP-ca. 625 BP) and (ca. 1810 AD-ca. 1860 AD) reported previously by Mighall *et al*., 2006 are observed in the oxygen isotope record. The warming episode (ca. 1750 AD-ca. 1800 AD) and the last cooling period in the LIA record (ca. 1800 AD-ca. 1850 AD) reported by Fischer *et al*. (1999) coincides well with the peat cellulose oxygen isotope record by showing substantial increase and subsequent decrease in isotopic ratios (**Figure 2.7**).

The isotopic composition of mercury in the top 5 cm of the core dominated by anthropogenic mercury released from modern industries (coal burning power plants, chlor-alkali plants etc.) is very similar to the isotopic composition of mercury from the bottom 10 cm of the core which represents mercury from pre-industrial times (mostly natural). The most plausible explanation is that the mercury emitted from modern industrial sources mostly in the form of Hg (0) joins the atmospheric pool of mercury vapor and get homogenized quickly before the average life time of 1 year. In the process of homogenization in atmosphere and deposition in the bog, the isotopic

signatures of individual sources are not preserved. A second explanation could be that since coal combustion releases all the mercury that has accumulated in the coal for thousands of years, essentially most of the modern anthropogenic mercury is representative of pre-industrial mercury, thus showing no difference in isotopic composition.

Temporal variations in the mercury isotope record over the past 2200 years were linked to various natural and anthropogenic sources. The two minima observed between ca. 498 AD–ca. 481 AD (ca.1452 BP-ca. 1469 BP) and (ca. 465 AD – ca. 449 AD (ca.1485 BP-ca. 1512 BP) were related to emissions from Mt. Vesuvius in 472 AD and 512 AD (**Figure 2.11**). The next prominent peak which probably coincides with the start of the Germanic Period (approximately 7th century AD) spans from ca. 617AD-ca. 579 AD (ca.1333BP- ca. 1371 BP) and is thought to be related to the intense vegetation and forest burning activity by the Visigoths (**Figure 2.11**). The largest peak observed in the mercury isotope record spanning from ca. 1779 AD-1723 AD (ca.171 BP-ca. 227 BP) and ca. 1666 AD-ca. 1609 AD (ca. 284 BP-ca. 341 BP) is probably caused by combination of natural and anthropogenic sources namely: volcanic eruptions in Iceland and Italy; higher oceanic productivity in the Northwest Iberia continental shelf and lastly the "second metallurgical revolution" where "patio" amalgamation process became prevalent for mining gold and silver throughout the world. Separating the percent contributions of any of these sources is beyond the scope of this study. The correlation of all these sources to the isotopic profile is suggestive and not conclusive. No meaningful paleoclimate information was obtained from the isotopic variations of mercury.

Table 2.1 Radiocarbon dates for bulk peat cellulose (from WHOI) for different depths at the Penido Vello peat bog (NW Iberian Pensinsula, Spain)

Depth (cm)	Age (BP)
9cm	> Mod
33cm	938±30
47cm	1363±25
63cm	1493±35
99cm	2183±25

Table 2.2 Mercury isotope $\delta^{198}Hg/^{202}Hg$ (‰) values for bulk peat samples from the Penido Vello peat core.

Sample	Depth (cm)	$\delta\ ^{198}Hg/^{202}Hg$	
		Average	2SE
Vegetation		4.06	0.04
Interface	0	3.79	0.03
0-2A	1	4.02	0.04
0-2B	1	3.97	0.02
0-2C	1	3.92	0.04
2-4	3	4.35	0.08
4-6*	5	3.95	0.02
6-8A	7	5.66	0.05
6-8B	7	5.58	0.06
10-12	11	5.00	0.06
12-14	13	4.13	0.03
14-16*	15	4.45	0.05
16-18	17	3.66	0.03
20-22*	21	4.24	0.04
22-24	23	3.77	0.07
26-28*	27	3.66	0.03
30-32	31	4.12	0.05
32-34	33	3.79	0.03
34-36	35	3.61	0.05
38-40	39	3.73	0.07
42-44	43	4.38	0.04
44-46	45	4.11	0.06
46-48*	47	5.26	0.06
50-52	51	3.52	0.04
54-56	55	4.16	0.04
56-58	57	3.78	0.04
58-60	59	2.97	0.05
62-64	63	2.97	0.04
64-66	65	4.26	0.04
66-68	67	3.44	0.04
70-72	71	4.12	0.04
74-76	75	4.08	0.05
78-80	79	3.66	0.03
82-84	83	4.53	0.03
84-86	85	3.74	0.06
86-88	87	4.07	0.04
90-92	91	4.05	0.04
92-94	93	3.80	0.05
94-96	95	3.42	0.09
96-98	97	3.25	0.06

*The internal precision of each measurement was calculated as the 2SE of the mean of n runs, where n=50, or multiples of 50 for larger samples. Samples indicated with an * correspond to samples for which replicate runs were not possible due to constraints on available sample mass and the errors represent internal precision from 50 scans of a single analysis.*

Table 2.3 Oxygen $\delta^{18}O$ (‰) values measured on bulk peat cellulose of the PV peat core

Sample	Depth (cm)	$\delta^{18}O$ (‰) Average	2SD
Vegetation		22.5	0.3
Interface	1	23.7	
2-4	3	22.3	1.5
4-6	5	17.6	0.5
6-8	7	22.9	0.7
10-12	11	20.4	1.0
12-14	13	17.9	1.3
14-16	15	20.2	0.3
16-18	17	20.3	0.2
18-20	19	14.4	0.3
20-22	21	20.1	1.0
22-24	23	17.4	0.2
24-26	25	23.8	0.8
26-28	27	21.1	0.8
28-30	29	24.7	1.8
30-32	31	22.2	0.3
32-34	33	24.0	0.5
34-36	35	20.4	0.6
36-38	37	22.0	0.6
38-40	39	24.3	0.6
42-44	43	21.6	1.1
44-46	45	22.1	0.1
46-48	47	22.8	0.4
48-50	49	24.9	0.4
52-54	53	21.1	1.5
54-56	55	17.0	0.2
58-60	59	17.8	0.2
60-62	61	20.7	1.4
62-64	63	20.0	0.4
64-66	65	21.3	0.2
66-68	67	21.6	0.3
68-70	69	21.3	0.3
70-72	71	18.9	0.2
74-76	75	19.5	1.0
76-78	77	24.5	1.0
78-80	79	22.2	2.1
80-82	81	23.7	1.7
82-84	83	17.4	0.6
84-86	85	20.5	1.5
86-88	87	18.7	0.3
88-90	89	20.4	0.8
90-92	91	16.6	0.4
92-94	93	26.4	0.4
94-96	95	23.4	1.1
96-98	97	17.0	0.4
98-100	99	19.8	1.8

The reported δ values for individual peat samples are the mean of δ values obtained from replicate analysis (varied from 4-10 depending on sample volume) and the reported uncertainty is the external reproducibility (±2 SD) on the mean

Table 2.4 Average monthly values of $\delta^{18}O$ (‰) precipitation, amount of precipitation, temperature & relative humidity for the IAEA sites La Coruna and Santander for 2000 to 2004.

LA CORUNA (0800101, Spain, 43° 22' 00" / -8° 25' 00" / 57m)						
Month	$\delta^{18}O$ (‰)	Precipitation (mm)	Temperature (ºC)	Water vapor pressure	Saturated vapor pressure	Relative Humidity (calculated)
January	-5.65	112	11.1	10.1	11.89	85
February	-4.58	65	11.5	10.1	12.20	83
March	-5.24	82	12.8	10.9	13.25	82
April	-5.51	96	12.8	10.7	13.25	81
May	-4.03	58	15.1	12.8	15.36	83
June	-4.89	41	18	15.2	18.50	82
July	-4.19	49	18.8	17	19.47	87
August	-4.01	50	20	18.1	21.03	86
September	-4.49	46	18.9	16.3	19.60	83
October	-5.41	179	16	14.1	16.27	87
November	-6.57	175	12.9	11.5	13.34	86
December	-5.50	118	11.6	10.6	12.27	86
SANTANDER (0802301, Spain, 43° 28' 60" / -3° 47' 60" / 52m)						
Month	$\delta^{18}O$ (‰)	Precipitation (mm)	Temperature (ºC)	Water vapor pressure	Saturated vapor pressure	Relative Humidity (calculated)
January	-6.11	93	10.8	9.6	11.66	82
February	-5.45	66	10.8	10	11.66	86
March	-7.18	68	12.1	11.1	12.67	88
April	-5.51	92	12.6	11.4	13.09	87
May	-3.2	54	14.5	13.7	14.78	93
June	-3.71	42	17.7	17.1	18.15	94
July	-4.12	52	19	18.4	19.72	93
August	-4.30	69	20.6	19.8	21.85	91
September	-4.95	91	18.7	17.4	19.35	90
October	-6.48	129	16.8	14.3	17.13	83
November	-6.66	136	12.9	11.7	13.34	88
December	-6.82	113	11.6	10.1	12.27	82

The relative humidity has been calculated from the water vapor pressure and temperature data provided by IAEA/GNIP and saturated water vapor pressure data from Donald 1994

Table 2.5 Mean annual values of $\delta^{18}O$ (‰) precipitation, amount of precipitation, temperature & relative humidity for the IAEA sites La Coruna and Santander for 2000 to 2004.

LA CORUNA (0800101, Spain, 43° 22' 00" / -8° 25' 00" / 57m)						
Year	Mean $\delta^{18}O$ (‰)	Sum Precipitation (mm)	Mean Temperature (ºC)	Mean Water vapor pressure	Saturated vapor pressure	Relative Humidity (calculated)
2000	-5.16	1274	14.9	12.8	15	84
2001	-5.25	1082.8	14.8	12.7	15	84
2002	-4.50	1142.5	15	13.6	15	89
2003	-6.00	1182.1	15.2	13.5	15	87
2004	-4.18	672.3	15	13.1	15	86
SANTANDER (0802301, Spain, 43° 28' 60" / -3° 47' 60" / 52m)						
Year	Mean $\delta^{18}O$ (‰)	Sum Precipitation (mm)	Mean Temperature (ºC)	Mean Water vapor pressure	Saturated vapor pressure	Relative Humidity (calculated)
2000	-5.33	1166.8	14.7	13.6	15	91
2001	-5.73	808.9	14.8	13.3	15	88
2002	-5.26	936.4	14.9	13.6	15	90
2003	-5.39	1020.6	15.3	14.3	16	92
2004	-5.10	1084.4	14.5	13.8	15	93

Table 2.6 $\delta^{18}O$ (‰) values of precipitation from IAEA GNIP stations and estimated $\delta^{18}O$ (‰) value of precipitation from modern bulk peat cellulose

Sample Site	Latitude	Longitude	Year	Average $\delta^{18}O$ precipitation
La Coruna*	43.37	-8.42	2000	-5.88
La Coruna	43.37	-8.42	2001	-5.65
La Coruna	43.37	-8.42	2002	-4.95
La Coruna	43.37	-8.42	2003	-6.84
La Coruna	43.37	-8.42	2004	-4.00
Santander*	43.48	-3.8	2000	-5.95
Santander	43.48	-3.8	2001	-6.09
Santander	43.48	-3.8	2002	-5.37
Santander	43.48	-3.8	2003	-6.22
Santander	43.48	-3.8	2004	-5.23
Penido Vello	43.63	-7.61		
Sample	Humidity	f	ε_b	Calculated Average $\delta^{18}O$ precipitation**
Vegetation (Penido Vello)***	**1.00**	**0.3**	**27**	**-4.46**
	0.95	**0.3**	**27**	**-5.79**
	0.90	0.3	27	-7.11
	0.85	0.3	27	-8.43
	0.80	0.3	27	-9.76

Table 2.6 continued

Sample	Humidity	*f*	ε_b	Calculated Average $\delta^{18}O$ precipitation**
Vegetation (Penido Vello)	1.00	0.3	25	-2.46
	1.00	0.3	26	-3.46
	0.95	0.3	25	-3.79
	0.95	**0.3**	**26**	**-4.79**
	0.90	**0.3**	**25**	**-5.11**
	0.90	**0.3**	**26**	**-6.11**
	0.85	**0.3**	**25**	**-6.43**
	0.85	0.3	26	-7.43
	0.80	0.3	25	-7.76
	0.80	0.3	26	-8.76
	1.00	**0.0**	**27**	**-4.46**
	1.00	**0.1**	**27**	**-4.46**
	1.00	**0.2**	**27**	**-4.46**
	0.95	**0.0**	**27**	**-6.35**
	0.95	**0.1**	**27**	**-6.16**
	0.95	**0.2**	**27**	**-5.98**
	0.90	0.0	27	-8.24
	0.90	0.1	27	-7.87
	0.90	0.2	27	-7.49
	0.95	**0.0**	**26**	**-5.35**
	0.95	**0.1**	**26**	**-5.16**
	0.95	**0.2**	**26**	**-4.98**
	0.95	**0.0**	**25**	**-4.35**
	0.95	**0.1**	**25**	**-4.16**
	0.95	0.2	25	-3.98
	0.90	0.0	26	-7.24
	0.90	0.1	26	-6.87
	0.90	**0.2**	**26**	**-6.49**
	0.90	**0.0**	**25**	**-6.24**
	0.90	**0.1**	**25**	**-5.87**
	0.90	**0.2**	**25**	**-5.49**
	0.85	0.0	26	-9.13
	0.85	0.1	26	-8.57
	0.85	0.2	26	-8.00
	0.85	0.0	25	-8.13
	0.85	0.1	25	-7.57
	0.85	0.2	25	-7.00
	0.80	0.0	26	-11.02
	0.80	0.1	26	-10.27
	0.80	0.2	26	-9.51
	0.80	0.0	25	-10.02
	0.80	0.1	25	-9.27
	0.80	0.2	25	-8.51

** Sites closest to the Penido Vello bog site sharing the same latitude*

*** Estimation done by using equation (2) in text. See text for more details*

**** Vegetation on the surface of the peat core chosen as representative of modern peat cellulose*

Table 2.7 Volcanic eruptions which possibly acted as natural sources of mercury to the Penido Vello peat core

Year	Volcano	Location	VEI	Abbreviation
1947 AD	Hekla	S Iceland	4	H
1918 AD	Katla	S Iceland	4	Ka
1902 AD	Grimsvotn	NE Iceland	4	G
1875 AD	Askja	NE Iceland	4	As
1875 AD	Vesuvius	Italy	4	Ve
1873 AD	Grimsvotn	NE Iceland	4	G
1845 AD	Hekla	S Iceland	4	H
1787 AD	Etna	Italy	4	Et
1783 AD	Grimsvotn	NE Iceland	4	G
1766 AD	Hekla	S Iceland	4	H
1755 AD	Katla	S Iceland	4+	Ka
1727 AD	Oraefajokull	SE Iceland	4	O
1721 AD	Katla	S Iceland	4+	Ka
1693 AD	Hekla	S Iceland	4	H
1660 AD	Katla	S Iceland	4	Ka
1631 AD	Vesuvius	Italy	4	Ve
1625 AD	Katla	S Iceland	4	Ka
1597 AD	Hekla	S Iceland	4	H
1510 AD	Hekla	S Iceland	4	H
1490? AD	Katla	S Iceland	4+	Ka
1477 AD	Bardarbunga	NE Iceland	5?	B
1416 AD	Katla	S Iceland	4?	Ka
1362 AD	Oraefajokull	SE Iceland	5	O
1357 AD	Katla	S Iceland	4	Ka
1311 AD	Katla	S Iceland	4?	Ka
1300 AD	Hekla	S Iceland	4	H
1179 AD	Krafla	NE Iceland	4?	Kr
1158 AD	Hekla	S Iceland	4	H
1104 AD	Hekla	S Iceland	5	H
1000? AD	Katla	S Iceland	4	Ka
934 AD	Katla	S Iceland	4	Ka
934 AD	Eldgja	S Iceland	4	El
512 AD	Vesuvius	Italy	4?	Ve
472 AD	Vesuvius	Italy	4	Ve
79 AD	Vesuvius	Italy	6	Ve
122 BC	Etna	Sicily	4?	Et
183 BC	Vulcano	Italy	4	Vu

All the ages of eruption and Volcano eruption index (VEI) compiled from Simkin and Siebert 1994 and Zielinski et al 1994

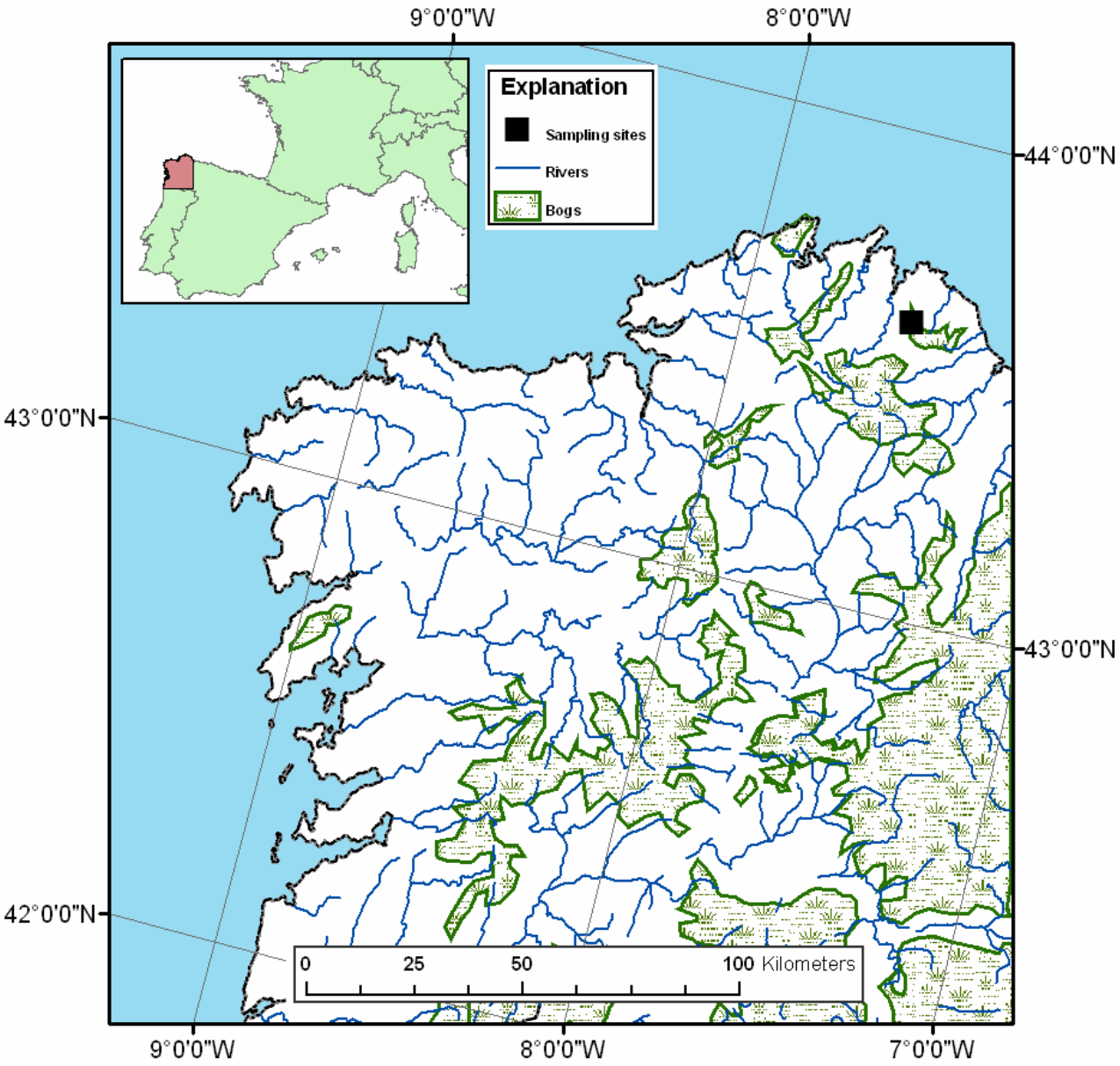

Figure 2.1 Location of sampling sites. The peat core sampled by Cortizas et al., 1997 and sampled for the current study are adjacent cores (meter scale).

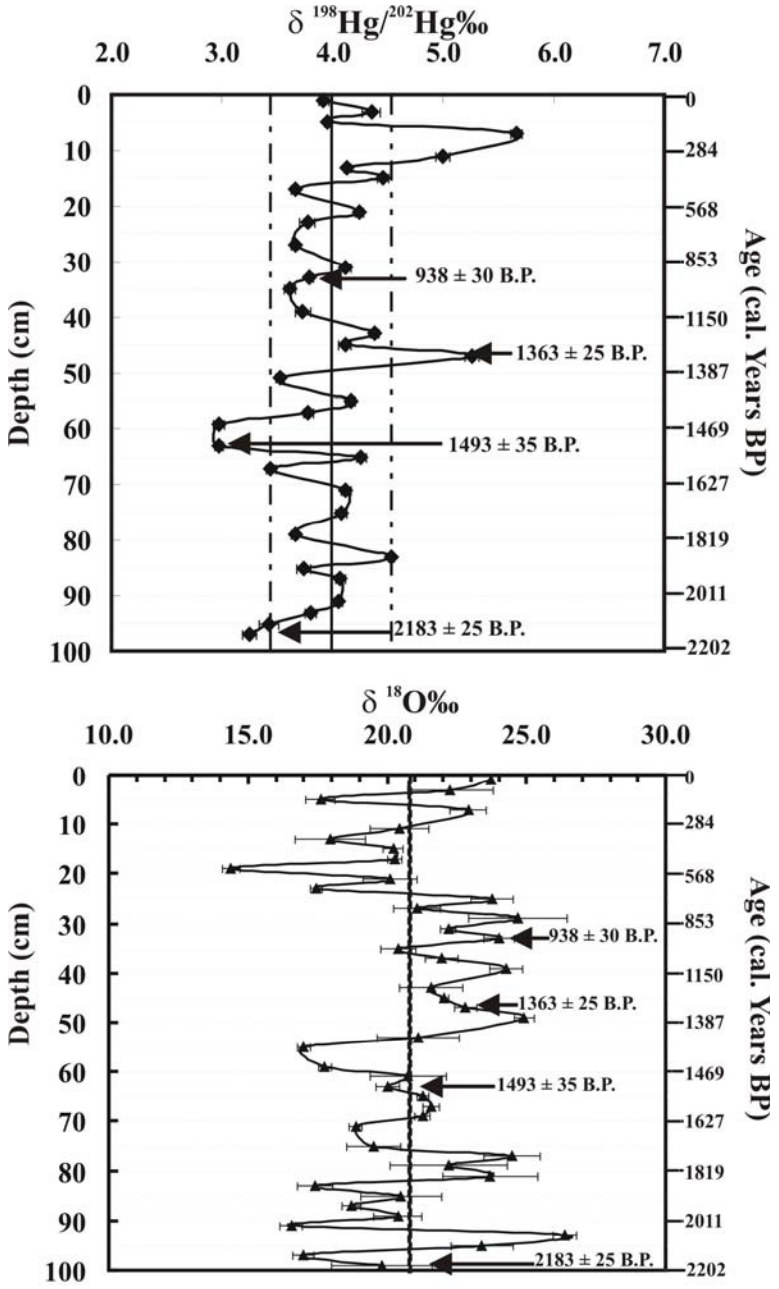

Figure 2.2 Variations in (a) $\delta^{198}Hg/^{202}$ Hg ‰ values measured on bulk peat and (b) $\delta^{18}O$ ‰ values measured on bulk peat cellulose with depth in the Penido Vello peat core down to 100 cm. The ^{14}C dated ages are marked inside the figure . The RHS age scale (calibrated years BP) is obtained by interpolation of ^{14}C dated horizons. For Hg, the internal precision of each analysis was calculated as the 2 SE of the mean of n runs, where n = 50, or multiples of 50 for larger samples For O_2 the error bars represent ±2SD on replicate runs (min. 4 to max. of 10). The bold line in (a) represents the overall average of Penido Vello peat core which is 3.99‰ and the dashed lined represents the 2σ error bar calculated from replicate runs of Almaden cinnabar of 0.55‰. The dotted line in (b) represents the overall average of the measured $\delta^{18}O_{cellulose}$ for the entire peat core profile, which is, 20.9 ‰.

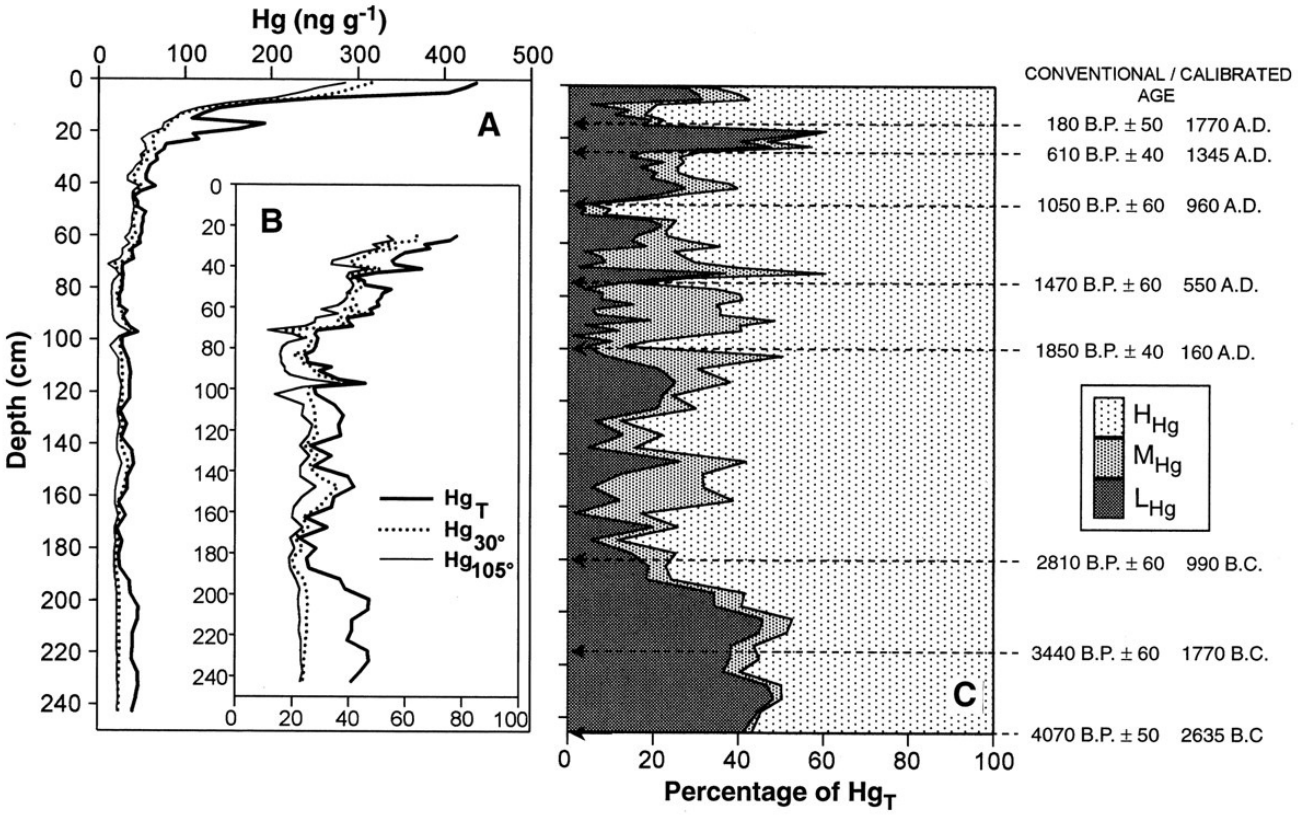

Figure 2.3 Mercury concentrations in the peat bog of Penido Vello analyzed by Cortizas *et al*., 1999. (A) Concentrations analyzed in wet peat are denoted by Hg_T and dried samples denoted by $Hg_{30°}$ and $Hg_{105°}$. (B) Magnified section of the core with mercury concentrations for peat samples below 25 cm. (C) Thermal stability of Hg: L_{Hg}, percentage of Hg lost at 30°C; M_{Hg}, percentage of Hg lost between 30° and 105°C; H_{Hg}, percentage of Hg retained by the peat after drying at 105°C. Radiocarbon and calibrated ages are also shown (Cortizas *et al*., 1999).

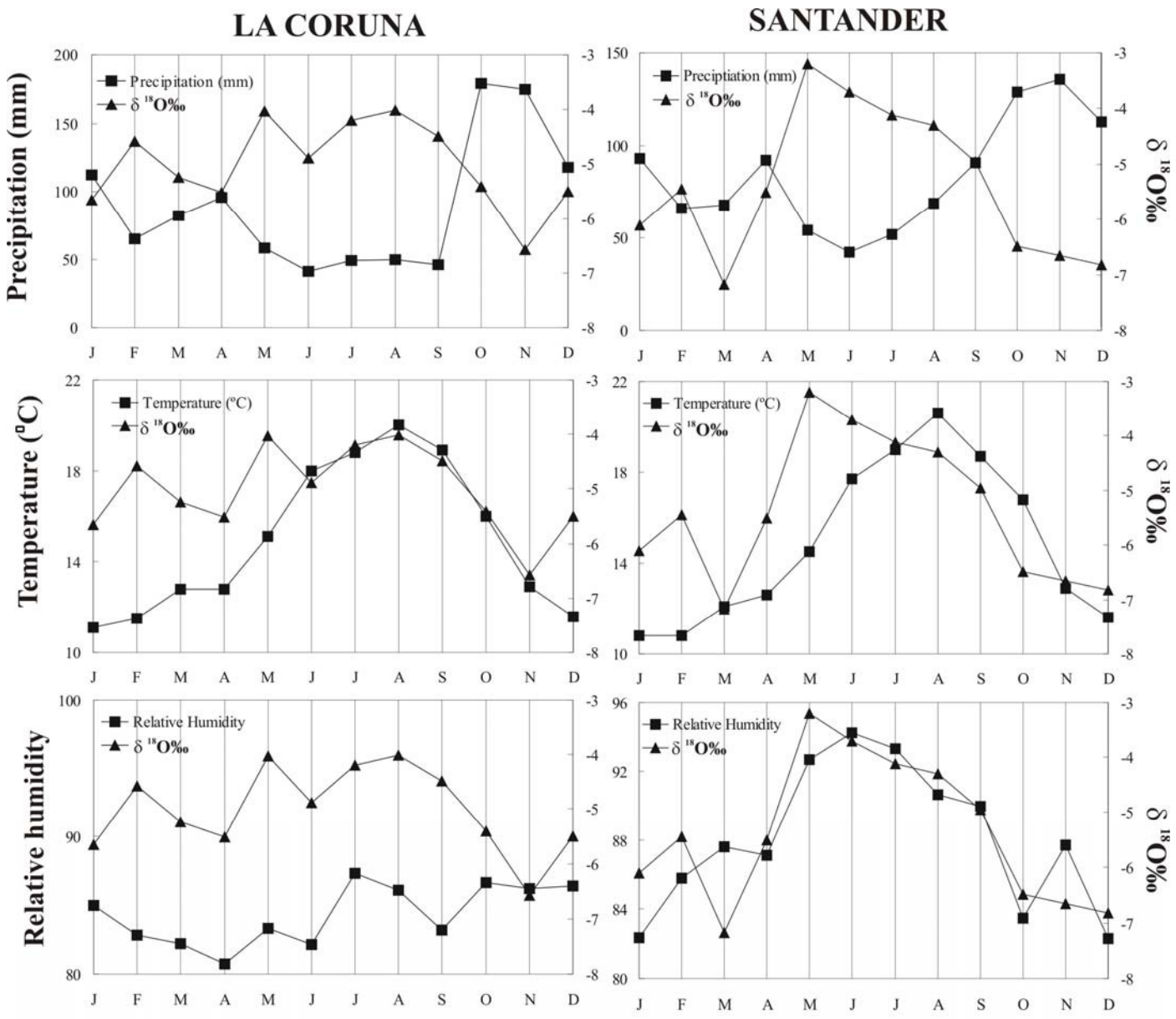

Figure 2.4 Comparisons of the averages of monthly precipitation (mm), monthly mean temperature(ºC) and monthly relative humidity from 2000 to 2004 with the averages of monthly $\delta^{18}O$(‰) values of precipitation for the IAEA meteorological sites La Coruna and Santander.

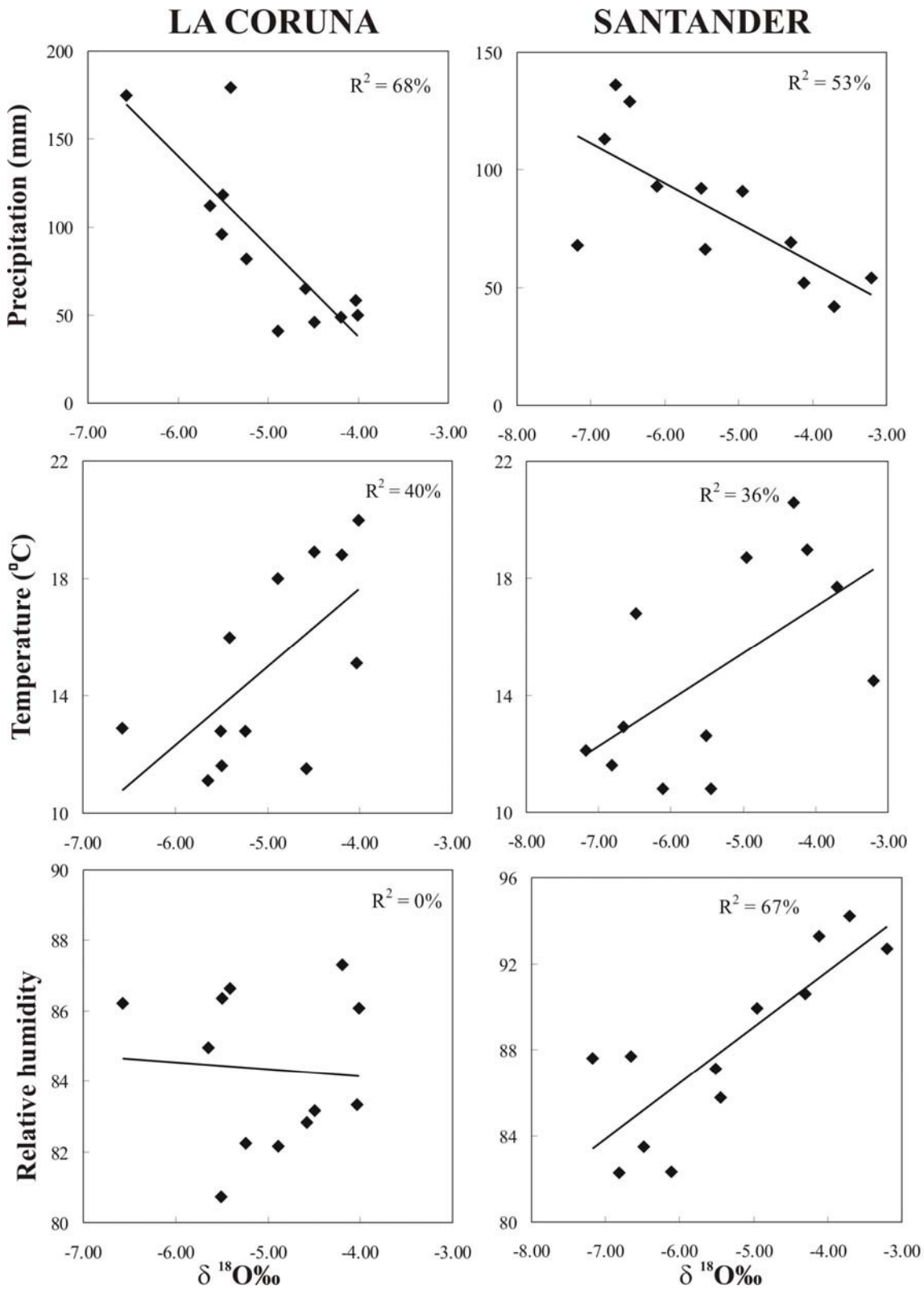

Figure 2.5 Linear correlations of the averages of monthly precipitation (mm), monthly mean temperature(ºC) and monthly relative humidity from 2000 to 2004 with the average monthly $\delta^{18}O$(‰) values of precipitation for the IAEA meteorological sites La Coruna and Santander.

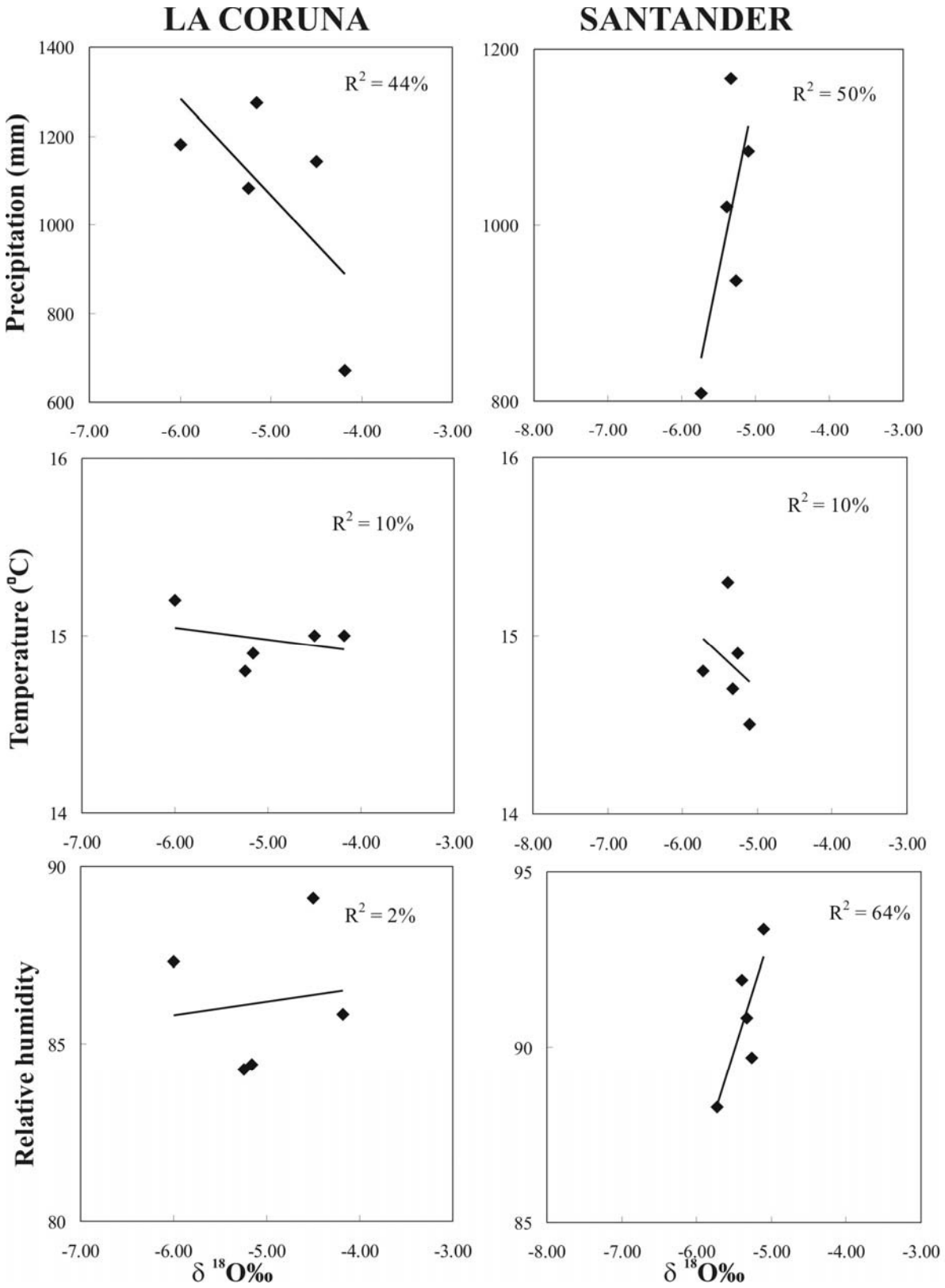

Figure 2.6 Linear correlations of the averages of annual precipitation (mm), annual mean temperature(ºC) and annual relative humidity from 2000 to 2004 with the annual average $\delta^{18}O$(‰) values of precipitation for the IAEA meteorological sites La Coruna and Santander.

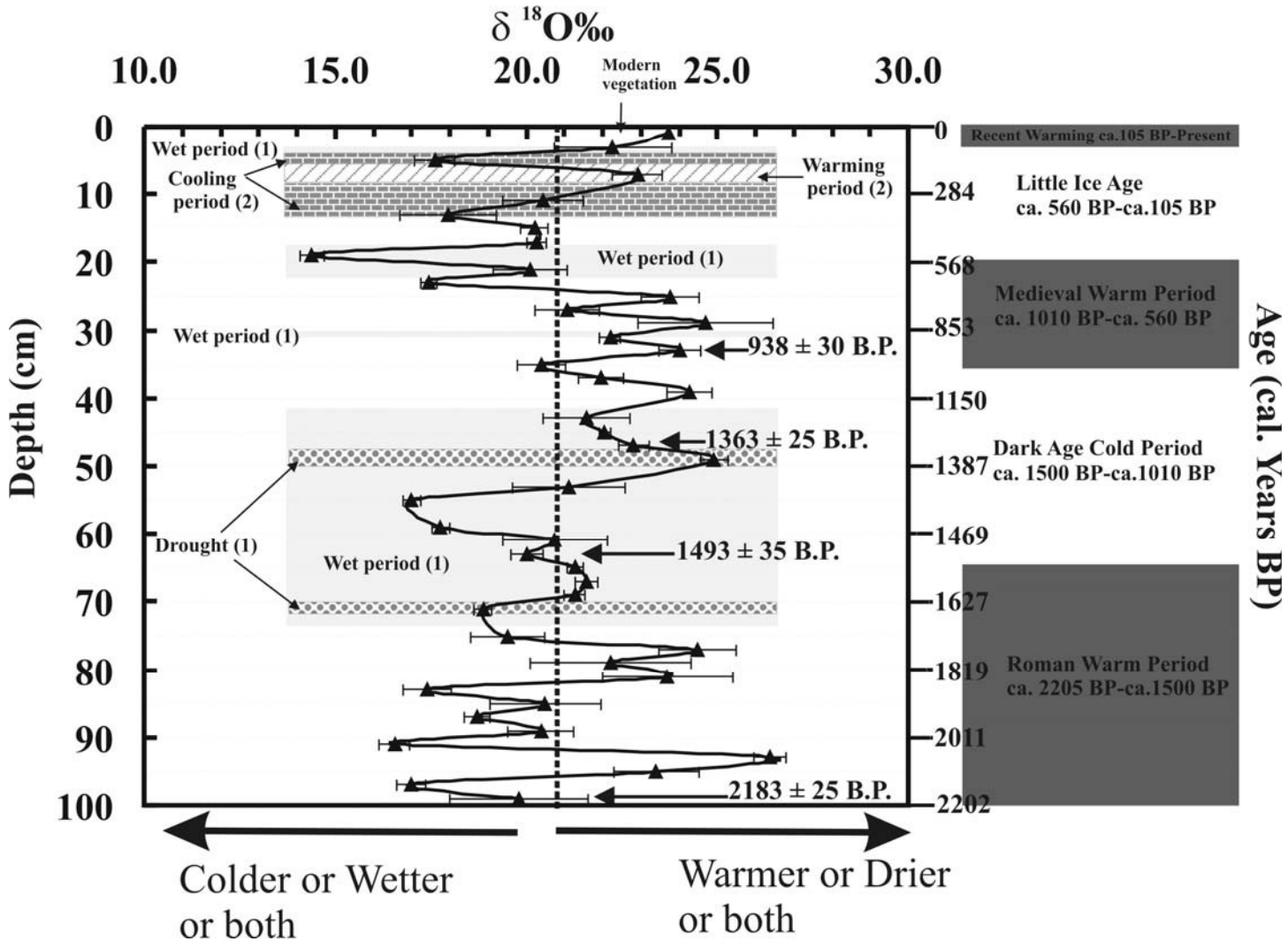

Figure 2.7 A comparison between $\delta^{18}O$ ‰ of bulk peat cellulose measured in the Penido Vello peat core and climatic reconstructions from previous records, 1= Mighall et al., 2006; 2= Fisher et al., 1999. Solid lines represent three-point running means.

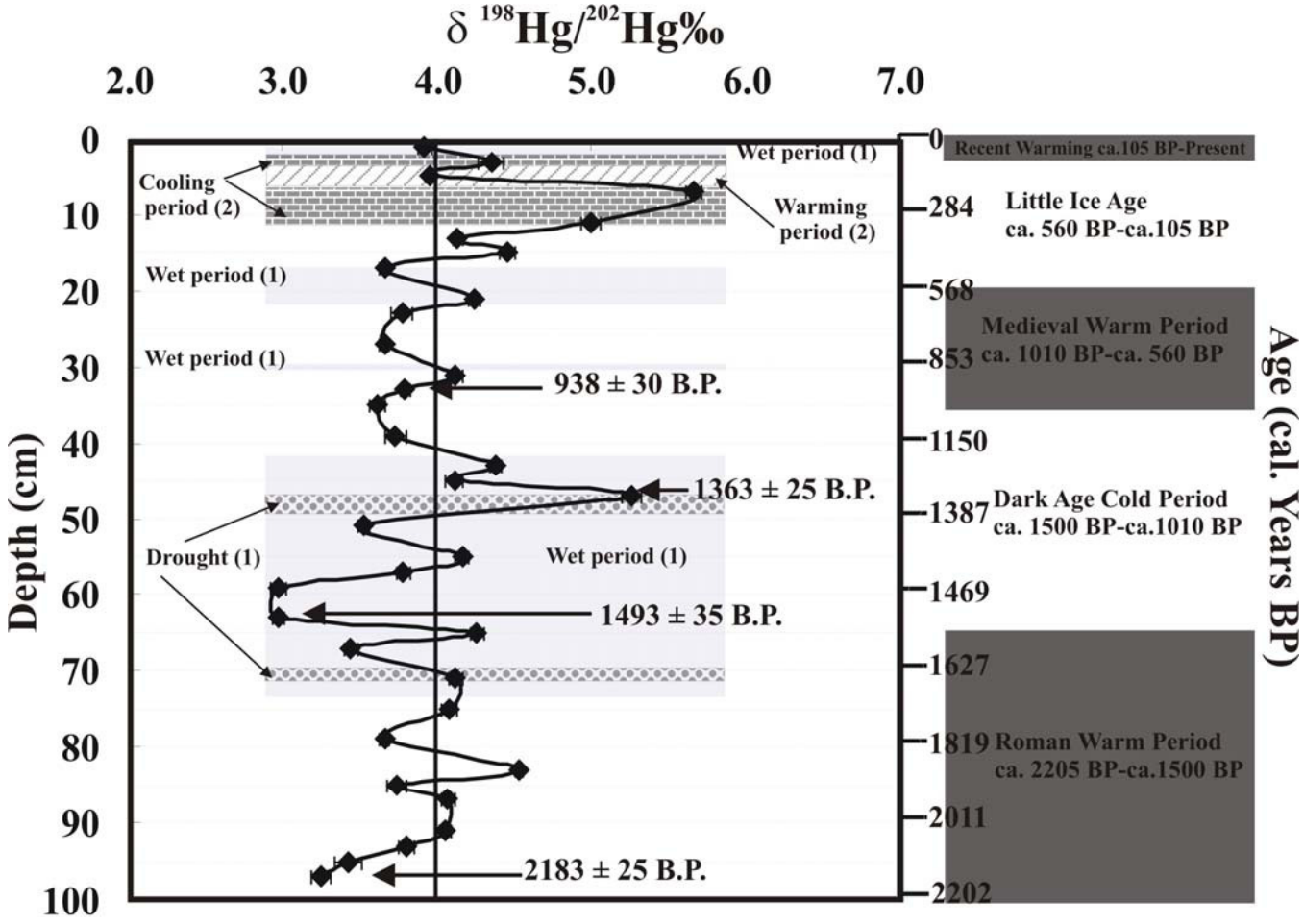

Figure 2.8 . A comparison between $\delta^{198}Hg/^{202}$ Hg ‰ of bulk peat measured in the Penido Vello peat core and climatic reconstructions from previous records, 1= Mighall et al., 2006; 2= Fisher et al., 1999.

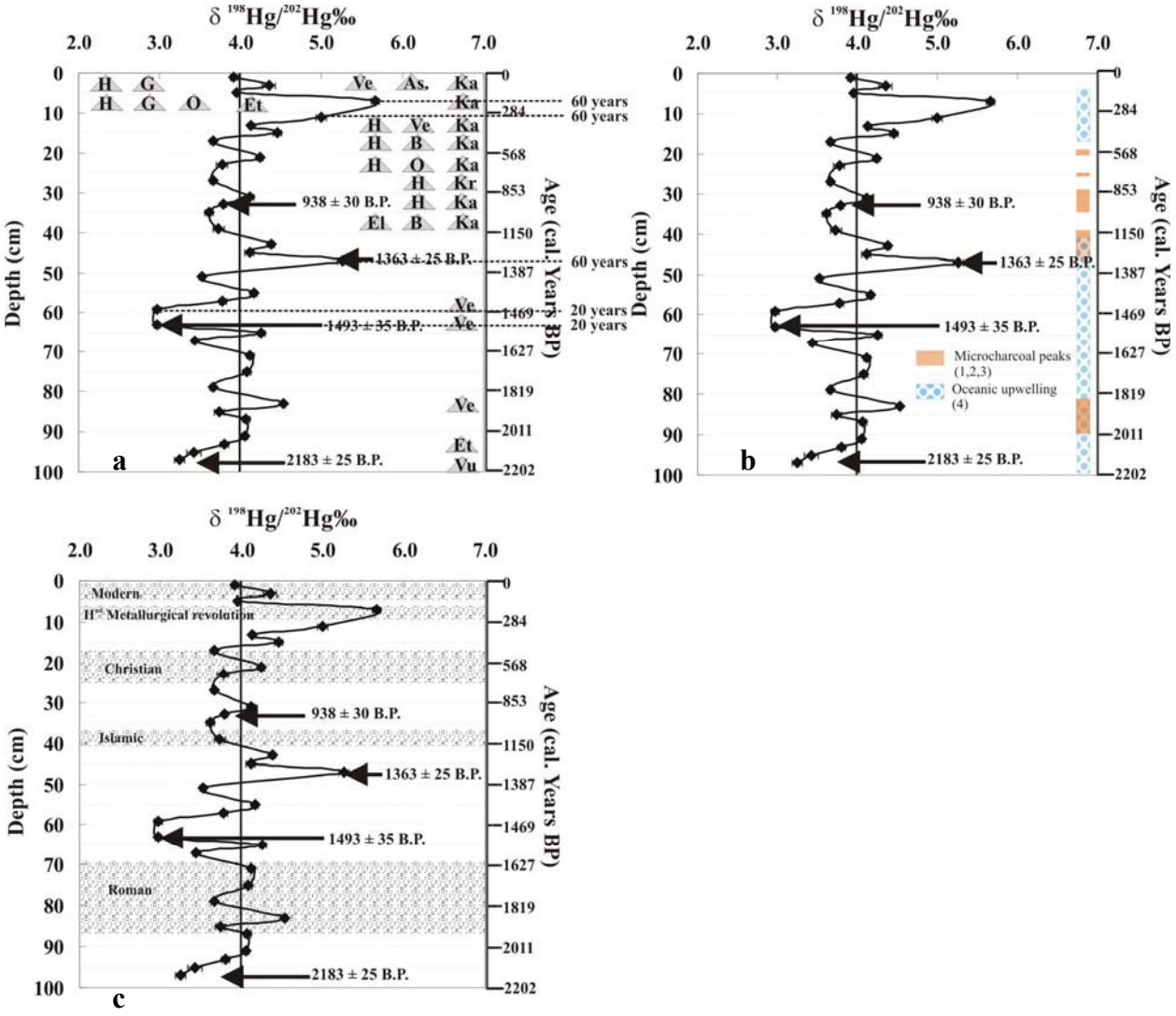

Figure 2.9 Comparison of $\delta^{198}Hg/^{202}$ Hg ‰ isotope profile of the Penido Vello peat core with probable mercury emission sources (a) Volcano eruptions in Italy and Iceland compiled from Simkin and Siebert, 1994 and Zielinski et al., 1994; As= Askja, B= Bardarbunga, El= Eldgja, Et= Etna, G= Grimsvotn, H= Hekla, Ka= Katla, Kr= Krafla, O= Oraefajokull, Ve= Vesuvius and Vu=Vulcan; the time resolution of relevant peaks vary from 20-60 years (b) Microcharcoal peak records in NW Iberia and oceanic upwelling periods in NW Iberian continental shelf, 1= Martinez-Cortizas et al., 2005; 2= Mighall et al., 2006; 3= Santos et al., 2000; 4= Martins et al., 2006, the microcharcoal peaks probably indicate biomass burning and (c) main historic phases of mercury exploitation in Spain.

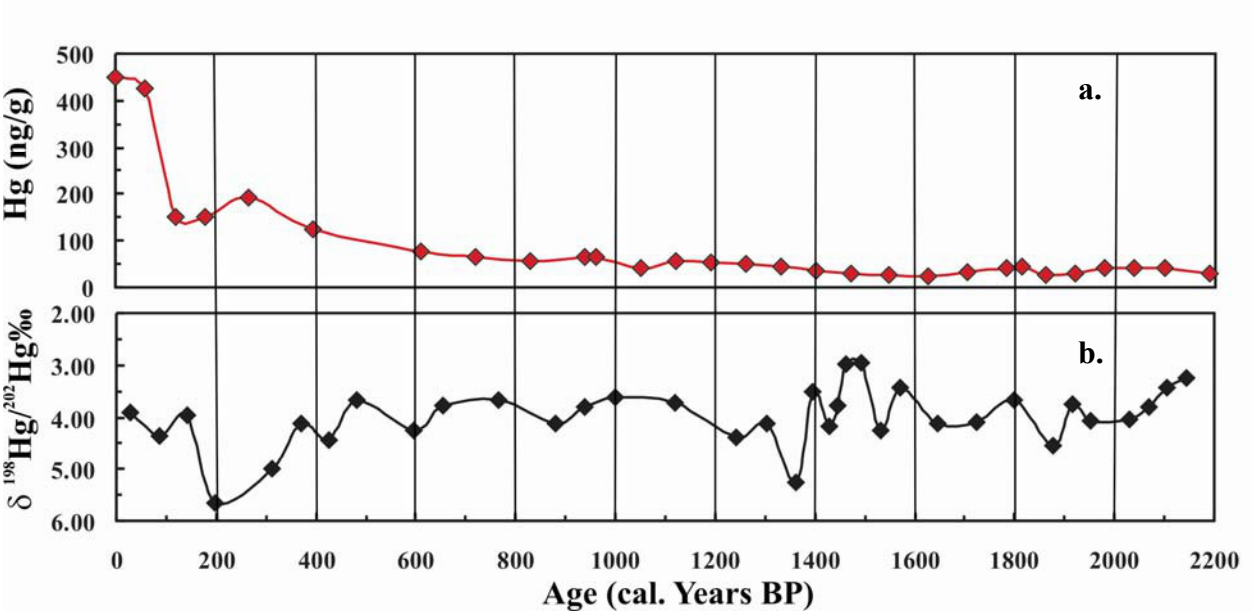

Figure 2.10 Comparison of (a) the total mercury concentration profile (ng/g) of an adjacent peat core (Cortizas et al., 1999) with the (b) mercury isotope profile of the peat core from the present study versus calibrated year BP.

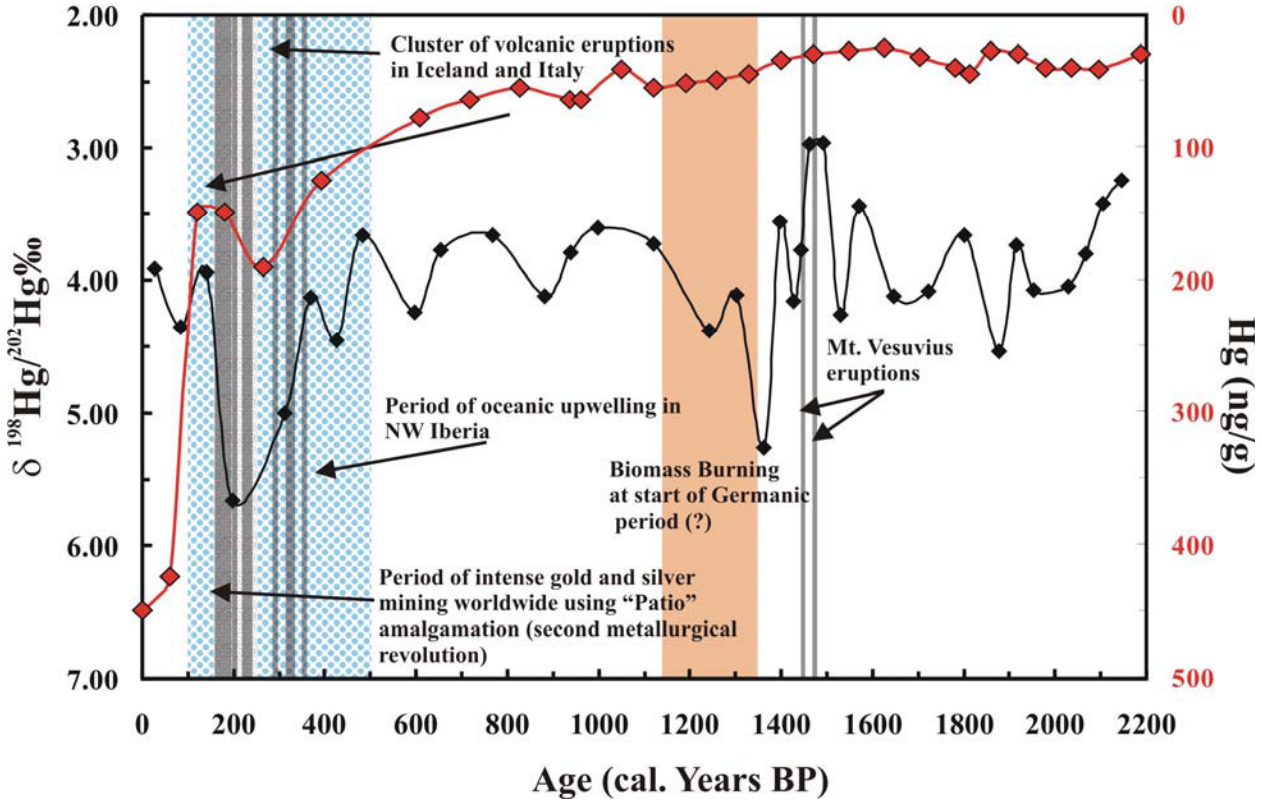

Figure 2.11 Chronology of mercury isotope ($\delta^{198}Hg/^{202}$ Hg ‰) (black diamonds) variation at Penido Vello peat core and known events which could have acted as sources of mercury to the bog since the last 2200 years. The total mercury concentration profile (ng/g) (red diamonds) from an adjacent peat core (Cortizas *et al*., 1999) is plotted for comparison

CHAPTER 3

MASS INDEPENDENT FRACTIONATION OF MERCURY ISOTOPES IN THE ENVIRONMENT

3.1 Introduction

Mercury is a global scale pollutant. Although it is well understood that atmospheric deposition plays a cardinal role in the global mercury cycle (Fitzgerald, 1995; Morel *et al*., 1998; Mason and Sheu, 2002) and that anthropogenic contributions to the annual atmospheric budget rival those of natural processes, crucial details of the mercury cycle and its fluxes are still uncertain. Mercury has seven stable isotopes (^{196}Hg, ^{198}Hg, ^{199}Hg, ^{200}Hg, ^{201}Hg, ^{202}Hg, ^{204}Hg), with a mass range of >3%, of which six are sufficiently abundant (7-30%) for precise measurement. Attempts at Hg isotope measurement have been limited by its high volatility, high first ionization potential, and ubiquitous contamination in mass spectrometers, until the recent advent of multi-collector ICP-MS. With new analytical techniques, variations in the isotopic composition of environmental mercury will become a powerful tool in constraining models of the mercury cycle.

Nearly a century ago, Bronsted and von Hevesy (1920) reported that they had achieved a partial separation of mercury isotopes by evaporation at low pressure. Nier (1950) suggested that the inability of researchers to obtain the same values for the isotopic composition of mercury might be due partly to real differences in isotope composition between the mercury reagents used. In recent years, several workers have reported variations in the isotopic composition of mercury of up to -5.5‰ (δ^{198}Hg/^{202}Hg relative to NIST SRM 3133) in hydrothermal ore deposits (Hintelmann and Lu 2003; Smith *et al*., 2005); -1‰ to +4 ‰ in sediments (Foucher and Hintelmann, 2006); relative variation of 2 ‰ in sediment cores (Jackson *et al*., 2004). In addition laboratory experiments conducted show a biologically induced -7‰ fractionation in δ^{198}Hg/^{202}Hg (relative to NIST SRM 3133) during reduction of Hg^{+2} to Hg^0 using a purely cultured bacterium *Escherichia coli* (Kritee *et al*., 2007). All these workers reported mass dependent fractionation for Hg isotopes. Controlling laboratory-induced mass dependent isotope fractionation in Hg remains a substantial analytical challenge due to the small intrinsic variations of Hg isotope composition (~1-2‰). While this manuscript was in review, Bergquist and Blum (2007) published an important paper that presented measurements of mercury isotopes in samples of fish muscles from different locations and of aqueous solutions of Hg^{+2} from which elemental mercury had been removed experimentally by photo-reduction. The fish samples and residual solutions exibited effects of MIF with ^{199}Hg and ^{201}Hg isotopes being enriched relative to the even-A isotopes. Bergquist and Blum (2007) suggested that the mechanism for such MIF enrichment (up to 2.5‰ in the photoreduction experiments and 4‰ in fish) is the magnetic isotope effect.

Recently Schauble (2007) has made estimations of equilibrium ^{198}Hg/^{202}Hg separation factors for a number of mercury species relative to Hg^0 vapor. He showed that the nuclear field shift (due to changes in nuclear volume) is far more significant than zero-point energy differences (vibrational frequency) in effecting isotopic separation. Although, nuclear radii are to first approximation a

simple function of mass, in detail the nuclei of odd isotopes exhibit a smaller Δr/A than the nuclei of the even isotopes so that the nuclear field shift deviates from mass-dependent isotope fractionation (Schauble, 2007). For mercury isotopes, Buchachenko *et al*., (2004, 2007) demonstrated a mass independent magnetic isotope effect in the thermal reaction between creatine kinase with methylmercury chloride (CH_3HgCl) and photochemical decomposition of an organomercury compound. Such effects are expressed in the odd-A Hg isotopes (^{199}Hg: -1/2, ^{201}Hg: -3/2), due to their non-zero nuclear spin, relative to the even-A Hg isotopes (^{198}Hg, ^{200}Hg, ^{202}Hg, ^{204}Hg). We present analyses of Hg isotope composition of environmental Hg by MC-ICP-MS corrected for mass dependent fractionation. We refined the calculations of nuclear field shift (Schauble, 2007) for the Hg isotopes using the most precise published nuclear radii available, and employ the slope of the correlation between ratios of ^{199}Hg/^{202}Hg and ^{201}Hg/^{202}Hg to establish what fraction of the mass independent effect is related to nuclear field shift. The difference is assigned to nuclear spin effects.

3.2 Materials and Methods

Samples from two peat cores, sediment and soil standards for Hg elemental abundances, and Spanish mosses, were analyzed for Hg isotope composition. A peat core representing about 2000 years of accumulation from an ombrotrophic peat bog of Penido Vello, Spain, previously identified as having an anthropogenic Hg profile (Martinez-Cortizas *et al*., 1999), was serially sampled for Hg isotope analysis. The core was collected jointly by researchers from University of Santiago de Compostela and NHMFL, FSU, adjacent to the core previously reported by Martinez-Cortizas *et al*. (1999). The peat was sampled by cutting cores of 25 × 25 × 25 cm with a serrated stainless steel knife, to a depth of 100 cm. The fresh core was then sliced into 2 cm slices and wrapped in plastic bags and shipped to the NHMFL laboratory. The samples were kept frozen until use. A peat sample from Patagonia was obtained from Harold Beister from University of Heidelberg. Spanish moss samples were collected in Tallahassee, Fl. The sediment and soil are NIST Standard Reference Materials Estuarine Sediment 1646 a and Montana I Soil 2710, respectively.

The ombrotrophic Penido Vello peat core in this study represents ~2000 years of atmospheric mercury deposition. Ombrotrophic bogs have always been assumed to represent reliable historical mercury repositories based on their homogeneous distribution and limited mercury migration after deposition (Benoit *et al*., 1994; Grigal 2003). Mercury is known to be immobile when bound to soil organic matter largely due to the affinity of Hg^{+2} to sulfur-containing functional groups in humic substances (Schuster, 1991; Xia *et al*., 1999; Yin *et al*., 1997). Hg^{+2} is also known to go into dissolved phase by getting absorbed onto soluble organics such as fulvic acids (Lindqvist *et al*., 1991; Meili, 1991; Mierle and Ingram, 1991). However, the amount of mercury that gets into a dissolved phase is considered to be a very small fraction of the amount of mercury that is bound to organic matter and stored in bogs (Biester *et al*., 2002). On the other hand, a recent report by Biester *et al*., 2003 demonstrated that biochemical alteration of the peat during humification can strongly influence concentrations and accumulation rates of mercury in peat cores.Due to mercury's strong affinity towards humic substances, the concentrations of mercury in peat increase as a result of mass losses during humification and the temporal changes in mercury concentrations in peat cores do not necessarily reflect the temporal changes in atmospheric mercury fluxes to the bog (Biester *et al*., 2003).

For sample preparation it is very important to recover mercury from the sample without introducing isotopic fractionation during sample chemistry. A cold acid leaching technique has proved to be excellent for high recovery of mercury in Standard Reference Materials NIST 2704 Buffalo River Sediment and NIST 1572 Citrus Leaves (98% to 100% yield). The same technique was applied to all samples for the current study. The leaching was done at room temperature. A mixture of ultrapure concentrated HCl and 30% H_2O_2 (45 ml, 2:1 v/v) was added to sample in a tightly capped 120 ml PFA vessel (Savillex). The samples were shaken for an hour on a C1 platform Shaker (New Brunswick Scientific Classic Series). The samples were then ultrasonicated for 48 hours in an ultrasonic bath of high purity water. The leachate was then filtered from the residual sample by passing through a 0.2 um Millipore Polycarbonate membrane filter in a vacuum filtration system. The quantity of sample leached varied from 1-30 g depending on the concentration of mercury and was adjusted to yield a final concentration of approximately 1ng/ml of mercury. The total procedural blank including cold acid leaching of sample and vacuum filtration were below 230 ρg.

The 1ppb (1ng/ml) mercury standard solutions were prepared fresh daily by dilution of the NIST SRM3133 mercury standard. A 2% tin chloride solution ($SnCl_2$, 98% purity, ACROS) was prepared in 1M HCl daily. The solution was purged everyday prior to use with argon gas for approximately thirty minutes in order to release any trace mercury present. Reagents used in this work included in-house doubly-distilled HNO_3 and HCl acids stored in PFA Teflon vessels, analytical grade H_2O_2 (30% Certified ACS, Fisher Chemical), and 18 MΩ QD H_2O.

Mercury isotopic measurements were performed on a Thermo-Finnigan *Neptune* multicollector inductively coupled plasma mass spectrometer (MC- ICPMS) equipped with eight movable faraday cups and a fixed Axial faraday collector. Elemental Hg vapor, formed by reacting sample solution with 2% $SnCl_2$, was introduced into the mass spectrometer by a CETAC HGX-200 Hydride Generation and Cold Vapor System (Klaue and Blum, 1999). A Perimax Spectec peristaltic pump controlled the uptake rates of $SnCl_2$ and Hg sample solutions. The peristaltic pump speed was adjusted to 22 rpm which made the solution uptake rate 1.4 ml/min. The mercury vapor generated from the reduction is transferred by Teflon PFA tubes to the plasma. In between samples the hydride generator system was washed with 1M HCl for 2-3 minutes until the signal intensity returned to background level.

For mercury isotope ratio measurements seven adjustable Faraday cups were used (**Table 3.1**). ^{204}Pb isobaric interference on ^{204}Hg was monitored at mass 206 (^{206}Pb). For a typical ^{202}Hg signal intensity of 800 mV, the ^{206}Pb intensity was $< 2 \times 10^{-2}$ mV, resulting in a correction of <0.006‰ on δ^{204}Hg, which is negligible. Operating conditions of the mass spectrometer are listed in **Table 3.2**. Data acquisition was done using 1 block of 50 cycles with an integration time of 8 seconds. A baseline measurement collecting 30 ratios (total time of 90 seconds) using the defocusing beam technique was performed at the beginning of each measurement. Peak centering was performed at the beginning of each measurement. Raw isotope ratios ^{198}Hg/^{202}Hg, ^{199}Hg/^{202}Hg, ^{200}Hg/^{202}Hg, ^{201}Hg/^{202}Hg and ^{204}Hg/^{202}Hg were calculated from signal intensities. Instrumental mass bias was determined to be about 3-4‰ based on replicate analyses of the NIST SRM 3133 solution. In order to minimize effects of instrumental fractionation, isotope ratios were determined by sample-standard bracketing technique and reported in δ (‰) notation relative to NIST SRM 3133 Hg elemental standard in 10% HNO_3,

$$\delta^{A}Hg = \left(\left(^{A}Hg/^{202}Hg\right)_{sample}/\left(^{A}Hg/^{202}Hg\right)_{NIST3133} -1\right) x1000 \quad (3.1)$$

Deviations from mass-dependent fractionation were calculated as:

$$\Delta^{A}Hg = \delta^{A}Hg_{measured} - \delta^{A}Hg_{MD} \quad (3.2)$$

The value $\Delta^{199}Hg$ and $\Delta^{201}Hg$ is defined as the difference between the measured $\delta^{199}Hg$ and $\delta^{201}Hg$ ($\delta^{A}Hg_{measured}$) of a sample and the $\delta^{199}Hg$ and $\delta^{201}Hg$ ($\delta^{A}Hg_{MD}$) obtained from the linear scaling defined by the even-mass isotopes. Linear and exponential mass bias correction laws yield $\Delta^{199}Hg$ and $\Delta^{201}Hg$ values within the uncertainty of our analyses (~±0.1‰). In this paper, the linear scaling factors are derived by least squares fitting of the δ values of the even A isotopes.

The internal precision of each measurement was calculated as the 2SE of the mean of n runs, where n=50, or multiples of 50 for larger samples, and is shown in **Table 3.4** for each analysis. The long term analytical reproducibility of mercury isotope measurements is demonstrated by repeated analysis of NIST SRM 3133 Hg standard (**Figure 3.1a**). The total number of measurements is 350 during 16 individual measurement sessions over a period of six months. From the entire set of raw $^{198}Hg/^{202}Hg$ ratios calculated directly from run intensities, an average of 0.327931 ± .000611 (± 2σ, n= 350) is obtained for the NIST SRM 3133 Hg standard. From the $\Delta^{199}Hg$ and $\Delta^{201}Hg$ values calculated for the NIST SRM 3133 Hg standard and Almaden cinnabar we infer that the external precision of our Hg measurements is better than 0.1‰ (2σ) for both $\Delta^{199}Hg$ and $\Delta^{201}Hg$ (**Figure 3.1b** and **3.1c**). In the distribution of the $\Delta^{199}Hg$ and $\Delta^{201}Hg$ ‰ values of the NIST and cinnabar (**Figure 3.1b** and **3.1c**) no systematic trend is observed. This precision can be compared with the reproducibility of the four replicates run on samples which involved both the chemical separation and mass spectrometry, which is always better than 0.1‰ (**Table 3.4**). Since mercury is introduced to the plasma in the elemental vapor form (Hg^0), no matrix effects are expected.

3.3 Results and Discussion

Figure 3.2 shows two features that consistently exist in our data for all samples analyzed. The δ values for even A isotopes are closely proportional to mass number. A second feature of the data is the mass-independent fractionation of odd-mass-number isotopes ^{199}Hg and ^{201}Hg. **Table 3.4** gives the $\Delta^{199}Hg$ and $\Delta^{201}Hg$ values for the samples. Such odd-mass-number isotopic excursions from the even-A array (odd-even staggering) are characteristic of the nuclear field effect on atomic spectra and atomic and molecular electron structure (Bigeleisen 1996; Gerstenkorn and Verges, 1975).

The mass-independent fractionation resulting from the nuclear volume effect for a pair of Hg isotopes ($^{i}Hg/^{202}Hg$) is given with respect to the fractionation in $^{198}Hg/^{202}Hg$ by:

$$\Delta^{i}Hg = \delta^{198}Hg(A^{i}_{NV} - A^{i}_{MD}) \quad (3.3)$$

where A_{NV} is the scale factor for the mass independent isotope shift, and A_{MD} is the scale factor for the zero-point energy (mass dependent) isotope shift. The scale factor, A_{MD}, is calculated entirely from the masses of the isotopes (Schauble, 2007) and the scale factor, A_{NV}, is calculated from the r.m.s. nuclear-charge radii of the isotopes (Schauble, 2007). The values of A_{NV} given by

Schauble (2007) are based on a compilation of nuclear radii (Angeli, 2004) and indicate important deviations in ^{199}Hg, ^{201}Hg and ^{204}Hg. However, isotope shifts in the Hg arc spectrum (Gerstenkorn and Verges, 1975) are linearly correlated with mass number for even-A mercury isotopes including ^{204}Hg, as are our measured δ values (**Figure 3.3**). We, therefore, re-examined the values of A_{NV} using the most precise empirically determined values of the nuclear radii, which were determined from muonic x-ray transitions in separated stable Hg isotopes (Hahn *et al*., 1979). These values of A_{NV} (**Table 3.3**) were close to those obtained by Schauble (2007), with the notable exception of the scale factor for ^{204}Hg. The scale factors calculated from nuclear radii determined by Hahn *et al*. (1979) in **Table 3.3** indicate that ^{204}Hg behaves in an entirely mass-dependent manner, consistent with fractionations observed in the natural samples. Mass-independent fractionations calculated from the revised A_{NV} values are shown in **Figure 3.3a** for each of the species for which δ^{198}Hg is available (Schauble, 2007). It can be seen that equilibrium isotope effects that include the nuclear field shift give rise to a non-zero value of Δ^{199}Hg the magnitude of which is a function of the chemical species (**Figure 3.3a**), with reduced species (Hg^0, methylmercury) featuring positive anomalies. Further, the nuclear field shift effect is larger in Δ^{199}Hg than in Δ^{201}Hg by about a factor of two. For comparison, **Figure 3.3b** is a plot of the data from our analyses (**Table 3.1**).

The magnetic isotope effect is a kinetic phenomenon and depends on reaction rates, reaction mechanisms involving radical pairs and their mean lives, and nuclear magnetic moments of reactant isotopes. This effect is observed in spin-selective reactions of paramagnetic particles and leads to fractionation into magnetic and nonmagnetic isotopes (Buchachenko *et al*., 1976; Turro, 1983). Only the odd-A isotopes of mercury have non zero nuclear spin quantum numbers (^{199}Hg and ^{201}Hg, have nuclear spins of 1/2 and 3/2 and magnetic moments +0.5029 and -0.5602 μ_B, respectively). Accordingly magnetic isotope effects can produce a partial separation of ^{199}Hg and ^{201}Hg from each other and from the even-A isotopes of mercury.

Samples including Patagonia peat, various sediments, and cinnabar plot close to the theoretical nuclear field shift relationship between Δ^{199}Hg and Δ^{201}Hg (**Figure 3.4**). The Penido Vello peat and the Spanish moss samples notably exhibit a Δ^{199}Hg approximately equal to Δ^{201}Hg. Thus if Hg nuclear radii are accurately determined, this additional source of mass-independent fractionation likely is due to magnetic isotope effects. For reference, two lines, one with Δ^{201}Hg = 0.4569 * Δ^{199}Hg (as predicted by nuclear volume effect and recalculated in this work) and other Δ^{201}Hg = 1.11 * Δ^{199}Hg (as predicted by magnetic isotope effect (Buchachenko *et al*., 2004)) fitted to go through the point (0.0, 0.0) are drawn on **Figure 3.4**. The third line (dashed) is the calculated nuclear volume fractionation line from Schauble (2007), which agrees well with the line calculated in this study, indicating that the R.M.S. nuclear charge radii of Hahn *et al*. (1979) agree well with those of Angeli (2004) for the odd isotopes. When considered altogether, the samples roughly follow the magnetic isotope effect line with a slope of 1.11. Values of the Δ^{199}Hg/Δ^{201}Hg ratios range from 0.54 to 2.00 (**Table 3.4**).

In **Figure 3.4** lines defining the Δ^{201}Hg/Δ^{199}Hg ratios produced by the effects of magnetic
Spin and nuclear volume are drawn for comparison. From the isotopic data it appears to be possible to differentiate the relative contribution of nuclear volume effect and magnetic spin effect (**Table 3.4**). Assuming that the MIF anomalies are artifacts of two different isotope effects, one producing Δ^{201}Hg / Δ^{199}Hg in a ratio of 0.4569 and the other in a ratio of 1.11 we

have calculated the relative contributions of each effect to the total MIF. In the sediment standards the nuclear field shift effect and magnetic isotope effect both seem to play an equivalent role in fractionating mass independently (**Table 3.4** and **Figure 3.4**) and samples plot in between the two trend lines defined by the two different processes. The dominant process for the Patagonia peat seems to be the nuclear field shift effect. The dominant process for the Penido Vello peat core and Spanish moss is consistent with the magnetic isotope effect.

3.4 Conclusion

Mass-independent fractionation has been an important tracer in light element geochemistry. Here, we show it to be an equally important tracer for heavy element geochemistry of Hg. The nuclear volume isotope shift is shown to induce a mass-independent isotope effect in the odd-A Hg isotopes in the ratio, $\Delta^{201}Hg/\Delta^{199}Hg \approx 0.5$, with the odd-A isotopes concentrated in the reduced Hg species (Hg^0 and methylmercury). After substitution of empirically determined nuclear radii as inputs in calculating separation factors for Hg isotopes, no mass-independent effect on $\Delta^{204}Hg$ is predicted, and none is observed. The sediment samples and the Patagonia peat are enriched in the odd-A Hg isotopes in approximately correct ratios for nuclear field shift effect, while the Penido Vello and Spanish moss samples are depleted in the odd-A Hg isotopes. Because the Penido Vello peat core samples and the Spanish moss, both of which receive their Hg from the atmosphere, exhibit $\Delta^{201}Hg/\Delta^{199}Hg \approx 1$ an additional source of mass-independent isotope fractionation based a magnetic isotope effect is inferred. The potential for isotopic tracing of Hg speciation in the environment should have important implications for a better understanding of the behavior of mercury in the environment and eventually provide important constraints on models of the mercury cycle, including both natural and anthropogenic influences.

Table 3.1 Configuration of the Faraday Collectors for mercury isotope ratio measurements

Measurement	L4	L3	L2	L1	C	H1	H2	H3	H4
Hg & Pb	------	------	198	199	200	201	202	204	206

Table 3.2 Operating conditions of Neptune mass spectrometer and Hydride Generator

Plasma tune parameters	Values
Cool gas (Ar)	15.00 L min^{-1}
Auxiliary gas (Ar)	0.75-0.85 L min^{-1}
Sample gas (Ar)	0.7-0.9 L min^{-1}
Additional gas (Ar)	0.23 L min^{-1}
RF Power	1200
Peripump Speed	22 rpm
Cetac HGX-200 Hydride Generation and Cold Vapor System	Values
Solution uptake rate	1.418 ml min^{-1}
Sensitivity for ^{202}Hg vapor	600-700 mV $(ng/mL^{-1})^{-1}$
Background	8-10 mV

Table 3.3 Nuclear Volume (NV) Scale factors calculated from nuclear radii determined by Hahn *et al*. (1979) and $\Delta^{m}Hg$ values calculated for various mercury bearing chemical species relative to $HgCl_2$

NV Scale factor	$^{198}Hg/^{202}Hg$ 1.0000	$^{199}Hg/^{202}Hg$ 0.9200	$^{200}Hg/^{202}Hg$ 0.5288	$^{201}Hg/^{202}Hg$ 0.3256	$^{202}Hg/^{202}Hg$ 0.0000	$^{204}Hg/^{202}Hg$ -0.4990
Chemical Species	$\Delta^{198}Hg$	$\Delta^{199}Hg$	$\Delta^{200}Hg$	$\Delta^{201}Hg$	$\Delta^{202}Hg$	$\Delta^{204}Hg$
Hg^0	0.00	0.22	0.04	0.10	0.00	-0.02
Hg^{+2}	0.00	-0.33	-0.06	-0.15	0.00	0.03
$Hg(CH_3)_2$	0.00	0.12	0.02	0.06	0.00	-0.01
$Hg(CH_3)Cl$	0.00	0.08	0.02	0.04	0.00	-0.01
$HgCl_2$	0.00	0.00	0.00	0.00	0.00	0.00
$HgBr_2$	0.00	0.01	0.00	0.00	0.00	0.00
$Hg(H_2O)_6^{+2}$	0.00	-0.26	-0.05	-0.12	0.00	0.02
$HgCl_4^{-2}$	0.00	-0.17	-0.03	-0.08	0.00	0.01

All nuclear volume fractionation factors are calculated at 25°C

Table 3.4 Δ^{199}Hg and Δ^{201}Hg ‰ values for natural samples and relative contributions of Magnetic Isotope Effect (MIE) and Nuclear Volume Effect (NV) on Δ^{199}Hg and Δ^{201}Hg.

Sample	Δ^{199}Hg	Δ^{201}Hg	$\frac{\Delta^{199}Hg}{\Delta^{201}Hg}$	MIE Contribution		NV Contribution	
				Δ^{199}Hg	Δ^{201}Hg	Δ^{199}Hg	Δ^{201}Hg
Patagonia Peat	0.20 ± 0.01	0.10 ± 0.01	2.00	9 ± 5 %	19 ± 5 %	91 ± 6 %	81 ± 5 %
Patagonia Peat (R)	0.22 ± 0.03	0.12 ± 0.01	1.83	15 ± 4 %	29 ± 3 %	85 ± 6 %	71 ± 6 %
SRM 2710	0.18 ± 0.04	0.13 ± 0.02	1.38	45%	65%	55%	35%
ES 1646	0.15 ± 0.03	0.12 ± 0.03	1.25	57 ± 4 %	75 ± 4 %	43 ± 4 %	25 ± 4 %
Spanish Moss	-0.83 ± .02	-0.98 ± .02	0.85	85%	93%	15%	7%
Spanish Moss (R)	-0.95 ± .02	-1.02 ± .02	0.93	96%	98%	4%	2%
Almaden Cinnabar	-0.07 ± 0.09	-0.06 ± 0.09	1.40	77 ± 7 %	89 ± 7 %	23 ± 7 %	11 ± 7 %
Penido Vello Peat Core							
0-2	-0.32 ± 0.02	-0.42 ± 0.02	0.76	77 ± 2 %	88 ± 1 %	23 ± 2 %	12 ± 1 %
0-2 (R)	-0.27 ± 0.03	-0.48 ± 0.03	0.56	64 ± 3 %	81 ± 3 %	36 ± 3 %	19 ± 3 %
2-4	-0.28 ± 0.05	-0.33 ± 0.07	0.85	83 ± 9 %	92 ± 9 %	17 ± 9 %	8 ± 9 %
4-6*	-0.23 ± 0.01	-0.30 ± 0.01	0.77	77 ± 3 %	89 ± 2 %	23 ± 3 %	11 ± 2 %
6-8	-0.16 ± 0.02	-0.27 ± 0.03	0.59	67 ± 6 %	82 ± 6 %	33 ± 6 %	18 ± 5 %
10-12	-0.24 ± 0.01	-0.32 ± 0.01	0.75	75 ± 2 %	87 ± 2 %	25 ± 2 %	13 ± 2 %
12-14	-0.28 ± 0.02	-0.33 ± 0.02	0.85	83 ± 4 %	92 ± 4 %	17 ± 3 %	8 ± 2 %
14-16*	-0.26 ± 0.03	-0.48 ± 0.03	0.54	64 ± 3 %	80 ± 2 %	36 ± 3 %	20 ± 2 %
16-18	-0.31 ± 0.02	-0.37 ± 0.02	0.84	84 ± 4 %	92 ± 3 %	16 ± 4 %	8 ± 4 %
20-22*	-0.25 ± 0.03	-0.42 ± 0.04	0.60	66 ± 7 %	81 ± 7 %	34 ± 5 %	19 ± 5 %
22-24	-0.35 ± 0.03	-0.35 ± 0.03	1.00	89 ± 6 %	95 ± 6 %	11 ± 6 %	5 ± 6 %
26-28*	-0.38 ± 0.03	-0.46 ± 0.03	0.83	84 ± 5 %	92 ± 4 %	16 ± 5 %	8 ± 4 %
30-32	-0.20 ± 0.03	-0.31 ± 0.05	0.65	68 ± 5 %	83 ± 5 %	32 ± 5 %	17 ± 5 %
32-34	-0.33 ± 0.03	-0.42 ± 0.03	0.79	80 ± 5 %	90 ± 4 %	20 ± 5 %	10 ± 4 %
34-36	-0.25 ± 0.03	-0.35 ± 0.03	0.71	74 ± 5 %	87 ± 4 %	26 ± 5 %	13 ± 4 %
38-40	-0.31 ± 0.01	-0.37 ± 0.02	0.84	85 ± 3 %	93 ± 3 %	15 ± 3 %	7 ± 3 %
42-44	-0.35 ± 0.04	-0.43 ± 0.03	0.81	82 ± 3 %	91 ± 3 %	18 ± 3 %	9 ± 3 %
44-46	-0.29 ± 0.02	-0.36 ± 0.03	0.81	81 ± 4 %	91 ± 4 %	19 ± 4 %	9 ± 4 %
46-48*	-0.28 ± 0.08	-0.24 ± 0.08	1.17	68 ± 14 %	83 ± 13 %	32 ± 14 %	17 ± 13 %
50-52	-0.39 ± 0.01	-0.38 ± 0.02	1.03	85 ± 5 %	93 ± 4 %	15 ± 5 %	7 ± 4 %
54-56	-0.36 ± 0.04	-0.37 ± 0.03	0.97	96 ± 8 %	98 ± 7 %	4 ± 8 %	2 ± 7 %
56-58	-0.43 ± 0.02	-0.39 ± 0.03	1.10	78 ± 6 %	89 ± 6 %	22 ± 6 %	11 ± 6 %
58-60	-0.41 ± 0.03	-0.43 ± 0.03	0.95	99 ± 6 %	100 ± 5 %	1 ± 5 %	0 ± 5 %
62-64	-0.50 ± 0.04	-0.41 ± 0.04	1.22	61 ± 7 %	78 ± 7 %	39 ± 7 %	22 ± 7 %
64-66	-0.39 ± 0.01	-0.48 ± 0.01	0.81	80 ± 2 %	90 ± 1 %	20 ± 2 %	10 ± 1 %
66-68	-0.35 ± 0.01	-0.36 ± 0.01	0.97	98 ± 1 %	99 ± 1 %	2 ± 1 %	1 ± 1 %

Table 3.4 continued

Sample	Δ^{199}Hg	Δ^{201}Hg	$\frac{\Delta^{199}Hg}{\Delta^{201}Hg}$	MIE Contribution		NV Contribution	
				Δ^{199}Hg	Δ^{201}Hg	Δ^{199}Hg	Δ^{201}Hg
70-72	-0.32 ± 0.02	-0.33 ± 0.03	0.97	98 ± 5 %	99 ± 5 %	2 ± 5 %	1 ± 5 %
74-76	-0.33 ± 0.03	-0.46 ± 0.02	0.72	72 ± 3 %	86 ± 2 %	28 ± 3 %	14 ± 2 %
78-80	-0.32 ± 0.03	-0.37 ± 0.03	0.86	86 ± 5 %	93 ± 4 %	14 ± 5 %	7 ± 4 %
82-84	-0.34 ± 0.03	-0.39 ± 0.04	0.87	88 ± 6 %	94 ± 5 %	12 ± 6 %	6 ± 5 %
84-86	-0.33 ± 0.03	-0.37 ± 0.02	0.89	91 ± 5 %	96 ± 4 %	9 ± 5 %	4 ± 4 %
86-88	-0.36 ± 0.03	-0.46 ± 0.04	0.78	79 ± 3 %	89 ± 2 %	21 ± 3 %	11 ± 2 %
90-92	-0.31 ± 0.03	-0.37 ± 0.03	0.84	84 ± 5 %	92 ± 4 %	16 ± 5 %	8 ± 4 %
90-92 (R)	-0.37 ± 0.02	-0.36 ± 0.02	1.03	88 ± 6 %	95 ± 3 %	12 ± 6 %	5 ± 3 %
92-94	-0.35 ± 0.02	-0.42 ± 0.02	0.83	86 ± 3 %	93 ± 3 %	14 ± 3 %	7 ± 3 %
94-96	-0.22 ± 0.03	-0.27 ± 0.04	0.81	82 ± 7 %	91 ± 6 %	18 ± 7 %	9 ± 6 %
96-98	-0.31 ± 0.02	-0.44 ± 0.02	0.70	73 ± 3 %	86 ± 2 %	27 ± 3 %	14 ± 2 %

*See text for details on how Δ^nHg ‰ has been calculated. The internal precision of each measurement was calculated as the 2SE of the mean of n runs, where n=50, or multiples of 50 for larger samples. For Almaden cinnabar, the error represents 2σ on sixty replicates. The sediments are NIST Standard Reference Materials Estuarine Sediment 1646 a and Montana I Soil 2710. Samples indicated with an * correspond to samples for which replicate runs were not possible due to constraints on available sample mass and the errors represent internal precision from 50 scans of a single analysis. (R) represents duplicate replicates run on samples which involved both the chemical separation and mass spectrometry*

Figure 3.1 Long term reproducibility for Hg isotope ratios determined at NHMFL by MC-ICP-MS: a) Raw ^{198}Hg/^{202}Hg calculated directly from signal intensities for 350 replicate measurements of NIST SRM 3133 Hg standard (1 ng mL^{-1}) collected over a time period of six months, b) Δ^{199}Hg (‰) for 55 replicate measurements of Hg from NIST SRM 3133 (1 ng mL^{-1}), and 60 replicate measurements of Hg from Almaden cinnabar (1 ng mL^{-1}), representing four months of data collection, and c) the same as in (b) for Δ^{201}Hg (‰). The bold lines represent the estimated average and the dashed lines represent the ± 2σ uncertainty.

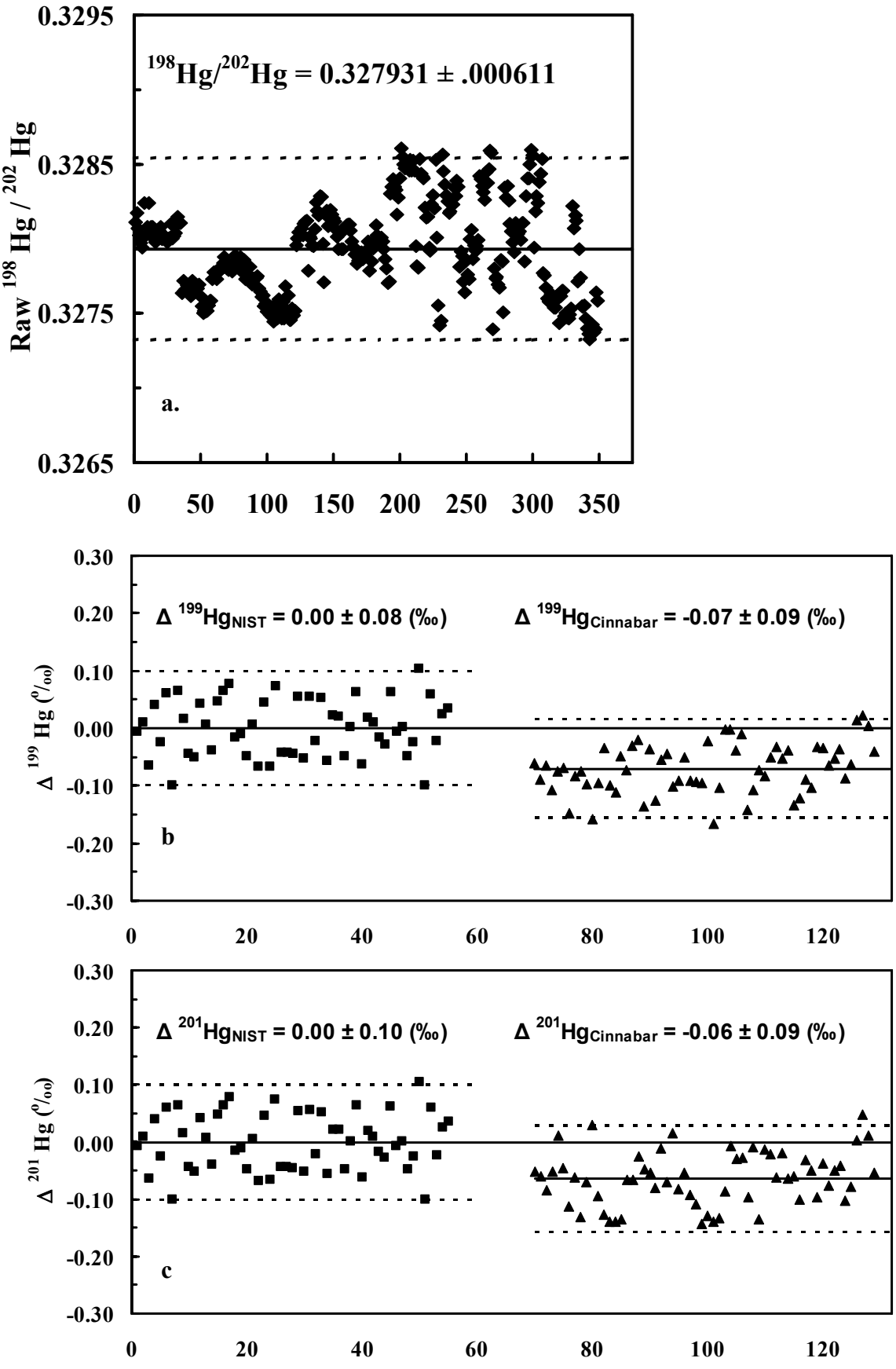
0.3295
0.3285
0.3275
0.3265
Raw 198 Hg / 202 Hg
198Hg/202Hg = 0.327931 ± .000611
a.
0
50
100
150
200
250
300
350
0.30
0.20
0.10
0.00
-0.10
-0.20
-0.30
Δ 199 Hg (‰)
Δ 199HgNIST = 0.00 ± 0.08 (‰)
Δ 199HgCinnabar = -0.07 ± 0.09 (‰)
b
0
20
40
60
80
100
120
Δ 201 Hg (‰)
Δ 201HgNIST = 0.00 ± 0.10 (‰)
Δ 201HgCinnabar = -0.06 ± 0.09 (‰)
c

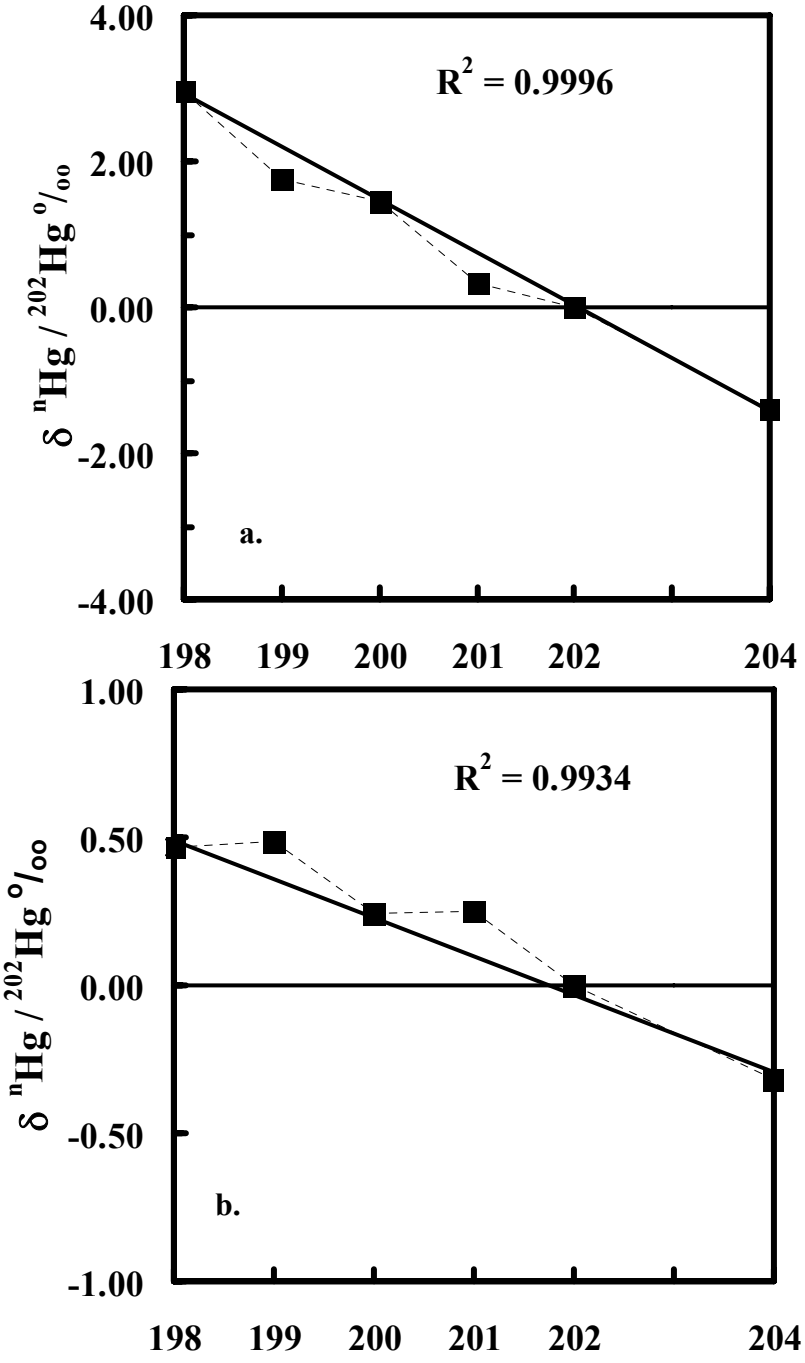

Figure 3.2 Selected $\delta\ ^{n}Hg/^{202}Hg$ (‰) (where n= 198, 199, 200, 201, 202 and 204) value of a) peat (58-60, peat core) and b) sediment standard (NIST SRM 2710) as a function of mass number of mercury isotopes, illustrating the mass-independent fractionation observed in odd-A isotopes of Hg. The measured isotopic ratio is converted to per mil (‰) deviation (δ notation) with respect to measurements of the NIST SRM3133 Hg Standard performed by standard-sample bracketing. The black lines represent a linear regression through the even-A isotopes of Hg which show only mass-dependent fractionation.

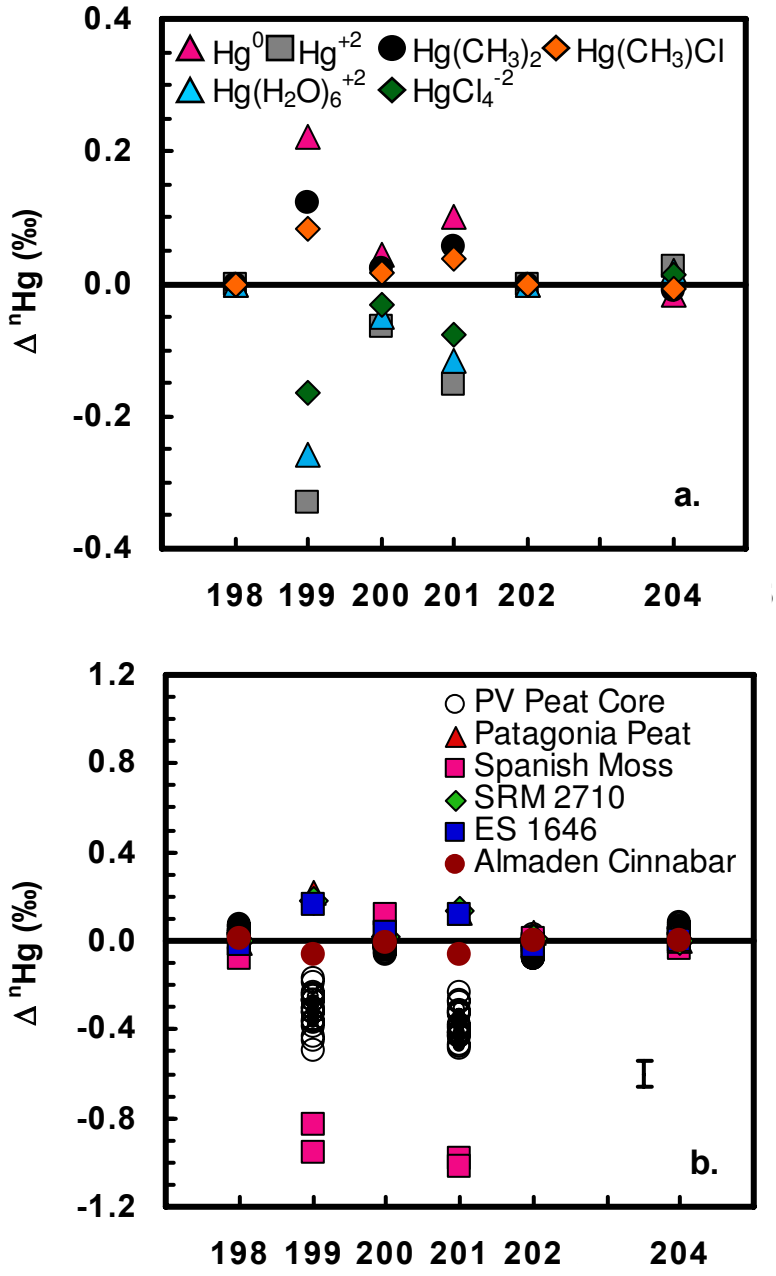

Figure 3.3 Mass independent fractionation, Δ^{n}Hg ‰ as a function of mass number of mercury isotopes (see text for details). **a**, The theoretical Δ^{n}Hg ‰ (from eqn. 3) for important oxidized and reduced mercury-bearing chemical species of environmental interest, normalized relative to fractionation factors for $HgCl_2$. The A_{NV} factors from **Table** 3 calculated using r.m.s. nuclear charge radii [Hahn *et al*., 1979] values from muonic x-ray transitions.**b**, Mass independent fractionation, Δ^{n}Hg ‰, for Hg from natural samples (this study). Sediment standards ES1646 & SRM 2710 and Patagonia peat show positive mass independent anomaly on the odd isotopes. The Penido Vello peat core (open circles) and Spanish moss show negative mass independent anomaly on odd isotopes. The average of Almaden cinnabar determined from sixty replicate runs shows very little deviation from mass dependent effect. A representative error bar is shown.

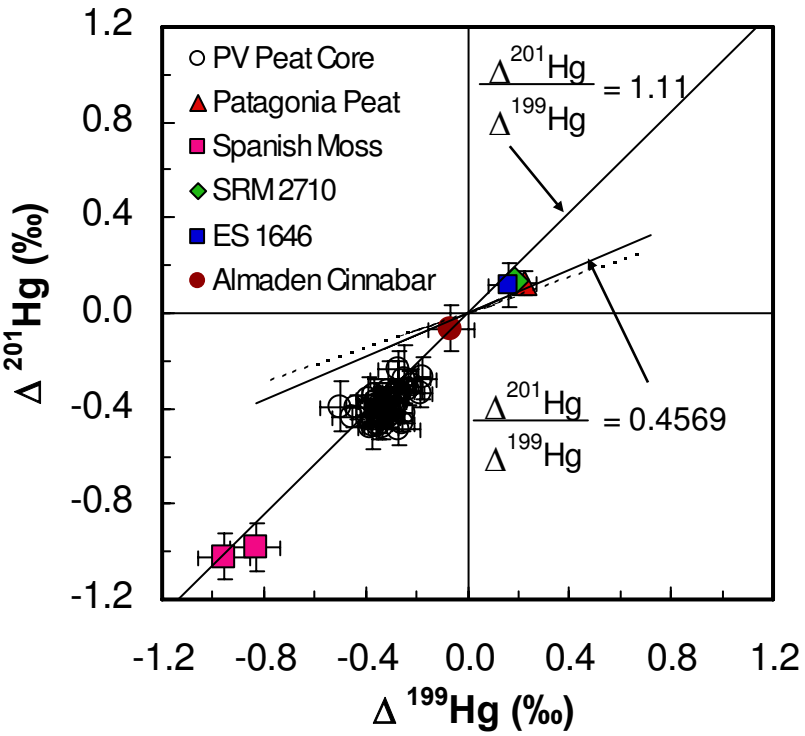

Figure 3.4 Calculated Δ^{199}Hg ‰ versus Δ^{201}Hg ‰ values in peat, sediments, moss and cinnabar. The dotted line and black line define the expected co-variation between Δ^{199}Hg and Δ^{201}Hg based on theoretical nuclear field shift from Schauble, 2007 and re-calculated in this work, respectively. The Δ^{201}Hg/Δ^{199}Hg =1.11 line is predicted from magnetic moments of the two isotopes and drawn for reference to facilitate discussion. The internal precision of each measurement was calculated as the 2SE of the mean of n runs, where n=50, or multiples of 50 for larger samples. For Almaden cinnabar, the error represents 2σ on 60 replicate measurements. Note that Hg from the Penido Vello peat and from the Spanish moss does not plot along the theoretical mass-independent line calculated from nuclear field shift alone.

CHAPTER 4

APPLICATION OF LEAD AND SULFUR ISOTOPES IN ARCHAEOLOGICAL STUDIES

4.1 Introduction

The mineral galena played a very important role in the early Native American culture of eastern North America. Galena has been reported from more than two hundred prehistoric archaeological sites in eastern North America (Austin *et al*., 2000, Walthall, 1981) (**Figure 4.1**). These burial and habitation sites range in age from the Middle Archaic to Mississippian (8000 B.C. - A.D. 1500) (Walthall, 1981). Finely ground galena was used as face paint by some cultures (Cole and Deuel, 1937; Swanton, 1946). It was also sometimes fashioned into beads and pendants or other objects. Sometimes unexpended pieces were buried with the dead in mortuary ceremonies (Walthall 1981, Austin *et al*., 2000). The appearance of galena with other exotic artifacts (for example mica, native copper, quartz) at the prehistoric sites has identified galena to be an exchangeable commodity in the hand-to-hand trade network between the native cultures of that age (Austin *et al*., 2000; Austin, 1993; Bullen, 1978; Sears, 1962; Walthall, 1981; Walthall *et al*., 1980; Walthall *et al*., 1979; Yerkes, 1988). This interregional exchange system allowed galena to travel long distances from probable source deposits. One of the consequences of the interregional trading system is the widespread occurrence of galena in the Coastal Plain of Southeastern United States and parts of the Mississippi and Tennessee River Valley systems (**Figure 4.1**).

4.2 Archaeological Background

Galena has been recovered in archaeological sites over much of North America and had been very important to the North American Indians for over 8000 years. Galena is very rare in sites predating the Late Archaic. It has been reported from only two sites of the Early-Middle Archaic period (8000-3500 B.C.): Rodgers Shelter in Missouri (Kay, 1980) and Modoc in Illinois (Fowler, 1959)**.** The presence of red ocher in these rock shelters suggests that galena was probably used as paint pigments or in ritual activities during these times (Walthall, 1981). It was not until Late Archaic period that galena started being used in burial ceremonies where pieces of galena were buried with the dead.

Galena used in the Late Archaic-Early Woodland (3500-500 B.C.) times is mainly found in the Eastern Great Lakes region, the upper and lower Mississippi Valley and Florida (Walthall, 1981; **Figure 4.1**). Very little galena has been reported (recovered mostly from burial mounds) in the Great Lakes region indicating that the mineral was not a major interregional exchange commodity during this period. However, numerous galenas have been recovered from the lower Mississippi Valley region and Florida indicating that galena was part of an important north-south exchange system (Walthall 1981).

The Middle Woodland period (200 B.C.-A.D. 500) saw a tremendous increase in regional and long-distance galena trade (Walthall, 1981). The occurrence of galena artifacts associated with

Middle Woodland period were mainly in the major river valleys of Mississippi, Illinois, Ohio, Scioto and Tennessee, and along the coastal area of Florida (**Figure 4.1**). Three important Middle Woodland cultures Havana Hopewell, Ohio Hopewell and Copena have been found to be the dominant users of galena during this period (Seeman 1977).

Galena from the Mississippian period (A.D. 900-1500) has been reported mainly from the upper Mississippi River valley, the lower Illinois River valley, parts of Tennessee River valley, the Caddoan region (mainly Oklahoma) and Florida. Although galena was still being exchanged in crystal and nodule forms, there is also evidence that galena was crushed and ground with a grinding stone and mortar or a paint palette (Griffin and Morse 1961; Keslin 1964). Apparently the crushed and powdered galena was also exchanged in this period (Walthall 1981). Crushed galena may have been stored in bags made from hides which have decomposed through time leaving the heaps (Walthall 1981).

4.3 Galena deposits in Eastern and Central United States

Most base metal (Zn, Pb, Cu) sulphide deposits in non igneous settings form from hot (50°C - 200°C), saline aqueous fluids. These fluids migrate out of deep basins, dissolve metals from host minerals and eventually reach shallow depths where they cool and precipitate metal sulphides (White 1968; Ohle 1980). The Coastal Plain of southeastern United States consists of mostly unconsolidated sedimentary rocks, which have never experienced elevated temperatures. As a result there is an absence of metal sulphide deposits in the Coastal Plain (**Figure 4.2**). Although there is no geological environment for galena deposits to form, there are many archaeological sites with abundant galena in the Coastal Plain. The major and minor galena deposits located in central and eastern North America can be classified into four groups (**Figure 4.2**):

A) Major Mississippi Valley ore occurrences- Upper Mississippi Valley (UMV) in the adjoining areas of northwestern Illinois, northeastern Iowa and southwestern Wisconsin; Southeast Missouri (SEM) - Central Missouri (CM) in the state of Missouri and Tri-State (TS) in southwestern Missouri and the adjacent areas of Kansas and Oklahoma. These large strata bound deposits occur in Paleozoic carbonate hosted rocks contain galena in commercial quantities in vugs and fracture zones. The Mississippi Valley type ore deposits formed as a result of warm concentrated saline fluids migrating through sedimentary basins (Goldhaber, *et al*. 1995). Before the modern mining of the Upper Mississippi Valley and Missouri deposits by the Europeans in the 1600's, the deposits were known and exploited by the Native Americans of Pre-European contact times (Logan 1976; Schockel 1916; Whitney 1866).

The galenas in UMV are occasionally found as open-air crevice type vein deposits, disseminated ore and as surface residues (Agnew 1955; Heyl 1968). The crevice type deposits are formed by solution weathering of the sedimentary host rock. Also there are numerous caves lined with sheets of galena crystals and chunks of loose galena occur on the floors of these caves (Hall and Whitney, 1858). Most of these caves are shallow and projectile points typical of Middle and Late Woodland period have been found near the mouth of some of these caves (Logan 1976). The SEM district can be separated into two sub districts: the Old Lead Belt (OLB) and the Viburnum Trend (VT). The VT sub-district is a subsurface lead deposit and was opened for mining only in the 1960s and was never a source for galena for prehistoric people. The ore in the OLB (sub-district of SEM) occurred in variety of ways, including bedded deposits replacing host rock, open

space fillings, disseminated ores and as surface residual chunks in clay accumulated due to solution weathering of host rock. Due to the surface concentrations of galena in both UMV and OLB, galena from both sources was easily procured by the prehistoric people by very primitive techniques like surface picking and mining in soft clays (Walthall 1981). In the OLB sub-district numerous small open-air and rock-shelter habitation sites as well as big settlements exists from which galena artifacts have been reported (Adams, 1949; Denny and McMillan, 1964). In fact there are evidences that the OLB deposits started being exploited for galenas from as early as 3000 B.C. (Walthall 1981) and continued until pre-European contact (Schoolcraft 1819; Swartzlow 1934, Walthall 1981). Galena in Central Missouri (CM) occurs as horizontal sheets, veins (Shumard, 1867; Broadhead, 1880) and as surface concentrations in residual clay (Kay, 1980). There is archaeological evidence that galena was mined by the aboriginal groups living within the CM mineral district. Rodgers Shelter, which is an Early Archaic-Middle Archaic site located within the CM district (Kay 1980), contains CM galenas (Walthall 1981). Galena in the TS district of Missouri occurs as disseminated ores, crystals in cavities and as residual concentrations in soil (Walthall 1981). Pieces of galena are found in clay or sand associated with dolomite or chert (Broadhead, 1894). There are no published reports or historical evidence of TS lead district being exploited before European contact.

B) Minor Mississippi Valley ore occurrences- The Illinois-Kentucky, Central Kentucky and Central Tennessee districts. Galena occurs in commercial quantities along with sphalerite, fluorite and barite in abundant fissure veins. In the Illinois-Kentucky (IK) district, galena occurs below the surface in subordinate amounts often coprecipitated with sphalerite. The IK was a main source of fluorspar to the Native American cultures from which statuettes were carved (Grogan and Bradbury, 1968) and no records of mining of galena from this district are found (Walthall, 1981). Galenas in Central Tennessee and Central Kentucky occur as vein deposits and in fissures filled with clay and there is no evidence that they occurred on the surface (Walthall 1981)

C) The zinc districts of the Appalachian Valley and Ridge province located from New Jersey to Tennessee. Galena is very rare in these strata bound deposits.

D) Massive sulfide deposits in Blue Ridge and Piedmont provinces of the Southern Appalachians from Virginia to Alabama. Galena generally occurs in very limited quantity in veins and as lenses along with other sulphide minerals.

4.4 Provenance Studies of Galena

Several previous studies have been conducted on the provenance of galenas from eastern North American archaeological sites. Walthall *et al*. (1979, 1980) and Walthall, 1981 performed trace element analysis of more than a hundred galena artifacts comparing silver, cadmium, cobalt, copper, manganese, nickel, zinc and antimony concentrations of the artifacts with galenas from ore deposits in the Mid-Continental United States. The trace element analyses were done by atomic absorption spectrophotometry and emission spectrography. In these studies a limited number of major ore deposits were selected as probable source locations. These were the Tri-State, Southeast Missouri, Central Missouri, Illinois-Kentucky and Upper Mississippi Valley deposits. The artifacts analyzed were associated with different archaeological periods (Archaic/Early Woodland, Middle Woodland and Mississippian). To differentiate the ore deposits chemically, multivariate discriminant analysis was used in which the possible source

areas served as groups, known galena ore samples as entities defining the groups and trace element concentrations as variables describing the entities. Through statistically generated models (based on trace element contents of the galena ore samples whose group is already known) an unknown artifact was allocated to a group it most closely resembled (Walthall *et al*. 1979, 1980; Walthall, 1981). The geochemical analysis showed that during the Late Archaic period both Upper Mississippi Valley (UMV) and South Eastern Missouri (SEM) deposits were exploited by nearby regional communities, but during the Middle Woodland period large quantities of ore were exploited mainly from UMV and traded to distant areas in the south such as the Tennessee valley. During the Mississippian period SEM dominated as the primary source and the use of UMV deposits sharply curtailed. The reports by Walthall could not unequivocally identify the source of an artifact because the data fields for ore sources overlapped with each other. Galena mineralization usually occurs from chemically heterogeneous solutions that cause large chemical zonings within an ore district. Also, chemical zoning within a single crystal of galena could cause a large variation in trace element concentrations.

Previously, lead isotope analyses also have served to determine the sources of trace amount of lead in artifacts like bronzes, glasses, coins, ceramics and other metallic lead objects (Barnes *et al*., 1974; Brill *et al*., 1979; Brill and Wampler, 1967; Farquhar and Vitali, 1989; *et al*., 1989; Yener *et al*., 1991). Farquhar and Fletcher (1980, 1984) were the first to use lead isotope ratios to determine the provenance of galena artifacts found in north eastern North American archaeological sites. Galena artifacts were analyzed from seven Late Archaic-Early Woodland period burial and habitation sites in the Great Lakes area by Farquhar and Fletcher in 1984. Six of these sites contained galenas that had relatively local sources (a few hundred kilometers from the sites) whereas the source of galena from one site was probably from the southern part of UMV mineral deposit (Farquhar and Fletcher, 1984). Austin *et al*. (2000) conducted a recent study on three archaeological sites in Florida and found from lead isotopic analysis that the galenas from these sites had a common source of origin in SEM. This indicated that the aboriginal people once living in central and south Florida had trade relations that extended northward and reached the Mississippi Valley.

4.5 Purpose of present study

The present study is to determine the potential provenance of galena artifacts recovered in prehistoric habitation and burial sites in parts of southeastern United States. This is the first study where provenance sourcing will be done by combining both lead and sulfur isotopes. The period of time spanned by the archaeological sites in this study is more than a millennium. It would be also be interesting to determine if the sources have changed through periods of time. If indeed that is the case then it could have major implications on sociological and economical interactions associated with Native American trade. A change of source area could indicate either depletion of sources or that some other source became more easily and readily available to the cultures. It could also indicate that two cultures developed hostile relations and stopped exchanging commodities. Given that in prehistoric times, mining technology was primitive, any galena available to the inhabitants would have to be readily available on or near the surface. This makes the following ore deposits the potential sources for galena artifacts: Missouri-Kansas-Oklahoma Tri-State (TS) area, Upper Mississippi Valley (UMV) and the Southeast and Central Missouri region (SEM-CM). There are evidences that prior to large scale mining, galena occurred as veins

in open-air crevices and caves or as surface residual deposits in these source areas. The other galena deposits known in eastern North America: Illinois-Kentucky (IK) district and the deposits located in the Tennessee Valley region: eastern Tennessee-Virginia, central Tennessee-central Kentucky and Alabama are close to the archaeological sites, but there is no published evidence that they were exploited for galena by the prehistoric cultures. Galena in the latter deposits occurs in subordinate amount, as small crystals co-precipitated with other sulphide phases like sphalerite (Heyl *et al*. 1966; Hoagland *et al*., 1965; Walthall 1981). The galena in these deposits are low in abundance and their mode of occurrence is such that they would have been more difficult to mine and less accessible sources for the Native Americans than the galena deposits in the UMV, SEM-CM and TS regions.

4.6 Material and Methods

4.6.1 Archaeological Site Locations

In general, the current study has attempted to analyze artifacts from those archaeological locations as Walthall 1981 did for his chemical analyses. The approach was to analyze at least two samples from any given site but there were certain limitations. First of all most of the sites are burial sites and the artifacts are protected as cultural heritage and second due to the destructive method employed for analyses the repositories were reluctant to distribute them.
Galena artifacts from five locations in Florida, four in Illinois, two in Alabama, two in Louisiana, two in Oklahoma and two in Missouri were analyzed for lead isotope ratios and a subset of samples were also analyzed for sulfur isotope ratios (**Table 4.1**). The locations of these sites are shown in **Figure 4.3**.

Eleven samples from Florida have been analyzed for this study, ten of which were obtained from the Florida Bureau of Archaeological Research and one from Harley Means of Florida Geological Survey (HM1) who discovered it in the bed of Wassica River. Out of the ten in Florida, four are from Miami Circle on Brickell Point off the Miami River (MC1A, MC1B, MC2A and MC2B). Tequesta were the first Native American tribes to settle in the Miami Circle area almost 2000 years ago. The Miami circle consists of a perfect circle 38 ft in diameter cut into the solid limestone bedrock (Carr and Ricisak 2000). One of the samples is from the Block-Sterns Site (BSI), which is the largest of the sixteen identified Swift Creek Sites in Leon County, encompassing some 80 acres (Jones *et al*., 1998). A variety of exotic trade goods have been recovered at the site, including galena, worked native copper and native copper ore (Jones *et al*., 1998). Another two are from the Lake Jackson mound (LJ1, LJ2) located on the south shore of Lake Jackson, north of Tallahassee, Florida. During the Mississippian period (1000 A.D. to 1500 A.D.) seven burial mounds were built probably by the Apalachee culture that lived in the Lake Jackson area when first encountered by European people (Jones and Tesar, 1996; Jones 1982). Found at the site are other objects such as copper breastplates, shell beaded necklaces, bracelets, anklets and galena. Three samples have been collected from the Oak Knoll site in Lee county (OK1A, OK1B and OK2) (Dickel and Carr, 1991). For Florida, every galena artifact recovered in the five archaeological sites been analyzed for lead isotopes in this study.

The artifacts from Louisiana are from two sites, the Morton Shell Mound (I61B3) in Iberia Parish and Poverty Point (W-4986) in West Carroll Parish. The Morton Shell Mound site is a shell midden some 700 feet long located along Weeks Bayou on the northwest flank of Week

Island salt dome. In addition to pottery shards and baked clay lumps, other artifacts recovered were modified pieces of bone, stone, wood, shell and four galena artifacts (Byrd, 1974). The Poverty Point site was the largest settlement of its time in North America (1700 B.C. – 100 B.C.) (Webb 1977). It was once the center of a major exchange network: large number of exotic raw materials including copper, steatite, sandstone, galena, hematite/magnetite and a variety of different kinds of chert were brought in thousands of miles away to be used in making tools and ornaments (Webb 1977). Only four of them could be acquired for this study (68GA69415, 9344N50E15, W4986 and Poverty Point).

The McQuorquodale Mound (ICK25) in Alabama, is a burial mound located in the west central part of Clarke County in the swamp of the Tombibgee River. The mound is circular with a diameter of sixty feet and the burial artifacts recovered include native copper, flint, six galena nodules, mica and siltstone (Wimberly *et al*., 1941). Samuel's site (IMS137) located near Guntersville Lake in Marshall County; Alabama has two mounds built during the Late Woodland period. A variety of artifacts have been recovered from this site such as copper reels, shell fragments, stone pipes, galena and projectile points (Webb and Wilder, 1951).

The Middle Archaic Barrington site (23JE600A) is located at the base of a ridge between two intermittent drainage systems of the Big River in Jefferson County, Missouri. The artifacts found at the site are fragmented cylindrical banner stone, one galena nodule and projectile points (Martin, 2001). Rodgers Shelter (RS-1074), a deeply stratified rock shelter and one of the oldest sites from where galena has been recovered (Early Archaic-Middle Archaic), is at the base of a south-facing bluff overlooking an intermediate terrace approximately 90 m north of the Pomme de Terre river in south central Benton County, Missouri (Kay, 1980). A large variety of artifacts have been recovered from this site such hammer stone, grinding stone, projectile points and different kinds of minerals such as hematite, limonite and 37 pieces of galena (Kay, 1980).

From Illinois, samples have been collected from four different sites. Crane (CR-102) in Greene County is a Middle Woodland habitation site. It is located within the Macoupin Valley. Native copper artifacts have also been excavated from this site (Winters, 1981) along with some minor galena (~11 pieces analyzed by Walthall 1981). Loy (LOY-2201) is a Middle Woodland habitation site located on the crest of the bluffs defining the southern boundary of the Macoupin Valley in Macoupin County. This site is well known for abundant Middle Woodland ceramics. Other artifacts such as projectile points and minor galena have also been found (Farnsworth, 1973). Walthall, 1981 analyzed five galena artifacts and LOY-2201 is one of them. The third site is Macoupin site (MAC-A), a predominantly Early Woodland occupation site in the lower Illinois Valley of Jersey County. Small quantities of Early Woodland ceramics and flint objects have been recovered (Farnsworth, 1973) along with galena. Walthall, 1981 had analyzed 14 artifacts from Macoupin. The Twenhafel site (TW) is located in the Mississippi River's flood plain northwest of Fountain Bluff in Jackson County, southern Illinois. Some 25 burial mounds are present on the site and large habitation areas are located on raised grounds. Mica, minor galena pieces (five analyzed in Walthall's 1981 report), native copper, marine shell, native copper, ceramic shards, chipped stones etc have been recovered from this site (Hofman 1979).

The Raymond Mackey site (34Lf29) is a large black midden mound in the Fourche Maline valley in southeastern Oklahoma. The artifacts found in the site are most commonly associated

with the Fourche Maline culture of Late Archaic/Early Woodland periods (Burns 1994; Leader 1997). Two artifacts from this site have been analyzed. The Hughes, a Mississippian mound site (34Ms4229) is located on the west bank of the Arkansas River near Muskogee in Muskogee County, Oklahoma. The various artifacts recovered from the mound include pottery sherds, manos, chipped flint axes, ovoid shaped flint knives, celt fragments and galena (Bell 1974).

4.6.2 Lead Isotopes

Lead consists of four stable isotopes. Of these, three isotopes ^{206}Pb, ^{207}Pb and ^{208}Pb have radioactive parents ^{238}U, ^{235}U and ^{232}Th respectively, the decay of which add to their primordial quantity. The fourth isotope ^{204}Pb is unchanged from its primordial quantity. The ratio of each of these isotopes in a lead ore deposit will depend on the geological age of the ore deposit and the age and relative quantity of uranium, thorium and lead present in the source of lead that went into the ore-forming fluid/reservoir. Hence, lead isotope ratios in an ore body are distinctive though not necessarily unique. On the basis of lead isotopic variations measured in a large number of ore deposits, there are two categories of ore lead, ordinary lead (Russell and Farquhar, 1960) and J-type "anomalous lead" (Holmes, 1946; Houtermans, 1953). Ordinary ore leads have homogenous lead isotope ratios within a given deposit and have an isotopic composition that can be related to the age of the earth. J-type (Joplin type) leads are enriched in radiogenic isotopes with respect to ordinary leads and indicate a "futuristic age". These anomalous leads have multistage and complex origins. Leads from galenas in all the Mississippi Valley type deposits are extremely radiogenic and thus yields future model ages, which suggest sources in the upper crust.

Provenance determination is done by comparing lead isotope ratios of the artifacts to similar data for galenas from naturally occurring ore deposits (Farquhar and Fletcher, 1980). Since this does not involve multi elements and the isotope ratios used are for a single element, any chemical alterations during metallurgical extractions or oxidation processes do not fractionate isotopes; thus preserving the original provenience information (Barnes *et al*., 1978). Variation in isotope ratios is produced by geological processes only. Thus, it is unnecessary to use statistics while assigning archaeological artifacts to source deposits (Farquhar and Fletcher, 1980). One of the potential problems could be mixing of different ores during smelting and refining processes of lead (Farquhar and Fletcher, 1980). Since this study deals with unprocessed pure galenas the above problem does not arise.

4.6.3 Sulfur Isotopes

Sulfur, the other principle component of galena has four stable isotopes (^{32}S, ^{33}S, ^{34}S, ^{36}S) whose natural abundances are approximately 94.93, 0.76, 4.29, and 0.02 respectively (McNamara and Thode, 1950). Isotope abundance variations are generally considered in terms of the abundance ratio ^{34}S and ^{32}S of the two principal isotopes. Natural variations in isotopic compositions are generally small and this makes it convenient to refer to fractional differences in isotope ratios ('del' values of samples relative to a standard (Canon Diablo meteorite), and to express these differences in parts per thousand (per mil) :

$$\delta^{34}S=\left[\frac{\left(\frac{^{34}S}{^{32}S}\right)_{sample}}{\left(\frac{^{34}S}{^{32}S}\right)_{standard}}-1\right]\times 1000\,‰ \qquad (4.1)$$

For SEM, CM and TS ore districts, sulfur isotopes in galena are very well correlated with the lead isotopic compositions (**Figure 4.6**) (Brown, 1967; Goldhaber, *et al*. 1995; Sverjensky, *et al*., 1979; Deloule *et al*., 1986). The galenas with more radiogenic lead have low $\delta^{34}S$ while galenas with less radiogenic lead have higher $\delta^{34}S$. In this study, sulfur isotopes have been analyzed in the galena artifacts to check for similar correlation between sulfur and lead isotopes. The sulfur isotope analysis would provide additional evidence for provenance determination

4.6.4 Analytical Technique

Approximately 1-2 mg of galena is dissolved in 7N ultrapure nitric acid solution in clean Teflon beakers. This allows the lead to go into solution while the elemental sulfur forms a white precipitate. A plastic syringe was used to remove the sulfur precipitate from solution. A small aliquot containing approximately 0.5 µg of lead was taken from the solution and evaporated to dryness.

10-12 µL of 0.25 N nitric acid solutions was added to the dried samples. Approximately one-tenth of the sample was taken up in a 1-2 µL phosphoric acid - silica gel solution, loaded on to a single rhenium ribbon filament (Cameron *et al*., 1969) and evaporated to dryness. The filament was then loaded into a solid source thermal ionization mass spectrometer and heated to 1200-1350 ºC for data acquisition. The mass spectrometer is a FINNIGAN MAT 262 magnetic sector multicollector mass spectrometer has a 90°, 23 cm magnetic sector. Lead isotope ratios are presented normalized to NBS 981 using a linear mass fractionation correction of 0.7‰ per amu based on replicate analysis of 50 ng of the lead isotopic standard. The accepted lead isotope ratios for NBS 981 are: $^{207}Pb/^{206}Pb$: 0.914585 ± 0.00004, $^{208}Pb/^{206}Pb$: 2.16701± 0.00013, $^{206}Pb/^{204}Pb$: 16.9356 ± 0.0007, $^{207}Pb/^{204}Pb$: 15.4891 ± 0.0009, $^{208}Pb/^{204}Pb$: 36.7006 ± 0.0034 (Todt et al., 1995). The external precision of NBS 981 from five separate sessions is $^{207}Pb/^{206}Pb$: 0.914004 ± 0.000496, $^{208}Pb/^{206}Pb$: 2.163690± 0.002315, $^{206}Pb/^{204}Pb$: 16.904727 ± 0.019019, $^{207}Pb/^{204}Pb$: 15.451021 ± 0.025071, $^{208}Pb/^{204}Pb$: 36.574869 ± 0.082189 (±2σ, n = 36) (**Table 4.2**). Some of the sample chemistry was performed in duplicate to test for sample homogeneity, accuracy and precision of lead isotopic analysis (**Table 4.3**).

Sulfur isotope analysis was done in Environmental Isotope Laboratory in University of Waterloo. Solid samples are run for sulfur analysis on an Isochrom Continuous Flow Stable Isotope Mass Spectrometer (Micromass) coupled to a Carlo Erba Elemental Analyzer (CHNS-O EA1108). Sulphide standards used in correcting $\delta^{34}S$ analysis are IAEA-S1, IAEA-S2 and IAEA-S3 (AgS), EIL-40 (CuS), EIL-43 (ZnS), NBS-122 and NBS-123 (Sphalerite ZnS). After each group of 100 samples, standards are run to check for bias and linearity corrections. Four replicates of different amounts are analyzed at the beginning and end of each run. This set allows for linearity corrections. Two sets of replicates of element standards are also run in each group. A sample replicate is run at least every eight samples and duplicates are run from previous

groups. The overall average number of repeats is about one every eight samples. A few sample replicates of different weights are analyzed to check linearity of the sample matrix.

4.7 Results

The measured lead and sulfur isotopic ratios for the galena artifacts and the mines are presented in **Table 4.3**. **Figure 4.4** shows lead isotope plots for galenas from ore deposits in Old Lead Belt (OLB), Viburnum Trend (VT), Central Missouri (CM), Upper Mississippi Valley (UMV) and Tri-State (TS) (**Appendix A.2**). Use of the $^{208}Pb/^{206}Pb$ and $^{207}Pb/^{206}Pb$ ratios are probably more useful since some of the lead isotope measurements of the ore data were done at times when mass spectrometric techniques were less accurate in measuring ratios relative to ^{204}Pb (very low abundance) compared to modern day analysis and it is a preferred presentation of data in archaeological studies. The data set for the different ore deposits have been presented as fields which define the limits of the source data available for use. Except for some small areas of data field overlaps, the lead isotope ratios of the ore deposits in general are distinct from each other. Some previous reports have recorded significant variations in lead isotopic composition of galena from SEM and TS. These variations can be between mines within a district (Doe and Delevaux, 1972), between samples within any given mine (Sverjensky *et al*., 1979) and even within individual galena crystals (Cannon *et al*., 1963; Crocetti *et al*., 1988, 1989; Deloule *et al*., 1986; Hart *et al*., 1981). In one study, a total variation of ~ 3 percent in $^{208}Pb/^{206}Pb$ and ~4 percent in $^{207}Pb/^{206}Pb$ was measured in a single crystal of galena from Buick Mine, Southeast Missouri (Hart *et al*., 1981). $^{207}Pb/^{204}Pb$ plot will not be utilized because it is insensitive to source variations. In spite of the variations within an ore district, overall the different ore districts can be distinguished from each other.

Galena artifacts analyzed for lead isotope ratios are plotted against the outlines of the UMV, OLB, CM and TS data fields for source comparison (**Figure 4.5**). The VT field is not shown since it never acted as a source in prehistoric times. Also plotted are three galena artifacts from Florida analyzed by Austin *et al*., 2000. Most of the artifacts except a few plot tightly within the CM and TS data field. MAC-A and one sample from Poverty point site (68GA69415) plot within the UMV data field. The sample collected from Hughes site (34Ms4229) plots on the border of the UMV field in **Figure 4.5a** and on the border of the OLB field in **Figure 4.5b**. One of the Raymond Mackey sample (34Lf291512) plots within the OLB field (**Figure 4.5**) and the other 34Lf291032 plots near the CM and TS data field (**Figure 4.5**). The lead isotope data set for the UMV field (**Figure 4.4** and **4.5**) is based on 26 analyses of mineral galena samples by Millen *et al*., 1995 and 2 analyses by Farquhar and Fletcher, 1980. Previous lead isotopic studies (Austin *et al*., 2000; Farquhar and Fletcher, 1980, 1984; Farquhar *et al*., 1995) did not separate SEM (OLB) and CM lead ore districts in the lead isotope plots. This study will treat SEM and CM lead districts as separate galena source areas. The data for Old Lead Belt (OLB) are from Doe and Delevaux, 1972; Farquhar *et al*., 1995 and Goldhaber etal., 1995 and for the Ciborium Trend (VT) from Doe and Delevaux, 1972; Farquhar *et al*., 1995 and Goldhaber et al., 1995; Hart *et al*., 1981; Sverjensky *et al*., 1979. Data field (**Figure 4.4** and **4.5**) for the CM has been defined from analyses done by Goldhaber *et al*., 1995; Farquhar *et al*., 1995 and 2 mine samples analyses (**Table 4.3**) done in current study. The VT field has not been used in the artifact lead isotope plots (**Figure 4.5**). Very limited lead isotope data is available for the TS district mineral (Deloule

et al., 1986; Doe and Zartman, 1979; Goldhaber *et al*., 1995 and 3 analyses done in the current study, **Table 4.3**).

In **Figure 4.6** the sulfur isotopic ratio analyzed for a subset of the artifacts is plotted against $^{206}Pb/^{204}Pb$. Brown (1967) observed that there is a correlation between lead isotope and sulfur isotope values of galenas. The galenas with most radiogenic lead (higher $^{206}Pb/^{204}Pb$) have low $\delta^{34}S$ and with low radiogenic lead (lower $^{206}Pb/^{204}Pb$) have higher $\delta^{34}S$. This is because the lead and sulfur had been derived from two sources: normal sulphide bearing sedimentary rocks and evaporites (Brown, 1967). Fluids that obtained sulfur and lead from evaporites had very high $\delta^{34}S$ but less radiogenic lead whereas fluids obtaining lead and sulfur from the sedimentary rocks had very radiogenic lead but low $\delta^{34}S$ values. All the artifacts analyzed for sulfur isotopes show this correlation. For TS galena, the $\delta^{34}S$ are not as variable as $^{206}Pb/^{204}Pb$ ratio. In contrast CM galena show moderate variation in $\delta^{34}S$ compared to $^{206}Pb/^{204}Pb$ (**Figure 4.6**). The artifacts have $\delta^{34}S$ values that are very similar to CM ores (**Figure 4.6**).

4.8 Discussion

For the seventeen archaeological site samples for which lead isotope ratio has been determined, **Figure 4.5** indicates that galena from the Middle Woodland Macoupin site in Illinois (MAC-A) and one from Late Archaic- Early Woodland Poverty Point site (68GA69415) in Louisiana almost certainly originated in the Upper Mississippi Valley (UMV) district. The other artifacts from the Poverty Point site (9344N50E15, W-4986 and Poverty Point) show a signature varying between Old Lead Belt and Central Missouri/Tri-State. The galena from Hughes site could have originated from UMV district (**Figure 4.5 a**) but it shows more of an OLB source signature in **Figure 4.5b** and plots in the area where no UMV mine samples are known. The Raymond Mackey site shows a mixed source signature between OLB (sample 34Lf291512) and CM /TS (sample 34Lf291032) districts (**Figure 4.5**). The galena artifacts from rest of the archaeological sites i.e. Illinois (Loy, Crane and Twenhafel), Missouri (Rodgers Shelter and Barrington Cache), Louisiana (Morton Shell Mound), Alabama (Samuels and McQuorquodale) and Florida (Harley Means, Oak Knoll, Lake Jackson, Block Sterns and Miami Circle) (**Table 4.3, Figure 4.5**) have lead isotope ratios that lie within or close to the field defined by Central Missouri (CM) and Tri-State (TS) mineral deposits and show a total variation of ~ 1.8 percent in $^{208}Pb/^{206}Pb$. The TS lead isotope data occurs as groups in both **Figures 4.4a** and **4.4b** and is not continuous like CM lead. Most of the artifacts fall in the gap where no TS data is known and have very similar lead isotopic ratios with CM ore data (**Figure 4.5a** and **4.5b**). For the nine galena artifacts analyzed for sulfur isotopes, except for MAC-A all other artifacts show very similar $^{206}Pb/^{204}Pb$ to each other but large variation in sulfur isotope ratios (**Figure 4.6**). This type of correlation is exhibited by CM ore galenas but not the TS ore galenas (**Figure 4.6**). There are no published reports or historical evidence of TS lead district being exploited before European contact. Based on these relationships and lack of archaeological evidence of prehistoric exploitation of galena from TS, the artifacts appear to be sourced from CM ore district.

For one of the oldest archaeological sites Finlan (Late Archaic period) located near Lake Ontario, Farquhar and Fletcher (1980, 1984) found galenas originating from the southern part of the UMV mineral district. The Finlan site is special since it is approximately 1000 km away from the proposed source. Within the UMV deposits there are large systematic differences in lead

isotopic composition that have been observed on a regional scale (Heyl *et al*., 1966; Millen *et al*., 1995). The lead isotopic ratios $^{206}Pb/^{204}Pb$ and $^{208}Pb/^{204}Pb$ across the UMV district revealed a spatial variation in which lower ratios occur on the western side of the district and higher ratios towards the northeast side. (Heyl *et al*., 1966). The Finlan galenas (seven samples) have almost 3.5 percent variation in $^{206}Pb/^{204}Pb$ ratio which probably suggests that more than one mineral outcrop in the UMV region was being exploited even during the Late Archaic culture (Farquhar and Fletcher, 1980, 1984). The MAC-A sample has higher $^{206}Pb/^{204}Pb$ and $^{208}Pb/^{204}Pb$ ratios and probably originated from the northeast side of the UMV district in Wisconsin. The Poverty Point sample (68GA69415) probably originated from the southern part of the UMV district in Illinois.

For the galena artifacts recovered from the Illinois Middle Woodland archaeological sites Loy, Twenhafel and Crane (LOY-2201, TW and CR-102 respectively) CM seems to be the most probable source area (**Figure 4.5**). Although Loy, Crane and Macoupin sites are located quite close to each other (**Figure 4.3**) and represent Middle Woodland cultures the source for Macoupin artifact is UMV. For the galena artifacts from Macoupin for whose trace elements were conducted by Walthall (1981) one (out of 15) was sourced to UMV, two out of fifteen were sourced to CM and rest twelve were sourced to SEM (Potosi Formation). All the Loy and Twenhafel samples (five of each) were assigned to SEM (Potosi Formation) deposits. Of the eleven artifacts tested from Crane two were assigned each to UMV and CM and seven to SEM (Potosi Formation). In the SEM deposits, mineralization occurs in two major formations, Bonneterre and Potosi. Based solely on trace element analysis Walthall, 1981 had subdivided the SEM lead belt into Potosi Trend and Bonneterre Trend and had assigned numerous artifacts to Potosi Formation. The Potosi lead ore data are isotopically very different from CM (**Figure 4.4**) and none of the artifacts analyzed in this study show any lead isotope similarity to galena from Potosi Formation.

The Missouri archaeological sites, Rodgers Shelter (Early-Middle Archaic) and Barrington Cache (Middle Archaic) are one of the oldest sites for which galena artifacts has been analyzed in this study. The Rodgers Shelter is located within the CM ore district and so galena found within the archaeological deposits was most likely collected in the immediate vicinity of the site. The Barrington Cache sample has slightly different lead isotope value than any of the other thirteen artifacts but still plots close to the CM ore field than any other.

The Poverty Point, in Louisiana, show a mixed source between UMV, OLB and CM (**Figure 4.5**) districts which confirms with Walthall's 1981 report, where he assigned eight samples to UMV and twenty to SEM (Potosi Formation) and demonstrated a north-south cultural contact along the Mississippi river. Large quantity of galena had been recovered from Poverty Point suggesting intensive early exploitation of this source by either local cultures residing near the source area or by Poverty Point culture people themselves. From lead isotopes plots only, it is unclear whether samples 9344N50E15 and Poverty Point (**Figure 4.5**, **Table 4.3**) originated from CM or OLB districts. Sulfur isotope analysis conducted on these samples might be able to resolve this issue. Further south and on the Gulf of Mexico coast is the Morton Shell Mound site whose galena shows a CM signature and could have been obtained by trading with the Poverty Point people or by some other cultures residing along the Mississippi river.

The Samuel's site and McQuorquodale mound in Alabama are both from the Mississippian period. On the basis of trace element analysis, six galena samples recovered from the McQuorquodale mound were assigned to UMV (Walthall *et al*., 1980). It is speculated, especially for the McQuorquodale mound in the Gulf Coast that there was a north south cultural exchange of galena for marine products with the Copena culture (Walthall *et al*., 1980). The Samuel's site group similarly could have obtained galena via exchange with the Copena culture or some other group.

For both the Oklahoma site Raymond Mackey (Late Archaic-Early Woodland site) and Hughes (Mississippian site) the OLB and CM region seems to be the most probable source area. Although TS district is closer to these sites and logically a more potential source, the cultures residing in Oklahoma probably exchanged these products with local cultures exploiting the OLB, CM ore districts. The galena artifacts sourced from the OLB-CM zone probably were traded south along the Mississippi river and then traded west along the Arkansas river. Sulfur isotope analysis on these samples needs to be done to confirm these observations.

The galenas found in Florida are exceptional in that their origin is so distant (1500 kilometers) from potential sources. Austin *et al*. (2000) analyses of galena samples from three sites in Florida (Royce Mound, Ft. Center and Pineland sites) indicated a common source of origin in SEM. The provenance of galena for the Ft Center is not precisely defined by the available data (**Figure 4.5a**). The sample plots in between the CM and SEM field. The Royce Mound sample plots within the OLB field. The Pineland sample is close to the CM field and was probably sourced from CM. More definite source signature is exhibited in $^{206}Pb/^{204}Pb$ and $^{208}Pb/^{204}Pb$ plot (**Figure 4.5b**); all the 3 sites have galena plotting near or within the CM field with ratios quite distinct from SEM. Similar to the artifacts analyzed in this study; Walthall, 1981 had indicated a major trade route linking the Mississippi Valley region of Missouri and communities inhabiting the Flint and Apalachicola rivers of northwest Florida. Austin *et al*. (2000) speculated that from northwest Florida galena may have been traded to central and south Florida gradually in a "down-the-line" fashion. Such trading is indicated by the comparatively small amounts of galena found in Florida sites. The rarity of this material probably would have made it more valuable and therefore only important people of a tribe would have possessed the galena (Austin *et al*., 2000).

Although the closest sources of galena for the southern and southeastern states of Louisiana, Alabama and Florida are in northern Alabama, central Tennessee-central Kentucky and the east Tennessee-Virginia district, in prehistorical times Missouri seems to be the most important source area. The remarkable point is that for most of the southern and eastern United States, except Poverty Point in Louisiana, the source area for the galena artifacts seems to be fairly unique, probably from the CM ore deposit and definitely not from UMV. One of the oldest sites in this study is the Rodgers Shelter in Missouri from the Early Archaic-Middle Archaic (8000 B.C. – 3500 B.C.) period in the southern United States whereas the youngest sites are the Alabama sites (Samuels and McQuorquodale) and the Florida site (Lake Jackson) from the Mississippian period (A. D. 900 - A.D. 1500). All these sites have galena artifacts sharing the same lead isotope signature. The period of time spanned by these sites and their wide geographic distribution (mid-eastern, southern and southeastern U.S.) indicate that trade networks linking the native cultures to the CM source area was active for thousands of years. It is surprising that perhaps a limited number of actual extraction localities (CM) were exploited to this extent while

nearby other ore districts were not. It would be of great interest to know whether a single mineral outcrop was utilized for this long period of time. Most of the site artifacts except Barrington Cache have very homogenous lead isotope compositions compared to typical source ore deposits. It could be possible that all these galena artifacts came from a single mineral outcrop rather than from several outcrops within the CM ore district. This cannot be demonstrated directly since surface ore has all been mined away and in-situ samples are no longer available for analysis.

4.9 Conclusions

The lead isotope database for the Mid Continental lead mineral deposits allows us to determine, with a high degree of certainty, the origin of galena artifacts found at Late Archaic – Mississippian archaeological burial and habitation sites in southern and central United States. Most of the archaeological burial/habitation sites contain galena artifacts which have lead isotopic ratios that imply Central Missouri as a single source. Eight of the nine galena artifacts analyzed for sulfur show identical sulfur and lead isotope correlation with the Central Missouri lead district. The sites in the states of Missouri and Illinois have galenas which have been derived relatively locally (a few miles to a few hundred miles from the Central Missouri source area). The analysis of Oklahoma site galena indicate that nearby Tri-State district was probably not exploited and galena was exchanged with cultures that exploited the Old Lead Belt-Central Missouri region and transported along the Mississippi river and Arkansas River. For the sites situated in Alabama and Florida and one of the site in Louisiana , the data shows that from the time of the Early Middle Woodland period some galena samples were reaching areas quite distant (approximately a thousand miles) from the Central Missouri ore district. The other site in Louisiana, Poverty Point, once a major trading centre shows a mixed signature between Upper Mississippi Valley, Old Lead Belt and Central Missouri. Only one site in Illinois has galena sourced from the Upper Mississippi Valley and from available lead isotope contouring seems to be from the northeast side of the ore district in Wisconsin. From chemical and isotopic analysis, it seems that only certain areas especially the northern and northeastern North America have galena artifacts sourced from Upper Mississippi Valley lead district. There is no evidence that southern and eastern USA, except Poverty Point in Louisiana had ever had any significant amounts of galena originating from Upper Mississippi Valley. Further the evidence doesn't show of any temporal change in galena sources over a time span of thousand years in the southern and eastern USA.

Table 4.1 Descriptions of galena artifacts and mine samples collected for the present study

Sample	Location	County	State	Coordinates		Type	Age
				Latitude	Longitude		
HM1	Harley Means 1	Jefferson	Fl	30.24	84.02	A	
BSI	Block Sterns	Leon	Fl	30.44	84.18	A	M. Woodland
OK1	Oak Knoll	Lee	Fl	26.34	81.83	A	M. Woodland
OK2	Oak Knoll	Lee	Fl	26.34	81.83	A	M. Woodland
LJ1	Lake Jackson 1	Leon	Fl	30.50	84.31	A	Mississippian
LJ2	Lake Jackson 2	Leon	Fl	30.50	84.31	A	Mississippian
MC1	Miami Circle	Miami-Dade	Fl	25.76	80.19	A	E. M. Woodland
MC2	Miami Circle	Miami-Dade	Fl	25.76	80.19	A	E. M. Woodland
Loy-2201	Loy	Macoupin	Il	39.21	90.22	A	M. Woodland
IMS-137	Samuels Site, Guntersville	Marshall	Al	34.36	86.35	A	Mississippian
ICK25	McQuorquodale Mound	Clarke	Al	31.58	88.03	A	Mississippian
W-4986	Poverty Point	West Carroll P	La	32.63	91.40	A	Archaic/E. Woodland
9344N50E15	Poverty Point	West Carroll P	La	32.63	91.40	A	Archaic/E. Woodland
68GA69415	Poverty Point	West Carroll P	La	32.63	91.40	A	Archaic/E. Woodland
Poverty Point	Poverty Point	West Carroll P	La	32.63	91.40	A	Archaic/E. Woodland
I61-B3	Morton Shell Mound	Iberia P	La	29.82	91.81	A	M. Woodland
CR-102	Crane	Greene	Il	39.24	90.36	A	M. Woodland
23JE600A	Barrington Cache	Jefferson	Mo	38.36	90.64	A	M. Archaic
RS-1074	Rodgers Shelter	Benton	Mo	38.20	93.44	A	Archaic/E. Woodland
TW	Twenhafel	Jackson	Il	37.72	89.54	A	M. Woodland
MAC-A	Macoupin	Greene	Il	39.19	90.54	A	M. Woodland
34Lf291032	Raymond Mackey	Le Flore	Ok	34.92	94.81	A	L. Archaic/E.Woodland
34Lf291512	Raymond Mackey	Le Flore	Ok	34.92	94.81	A	L. Archaic/E.Woodland
34Ms4/229	Hughes	Muskogee	Ok	35.79	95.31	A	Mississippian
MW2	Dresser Minerals Pit, Mineral Point	Washington	Mo	38.12	90.69	M	
MC-3	Quigley Mine, Fortuna, CM	Morgan	Mo	38.34	92.47	M	
MS-9	Mine La Motte Corp	Madison	Mo	37.36	90.14	M	
MJ-1	Bill Shaft , Potosi	Jefferson	Mo	38.23	90.30	M	
MF-3	Jackson Mine (Ba-Pb)	Franklin	Mo	38.20	90.58	M	
MC-1	Circle Mines, CM	Miller	Mo	38.21	92.24	M	
B. Goose	Blue Goose, Picher Field, TS	Ottawa	Ok	36.96	94.86	M	
MCM	Mid Continent Mine, Picher Field, Treece, TS	Cherokee	Ks	37.00	91.86	M	
8HG676*	Royce Mound	Highlands	Fl	27.36	81.32	A	M. Woodland
8GL13*	Fort Center's Mound A	Glades	Fl	26.96	81.16	A	M. Woodland
8LL33*	Mound, Pineland	Lee	Fl	26.66	82.15	A	Mississippian

Under "Location", CM = Central Missouri, TS= Tri-States mineral district; Under "Type", A = artifact sample, M= mine sample.= data from Austin et al., 2000*

Table 4.2 Lead isotope ratios for replicate analyses of NBS 981

NBS 981	$^{207}Pb/^{208}Pb$	$^{207}Pb/^{206}Pb$	$^{208}Pb/^{206}Pb$	$^{206}Pb/^{204}Pb$	$^{207}Pb/^{204}Pb$	$^{208}Pb/^{204}Pb$
uncorr Average	0.422371	0.914236	2.164534	16.909030	15.459210	36.600448
	0.422570	0.913820	2.162495	16.893424	15.437561	36.535350
	0.422551	0.913624	2.162193	16.894727	15.435245	36.528571
	0.422473	0.913939	2.163321	16.900986	15.446306	36.562190
	0.422425	0.914020	2.163744	16.903539	15.450150	36.574837
	0.422218	0.914599	2.166169	16.924806	15.479515	36.662035
	0.422189	0.914533	2.166167	16.923525	15.477271	36.659456
	0.422367	0.914266	2.164632	16.909506	15.459803	36.602828
	0.422301	0.914085	2.164539	16.909898	15.457096	36.602030
	0.422415	0.913930	2.163606	16.909550	15.454273	36.585498
	0.422464	0.913876	2.163195	16.906382	15.450154	36.571440
	0.422448	0.913895	2.163333	16.909527	15.453637	36.580853
	0.422246	0.913952	2.164508	16.915176	15.459713	36.612975
	0.422266	0.913928	2.164321	16.912872	15.457238	36.604951
	0.422509	0.913717	2.162604	16.897445	15.439507	36.542443
	0.422277	0.914125	2.164758	16.919884	15.466933	36.628065
	0.422647	0.913622	2.161650	16.890412	15.431540	36.511817
	0.422371	0.914236	2.164534	16.909030	15.459210	36.600448
	0.422570	0.913820	2.162495	16.893424	15.437561	36.535350
	0.422551	0.913624	2.162193	16.894727	15.435245	36.528571
	0.422606	0.913669	2.161972	16.885671	15.427622	36.505642
	0.422216	0.914599	2.166180	16.925160	15.479901	36.663077
	0.422418	0.914025	2.163796	16.903794	15.450476	36.576286
	0.422474	0.913935	2.163302	16.900751	15.446016	36.561391
	0.422407	0.914074	2.163949	16.906270	15.453499	36.585010
	0.422529	0.913833	2.162755	16.897821	15.442030	36.546697
	0.422419	0.914102	2.164510	16.905207	15.453214	36.581751
	0.422518	0.913966	2.163143	16.899300	15.445304	36.555888
	0.422397	0.914205	2.164310	16.908776	15.458077	36.595740
	0.422567	0.913855	2.162627	16.896093	15.440661	36.514274
	0.422407	0.914074	2.163949	16.906270	15.453499	36.585010
	0.422529	0.913833	2.162755	16.897821	15.442030	36.546697
	0.422419	0.914102	2.164510	16.905207	15.453214	36.581751
	0.422518	0.913966	2.163143	16.899300	15.445304	36.555888
	0.422397	0.914205	2.164310	16.908776	15.458077	36.595740
	0.422567	0.913855	2.162627	16.896093	15.440661	36.514274
Average	0.422434	0.914004	2.163690	16.904727	15.451021	36.574869
2Stdev	0.000238	0.000496	0.002315	0.019019	0.025071	0.082189

Table 4.3 Lead and sulfur isotope ratios for artifacts and mine samples analyzed in this study

Sample	$^{206}Pb/^{204}Pb$	$^{207}Pb/^{204}Pb$	$^{208}Pb/^{204}Pb$	$^{207}Pb/^{206}Pb$	$^{208}Pb/^{206}Pb$	$^{207}Pb/^{208}Pb$	$\delta^{32}S$
HM1	22.102544	15.926587	40.991554	0.720582	1.854611	0.389088	-6.0
BSI	21.938606	15.933132	40.965247	0.726266	1.867285	0.389496	1.4
OK1	21.910650	15.917629	40.972677	0.726471	1.869992	0.389042	
OK1 (d)	21.931381	15.948090	41.074107	0.727182	1.872840	0.388830	2.1
OK2	21.835596	15.920862	40.951678	0.729125	1.875466	0.389319	5.3
LJ1	21.828556	15.898168	40.856640	0.728316	1.871710	0.389673	2.7
LJ2	21.931993	15.920128	40.940608	0.725884	1.866683	0.389416	-3.9
LJ1(dup)	21.835120	15.904681	40.879166	0.728404	1.872175	0.389622	
MC2	22.052909	15.921733	40.961687	0.721980	1.857432	0.389250	-6.7
MC2 (d)	22.070475	15.940450	41.028479	0.722252	1.858978	0.389075	
MC1	21.914199	15.906743	40.949891	0.725871	1.868651	0.388997	
MC1 (d)	21.924849	15.912270	40.972697	0.725767	1.868786	0.388915	
LOY-2201	21.893862	15.906272	40.951093	0.726502	1.870391	0.389005	
IMS-137	21.880235	15.908245	40.933140	0.727056	1.870780	0.389223	4.4
ICK25	21.900054	15.926642	40.999903	0.727243	1.872107	0.389028	
W-4986	21.873053	15.917262	40.906840	0.727711	1.870188	0.389681	-3.8
9344N50E15	21.905371	15.935548	41.024590	0.727472	1.872772	0.388439	
9344 N50E15 (d)	21.905582	15.935336	41.023222	0.727455	1.872750	0.388447	
Poverty Point	21.840381	15.931229	40.970634	0.729439	1.875933	0.388845	
68GA69415	22.233693	16.008838	42.119107	0.720026	1.894382	0.380085	
68GA69415 (d)	22.236112	16.009750	42.121965	0.719989	1.894333	0.380081	
I61-B3	21.871282	15.927769	40.994400	0.728243	1.874357	0.389099	
CR-102	21.967625	15.945653	41.092899	0.725878	1.870641	0.388608	
23JE600A	22.024872	15.989009	41.285961	0.725953	1.874790	0.387788	
RS-1074	22.022817	15.969794	41.135085	0.725134	1.867638	0.388801	-4.3
RS-1074 (d)	21.802000	15.959064	40.930000	0.732000	1.878000	0.3899112	
TW	21.854505	15.930706	40.954034	0.728924	1.873913	0.389574	
MAC-A	23.237500	16.083868	42.743600	0.692144	1.839408	0.376848	4.0
34Lf291032	21.982439	15.946597	41.026957	0.725424	1.866357	0.388686	
34Lf291032(d)	21.981046	15.943982	41.019167	0.725351	1.866431	0.388696	
34Lf291512	21.630471	15.929772	40.922898	0.736451	1.891937	0.389263	
34Lf291512(d)	21.634076	15.932317	40.930373	0.736445	1.891926	0.389254	
34Ms4/229	20.578215	15.762769	39.919586	0.765993	1.939876	0.394863	
34Ms4/229 (d)	20.579134	15.763526	39.920983	0.765996	1.939868	0.394868	
MW2	22.060630	15.942400	41.025844	0.722662	1.859670	0.389179	
MC-3	22.048465	15.928693	41.063991	0.722438	1.862453	0.388475	-5.9
MS-9	21.127468	15.891517	40.059061	0.752172	1.896068	0.397296	
MJ-1	20.828209	15.835565	40.064143	0.760303	1.923560	0.395837	
MF-3	22.232695	15.968782	41.208861	0.718255	1.853551	0.388077	
MC-1	21.998611	15.949773	41.136393	0.725045	1.869963	0.388305	
Bgoose	22.080796	15.873599	41.091827	0.718887	1.860976	0.386296	-8.5
MCM	22.426409	15.938048	41.411341	0.710682	1.846544	0.384872	
8HG676*	21.802000	15.959064	40.930000	0.732000	1.878000	0.389776	
8GL13*	21.867000	15.976030	41.040000	0.730600	1.876000	0.389446	
8LL33*	22.005000	15.977831	41.010000	0.726100	1.863000	0.389748	

**= samples from Austin et al., 2000. d= duplicate, where sample chemistry was replicated*

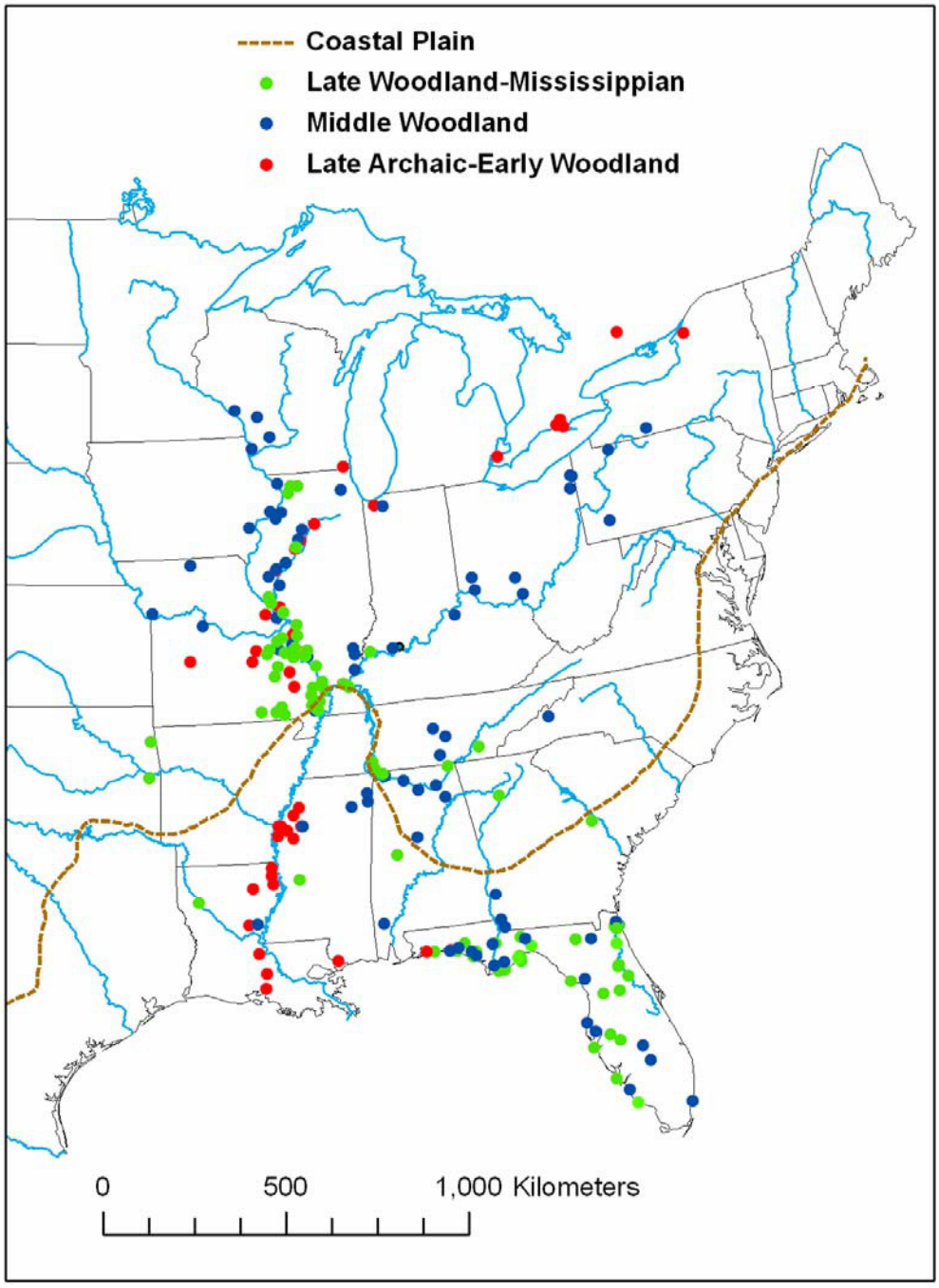

Figure 4.1. Distribution of galena artifacts at Late-Archaic – Mississippian archaeological habitation and burial sites. Figure modified from Walthall, 1981 and Austin et al., 2000.

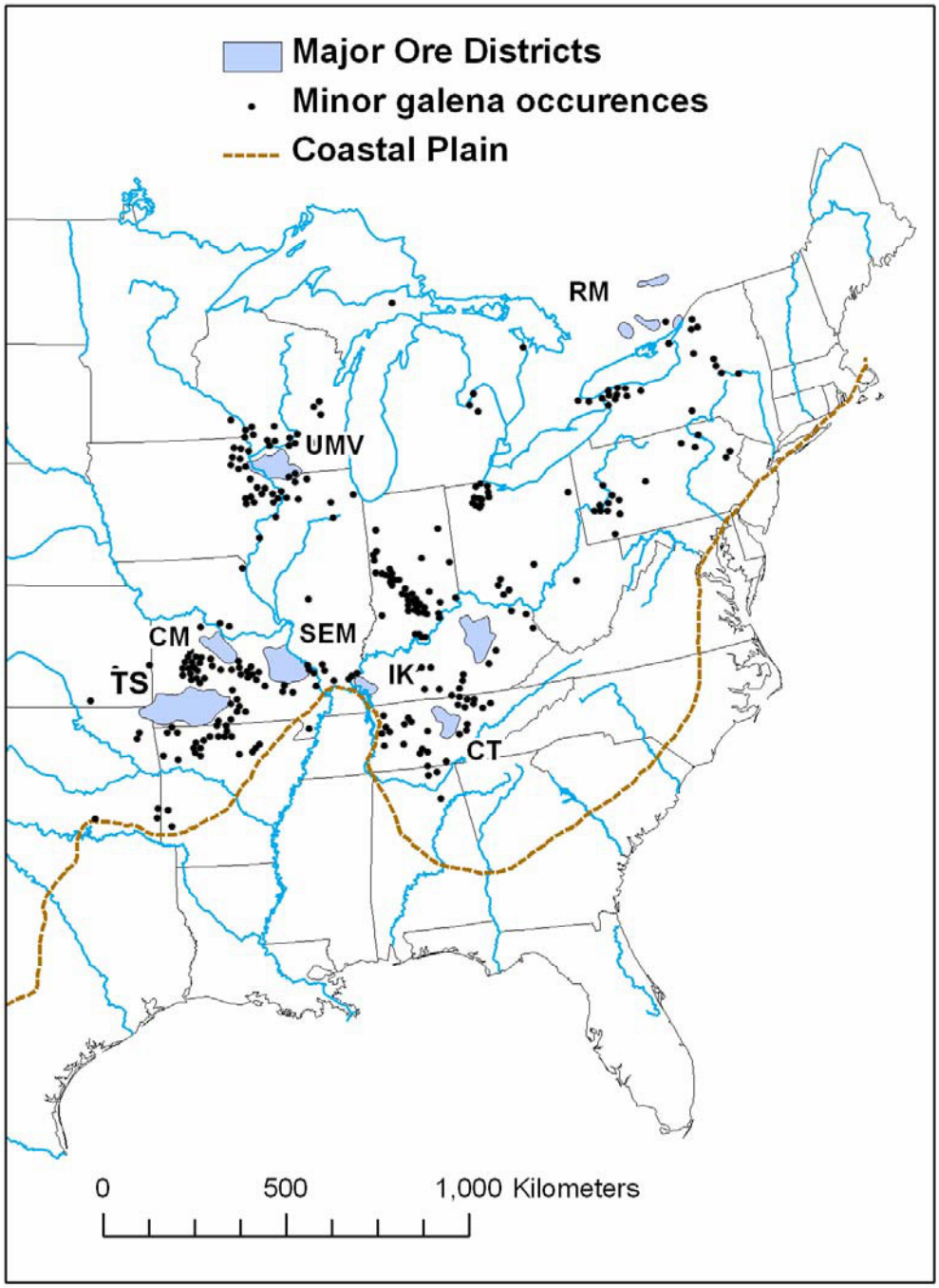

Figure 4.2. Map of major and minor galena ore sources in USA. UMV= Upper Mississippi Valley district in Illinois, Wisconsin and Iowa; CM= Central Missouri District, SEM= South-Eastern Missouri District; TS= Tri-Stats District in Missouri, Oklahoma and Kansas; IK= Illinois-Kentucky Fluorspar District; CK= Central Kentucky, CT= Central Tennessee, RS= Rossie Mines, New York. Adapted from Heyl 1968.

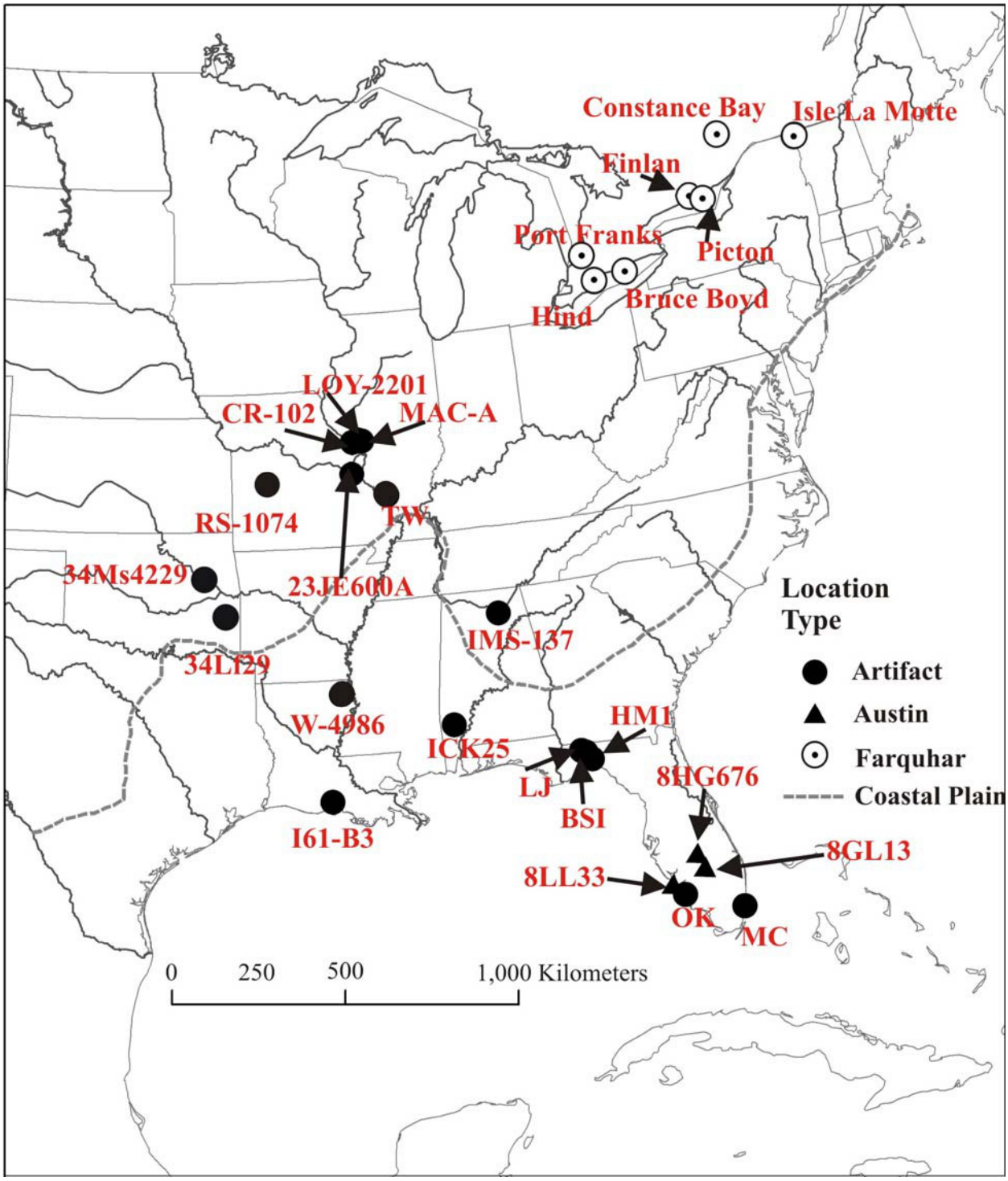

Figure 4.3 Location of archaeological burial/habitation sites from where galena artifacts were sampled for present study. MC= Miami Circle; OK= Oak Knoll; LJ= Lake Jackson; BSI= Block Stern; HM1 = Harley Means; I61B3 = Morton Shell Mound; ICK25 = McQuorquodale Mound; W-4986= Poverty Point; IMS-137 = Samuels; TW= Twenhafel; 23JE600A= Barrington Cache; RS-1074= Rodgers Shelter; CR-102= Crane; LOY-2201= Loy; MAC-A= Macoupin, 34Ms4229 = Hughes, 34L29= Raymond Mackey. For more details on samples please see Table 4.1.

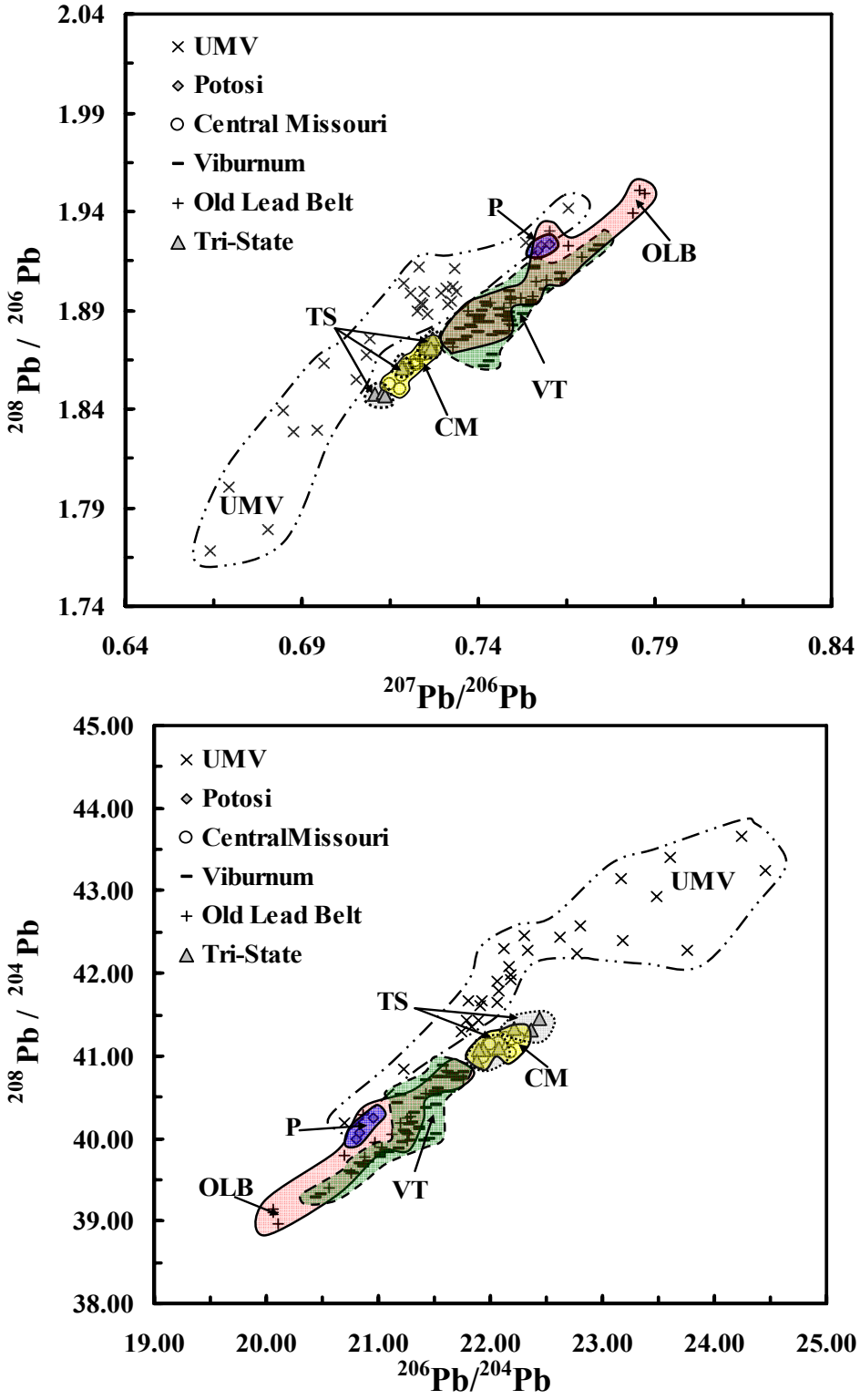

Figure 4.4 Bivariate lead isotope ratio plots a) ^{208}Pb / ^{206}Pb vs. ^{207}Pb / ^{206}Pb and b) ^{208}Pb / ^{204}Pb vs. ^{206}Pb / ^{204}Pb for galenas from the Upper Mississippi Valley (UMV), Potosi (P), Central Missouri (CM), Ciborium (VT), Old Lead Belt (OLB) and Tri-State (TS) ore districts. Data sources are: Deloule *et al*., 1986; Doe and Delevaux, 1972; Doe and Zartman, 1979; Farquhar *et al*., 1995; Farquhar and Fletcher, 1980; Goldhaber *et al*., 1995; Hart *et al*., 1981; Millen *et al*., 1995 and Sverjensky *et al*., 1979.

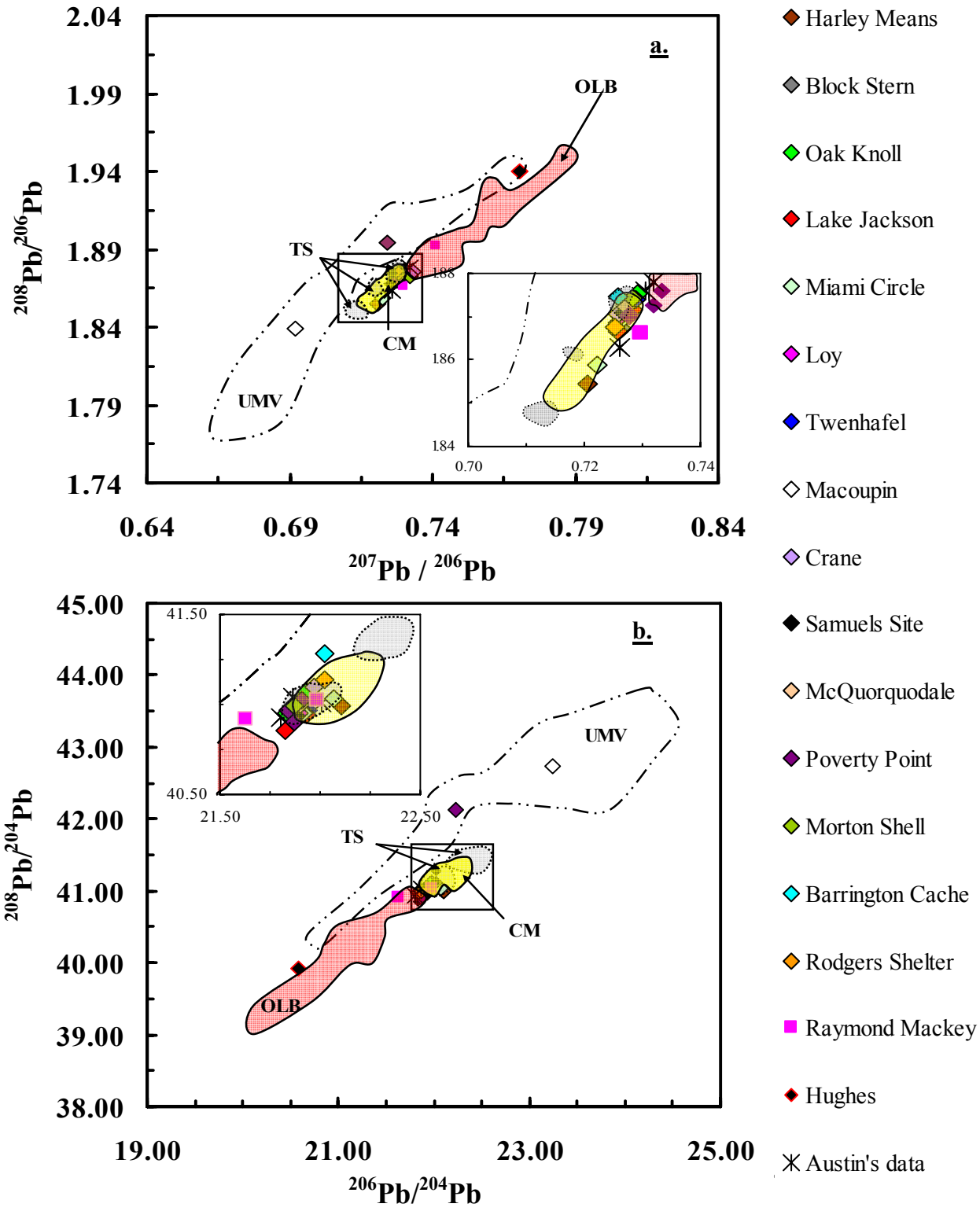

Figure 4.5 Bivariate lead isotope ratio plots a) ^{208}Pb / ^{206}Pb vs. ^{207}Pb / ^{206}Pb and b) ^{208}Pb / ^{204}Pb vs. ^{206}Pb / ^{204}Pb for galena artifacts analyzed in this study. The data field boundaries for galenas from UMV, CM, OLB and TS are shown for comparison. Three galena artifacts analyzed by Austin *et al*., 2000 are also shown for comparison. The inset shows an enlarged view of the lead isotope ratio for the galena artifacts.

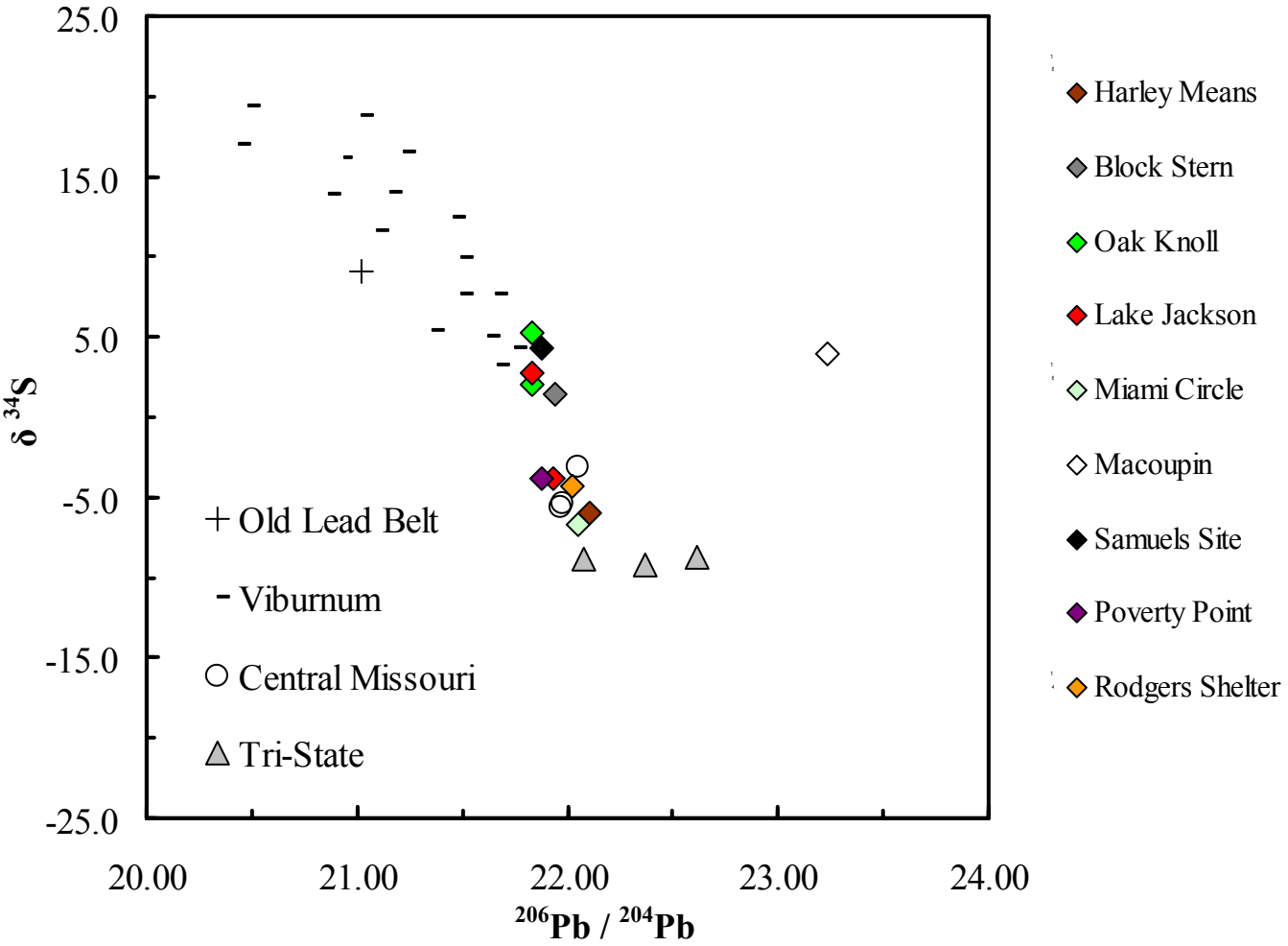

Figure 4.6 Lead and sulfur isotopic composition of archaeological galena artifacts analyzed in this study. Plotted for comparison are galena mine data from South – East Missouri (Old Lead Belt and Ciborium Trend), Central Missouri and Tri-State lead ore districts. Data has been compiled from Deloule *et al*., 1986, Goldhaber *et al*., 1995 and Sverjensky *et al*., 1979.

APPENDIX

Table A.1 Mercury isotope ratios for Penido Vello peat core

Sample	$\delta\ ^{198}Hg/^{202}Hg$	$\delta\ ^{199}Hg/^{202}Hg$	$\delta\ ^{200}Hg/^{202}Hg$	$\delta\ ^{201}Hg/^{202}Hg$	$\delta\ ^{204}Hg/^{202}Hg$
Vegetation	4.22	2.81	2.06	0.71	-2.02
	4.05	2.76	2.00	0.73	-1.98
	3.89	2.62	1.90	0.75	-1.82
Interface	3.84	2.58	1.90	0.55	-1.92
	3.73	2.39	1.80	0.49	-1.79
0-2A	3.90	2.64	1.93	0.53	-1.71
	3.70	2.50	1.92	0.43	-1.98
	4.35	2.86	2.15	0.65	-2.28
	4.03	2.88	1.95	0.46	-2.39
	4.10	2.80	1.96	0.47	-1.82
0-2B	4.05	2.62	2.02	0.46	-1.99
	3.94	2.62	2.01	0.47	-2.04
	3.93	2.57	1.97	0.47	-2.02
0-2C	3.97	2.64	1.94	0.58	-1.92
	4.37	2.90	2.18	0.57	-1.98
	3.75	2.45	1.84	0.49	-1.92
	3.73	2.37	1.82	0.53	-1.84
	3.77	2.47	1.89	0.41	-1.94
2-4	4.30	3.01	2.17	0.69	-2.19
	4.43	3.00	2.19	0.85	-1.99
4-6	4.04	2.80	1.99	0.71	-2.01
	3.85	2.63	1.90	0.67	-1.91
6-8A	5.72	4.11	2.81	1.23	-2.85
	5.80	4.15	2.88	1.11	-2.87
	5.58	4.02	2.78	1.17	-2.61
6-8B	5.83	4.34	2.91	1.25	-2.58
	5.87	4.27	2.89	1.12	-2.65
	5.80	4.24	2.84	1.32	-2.69
	5.87	4.18	2.82	1.19	-2.97
10-12	5.33	3.79	2.67	1.05	-2.55
	5.02	3.49	2.46	0.96	-2.34
	4.74	3.26	2.32	0.79	-2.23
	4.47	3.12	2.22	0.88	-2.22
12-14	3.90	2.62	1.94	0.61	-1.94
	4.09	2.77	2.01	0.66	-2.05
	4.19	2.85	2.08	0.70	-2.06
	4.33	2.98	2.16	0.79	-2.14
	4.16	2.84	2.09	0.74	-2.02
14-16	4.55	3.05	2.22	0.66	-2.21
	4.35	2.99	2.07	0.59	-1.99
16-18	3.64	2.41	1.83	0.54	-1.89
	3.73	2.49	1.84	0.54	-1.95
	3.60	2.38	1.81	0.49	-1.93

Table A.1 continued

Sample	$\delta^{198}Hg/^{202}Hg$	$\delta^{199}Hg/^{202}Hg$	$\delta^{200}Hg/^{202}Hg$	$\delta^{201}Hg/^{202}Hg$	$\delta^{204}Hg/^{202}Hg$
20-22	4.20	2.87	2.06	0.68	-2.12
	4.29	2.96	2.10	0.65	-1.99
22-24	4.20	2.78	2.16	0.62	-2.07
	3.73	2.42	1.82	0.63	-1.86
22-24	3.44	2.15	1.67	0.56	-1.63
	3.66	2.40	1.76	0.60	-1.71
26-28	3.64	2.40	1.80	0.44	-1.75
	3.67	2.30	1.79	0.51	-1.72
30-32	4.28	3.03	2.06	0.71	-1.85
	4.29	2.93	2.04	0.81	-1.72
	4.40	2.98	2.16	0.94	-2.06
	4.03	2.89	2.06	0.68	-1.91
	3.93	2.81	2.06	0.69	-1.77
	3.81	2.71	1.96	0.62	-1.91
32-34	3.79	2.53	1.86	0.59	-1.87
	3.87	2.59	1.98	0.61	-1.90
	3.70	2.47	1.88	0.47	-1.92
	3.81	2.49	1.85	0.47	-1.95
34-36	3.64	2.55	1.77	0.59	-1.68
	3.52	2.35	1.77	0.52	-1.77
	3.67	2.38	1.76	0.62	-1.74
38-40	4.02	2.68	2.03	0.80	-1.94
	3.73	2.52	1.81	0.49	-1.75
	3.79	2.48	1.77	0.59	-1.69
	3.79	2.51	1.89	0.55	-1.85
	3.39	2.23	1.66	0.50	-1.63
42-44	4.61	3.06	2.25	0.68	-2.18
	4.38	3.03	2.27	0.82	-2.27
	4.01	2.76	1.89	0.49	-2.04
	4.27	2.77	2.12	0.52	-2.08
	4.58	2.96	2.20	0.79	-2.25
44-46	4.38	3.02	2.17	0.80	-2.11
	3.67	2.45	1.92	0.55	-1.82
	4.26	2.93	2.14	0.62	-2.32
46-48	5.26	3.67	2.68	1.15	-2.44
50-52	3.72	2.35	1.80	0.55	-1.76
	3.45	2.27	1.73	0.61	-1.84
	3.51	2.30	1.95	0.52	-1.54
	3.54	2.17	1.70	0.49	-1.71
	3.57	2.31	1.78	0.52	-1.79
54-56	4.16	2.80	2.14	0.75	-1.88
	4.10	2.67	2.06	0.73	-1.91
	4.22	2.81	2.12	0.62	-2.00
56-58	3.80	2.42	1.89	0.61	-1.80
	3.80	2.48	1.82	0.57	-1.90
	3.81	2.41	1.88	0.49	-1.91
	3.75	2.29	1.84	0.55	-1.77

Table A.1 Continued

Sample	$\delta^{198}Hg/^{202}Hg$	$\delta^{199}Hg/^{202}Hg$	$\delta^{200}Hg/^{202}Hg$	$\delta^{201}Hg/^{202}Hg$	$\delta^{204}Hg/^{202}Hg$
	3.62	2.27	1.78	0.58	-1.82
	3.89	2.42	1.89	0.51	-1.83
58-60	2.78	1.72	1.35	0.29	-1.21
	2.77	1.59	1.31	0.27	-1.25
58-60	3.15	1.76	1.52	0.36	-1.58
	3.03	1.81	1.51	0.26	-1.47
	3.11	1.91	1.51	0.42	-1.49
62-64	2.91	1.62	1.36	0.50	-1.31
	2.88	1.64	1.42	0.32	-1.25
	2.95	1.59	1.41	0.31	-1.16
	3.09	1.90	1.52	0.40	-1.32
64-66	4.38	2.81	2.13	0.66	-1.94
	4.34	2.86	2.10	0.61	-2.19
	4.29	2.85	2.05	0.63	-1.91
	4.03	2.59	1.98	0.58	-1.78
66-68	3.55	2.28	1.78	0.55	-1.64
	3.69	2.41	1.80	0.54	-1.78
	3.35	2.25	1.68	0.53	-1.65
	3.12	1.90	1.53	0.41	-1.40
70-72	4.30	2.87	2.09	0.68	-1.91
	4.10	2.70	2.00	0.80	-1.82
	3.95	2.68	2.02	0.78	-1.73
74-76	3.86	2.55	1.94	0.59	-1.73
	4.37	2.86	2.14	0.59	-2.10
	4.01	2.74	2.02	0.52	-2.05
78-80	3.67	2.35	1.83	0.64	-1.76
	3.68	2.54	1.90	0.55	-1.91
	3.63	2.39	1.79	0.51	-1.75
82-84	4.44	2.93	2.12	0.72	-2.13
	4.53	3.12	2.29	0.75	-2.15
	4.63	3.10	2.29	0.72	-2.19
	4.54	3.04	2.24	0.87	-2.21
84-86	4.17	2.74	2.04	0.71	-1.89
	3.91	2.51	1.88	0.57	-1.96
	3.67	2.40	1.87	0.61	-1.68
	3.39	2.32	1.72	0.51	-1.62
	3.63	2.39	1.81	0.52	-1.67
86-88	4.11	2.65	1.99	0.64	-1.85
	4.15	2.72	2.07	0.48	-1.98
	3.81	2.56	1.92	0.68	-1.82
	4.09	2.72	2.06	0.55	-1.93
	4.21	2.69	2.00	0.54	-1.86
90-92	3.95	2.61	1.98	0.59	-1.84
	5.37	3.75	2.65	1.06	-2.51
	4.14	2.77	2.03	0.77	-1.76
	4.06	2.65	1.94	0.67	-1.93
92-94	3.58	2.29	1.74	0.45	-1.92

Table A.1 Continued

Sample	$\delta^{198}Hg/^{202}Hg$	$\delta^{199}Hg/^{202}Hg$	$\delta^{200}Hg/^{202}Hg$	$\delta^{201}Hg/^{202}Hg$	$\delta^{204}Hg/^{202}Hg$
	4.36	2.92	2.12	0.72	-2.02
	3.78	2.49	1.93	0.55	-1.70
	3.79	2.47	1.87	0.56	-1.84
	3.52	2.26	1.78	0.50	-1.61
94-96	3.39	2.35	1.77	0.59	-1.65
	3.37	2.25	1.67	0.49	-1.62
	3.50	2.46	1.95	0.85	-1.26
96-98	3.67	2.36	1.78	0.51	-1.62
	3.16	2.09	1.58	0.35	-1.41
	2.92	1.88	1.43	0.35	-1.41

Table A.2 Lead isotope data for ore deposits

Name of mine	State	Ore District	Lead Isotopic Ratios			Ref
			$^{206}Pb/^{204}Pb$	$^{207}Pb/^{204}Pb$	$^{208}Pb/^{204}Pb$	
Waukon (Mineral Creek) mines	IA	UMV	20.70	15.85	40.19	1
Captain Turner mine	IA	UMV	21.22	15.99	40.83	1
Holmes mine	IA	UMV	21.74	15.95	41.29	1
Skene mine	IL	UMV	21.92	16.02	41.67	1
Amelia mine	IL	UMV	21.91	15.98	41.60	1
Rockville mine	WI	UMV	21.89	16.01	41.44	1
Piquette mine	WI	UMV	22.06	16.01	41.64	1
Bautsch mine	IL	UMV	22.18	16.06	41.98	1
Nigger Jim mine	WI	UMV	22.07	15.97	41.79	1
New Hoskins mine	WI	UMV	22.17	15.98	42.09	1
Calumet mine (cubic c.)	WI	UMV	22.80	16.15	42.58	1
Calumet mine (octahedral c.)	WI	UMV	22.62	16.04	42.43	1
Ohlerking mine	WI	UMV	23.18	16.10	42.40	1
Old Slack mine	WI	UMV	23.48	16.14	42.93	1
Ivey mine	WI	UMV	23.76	16.17	42.27	1
North Yellowstone mine	WI	UMV	23.60	16.16	43.40	1
Demby-Weist mine	WI	UMV	24.24	16.22	43.65	1
Spring Grove mine	MN	UMV	21.83	15.99	41.36	1
Pints Quarry mine	IA	UMV	18.29	15.62	38.24	1
Fessler mine	IA	UMV	22.06	15.99	41.91	1
Orion mine	WI	UMV	22.77	16.06	42.24	1
Doylestown mines	WI	UMV	24.46	16.24	43.25	1
Blue Mounds mines*	WI	UMV	23.16	16.12	43.15	1
Vinegar Hill mine	IL	UMV	22.30	16.03	42.45	1
Ten Strike mine	IL	UMV	21.79	15.97	41.44	1
Mt. Carroll mines	IL	UMV	21.80	15.99	41.66	1
Stebbins mine	IL	UMV	22.12	16.00	42.3	1
Milliken	MO	VT	21.32	15.91	40.30	2
Milliken	MO	VT	21.36	15.93	40.14	2

Table A.2 Continued

Name of mine	State	Ore District	Lead Isotopic Ratios			Reference
			$^{206}Pb/^{204}Pb$	$^{206}Pb/^{204}Pb$	$^{206}Pb/^{204}Pb$	
Fletcher	MO	VT	21.25	15.91	40.08	2
Fletcher	MO	VT	21.16	15.99	40.43	2
Fletcher	MO	VT	21.19	16.02	40.52	2
Fletcher	MO	VT	21.62	15.96	40.80	2
Fletcher	MO	VT	21.67	15.98	40.79	2
Fletcher	MO	VT	21.49	15.90	40.52	2
Fletcher	MO	VT	21.58	16.01	40.87	2
Fletcher	MO	VT	21.53	15.93	40.61	2
Fletcher	MO	VT	21.56	15.98	40.74	2
Fletcher	MO	VT	21.53	15.98	40.74	2
Fletcher	MO	VT	21.70	15.99	40.71	2
Buick	MO	VT	21.26	15.90	40.06	2
Buick	MO	VT	21.02	15.87	39.82	2
Buick	MO	VT	21.36	15.89	40.10	2
Buick	MO	VT	21.63	15.92	40.56	2
Buick	MO	VT	21.51	15.91	40.41	2
Buick	MO	VT	21.51	15.91	40.53	2
Buick	MO	VT	21.51	15.91	40.41	2
Buick	MO	VT	21.75	15.92	40.73	3
Buick	MO	VT	21.66	15.92	40.73	3
Buick	MO	VT	21.50	15.92	40.56	3
Buick	MO	VT	21.23	15.89	40.10	3
Buick	MO	VT	21.10	15.87	39.83	3
Buick	MO	VT	21.02	15.87	39.78	3
Buick	MO	VT	20.48	15.83	39.33	3
Buick	MO	VT	20.44	15.82	39.28	3
Magmont	MO	VT	21.21	15.89	39.96	2
Magmont	MO	VT	21.29	15.90	39.98	2
Magmont	MO	VT	21.06	15.87	39.85	2
Ciborium 28	MO	VT	22.58	15.99	41.69	2
Ciborium 28	MO	VT	21.18	15.88	39.87	2
Ciborium 29	MO	VT	21.46	15.95	40.00	2
Ciborium 29	MO	VT	21.41	15.93	39.97	2
Ciborium 29	MO	VT	21.52	15.96	40.06	2
Ciborium 29	MO	VT	21.36	16.00	40.49	2
Ciborium 29	MO	VT	21.43	16.05	40.71	2
Ciborium 29	MO	VT	21.28	15.91	40.16	2
Bixby	MO	VT	21.02	15.87	39.81	4
Bixby	MO	VT	21.30	15.89	40.20	4
Bixby	MO	VT	20.75	15.83	39.60	4
Number 8	MO	VT	20.78	15.85	39.59	4
Number 8	MO	VT	20.91	15.87	39.72	4
Number 8	MO	VT	21.56	15.91	40.56	4
Indian Creek Mine	MO	VT	21.76	15.93	40.80	5
Derby-Doe Run	MO	OLB	20.88	15.85	39.78	2
Hayden Creek	MO	OLB	20.97	15.86	39.95	2
Madison	MO	OLB	21.60	15.93	40.82	2

Table A.2 Continued

Name of mine	State	Ore District	Lead Isotopic Ratios			Reference
			$^{206}Pb/^{204}Pb$	$^{206}Pb/^{204}Pb$	$^{206}Pb/^{204}Pb$	
Goose Creek	MO	Indian Creek	21.03	15.88	39.89	2
Potosi core	MO	OLB	20.96	15.87	40.25	2
Surface	MO	OLB	21.25	15.92	40.25	2
Doe Run Lead Company	MO	OLB	20.56	15.81	39.39	5
National Mine 1	MO	OLB	20.10	15.75	38.97	5
Park City	MO	OLB	20.87	15.86	40.28	5
La Motte Prop	MO	OLB	21.19	15.87	40.20	5
Mine LaMotte	MO	OLB	20.06	15.79	39.09	5
Anapolis	MO	Annapolis	21.28	15.92	40.06	2
Anapolis	MO	Annapolis	21.26	15.92	39.96	2
Fredricktown	MO	Fredericktown	21.29	15.91	40.27	2
Fredericktown	MO	Fredericktown	21.42	15.92	40.55	2
Mine La Motte	MO	Fredericktown	20.07	15.77	39.14	2
Mine La Motte	MO	Fredericktown	20.70	15.85	39.79	2
Indian Creek	MO	Indian Creek	20.76	15.86	39.58	2
Indian Creek	MO	Indian Creek	21.76	15.94	40.72	2
Kingstone	MO	Washing Co Barite	22.18	15.96	41.17	2
Goller lease	MO	CM	22.19	15.94	41.19	2
Goller 2	MO	CM	21.98	15.96	41.12	4
Silvermine	MO	SEM	16.07	15.28	35.76	4
Iron Mountain	MO	SEM	16.15	15.30	35.86	4
Pea Ridge	MO	SEM	33.55	17.01	54.10	4
Ford & Gray lease	MO	CM	21.95	15.92	41.05	2
High Point	MO	CM	21.92	15.94	40.97	2
Simpson	MO	CM	21.93	15.94	41.06	2
Grunding	MO	CM	21.91	15.92	40.98	2
Lamb	MO	CM	22.00	15.92	41.06	2
Buckshot	MO	CM	22.10	15.97	41.16	2
Hill Lead and Zinc	MO	CM	22.18	15.92	41.03	2
Brown	MO	CM	21.94	15.91	40.97	2
Blackwater	MO	CM	21.98	15.97	41.14	2
Blackwater	MO	CM	21.97	15.96	41.08	2
Jackson Mine	MO	CM	22.25	15.91	41.22	5
Circle Mines	MO	CM	22.13	15.93	41.22	5
Buckshot Mines	MO	CM	22.11	15.93	41.11	5
Quigley Mines	MO	CM	22.08	15.94	41.15	5
Tri-State - Blue Goose	OK	TS	21.94	15.92	41.08	2
Tri-State - Blue Goose	OK	TS	21.90	15.92	41.07	2

References: 1= Millen et al., 1995, 2= Goldhaber et al., 1995, 3= Sverjensky et al., 1979, 4= Doe and Delevaux, 1972, 5= Farquhar et al., 1995

REFERENCES

Chapter 1

Alberts, J. J., Je. Schindle, R. W. Miller, and D. E. Nutter (1974), Elemental Mercury Evolution Mediated by Humic Acid, *Science, 184*(4139), 895-896.

Allard, B. and I. Arsenie (1991), Abiotic Reduction of Mercury by Humic Substances in Aquatic System - an Important Process for the Mercury Cycle, *Water Air and Soil Pollution, 56*, 457-464.

Amyot, M., G. Mierle, D. R. S. Lean, and D. J. Mcqueen (1994), Sunlight-Induced Formation of Dissolved Gaseous Mercury in Lake Waters, *Environmental Science & technology, 28*(13), 2366-2371.

Barkay, T., J. K. Schaefer, A. J. Poulain and M. Amyot (2005), Microbial transformations in the mercury geochemical cycle, *Geochimica et Cosmochimica Acta, 69*(10), A702-A702.

Biester, H., A.M. Cortizas, S. Birkenstock and R. Kilian (2003), Effect of Peat Decomposition and Mass Loss on Historic Mercury Records in Peat Bogs from Patagonia, *Environmental Science & technology*, *37*, 32-39.

Bronsted, J. N. and G. Hevesy (1921), The separation of the isotopes of mercury, *Nature*, *106*, 144-144.

Buat-Menard, P. and North Atlantic Treaty Organization, Scientific Affairs Division (1986), The role of air-sea exchange in geochemical cycling. D. Reidel Pub. Co; Sold and distributed in the U.S.A. and Canada by Kluwer Academic Publishers, Dordrecht ; Boston; Norwell, MA, U.S.A.

Cortizas, A.M., X. Pontevedra-Pombal, E. García-Rodeja, J.C. Nóvoa-Muñoz and W. Shotyk (1999), Mercury in a Spanish Peat Bog: Archive of Climate Change and Atmospheric Metal Deposition, *Science*, *284*, 939-942.

Dickel, D. and R. S. Carr (1991), Archaeological investigations at the Oak Knoll Mound, 8LL729, Lee County, *Florida Archaeological and History Conservancy*, Technical Report # 21, Miami, Florida

England, J.G. and A. Zindler (1992), The Lamont-Doherty Geological Observatory Isolab 54 isotope ratio mass spectrometer, *Int. J. Mass Spec. Ion Proc*, *121*, 201-240

Fitzgerald, W. F. (1986), In *The Role of Air-Sea Exchange in Geochemical Cycling*; Buat-Menard, P., Ed.; NATO ASI Series; Reidel Press: Dordrecht, C185, 363-408.

Fitzgerald, W. F. (1989). In *Chemical Oceanography*; Riley, J. P., Chester, R., Eds.; Academic Press: London. 10, 151-186.

Fitzgerald, W. F. (1995), Is mercury increasing in the atmosphere? The need for an atmospheric mercury network (AMNET), *Water, Air, & Soil Pollution*, *80*, 245-254.

Fitzgerald, W. F. and T.W. Clarkson (1991), Mercury and Monomethylmercury: Present and Future Concerns, *Environmental Health Perspectives*, *96*, 159-166

Foucher, D. and H. Hintelmann (2006), High-precision measurement of mercury isotope ratios in sediments using cold-vapor generation multi-collector inductively coupled plasma mass spectrometry, *Analytical Bionanalytical Chemistry*, *384*, 1470-1478

Goel, P.S. and A.N. Thakur (1987), Isotopically anomalous Hg in meteorites, *Meteoritics, 22*, 389–390.

Gustin, M. S., G.E. Taylor, T.L. Leonard and R.E. Keislar (1996), Atmospheric Mercury Concentrations Associated with Geologically and Anthropogenically Enriched Sites in Central Western Nevada, *Environmental Science & Technology*, *30*, 2572-2579

Gustin, M. S., G.E. Taylor and R.J. Callan (1997), Anthropogenic and natural sources of atmospheric mercury in central western Nevada, *Abstracts of Papers of the American Chemical Society*, *214*, 135-ENVR.

Hintelmann, H. and S. Lu (2003), High Precision isotope ratio measurements of mercury isotopes in cinnabar ores using multi-collector inductively coupled plasma mass spectrometry. *Analyst*, *128*, 635-639

Hudson, R. J. M., S. A. Gherini, W.F. Fitzgerald and D.B. Porcella (1995), Anthropogenic influences on the global mercury cycle: a model-based analysis, *Water, Air, & Soil Pollution*, *80*, 265-272.

Jackson, T. A. (2001), Variations in the isotope composition of mercury in a freshwater sediment sequence and food web, *Canadian Journal of Fish and Aquatic Science*, *58*, 185-196.

Jackson, T.A., D.C.G. Muir and V.F. Warwick (2004), Historic variations in the s**Table** isotope composition of mercury in Arctic lake sediments, *Environmental Science and Technology*, *38*, 2813-2821

Jovanovic, S. and G.W. Reed (1976a), ^{196}Hg and ^{202}Hg isotopic ratios in chondrites: revisited, *Earth Planet Science Letters*, *31*, 95–100

Jovanovic, S. and G.W. Reed (1976b), Interrelations among isotopically anomalous mercury fractions from meteorites and possible cosmological inferences, *Science*, *193*, 888–891

Jovanovic, S. and G.W. Reed (1987), Isotopically anomalous ^{196}Hg and ^{202}Hg in Antarctic achondrites, *Geophyical Research Letters, 14*, 1127–1130.

Jovanovic, S. and G.W. Reed (1990), Hg isotopes on the Moon and in achondrites, *Chemical Geology*, *80*, 181–191

Klaue, B. and J.D. Blum (1999), Trace element analysis of arsenic in drinking water by inductively coupled mass spectrometry: high resolution versus hydride generation, *Analytical Chemistry*, *71*, 1408-1414

Kumar, P. and P.S. Goel (1992a), Variable ^{196}Hg / ^{202}Hg ratio in stone meteorites and in some of their carbon-rich residues, *Chemical Geology*, *102*, 171–183.

Kumar, P. and P.S. Goel (1992a), Further measurements on isotopic anomalies of ^{196}Hg / ^{202}Hg ratio in some acid insoluble residues of Sikhote Alin and other iron meteorites, *Geochem. J.*, *26*, 51–56

Kumar, P., M. Ebihara and S.K. Bhattacharya (2001), ^{196}Hg / ^{202}Hg ratio and Hg content in meteorites and terrestrial standard rocks, *Geochem. J.*, *35*, 101–116.

Kritee, K., B. Klaue, J.D. Blum and T. Barkay (2005), Biological Hg isotope fractionation; Abstracts of the 15th annual V. M. Goldschmidt conference, *Geochimica et Cosmochimica Acta*, *69*, 708.

Kritee, K., J. D. Blum, M. W. Johnson, B. A. Bergquist, and T. Barkay (2007), Mercury stable isotope fractionation during reduction of Hg(II) to Hg(0) by mercury resistant microorganisms, *Environmental science & technology, 41*(6), 1889-1895.

Krupp, E. M. and O.F.X. Donard (2005), Isotope ratios on transient signals with GC–MC–ICP-MS, *International Journal of Mass Spectrometry*, *242*, 233-242.

Lindqvist, O. and H. Rodhe (1985), Atmospheric Mercury - a Review, Tellus Series B-*Chemical and Physical Meteorology*, *37*, 136-159.

Lindqvist, O., K. Johansson, L. Bringmark, B. Timm, M. Aastrup, A. Andersson, G. Hovsenius, Lars H ├Ñkanson, ├åke Iverfeldt, Meili, M., 1991. Mercury in the Swedish environment ΓÇö Recent research on causes, consequences and corrective methods. *Water, Air, & Soil Pollution. 55*, xi-261.

Mackay, D. and F. Wania, F. (1995), Prospects for modeling the behavior and fate of mercury, globally and in aquatic systems, *Water, Air, & Soil Pollution*, *80*, 941-950.

Madsen, P. P. (1981), Peat bog records of atmospheric mercury deposition, *Nature*, *293*, 127-130.

Mason, R. P. and W.F. Fitzgerald (1990), Alkylmercury species in the equatorial Pacific, *Nature*, *347*, 457-459.

Mason, R. P., W.F. Fitzgerald and F.M.M. Morel (1994), The biogeochemical cycling of elemental mercury: Anthropogenic influences, *Geochimica et Cosmochimica Acta*, *58*, 3191-3198.

Mason, R. P., F. M. M. Morel, and H. F. Hemond (1995), The Role of Microorganisms in Elemental Mercury Formation in Natural-Waters, *Water Air and Soil Pollution, 80*(1-4), 775-787.

Mason, R. P., K.R. Rolfhus and W.F. Fitzgerald (1995), Methylated and elemental mercury cycling in surface and deep ocean waters of the North Atlantic, *Water, Air, & Soil Pollution*, *80*, 665-677.

Mason, R. P. and G.R. Sheu (2002), Role of the ocean in global mercury cycle. *Global Biogeochemical Cycles*, *16*, 40-1 - 40-14.

Mitchell, S. (1999), The natural and anthropogenic fractionation of mercury isotopes, M.S. Thesis, 1-90, Florida State University.

Morel, F. M. M., A.M.L. Kraepiel and M. Amyot (1998), The Chemical Cycle and Bioaccumulation of Mercury, *Annual Review of Ecology and Systematics*, *29*, 543-566.

Munthe, J. (1992), The Aqueous Oxidation of Elemental Mercury by Ozone, Atmospheric *Environment Part A-General Topics*, *26*, 1461-1468.

Munthe, J. and W.J. McElroy (1992), Some aqueous reactions of potential importance in the atmospheric chemistry of mercury**,** *Atmospheric Environment*, *26A*, 553-557.

Munthe, J., Z.F. Xiao and O. Lindqvist (1991), The aqueous reduction of divalent mercury by sulfite, *Water, Air, & Soil Pollution*, *56*, 621-630.

Nier, A. O. (1950), A Redetermination of the Relative Abundances of the Isotopes of Neon, Krypton, Rubidium, Xenon, and Mercury, *Physical Review*, *79*, 450.

Nriagu, J. O. (1989), A global assessment of natural sources of atmospheric trace metals, *Nature*, *338*, 47-49.

Pacyna, J., J. Munthe, K. Larjava and E. Pacyna (2005), Mercury Emissions from Anthropogenic Sources: Estimates and Measurements for Europe, Dynamics of Mercury Pollution on Regional and Global Scales, 51-64.

Rasmussen, P. E. (1994), Current Methods of Estimating Atmospheric Mercury Fluxes in Remote Areas, *Environmental Science & Technology*, *28*, 2233-2241.

Reed, G. W. and S. Jovanovic (1967), Mercury in Chondrites, *Journal of Geophysical Research*, *72*, 2219.

Reed, G. W. and S. Jovanovic (1990), Isotopic Hg in an Allende Carbon-Rich Residue, *Meteoritics, 25*, 345-346.

Sellers, P., C. A. Kelly, J. W. M. Rudd, and A. R. MacHutchon (1996), Photodegradation of methylmercury in lakes, *Nature, 380*(6576), 694-697.

Slemr, F. and E. Langer (1992), Increase in global atmospheric concentrations of mercury inferred from measurements over the Atlantic Ocean, *Nature*, *355*, 434-437.

Smith, C.N., S.E. Kesler, B. Klaue and J.D. Blum (2005), Mercury isotope fractionation in fossil hydrothermal systems, *Geology*, *33*, 825-828

Streets, D., J. Hao, Y. Wu, J. Jiang, M. Chan, H. Tian and X. Feng (2005), Anthropogenic mercury emissions in China, *Atmospheric Environment*, *39*, 7789-7806.

Swain, E. B., D.R. Engstrom, M.E. Brigham, T.A. Henning and P.L. Brezonik (1992), Increasing Rates of Atmospheric Mercury Deposition in Midcontinental North America, *Science*, *257*, 784-787

Thakur, A.N. and P.S. Goel (1989), Huge variations in the isotopic ratio $^{196}Hg/^{202}Hg$ in some acid-insoluble residues of Sikhote and other iron meteorites, *Earth Planetary Science Letters*, *96*, 235–246.

Zadnik, M.G., S. Specht and F. Begemann (1989), Revised isotopic composition of terrestrial mercury, *Int. J. of Mass Spectrom. and Ion Proc*, *89*, 103-110

Chapter 2

Allard, B., and I. Arsenie (1991), Abiotic Reduction of Mercury by Humic Substances in Aquatic System - an Important Process for the Mercury Cycle, *Water Air and Soil Pollution, 56*, 457-464.

Allison, G.B., J.R. Gat and F.W.D. Leaney (1985), The relationship between deuterium and oxygen 18 delta values in leaf water. *Chem. Geol*, 58, pp. 145–156.

Amyot, M., G. Mierle, D. R. S. Lean, and D. J. Mcqueen (1994), Sunlight-Induced Formation of Dissolved Gaseous Mercury in Lake Waters, *Environmental science & technology, 28*(13), 2366-2371.

Anderson, W.T., S.M. Bernasconi, J.A. McKenzie and M. Saurer (1998), Oxygen and carbon isotopic record of climatic variability in tree-ring cellulose (Picea abies): An example from central Switzerland (1913-1995). *Journal of Geophysical Research*, v. 103, no. D24, p. 31,625-31,636

Aravena, R. and B.G. Warner (1992), Oxygen-18 composition of Sphagnum, and microenvironmental water relations, *Bryologist,* 95, pp. 445-448.

Aucour, A.M., C. Hillaire-Marcel and R. Bonnefille (1996), Oxygen isotopes in cellulose from modern and Quaternary intertropical peatbogs: implications for paleohydrology. Chem. Geol. 129, pp. 341–359.

Baertschi, P. and M. Thürkauf 1969), Isotopie-Effekt für die Trennung der Sauersto!-Isotopen ^{16}O and ^{18}O bei der Rekti-fikation von leichtem und schwerem. Wassers, Helv. Chim. Acta 43, pp. 80-89.

Bariac, T., C. Jusserand and A. Mariotti (1990), Evolution spatiotemporelle de la composition isotopique dam le continuum sol-plante-atmosphere. Geochim. Cosmochim. Acta, 54, pp. 413-424.

Barkay, T., J. K. Schaefer, A. J. Poulain, and M. Amyot (2005), Microbial transformations in the mercury geochemical cycle, *Geochimica et Cosmochimica Acta, 69*(10), A702-A702.

Benoit, J. M., W. F. Fitzgerald, and A. W. H. Damman (1998), The biogeochemistry of an ombrotrophic bog: Evaluation of use as an archive of atmospheric mercury deposition, *Environmental research, 78*(2), 118-133.

Biester, H., A. M. Cortizas, S. Birkenstock, and R. Kilian (2003), Effect of Peat Decomposition and Mass Loss on Historic Mercury Records in Peat Bogs from Patagonia, *Environmental science & technology, 37*, 32-39.

Biester, H., G. Muller, and H. F. Scholer (2002), Estimating distribution and retention of mercury in three different soils contaminated by emissions from chlor-alkali plants: part I, *Science of the Total Environment, 284*(1-3), 177-189.

Biester, H., R. Kilian, C. Franzen, C. Woda, A. Mangini, and H. F. Scholer (2002), Elevated mercury accumulation in a peat bog of the Magellanic Moorlands, Chile (53 degrees S) - an anthropogenic signal from the Southern Hemisphere, *Earth and Planetary Science Letters, 201*(3-4), 609-620.

Biester, H., and C. Scholz (1997), Determination of mercury binding forms in contaminated soils: Mercury pyrolysis versus sequential extractions, *Environmental science & technology, 31*(1), 233-239.

Biester, H. and C. Scholz (1996), Determination of Mercury Binding Forms in Contaminated Soils: Mercury Pyrolysis versus Sequential Extractions. Environ. Sci. Technol., 31, pp. 233 -239

Bindler, R. (2002), Estimating the Natural Background Atmospheric Deposition Rate of Mercury Utilizing Ombrotrophic Bogs in Southern Sweden, *Environmental science & technology, 37*(1), 40-46.

Bond, G., H. Heinrich, W. Broecker, L. Labeyrie, J. McManus, J. Andrews, S. Huon, R. Jantschik , S. Clasen, C. Simet , K. Tedesco, M. Klas, G. Bonani and S. Ivy (1992), Evidence for Massive Discharges of Icebergs into the North-Atlantic Ocean during the Last Glacial Period, *Nature, 360*(6401), 245-249.

Brading, D.A. and H.E. Cross (1972), Colonial silver mining: Mexico and Peru. *Hisp Am Hist Rev,* 52:545–579.

Bradley, R. (2000), Paleoclimate - 1000 Years of climate Change, *Science, 288*(5470), 1353

Brenninkmeijer, C.A.M. (1983), Deuterium, Oxygen-18 and Carbon- 13 in Tree Rings and Peat Deposits in Relation to Climate, Groningen.

Brenninkmeijer, C.A.M., B. Van Geel and W.G. Mook (1982), Variations in the D/H and $^{18}O/^{16}O$ ratios in cellulose extracted from a peat bog core. Earth Planet. Sci. Lett. 61, pp. 283–290.

Bricout, J. (1978), Recherches sur le fractionnement des isotopes s**Table**s de l'hydrogène et de l'oxygène dans quelques végétaux. Rev. Cytol. Biol. Végét. Bot. 1, pp. 133–209.

Broecker, W. S. (2001), Paleoclimate - Was the medieval warm period global? *Science, 291*(5508), 1497-1499.

Bronsted, J. N., and G. Hevesy (1921), The separation of the isotopes of mercury, *Nature, 106*, 144-144.

Brunke, E. G., C. Labuschagne, and F. Slemr (2001), Gaseous mercury emissions from a fire in the Cape Peninsula, South Africa, during January 2000, *Geophysical Research Letters, 28*(8), 1483-1486.

Buat-Menard, P., North Atlantic Treaty Organization, and Scientific Affairs Division (1986), The role of air-sea exchange in geochemical cycling, D. Reidel Pub. Co; Sold and distributed in the U.S.A. and Canada by Kluwer Academic Publishers, Dordrecht; Boston; Norwell, MA, U.S.A.

Buhay, W.M., T.W.D. Edwards, and R. Aravena (1996), Evaluating kinetic fractionation factors used for ecologic and paleoclimatic reconstructions from oxygen and hydrogen isotope ratios in plant water and cellulose. *Geochim. Cosmochim. Acta* 60, pp. 2209-2218.

Burk, R.L. and M. Stuiver (1981), Oxygen isotope ratios in trees reflect mean annual temperature and relative humidity. Science 211, pp. 1417-1419.

Cordeiro, R.C. (1995), Mudanças paleoambientais e ocorrência de incêndios nos últimos 7400 anos, na região de Carajás, Pará. Master Degree Thesis. Universidade Federal Fluminense. Niteroi, Brazil. 144 pp

Cordeiro, R.C., B. Turcq, da S. A. Oliveira and K. Suguio (1997), Holocene environmental changes in Carajás region (Pará, Brazil) recorded by lacustrine deposits. *Verh. Internat. Verein. Limnol*. 26: 814–817

Cortizas, A. M., E. Garcia-Rodeja, X. P. Pombal, J. C. N. Munoz, D. Weiss, and A. Cheburkin (2002), Atmospheric Pb deposition in Spain during the last 4600 years recorded by two ombrotrophic peat bogs and implications for the use of peat as archive, *Science of the Total Environment, 292*(1-2), 33-44.

Cortizas, A. M., T. Mighall, X. P. Pombal, J. C. N. Munoz, E. P. Varela, and R. P. Rebolo (2005), Linking changes in atmospheric dust deposition, vegetation change and human activities in northwest Spain during the last 5300 years, *Holocene, 15*(5), 698-706.

Cortizas, A. M., X. P. Pombal, E. García-Rodeja, J. C. Nóvoa-Muñoz and W. Shotyk (1999), Mercury in a Spanish Peat Bog: Archive of Climate Change and Atmospheric Metal Deposition, *Science, 284*(541), 939-942.

Cortizas, A. M, X. P. Pombal, J. C. N. Munoz, and E. García-Rodeja (1997), Four Thousand Years of Atmospheric Pb, Cd and Zn Deposition Recorded by the Ombrotrophic Peat Bog of Penido Vello (Northwestern Spain), *Water, Air, & Soil Pollution, 100*, 387-403.

Craig, H.(1961), Isotopic variations in meteoric waters. *Science,* 133, 1702–1703.

Cuadra, W. A., and P. M. Dunkerley (1991), A History of Gold in Chile, *Economic Geology and the Bulletin of the Society of Economic Geologists, 86*(6), 1155-1173.

Dansgard, W. (1964), Stable isotopes in precipitation. Tellus, 16, pp. 436-468

DeNiro, M.J. and L.W. Cooper (1989), Postphotosynthetic modification of oxygen isotope ratios of carbohydrates in the potato: implications for paleoclimatic reconstruction based upon isotopic analysis of wood cellulose. Geochim. Cosmochim. Acta 53, pp. 2573–2580

DeNiro, M.J. and S. Epstein (1981), Isotopic composition of cellulose from aquatic organisms. Geochim. Cosmochim. Acta 45, pp. 1885–1894

DeNiro, M.J. and S. Epstein (1979), Relationships between the oxygen isotope ratios of terrestrial plant cellulose, carbon dioxide, and water, Science 204, pp. 51-53

De Lacerda, Luiz Drude (1995), Amazon mercury emissions, *Nature, 374*(6517), 20-21.

Desprat, S., M. F. S. Goni, and M. F. Loutre (2003), Revealing climatic variability of the last three millennia in northwestern Iberia using pollen influx data, *Earth and Planetary Science Letters, 213*(1-2), 63-78.

Donald, A. (1994) Meteorology Today: An introduction to weather, climate and the environment Fifth Edition, West Publishing Co, 591 pp.

Dongman, G., H.W. Nimberg, H. Wrstel and K. Wagener (1974), On the enrichment of $H_2{}^{18}0$ in the leaves of transpiring plants. Rad. Environ. Biophys., 11, pp. 41-52.

Edner, H., P. Ragnarson, S. Svanberg, E. Wallinder, R. Ferrara, R. Cioni, B. Raco, and G. Taddeucci (1994), Total Fluxes of Sulfur-Dioxide from the Italian Volcanos Etna, Stromboli, and Vulcano Measured by Differential Absorption Lidar and Passive Differential Optical-Absorption Spectroscopy, *Journal of Geophysical Research-Atmospheres, 99*(D9), 18827-18838.

Edwards, T.W.D. and P. Fritz (1986), Assessing meteoric water composition and relative humidity from ^{18}O and ^{2}H in wood cellulose: paleoclimatic implications for southern Ontario, Canada. Applied Geochemistry 1, pp. 715-723.

Edwards T.W.D., R.O. Aravena, P. Fritz and A.V. Morgan (1985), Interpreting paleoclimate from ^{18}O and ^{2}H in plant cellulose: comparison with evidence from fossil insects and relict permafrost in southwestern Ontario. Can. J. Earth Sci., pp. 1720-1726

Environment Canada, (2000),
http://www.cec.org/Programs_projects/pollutants_health/smoc/pdfs/hgcan-e.pdf.

Epstein, S., P. Thompson, and C. J. Yapp (1977), Oxygen and Hydrogen Isotopic Ratios in Plant Cellulose, *Science, 198*(4323), 1209-1215.

Ferrara, R., and B. E. Maserti (1990), Atmospheric Mercury Levels in the Mount Etna Volcanic Area after an Eruptive Phase, *Environmental technology, 11*(1), 51-56.

Ferrara, R., B. E. Maserti, M. Andersson, H. Edner, P. Ragnarson, and S. Svanberg (1997), Mercury degassing rate from mineralized areas in the Mediterranean basin, *Water Air and Soil Pollution, 93*(1-4), 59-66.

Ferrara, R., B. Mazzolai, E. Lanzillotta, E. Nucaro, and N. Pirrone (2000), Volcanoes as emission sources of atmospheric mercury in the Mediterranean basin, *Science of the Total Environment, 259*(1-3), 115-121.

Fischer, H., M. Wahlen, J. Smith, D. Mastroianni, and B. Deck (1999), Ice Core Records of Atmospheric CO2 Around the Last Three Glacial Terminations, *Science, 283*(5408), 1712-1714, doi: 10.1126/science.283.5408.1712.

Fisher, J. R. (1977), *Silver Mines and Silver miners in Colonial Peru, 1776-1824*, Centre for Latin American Studies, University of Liverpool.

Fitzgerald, W.F. (1989), Atmospheric and oceanic cycling of mercury. In: J.P. Riley and R. Chester, Editors, *Chemical Oceanography* Vol. 10**,** Academic Press, London, pp. 151–186.

Fitzgerald, W. F. (1986), *In The Role of Air-Sea Exchange in Geochemical Cycling*, 363-408 pp., Reidel Press, Dordrecht.

Fitzgerald, W. F. (1995), Is mercury increasing in the atmosphere? The need for an atmospheric mercury network (AMNET), *Water, Air, & Soil Pollution, 80*(1-4), 245-254.

Fitzgerald, W. F., and T. W. Clarkson (1991), Mercury and Monomethylmercury: Present and Future Concerns, *Environmental health perspectives, 96*, 159-166.

Förstel, F. and H. Hutzen (1983), $^{18}O/^{16}O$ ratio of water in a local ecosystem as a basis of climate record, in: Paleoclimates and Paleowaters: a Collection of Environmental Isotope Studies, IAEA, Vienna, 67-81.

Fricke, H.C. and J.R. O'Neil (1999), The correlation between $^{18}O/^{16}O$ ratios of meteoric water and surface temperature: its use in investigating terrestrial climate change over geologic time. *Earth Planet. Sci. Lett*. 170, 181– 196.

Friedli, H. R., L. F. Radke, and J. Y. Lu (2001), Mercury in smoke from biomass fires, *Geophysical Research Letters, 28*(17), 3223-3226.

Friedli, H. R., L. F. Radke, J. Y. Lu, C. M. Banic, W. R. Leaitch, and J. I. MacPherson (2003), Mercury emissions from burning of biomass from temperate North American forests: laboratory and airborne measurements, *Atmospheric Environment, 37*(2), 253-267.

Galbreath, K.C. and C.J. Zygarlicke (2000), Mercury transformations in coal combustion flue gas, *Fuel Proceesing Technology*, 65-66, 289-310.

García Codrón, J.C. (1996), *Un Clima para la Historia Una Historia para el Clima* (Servicio de Publicaciones de la Universidad de Cantabria, Lecciones 2/96, Santander, Spain.

Gonfiantini, R., S. Gratziu and E. Tongiorgi (1965), Oxygen isotopic composition of water in leaves. In: Isotopes and Radiation in Soil-Plant Nutrition Studies. Int. At. Energy Agency, Vienna, pp. 405-410

Gray, J. E., M. E. Hines, P. L. Higueras, I. Adatto and B.K. Lasoras (2004), Mercury Speciation and Microbial Transformations in Mine Wastes, Stream Sediments, and Surface Waters at the Almaden Mining District, Spain, *Environmental Science and Technology*, 38, 4285-4292

Gray, J. E., J. G. Crock, and D. L. Fey (2002), Environmental geochemistry of abandoned mercury mines in West-Central Nevada, USA, *Applied Geochemistry, 17*(8), 1069-1079.

Gray, J. E., P. M. Theodorakos, E. A. Bailey, and R. R. Turner (2000), Distribution, speciation, and transport of mercury in stream-sediment, stream-water, and fish collected near abandoned mercury mines in southwestern Alaska, USA, *Science of the Total Environment, 260*(1-3), 21-33.

Green, J. W. (1963), Wood cellulose, in *Methods in Carbohydrate Chemistry*edited by Green, R.L. and Green, J.W., pp. 9-21, Academic Press, New York, N.Y., .

Grove, J. M. (1988), *The Little Ice Age*, Methuen., New York.

Gustin, M. S., M. Coolbaugh, M. Engle, B. Fitzgerald, R. Keislar, S. Lindberg, D. Nacht, J. Quashnick, J. Rytuba, C. Sladek, H. Zhang, R. Zehner (2003), Atmospheric mercury emissions from mine wastes and surrounding geologically enriched terrains, *Environmental Geology, 43*(3), 339-351.

Gustin, M. S., G. E. Taylor, and R. J. Callan (1997), Anthropogenic and natural sources of atmospheric mercury in central western Nevada. *Abstracts of Papers of the American Chemical Society, 214*, 135-ENVR.

Gustin, M. S., G. E. Taylor, T. L. Leonard, and R. E. Keislar (1996), Atmospheric Mercury Concentrations Associated with Geologically and Anthropogenically Enriched Sites in Central Western Nevada, *Environmental science & technology, 30*(8), 2572-2579.

Haas, J. N., I. Richoz, W. Tinner, and L. Wick (1998), Synchronous Holocene climatic oscillations recorded on the Swiss Plateau and at timberline in the Alps, *Holocene, 8*(3), 301-309.

Hass, H. C. (1996), Northern Europe climate variations during late Holocene: Evidence from marine Skagerrak, *Palaeogeography Palaeoclimatology Palaeoecology, 123*(1-4), 121-145.

Hines, M. E., M. Horvat, J. Faganeli, J. C. J. Bonzongo, T. Barkay, E. B. Major, K. J. Scott, E. A. Bailey, J. J. Warwick, and W. B. Lyons (2000), Mercury biogeochemistry in the Idrija River, Slovenia, from above the mine into the Gulf of Trieste, *Environmental research, 83*(2), 129-139.

Hong, Y. T., H. B. Jiang, T. S. Liu, L. P. Zhou, J. Beer, H. D. Li, X. T. Leng, B. Hong, and X. G. Qin (2000), Response of climate to solar forcing recorded in a 6000-year delta O-18 time-series of Chinese peat cellulose, *Holocene, 10*(1), 1-7.

Hudson, R. J. M., S. A. Gherini, W. F. Fitzgerald, and D. B. Porcella (1995), Anthropogenic Influences on the Global Mercury Cycle - a Model-Based Analysis, *Water Air and Soil Pollution, 80*(1-4), 265-272.

Hudson, R. J. M., S. A. Gherini, W. F. Fitzgerald, and D. B. Porcella (1995), Anthropogenic influences on the global mercury cycle: a model-based analysis, *Water, Air, & Soil Pollution, 80*(1-4), 265-272.

Jackson, T. A. (2001), Variations in the isotope composition of mercury in a freshwater sediment sequence and food web, *Can. J. Fish. Aquat. Sci. /J. Can. Sci. Halieut. Aquat, 58*(1), 185-196.

Kaufman, Y. J., A. Setzer, D. Ward, D. Tanre, B. N. Holben, P. Menzel, M. C. Pereira, and R. Rasmussen (1992), Biomass burning airborne and spaceborne experiment in the Amazonas (BASE-A), *Journal of Geophysical Research, 97*(D13), 14581-14599.

Kaufman, Y. J., A. Setzer, D. Ward, D. Tanre, B. N. Holben, P. Menzel, M. C. Pereira, and R. Rasmussen (1992), Biomass Burning Airborne and Spaceborne Experiment in the Amazonas (Base-A), *Journal of Geophysical Research-Atmospheres, 97*(D13), 14581-14599.

Kim, J. P., and W. F. Fitzgerald (1986), Sea-Air Partitioning of Mercury in the Equatorial Pacific-Ocean, *Science, 231*(4742), 1131-1133.

Klaue, B. and J.D. Blum (1999), Trace element analysis of arsenic in drinking water by inductively coupled mass spectrometry: high resolution versus hydride generation. *Analytical Chemistry*. 71, 1408-1414

Kritee, K., B. Klaue, J. D. Blum, and T. Barkay (2005), Biological Hg isotope fractionation; Abstracts of the 15th annual V. M. Goldschmidt conference, *Geochimica et Cosmochimica Acta, 69*(10), 708.

Krupp, E. M., and O. F. X. Donard (2005/4/1), Isotope ratios on transient signals with GC–MC–ICP-MS, *International Journal of Mass Spectrometry, 242*(2-3), 233-242.

Lacerda, L. D. (1997), Global mercury emissions from gold and silver mining, *Water Air and Soil Pollution, 97*(3-4), 209-221.

Lamb, H. H. (1985), *Climatic History and the Future*, 835 pp., Princeton University PRess, Princeton, NJ.

Lindqvist, O., and H. Rodhe (1985), Atmospheric Mercury - a Review, *Tellus Series B-Chemical and Physical Meteorology, 37*(3), 136-159.

Lindqvist, O., K. Johansson, L. Bringmark, B. Timm, M. Aastrup, A. Andersson, G. Hovsenius, Lars H ├Ñkanson, ├åke Iverfeldt, and M. Meili (1991), Mercury in the Swedish environment ΓÇö Recent research on causes, consequences and corrective methods, *Water, Air, & Soil Pollution, 55*(1), xi-261.

Lipp, J., P. Trimborn, T. Edwards, Y. Waisel and D. Yakir (1996), Climatic effects on the $\delta^{18}O$ and the $\delta^{13}C$ of cellulose in the desert tree Tamarix jordanis. *Geochim. Cosmochim. Acta* 60, pp. 3305–3309.

Lockhart, W. L., R. W. Macdonald, P. M. Outridge, P. Wilkinson, J. B. DeLaronde, and J. W. M. Rudd (2000), Tests of the fidelity of lake sediment core records of mercury deposition to known histories of mercury contamination, *Science of the Total Environment, 260*(1-3), 171-180.

Loredo, J., J. Soto, R. Alvarez, and A. Ordonez (2007), Atmospheric monitoring at abandoned mercury mine sites in Asturias (NW Spain), *Environmental monitoring and assessment, 130*(1-3), 201-214.

Luken, J. O. (1985), Zonation of Sphagnum Mosses - Interactions among Shoot Growth, Growth Form, and Water-Balance, *Bryologist, 88*(4), 374-379.

Luque, J. A., and R. Julia (2002), Lake sediment response to land-use and climate change during the last 1000 years in the oligotrophic Lake Sanabria (northwest of Iberian Peninsula), *Sedimentary Geology, 148*(1-2), 343-355.

Mackay, D., F. Wania, and W. H. Schroeder (1995), Prospects for Modeling the Behavior and Fate of Mercury, Globally and in Aquatic Systems, *Water Air and Soil Pollution, 80*(1-4), 941-950.

Madsen, P. P. (1981), Peat bog records of atmospheric mercury deposition, *Nature, 293*(582), 127-130.

Madsen, P. P. (1981), Peat bog records of atmospheric mercury deposition, *Nature, 293*(5828), 127-130.

Mann, M. E., R. S. Bradley, and M. K. Hughes (1998), Global-scale temperature patterns and climate forcing over the past six centuries, *Nature, 392*(6678), 779-787.

Martins, V., J. M. Jouanneau, O. Weber, and F. Rocha (2006), Tracing the late Holocene evolution of the NW Iberian upwelling system, *Marine Micropaleontology, 59*(1), 35-55.

Mason, R. P., and W. F. Fitzgerald (1990), Alkylmercury species in the equatorial Pacific, *Nature, 347*(6292), 457-459.

Mason, R. P., W. F. Fitzgerald, and F. M. M. Morel (1994/8), The biogeochemical cycling of elemental mercury: Anthropogenic influences, *Geochimica et Cosmochimica Acta, 58*(15), 3191-3198.

Mason, R. P., K. R. Rolfhus, and W. F. Fitzgerald (1995), Methylated and elemental mercury cycling in surface and deep ocean waters of the North Atlantic, *Water, Air, & Soil Pollution, 80*(1-4), 665-677.

McDermott, F., D. P. Mattey, and C. Hawkesworth (2001), Centennial-scale holocene climate variability revealed by a high-resolution speleothem delta O-18 record from SW Ireland, *Science, 294*(5545), 1328-1331.

Mellor, J. W. (1952), *A Comprehensive Treatise on Inorganic and Theoretical Chemistry*, Longmans, Green & Co., London.

Ménot-Combes, G., S.J. Burns and M. Leuenberger (2002), Variations of $^{18}O/^{16}O$ in plants from temperate peat bogs (Switzerland): implications for paleoclimatic studies. *Earth Planet. Sci. Lett*, 202, pp. 419-434

Mighall, T. M., A. M. Cortizas, H. Biester, and S. E. Turner (2006), Proxy climate and vegetation changes during the last five millennia in NW Iberia: Pollen and non-pollen palynomorph data from two ombrotrophic peat bogs in the North Western Iberian Peninsula, *Review of palaeobotany and palynology, 141*(1-2), 203-223.

Morel, F. M. M., A. M. L. Kraepiel, and M. Amyot (1998), The Chemical Cycle and Bioaccumulation of Mercury, *Annual Review of Ecology and Systematics, 29*, 543-566.

Munõz Sobrino, C., P. Ramil-Rego, M. Rodríguez Guitián (1997), Upland vegetation in the north-west Iberian Peninsula after the last glaciation: forest history and deforestation dynamics. *Vegetation History and Archaeobotany,* 6, 215–233.

Munthe, J. and McElroy, WJ (1992), Some aqueous reactions of potential importance in the atmospheric chemistry of mercury, *Atmospheric Environment., 26A*(4), 553-557.

Munthe, J. (1992), The Aqueous Oxidation of Elemental Mercury by Ozone, *Atmospheric Environment Part A-General Topics, 26*(8), 1461-1468.

Munthe, J., Z. F. Xiao, and O. Lindqvist (1991), The aqueous reduction of divalent mercury by sulfite, *Water, Air, & Soil Pollution, 56*, 621-630.

Nevado, J. J. B., L. F. G. Bermejo, and R. C. R. Martin-Dolmeadios (2003), Distribution of mercury in the aquatic environment at Almaden, Spain, *Environmental Pollution, 122*(2), 261-271.

Nier, A. O. (1950), A Redetermination of the Relative Abundances of the Isotopes of Neon, Krypton, Rubidium, Xenon, and Mercury, *Physical Review, 79*(3), 450-454.

Nriagu, J. O. (1994), Mercury Pollution from the Past Mining of Gold and Silver in the America, *Science of the Total Environment, 149*(3), 167-181.

Nriagu, J. O. (1989), A global assessment of natural sources of atmospheric trace metals, *Nature, 338*(6210), 47-49.

Nriagu, J., and C. Becker (2003), Volcanic emissions of mercury to the atmosphere: global and regional inventories, *The Science of The Total Environment, 304*(1-3), 3-12.

Oldfield, F., K. Tolonen, and R. Thompson (1981), History of Particulate Atmospheric-Pollution from Magnetic Measurements in Dated Finnish Peat Profiles, *Ambio, 10*(4), 185-188.

Pacyna, J. M., and J. Munch (1991), Anthropogenic Mercury Emission in Europe, *Water Air and Soil Pollution, 56*, 51-61.

Pacyna, J., J. Munthe, K. Larjava, and E. Pacyna (2005), Mercury Emissions from Anthropogenic Sources: Estimates and Measurements for Europe, *Dynamics of Mercury Pollution on Regional and Global Scales:,* , 51-64.

Pessenda, L. C. R., B. M. Gomes, R. Aravena, A. S. Ribeiro, R. Boulet, and S. E. M. Gouveia (1998), The carbon isotope record in soils along a forest-cerrado ecosystem transect: implications for vegetation changes in the Rondonia state, southwestern Brazilian Amazon region, *Holocene, 8*(5), 599-603.

Pessenda, L.C.R., E.P.E. Valencia, R. Aravena, E.C.C. Telles, R. Boulet (1998b), Paleoclimate studies in Brazil using carbon isotope studies in soils. In: Wasserman JC, Silva Filho EV, Villas-Boas R, editors. *EnvironmentalGeochemistry in the Tropics*. Springer Verlag.

Pfister, C. (1985), CLIMHIST, a weather data bank for Central Europe 1525 to 1863. METEOTEST, Bern.

Pirrone, N., I. Allegrini, G. J. Keeler, J. O. Nriagu, R. Rossmann, and J. A. Robbins (1998), Historical atmospheric mercury emissions and depositions in North America compared to mercury accumulations in sedimentary records, *Atmospheric Environment, 32*(5), 929-940.

Pongratz, R., and K. G. Heumann (1999), Production of methylated mercury, lead, and cadmium by marine bacteria as a significant natural source for atmospheric heavy metals in polar regions, *Chemosphere, 39*(1), 89-102.

Porcella, D.B., P. Chu, M.A. Alla (1996), Inventory of North America Hg Emissions to the Atmosphere; Relationship to the Global Hg Cycle. In; Global and Regional Mercury Cycles: Sources, Fluxes, and Mass Balances, 179-190.

Pyle, D. M., and T. A. Mather (2003), The importance of volcanic emissions for the global atmospheric mercury cycle, *Atmospheric Environment, 37*(36), 5115-5124.

Ramesh, R., S.K. Bhattacharya and K. Gopalan (1986), Climatic correlations in the s**Table** isotope records of silver fir (Abies pindrow) trees from Kashmir, India. *Earth Planet. Sci. Lett*, 79, pp. 66–74.

Ramil-Rego, P., C. Munoz-Sobrino, M. Rodriguez-Guitian, and L. Gomez-Orellana (1998), Differences in the vegetation of the North Iberian Peninsula during the last 16,000 years, *Plant Ecology, 138*(1), 41-62.

Ramil, P., M. Rodriguez-Guitian., and C. Munoz-Sobrino (1996), *Real Soc. Esp. Hist. Nat*, Tomo Extraordinario, pp. 253–256

Rasmussen, P. E. (1994), Current Methods of Estimating Atmospheric Mercury Fluxes in Remote Areas, *Environmental science & technology, 28*(13), 2233-2241.

Robertson, I., Waterhouse, JS., Barker, AC., Carter, AHC. and Switsur, VR., 2001, Reconstructing oxygen isotope ratios of precipitation. Earth and Planetary Science Letters 191(1-2), pp. 21-31

Roos-Barraclough, F., A. M. Cortizas, E. Garcia-Rodeja, and W. Shotyk (2002), A 14 500 year record of the accumulation of atmospheric mercury in peat: volcanic signals, anthropogenic influences and a correlation to bromine accumulation, *Earth and Planetary Science Letters, 202*(2), 435-451.

Rose, T. K. (1915), *The Metallurgy of Gold*, C. Griffin & Co. Ltd., New York.

Rydin, H. (1985), Effect of Water Level on Desiccation of Sphagnum in Relation to Surrounding Sphagna, *Oikos, 45*(3), 374-379.

Rytuba, J. J. (2003), Mercury from mineral deposits and potential environmental impact, *Environmental Geology, 43*(3), 326-338.

Santos, G. M., R. Cordeiro, E. V. Silva, B. Turcq, L. D. Lacerda, L. K. Fifield, P. R. S. Gomes, P. A. Hausladen, A. Sifeddine, and A. L. S. Albuquerque (2001), Chronology of the atmospheric mercury in Lagoa da Pata Basin, Upper Rio Negro region of Brazilian Amazon, *Radiocarbon, 43*(2B), 801-808.

Santos, L. (2004), Late Holocene Forest History and Deforestation Dynamics in the Queixa Sierra, Galicia, Northwestern Iberian Peninsula, *Mountain Research and Development, 24*(3), 251-257.

Santos, L., J. R. V. Romani, and G. Jalut (2000), History of vegetation during the Holocene in the Courel and Queixa Sierras, Galicia, northwest Iberian Peninsula, *Journal of Quaternary Science, 15*(6), 621-632.

Schuster, P. F., D. P. Krabbenhoft, D. L. Naftz, L. D. Cecil, M. L. Olson, J. F. Dewild, D. D. Susong, J. R. Green, and M. L. Abbott (2002), Atmospheric mercury deposition during the last 270 years: A glacial ice core record of natural and anthropogenic sources, *Environmental science & technology, 36*(11), 2303-2310.

Sellers, P., C. A. Kelly, J. W. M. Rudd, and A. R. MacHutchon (1996), Photodegradation of methylmercury in lakes, *Nature, 380*(6576), 694-697.

Serrano, A., J. A. Garcı´a, V. L. Mateos, M. L. Cancillo, and J. Garrido (1999), Monthly modes of variation of precipitation over the Iberian peninsula. *J. Climate,* 12**,** 2894–2919.

Shotyk, W., M. E. Goodsite, F. Roos-Barraclough, R. Frei, J. Heinemeier, G. Asmund, C. Lohse, and T. S. Hansen (2003), Anthropogenic contributions to atmospheric Hg, Pb and As accumulation recorded by peat cores from southern Greenland and Denmark dated using the 14C "bomb pulse curve", *Geochimica et Cosmochimica Acta, 67*(21), 3991-4011.

Shotyk, W., H. W. Nesbitt, and W. S. Fyfe (1990), The Behavior of Major and Trace-Elements in Complete Vertical Peat Profiles from 3 Sphagnum Bogs, *International Journal of Coal Geology, 15*(3), 163-190.

Shotyk, W., D. Weiss, P. G. Appleby, A. K. Cheburkin, R. Frei, M. Gloor, J. D. Kramers, S. Reese, and W. O. Van der Knaap (1998), History of atmospheric lead deposition since 12,370 C-14 yr BP from a peat bog, Jura Mountains, Switzerland, *Science, 281*(5383), 1635-1640.

Siegel, S. M., and B. Z. Siegel (1984), 1st Estimate of Annual Mercury Flux at the Kilauea Main Vent, *Nature, 309*(5964), 146-147.

Sigler, J. M., X. Lee, and W. Munger (2003), Emission and long-range transport of gaseous mercury from a large-scale Canadian boreal forest fire, *Environmental science & technology, 37*(19), 4343-4347.

Simkin, T., and L. Siebert (1994), *Volcanoes of the world*, Geoscience Press Inc., Tucson, Arizona.

Slemr, F., and E. Langer (1992), Increase in global atmospheric concentrations of mercury inferred from measurements over the Atlantic Ocean, *Nature, 355*(6359), 434-437.

Steinnes, E., and E. M. Andersson (1991), Atmospheric Deposition of Mercury in Norway - Temporal and Spatial Trends, *Water Air and Soil Pollution, 56*, 391-404.

Sternberg, L.S.L. (1989), Oxygen and hydrogen isotope measurements in plant cellulose analysis, in: Modern Methods of Plant Analysis,. H.F.L.a.J.F. Jackson (Ed.), Springer, Berlin, pp. 89-99.

Sternberg, L.S.L., M.J. DeNiro and R.A. Savidge (1986a), Oxygen isotope exchange between metabolites and water during biochemical reactions leading to cellulose synthesis. *Plant Physiol*, 82, pp. 423–427.

Streets, D., J. Hao, Y. Wu, J. Jiang, M. Chan, H. Tian, and X. Feng (2005), Anthropogenic mercury emissions in China, *Atmospheric Environment, 39*(40), 7789-7806.

Strode, S. A., L. Jaegle, N. E. Selin, D. J. Jacob, R. J. Park, R. M. Yantosca, R. P. Mason, and F. Slemr (2007), Air-sea exchange in the global mercury cycle, *Global Biogeochemical Cycles, 21*(1), GB1017.

Sun, L. G., X. B. Yin, X. D. Liu, R. B. Zhu, Z. Q. Xie, and Y. H. Wang (2006), A 2000-year record of mercury and ancient civilizations in seal hairs from King George Island, West Antarctica, *Science of the Total Environment, 368*(1), 236-247.

Sundelin, B., and A. K. Eriksson (2001), Mobility and bioavailability of trace metals in sulfidic coastal sediments, *Environmental Toxicology and Chemistry, 20*(4), 748-756.

Swain, E. B., D. R. Engstrom, M. E. Brigham, T. A. Henning, and P. L. Brezonik Increasing Rates of Atmospheric Mercury Deposition in Midcontinental North America, *Science, 257*(5071), 784-787.

Switsur, R. and J.S. Waterhouse (1998), Stable isotopes in tree ring cellulose, in H. Griffiths (Ed.), Stable Isotopes: the Integration of Biological, Ecological and Geological Processes, BIOS Scientific Publishers, 1998, pp. 303-321

Thompson, L. G., E. Mosley-Thompson, Dansgaard W., and P. M. Grootes (1986), The Little Ice Age as Recorded in the Stratigraphy of the Tropical Quelccaya Ice Cap, *Science, 234*(4774), 361-364, doi: 10.1126/science.234.4774.361.

Titus, J. E., and D. J. Wagner (1984), Carbon Balance for 2 Sphagnum Mosses - Water-Balance Resolves a Physiological Paradox, *Ecology, 65*(6), 1765-1774.

Tullot, I.F. (1988), *Historia del Clima de España: Cambios Climáticos y sus Causas* (Instituto Nacional de Meteorología, Madrid.

Turcq, B., A., L. Siffedine, M.L. Martin, F. Absy, K. Soubies, C. Suguio, Volkeimer-Ribeiro (1998), Amazon forest fires: a Lacustrine report of 7000 years. *Ambio 27*(2): 139–142.

Valero-Garcés, B.L., K. Kelts, A. Delgado-Huertas, P. González-Sampériz, A. Navas, J. Machín (1999), Sedimentary facies analyses as paleohydrological proxies for saline lakes, Centro Ebro Basin, Spain, in: E. Eldp (Ed.), 4th Workshop of the European Lake Drilling Programme: Correlations of Late Weichselian and Holocene Palaeoenvironment
Proxy Data, Terra Nostra 99 (10), 101-106.

Vandal, G. M., W. F. Fitzgerald, C. F. Boutron, and J. P. Candelone (1993), Variations in Mercury Deposition to Antarctica Over the Past 34,000 Years, *Nature, 362*(6421), 621-623.

Varekamp, J. C., and P. R. Buseck (1981), Mercury Emissions from Mount St-Helens during September 1980, *Nature, 293*(5833), 555-556.

Varekamp, J. C., and P. R. Buseck (1986), Global mercury flux from volcanic and geothermal sources, *Applied Geochemistry, 1*(1), 65-73

Veiga, M.M. and J.J. Hinton (2002), Abandoned artisanal gold mines in the Brazilian Amazon: A legacy of mercury pollution, *Natural Resources Forum,* 26 (1) , 15–26 doi:10.1111/1477-8947.00003

Wagner, D. J., and J. E. Titus (1984), Comparative Desiccation Tolerance of 2 Sphagnum Mosses, *Oecologia, 62*(2), 182-187.

Webb, W. S. and C. G. Wilder (1951), *An archaeological survey of Guntersville Basin on the Tennessee River in Northern Alabama*, 278 pp., University of Kentucky Press, Lexington.

Weiss, D., W. Shotyk and O. Kempf, 1999, Archives of atmospheric lead pollution. *Naturwissenschaften* 86 (6), 10.1007/s001140050612, 262-275

Xia, K., U. L. Skyllberg, W. F. Bleam, P. R. Bloom, E. A. Nater, and P. A. Helmke (1999), X-ray absorption spectroscopic evidence for the complexation of Hg(II) by reduced sulfur in soil humic substances, *Environmental science & technology, 33*(2), 257-261.

Yudovich, Y. E., and M. P. Ketris (2005), Mercury in coal: a review: Part 1. Geochemistry, *International Journal of Coal Geology, 62*(3), 107-134.

Zanazzi, A., and G. Mora (2005), Paleoclimatic implications of the relationship between oxygen isotope ratios of moss cellulose and source water in wetlands of Lake Superior, *Chemical Geology, 222*(3-4), 281-291.

Zapata, B.R. (1999), El cambio climático en la Península Ibérica. In Ruiz Zapata, B., Dorado Valinó, M., Gil García, M. J. & Valdeolmillos Rodríguez, A. (eds.): Efectos del cambio climático en la región mediterránea durante los últimos 3000 anâôs, 86–95.Universidad de Alcalôá, Madrid.

Chapter 3

Angeli, I. (2004), A consistent set of nuclear rms charge radii: properties of the radius surface R(N,Z), *Atomic Data and Nuclear Data Tables, 87*(2), 185-206.

Benoit, J. M., W. F. Fitzgerald, and A. W. H. and Damman (1994), Historical atmospheric mercury deposition in the Mid-Continental U.S. as recorded in an ombrotrophic peat bog. in *Mercury pollution: Integration and synthesis*edited by C. J. Watras and J. W. and Huckabee, pp. 187-202, Lewis Publication, Boca Raton, Florida.

Bergquist, B. A., and J. D. Blum (2007), Mass-dependent and -independent fractionation of Hg isotopes by photoreduction in aquatic systems, *Science, 318*(5849), 417-420.

Biester, H., A. Martinez-Cortizas, S. Birkenstock, and R. Kilian (2003), Effect of peat decomposition and mass loss on historic mercury records in peat bogs from Patagonia, *Environmental science & technology, 37*(1), 32-39.

Biester, H., G. Muller, and H. F. Scholer (2002), Binding and mobility of mercury in soils contaminated by emissions from chlor-alkali plants, *Science of the Total Environment, 284*(1-3), 191-203.

Bigeleisen, J. (1996), Nuclear Size and Shape Effects in Chemical Reactions. Isotope Chemistry of the Heavy Elements, *Journal of the American Chemical Society, 118*(15), 3676-3680, doi: 10.1021/ja954076k [doi].

Blum, J., and B. Bergquist (2007), Reporting of variations in the natural isotopic composition of mercury, *Analytical and Bioanalytical Chemistry, 388*(2), 353-359.

Bronsted, J. N., and G. Von Hevesy (1920), The separation of the isotopes of mercury. *Nature, 106*, 144.

Buchachenko, A. L., E. M. Galimov, V. V. Ershov, G. A. Nikiforov, and A. D. Pershin (1976), Isotope enrichment induced by magnetic interactions in chemical reactions, *228*, 379-381.

Buchachenko, A. L., D. A. Kouznetsov, and A. V. Shishkov (2004), Spin Biochemistry: Magnetic Isotope Effect in the Reaction of Creatine Kinase with CH_3HgCl, *Journal of Physical Chemistry A, 108*(5), 707-710.

Buchachenko, A. L., V. L. Ivanov, V. A. Roznyatovskii, G. A. Artamkina, A. K. Vorob'ev, and Y. A. Ustynyuk (2007), *Magnetic Isotope Effect for Mercury Nuclei in Photolysis of Bis(p-trifluoromethylbenzyl)mercury*, *Doklady Physical Chemistry, 413*, 39-41.

Fitzgerald, W. F. (1995), Is mercury increasing in the atmosphere? The need for an atmospheric mercury network (AMNET), *Water, Air, & Soil Pollution, 80*(1), 245-254.

Foucher, D., and H. Hintelmann (2006), High-precision measurement of mercury isotope ratios in sediments using cold-vapor generation multi-collector inductively coupled plasma mass spectrometry, *Analytical and Bioanalytical Chemistry, 384*(7), 1470-1478.

Gerstenkorn, S., and J. Verges (1975), Interpretation of the anomalous odd-even isotopes in the arc spectra of mercury. *Journal of Physics (Paris), 36*, 481-486.

Grigal, D. F. (2003), Mercury sequestration in forests and peatlands: A review, *Journal of environmental quality, 32*(2), 393-405.

Hahn, A. A., J. P. Miller, R. J. Powers, A. Zehnder, A. M. Rushton, R. E. Welsh, A. R. Kunselman, P. Roberson, and H. K. Walter (1979), An experimental study of muonic x-ray transitions in mercury isotopes, *Nuclear Physics, A314*, 361-386.

Hintelmann, H., and S. Lu (2003), High precision isotope ratio measurements of mercury isotopes in cinnabar ores using multi-collector inductively coupled plasma mass spectrometry, *Analyst, 128*, 635-639.

Jackson, T. A., D. C. G. Muir, and W. F. Vincent (2004), Historical Variations in the Stable Isotope Composition of Mercury in Arctic Lake Sediments, *Environmental Science & Technology, 38*(10), 2813-2821.

Kritee, K., Blum, J. D., Johnson, M. W., Bergquist, B. A. and Barkay, T. (2007), Mercury Stable Isotope Fractionation during Reduction of Hg(II) to Hg(0) by Mercury Resistant Microorganisms, *Environmental science & technology, 41*, 1889-1895.

Klaue B., and Blum J.D. (1999), Trace Element analyses of arsenic in drinking water by inductively coupled plasma mass spectrometry: high resolution versus hydride generation. *Anal Chem*., 71, 1408-1414

Lindqvist, O., K. Johansson, M. Aastrup, A. Andersson, L. Bringmark, G. Hovsenius, L. Hakanson, A. Iverfeldt, M. Meili, and B. Timm (1991), Mercury in the Swedish Environment - Recent Research on Causes, Consequences and Corrective Methods, *Water Air and Soil Pollution, 55*(1-2), R11.

Martínez-Cortizas, A., Pontevedra-Pombal, X., García-Rodeja, E., Nóvoa-Muñoz, J. C. and Shotyk, W. (1999), Mercury in a Spanish Peat Bog: Archive of Climate Change and Atmospheric Metal Deposition, *Science, 284*(541), 939-942.

Mason, R. P., and G. R. Sheu (2002), Role of the ocean in the global mercury cycle, *16*(4), 40-1-40-14.

Meili, M. (1991), The Coupling of Mercury and Organic-Matter in the Biogeochemical Cycle - Towards a Mechanistic Model for the Boreal Forest Zone, *Water Air and Soil Pollution, 56*, 333-347.

Mierle, G., and R. Ingram (1991), The Role of Humic Substances in the Mobilization of Mercury from Watersheds, *Water Air and Soil Pollution, 56*, 349-357.

Morel, F. M. M., A. M. L. Kraepiel, and M. Amyot (1998), The Chemical Cycle and Bioaccumulation of Mercury, *Annual Review of Ecology and Systematics, 29*(1), 543-566.

Nier, A. O. (1950), A Redetermination of the Relative Abundances of the Isotopes of Neon, Krypton, Rubidium, Xenon, and Mercury, *Physical Review, 79*(3), 450.

Schauble, E. A. (2007), Role of nuclear volume in driving equilibrium stable isotope fractionation of mercury, thallium, and other very heavy elements, *Geochimica et Cosmochimica Acta, 71*(9), 2170-2189.

Schuster, E. (1991), The Behavior of Mercury in the Soil with Special Emphasis on Complexation and Adsorption Processes - a Review of the Literature, *Water Air and Soil Pollution, 56*, 667-680.

Smith, C. N., S. E. Kesler, B. Klaue, and J. D. Blum (2005), Mercury isotope fractionation in fossil hydrothermal systems, *Geology, 33*(10).

Thiemens, M. H. (1999), Mass-Independent Isotope Effects in Planetary Atmospheres and the Early Solar System, *Science, 283*(5400), 341-345.

Turro, N. J. (1983), Influence of nuclear spin on chemical, reactions: Magnetic isotope and magnetic field effects (A Review), Proc. Natl. Acad. Sci. *80*, 609-621.

Xia, K., U. L. Skyllberg, W. F. Bleam, P. R. Bloom, E. A. Nater, and P. A. Helmke (1999), X-ray absorption spectroscopic evidence for the complexation of Hg(II) by reduced sulfur in soil humic substances, *Environmental science & technology, 33*(2), 257-261.

Yin, Y. J., H. E. Allen, C. P. Huang, D. L. Sparks, and P. F. Sanders (1997), Kinetics of mercury(II) adsorption and desorption on soil, *Environmental science & technology, 31*(2), 496-503.

Chapter 4

Adams, R. M. (1949), Archaeological Investigations in Jefferson County, Missouri, *The Missouri Archaeologist, 11*(3 and 4).

Agnew, A. F. (1955), Application of geology to the discovery of zinc-lead ore in the Wisconsin-Illinois-Iowa district, *Transactions of the American Institute of Mining, Metallurgical and Petroleum Engineers, 202*, 781-794.

Austin, R.J. (1993), The Royce Mound: Middle Woodland exchange and mortuary customs in south Florida. *Florida Anthropologist*, *46*, 291-309

Austin, R.J., R.M. Farquhar and K.J. Walker (2000), Isotope Analysis of Galena from Prehistoric Archaeological Sites in South Florida, *Florida Scientist*, *63*(2), 118-122

Barnes, I. L., J.W. Gramlich, M.C. Diaz, and R.H. Brill, R. H. (1978), The possible change in lead isotope ratios in the manufacture of pigments: a fractionation experiment. In (G. F. Carter, Ed.) *Advances in Chemistry Series 171, Archaeological Chemistry II.* Washington, DC: American Chemical Society, 273-277

Barnes, I.L., W.R. Shields, T.J. Murphy and R.H. Brill (1974), Isotopic Analysis of Laurion Lead Ores, *In* C. W. Beck, ed. *Archaeological Chemistry*, *138*. American Chemical Society, Washington, D. C.

Bell, R.E. (1974), Mounds and Fieldwork near Muskogee, Oklahoma, *Oklahoma Anthroplogical Society Newsletter*, *22* (8), 6-9

Brill, R. H., and J. M. Wampler (1967), Isotope Studies of Ancient Lead, *American Journal of Archaeology, 71*(1), 63-77.

Brill, R.H., K. Yamasaki, L. Barnes, K.J.R. Rosman and M. Diaz (1979), Lead Isotopes in some Japanese and Chinese Glasses., *Ars Orientalis XI*: 87-109

Broadhead, G. C. (1894), Report of the Geological Survey of Missouri, , 380 pp., Rolla.

Broadhead, G. C. (1880), Geological Report on the Mineral Lands of R. H. Melton, , Eagle Print, Sedalia, Missouri.

Brown J. S. (1967), Isotopic zoning of lead and sulfur in southeast Missouri. *Econ. Geol. Monogr. 3***,** 410–426

Bullen, R.P. (1978), Pre-columbian trade in eastern United States as reviewed from Florida. *Florida Anthropologist*, *31*, 92-108

Burns, S. (1994), Bioarchaeology of the Mackey site in Southeastern Oklahoma. Master's Thesis. Department of Anthropology, University of Oklahoma

Byrd, K.M. (1974), Tchefuncte subsistence patterns: Morton Shell Mound, Iberia Parish, Louisiana State University

Cameron, A. E., D. H. Smith, and R. L. Walker (1969), Mass Spectrometry of Nanogram-Size Samples of Lead, *Analytical Chemistry, 41*(3), 525-&.

Cannon, R.,Jr., A. Pierce, and M. Delevaux (1963), Lead Isotope Variation with Growth Zoning in a Galena Crystal, *Science, 142*(3592), 574-576, doi: 10.1126/science.142.3592.574.

Carr, R. S., and J. Ricisak (2000), Preliminary report on salvage archaeological excavations of the Brickell Point site (8DA12), including the Miami Circle. *The Florida Anthropologist, 53*, 260-284.

Cole, F. and T. Deuel (1937), *Rediscovering Illinois; archaeological explorations in and around Fulton County*, 295 pp., Ill., University of Chicago Press, Chicago.

Crocetti, C. A. and H. D. Holland (1989), Sulfur-lead isotope systematics and the composition of fluid inclusions in galena from the Viburnum Trend, Missouri, *Economic Geology, 84*(8), 2196-2216.

Crocetti, C. A., H. D. Holland and L. W. McKenna (1988), Isotopic composition of lead in galenas from the Viburnum Trend, Missouri, *Economic Geology, 83*(2), 355-376.

Deloule, E., C. Allegre, and B. Doe (1986), Lead and sulfur isotope microstratigraphy in galena crystals from Mississippi valley-type deposits (USA), *Economic Geology, 81*(6), 1307-1321.

Denny, S., and R. B. McMillan (1964), Report on the Archaeological Resources in the Bourbeuse River Valley and Lower Meramec Valley of the Meramec Basin Project Area, Missouri, , National Park Service, Midwest Region, Omaha, Nebraska.

Doe, B. R., and Z. E. Zartman (1979), Plumbotectonics, the Phanerozoic in *Geochemistry of hydrothermal ore deposits,* edited by H. L. Barnes, 22-70, Wiley, New York, .

Doe, B., and M. H. Delevaux (1972), Source of Lead in southeast Missouri galena ores, *Economic Geology*, *67*, 409-425.

Farnsworth, K.B. (1973), An Archaeological Survey of the Macoupin Valley. Illinois *State Museum Reports of Investigations*, No. 26. Springfield

Farquhar, R. M., and I. R. Fletcher (1980), Lead Isotope Identification of Sources of Galena from Some Prehistoric Indian Sites in Ontario, Canada, *Science, 207*(4431), 640-643, doi: 10.1126/science.207.4431.640.

Farquhar, R. M., and I. R. Fletcher (1984), The Provenience of Galena from Archaic/Woodland Sites in Northeastern North America: Lead Isotope Evidence, *American Antiquity, 49*(4), 774-785.

Farquhar, R. M. and V. Vitali (1989), Lead isotope measurements and their application to Roman lead and bronze artifacts from Carthage. *MASCA Research Papers in Science and Archaeology, 6,* 9-45.

Farquhar, R. M., J. A. Walthall, and R. G. V. Hancock (1995), 18th-Century Lead Smelting in Central North-America - Evidence from Lead-Isotope and Inaa Measurements, *Journal of Archaeological Science, 22*(5), 639-648.

Fowler, M. L. (1959), Modoc Rock Shelter: An Early Archaic Site in Southern Illinois, *American Antiquity, 24*(3), 257-270.

Goldhaber, M. B., S. E. Church, B. R. Doe, J. N. Aleinikoff, J. C. Brannon, F. A. Podosek, E. L. Mosier, C. D. Taylor, and C. A. Gent (1995), Lead and sulfur isotope investigation of Paleozoic sedimentary rocks from the southern Midcontinent of the United States; implications for paleohydrology and ore genesis of the Southeast Missouri lead belts, *Economic Geology, 90*(7), 1875-1910.

Griffin, J. B., and D. F. Morse (1961), The Short-Nosed God from the Emmons Site, Illinois, *American Antiquity, 26*(4), 560-563.

Grogan, R.M. and J.C. Bradbury (1968), Fluorite-zinc-lead deposits of the Illinois-Kentucky mining district. In *Ore deposits of the United States*, J.R. Ridge (ed)., New York, American Institute of Mining, Metallurgical and Petroleum Engineers, 370-399

Hall, J. and J. D. Whitney (1858), Report of the Geological Survey of the State of Iowa, , 473 pp

Hart, S., N. Shimizu, and D. Sverjensky (1981), Lead isotope zoning in galena; an ion microprobe study of a galena crystal from the Buick Mine, Southeast Missouri, *Economic Geology, 76*(7), 1873-1878.

Heyl, A. V. (1968), The Upper Mississippi Valley base metal district, in *Ore deposits of the United States,* edited by J. R. Ridge, pp. 431-459, American Institute of Mining, Metallurgical and Petroleum Engineers, New York .

Heyl, A. V., M. H. Delevaux, R. E. Zartman, and M. R. Brock (1966), Isotopic study of galenas from the upper Mississippi Valley, the Illinois-Kentucky, and some Appalachian Valley mineral districts, *Economic Geology, 61*(5), 933-961.

Hoagland, A. D., W. T. Hill, and R. E. Fulweiler (1965), Genesis of the Ordovician zinc deposits in east Tennessee, *Economic Geology, 60*(4), 693-714.

Hofman, J.L. (1979), Twenhafel, A Prehistoric community on the Mississippi 500 B.C. - A.D. 1500, *The Living Museum*, *41*(3): 34--38.

Holmes, A. (1946), An estimate of the age of the Earth, *Nature, 157*, 680-684.

Houtermans, F. G. (1953), Determination of the age of the Earth from the isotopic composition of meteoritic lead. *Nuovo Cimento, 10*, 1623-1633.

Jones, B.C. (1982), Southern cult manifestations at the Lake Jackson site (8Le1), Leon County, Florida: salvage excavations of Mound 3, *Midcontinental Journal of Archaeology*, *7*, 3-44

Jones, B. C. and L. D. Tesar (1996), Emergency Archaeological Salvage Excavation Within the Swift Creek Subarea of the Block-Sterns Site (8LE148), Leon County, Florida: A Public Archaeology Project. Bureau of Archaeological Research, Division of Historical Resources. , Florida Department of State, Tallahassee.

Jones, B.C, D.T. Penton and L.D. Tesar (1998), Excavations at the Block-Sterns Site, Leon County, Florida. In *A World Engraved: Archaeology of the Swift Creek Culture*, edited by Mark Williams and Daniel T. Elliott, 222–246. University of Alabama Press, Tuscaloosa.

Kay, M. (1980), Holocene Adaptations within the Lower Pomme de Terre River Valley, Missouri. Report of the Corps of Engineers, Kansas City.

Keslin, R. O. (1964), *Archaeological implications on the role of salt as an element of cultural diffusion*, 181 pp., State Archaeological Society of Missouri, Columbia, Mo.

Leader, P.M. (1997), Chipped stone artifacts from the Mackey site, large black midden mound in the Fourche Maline Valley, Master's thesis, Department of Anthropology, University of Oklahoma

Logan, W. D. (1976), Woodland complexes in northeastern Iowa*: Publications in Archaeology 15*, 203 pp., National Park Service, U.S. Department of the Interior, Washington, D.C.

Martin, T.L. (2001), The Barrington Site: A Middle Archaic Cache from the St. Luois area, *Plains Anthropologist*, *46*, 95-108

McNamara, J. and Thode, H.G. (1950), Comparison of the isotopic constitution of terrestrial and meteoritic sulfur. *Physical Review, 78*, 307-308.

Millen, T. M., R. E. Zartman, A. V. Heyl, J. L. Ridgley, and Geological Survey (U.S.) (1995), *Evolution of sedimentary basins - Illinois Basin*, United States Gov. Print. Off, Washington, DC.

Ohle, E. L. (1980), Some considerations in determining the origin of ore deposits of the Mississippi Valley-type--Part II. *Economic Geology, 75*, 161-172.

Russell, R. D. and R. M. Farquhar (1960), *Lead isotopes in geology*, Interscience Publishers, New York.

Schockel, B.H. (1916), Settlemen and Development of Jo Daviess County*, Geology and geography of the Galena and Elizabeth quadrangles*, 173-228.

Schoolcraft, H. R. (1819), A view of the lead mines of Missouri : including some observations on the mineralogy, geology, geography, antiquities, soil, climate, population, and productions of Missouri and Arkansas, and other sections of the western country : accompanied by three engravings, Charles Wiley & Co., J. Seymour), New-York.

Sears, W.H. (1962), Hopewellian affiliations of certain sites on the Gulf coast of Florida. *American Antiquity*, *28*, 5-18

Seeman, M. F. (1977), *The Hopewell Interaction Sphere: The Evidence for Interregional. Trade*

Shumard, B. F. (1867), A Geological Report on the Mineral Lands Belonging to R. H. Melton, Esq. in Benton and Hickory Counties, Missouri. St. Louis

Sverjensky, D. A., D. M. Rye, and B. R. Doe (1979), The lead and sulfur isotopic compositions of galena from a mississippi valley-type deposit in the New Lead Belt, Southeast Missouri, *Economic Geology, 74*(1), 149-153.

Swanton, J.R. (1946), The Indians of the Southeastern United States. *Bureau of American Ethnology Bulletins,* No 137. Washington, D.C.

Swartzlow, R.J. (1934), Missouri Historical Review, Columbia, Mo.

Todt, W., R. A. Cliff, A. Hanser, and A. W. Hofmann (1995), Evaluation of a ^{202}Pb-^{205}Pb Double spike for high precision lead isotope analysis, in *Earth Processes Reading the Isotopic Code*edited by A. Basu and S. Hart, pp. 429-437, AGU, .

Walthall, J.A. (1981), Galena and Aborigical Trade in Eastern North America. III. *St. Mus., Scientific Paper*, Vol. XVII. Springfield, IL.

Walthall, J.A., S.H. Stow and M.J. Karson (1979), Ohio Hopewell Trade: Galena Procurement and Exchange. In *Hopewell Archaeology*, D.S. Brose ands N.M.B. Greber (Eds.). Kent, Ohio, Kent State University Press

Walthall, J.A., S.H. Stow and M.J, Karson (1980), Copena Galena: Source Identification and Analysis. *American Antiquity*, *45*, 21-42

Webb, C.H. (1977), The Poverty Point Culture, Louisiana State University Geoscience and Man, 17. Baton Rouge

Webb, W. S. and C. G. Wilder (1951), *An archaeological survey of Guntersville Basin on the Tennessee River in Northern Alabama*, 278 pp., University of Kentucky Press, Lexington.

White, D. E. (1968), Environments of generation of some base-metal ore deposits, *Economic Geology, 63*(4), 301-335.

Whitney, J. D. (1866), Geology of the lead region, *Geological survey of Illinois 1,* 153-207.

Wimberly, S. B. and H. A. Tourtelot, United States, and Work Projects Administration (1941), *The McQuorquodale mound; a manifestation of the Hopewellian phase in south Alabama*, Alabama University.

Winters, H.D., 1981, Excavating in Museums: Notes on Mississippian Hoes and Middle Woodland Copper Gouges and Celts. *Annals of the New York Academy of Sciences,* 376 1, pp. 17–34.

Yener, K. A., Sayre, E. V., Joel, E. C., Ozbal, H., Barnes, I. L. & Brill, R. H., 1991, Stable lead isotope studies of central Taurus ore sources and related artifacts from eastern Mediterranean Chalcolithic and Bronze Age sites. *Journal of Archaeological Science* 18, pp. 541-577

Yerkes, R.W., 1988, The Woodland and Mississippian traditions in the prehistory of Midwestern North America. *Journal of World Prehistory*, Vol. 2, No. 3, pp. 307-358

BIOGRAPHICAL SKETCH

Sanghamitra Ghosh

Education

- Doctor of Philosophy, Environmental Geochemistry, Dept. of Geological Sciences, Florida State University & National High Magnetic Field Laboratory, Tallahassee, FL — August, 2008
- Master of Science, Geochemistry, Dept. of Earth Sciences, Simon Fraser University, Burnaby, BC, Canada — April, 2003
- Master of Science, Geology, Dept. of Geology and Geophysics, Indian Institute of Technology, India — May, 2000
- Bachelor of Science, Geology, Dept. of Geology and Geophysics, Indian Institute of Technology, India — May, 1998